Recognition, Reactivity and Transport with Biomimetic Zinc Complexes

Layla Jasim Abbas Alajmee

The Supervisor: Prof. N.H.Williams

The University of Sheffield - Faculty of Science - Department of Chemistry

Submitted to the University of Sheffield in part –fulfilment of the requirements for the degree of Doctor of Philosophy

November 2019

Declaration

I declare that the data presented in this work were obtained from experiments carried out by myself at the Chemistry Department, The University of Sheffield since October 2015 to September 2019 under the supervision of Professor N.H.Williams. This thesis and the data presented within it were completed solely by the author and has not previously been submitted, in whole or in part for any other degree at this or any other institution.

Sep.2019

Layla Alajmee

Department of Chemistry

University of Sheffield

Dainton Building

Brook Hill

Sheffield

S3 7HF

Acknowledgements

Abstract

This thesis describes the activity of a range of oxime-Zn^{2+} complexes as catalysts in solution and in bilayer membranes to develop greater insights into the parameters that will allow the development of more effective transducers in artificial signal transduction systems. This is followed by studies where a membrane-embedded thiol is used to try and activate an inhibited enzyme to exploit the greater efficiency of biological catalysts.

Chapter one describes key terms in the bilayer membrane field and describes the research that have been achieved in making supramolecular systems that can transfer information across a bilayer membrane.

Chapter two presents the design and the investigation of Zn^{2+} complexes of small ligands containing oxime moieties. The ability of the complexes to catalyse the hydrolysis of two different ester substrates in solution under physiological conditions has been studied using UV-Visible spectroscopy. The stability of the complexes, the dependence of the activity on both ligand and Zn^{2+} ion concentration was determined. The findings showed the underlying characteristics of these complexes to allow comparison with the activity of analogues that can be used as part of a membrane signalling.

Chapter three focuses on using the ligands which were designed and studied in chapter two as headgroups that were attached to cholesterol and lithocholic acid as a lipophilic moiety. These compounds allowed the investigation of the effect of varying the linker between the hydrophilic and lipophilic moieties, and of the effect of the membrane interface, on the characteristics of the complexes. Moreover, the system used in this chapter is compared to the previously reported membrane transducers. In this chapter, we sought to control the reactivity of this metallovesicular system and enhance the catalytic efficiency of the reaction.

Chapter four aims to see if a molecule containing a thiol group that is anchored in a lipid bilayer membrane (in the form of a vesicle) could be utilised to activate an inhibited enzyme in the aqueous phase and whether the enzyme was capable of amplifying a signal once activated. The second aim was to study whether this would provide a system with the ability to be completely inactive in an '**off**' state so that it could be used in a membrane translocation system for signal transduction. The final aim was to see if a transducer molecule with a polar headgroup could be made, which could hold the enzyme-activating moiety held inside the vesicle membrane until a primary signal was inputted.

Chapter five presents the experimental procedures which used to obtain the synthetic compounds with the yield and characterisation data (NMR, Mass Spectra, IR and HPLC traces).

Abbreviations

Adenosine diphosphate	ADP
Adenosine triphosphate	ATP
Angstrom	Å
Benzoylglycinamide	BGA
Bis(2-Hydroxyethyl)iminotris(hydroxymethyl)methane	Bis-Tris
Bis(4-nitrophenyl)- phosphate	BNPP
Capillary Electrophoresis	CE
Carbobenzoxyglycylglycine	CGG
Carbobenzoxy-L-histidinamide	CHA
Carbon Nuclear magnetic resonance	^{13}CNMR
Cetyltrimethylammonium bromide	CTAB
Chemical warfare agents	CWAs
Critical Micelle Concentration	CMC
Deoxyribonucleic acid	DNA
Dicyclohexylcarbodiimide	DCC
Dicyclourea	DCU
4-Dimethylaminopyridine	DMAP
Dimethyl sulfoxide	DMSO
2,4-Dinitrophenyl diethyl phosphate	DNPDEP
2,4-Dinitrophenyl ethyl methyl phosphonate	DNPEMP

1,2-Dioleoyl-sn-glycero-3-phosphocholine	DOPC
1,2-Dioleoyl-sn-glycero-3-phosphoethanolamine	DOPE
Dipicolylamine	DPA
5,5-dithiobis(2-nitrobenzoic acid) (Ellman's reagent)	DTNB
Dodecyl trimethylammonium bromide	DTAB
Dye Encapsulation	DE
Dynamic light scattering	DLS
Egg yolk phosphatidylcholine	EYPC
Ethylenediaminetetraacetic acid	EDTA
Fluorescein diacetate	FDA
Gel permission chromatography	GPC
Guanosine-5'-triphosphate	GTP
High-performance liquid chromatography	HPLC
2-Hydroxypropyl *p*-nitrophenyl phosphate	HPNP
4-(2-hydroxyethyl)-1-piperazineethanesulfonic acid	HEPES
8-Hydroxypyrene-1,3,6-trisulfonate trisodium salt	HPTS
Metal	M
microliter	μL
micromolar	μM
Nanometer	Nm
N,N-Diisopropylethylamine	DIPEA
*N*α-benzoyl-L-arginine *p*-nitroanilide	L-BAPNA

O-Isopropyl methylphosphonofluoridate	(Sarin)
P-Nitrophenyl diphenyl phosphate	PNPDPP
P-Nitrophenyl acetate	PNPA
p-Nitrophenyl picolinate	PNPP
Polymerase chain reaction	PCR
Proton nuclear magnetic resonance	^{1}HNMR
1,3,6-pyrenetrisulfonic acid, 8-(acetyloxy)-, sodium salt	HPTSA
Pyrophosphate	ppi
Ribonucleic acid	RNA
Sodium dodecylbenzenesulfonate	SDBS
Substrate	S
Tetrahedral transition state	(T.T.S)
Tetrahydrofuran	THF
Transmission electron microscopy	TEM
Ultraviolet–visible spectroscopy	UV-Vis
Uridine-5'-triphosphate	UTP

Table of Contents

XIII

XIV

Table of Figures

Table of Schemes

Chapter 1 -   General Introduction

1.1   Transporting Information through Cell Membranes

The cell membranes of organisms are unique structures, which enable the cell to sense, respond to, and then transform information and signals. Cells are isolated from their environments by a lipid bilayer membrane (Figure 1-1) that plays a vital role in cell signalling.[1] Cells cannot survive unless they sense and respond to the changes in their surroundings (*e.g.* the levels of extracellular hormones, cytokines, nutrients, growth factors, and pathogens).[2] These molecular signals can change the cell's intracellular chemistry by being transported into the cell through pores in the membrane or by active transport (Figure 1-2A).[3, 4] The communication between the outside and the inside of a cell can also take place by a reorganisation of a receptor spanning the membrane upon binding of a ligand, causing the release of another messenger within the bilayer membrane (Figure 1-2B).
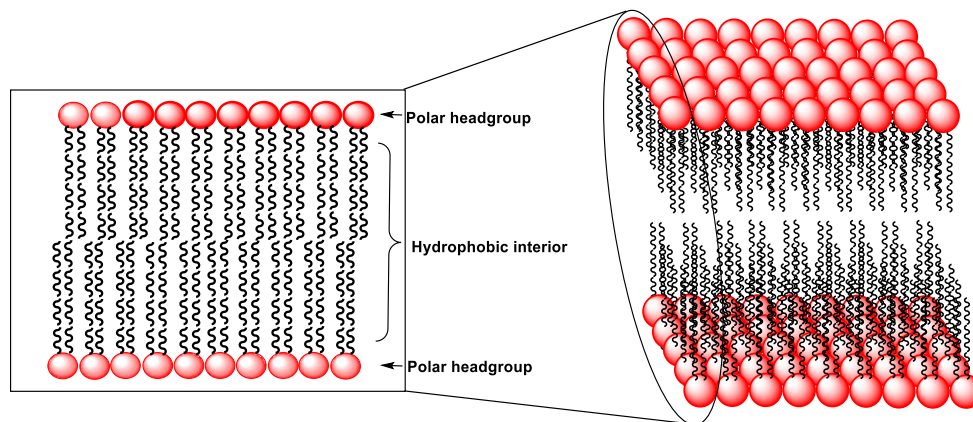
Figure 1-1. *Cell bilayer membrane*
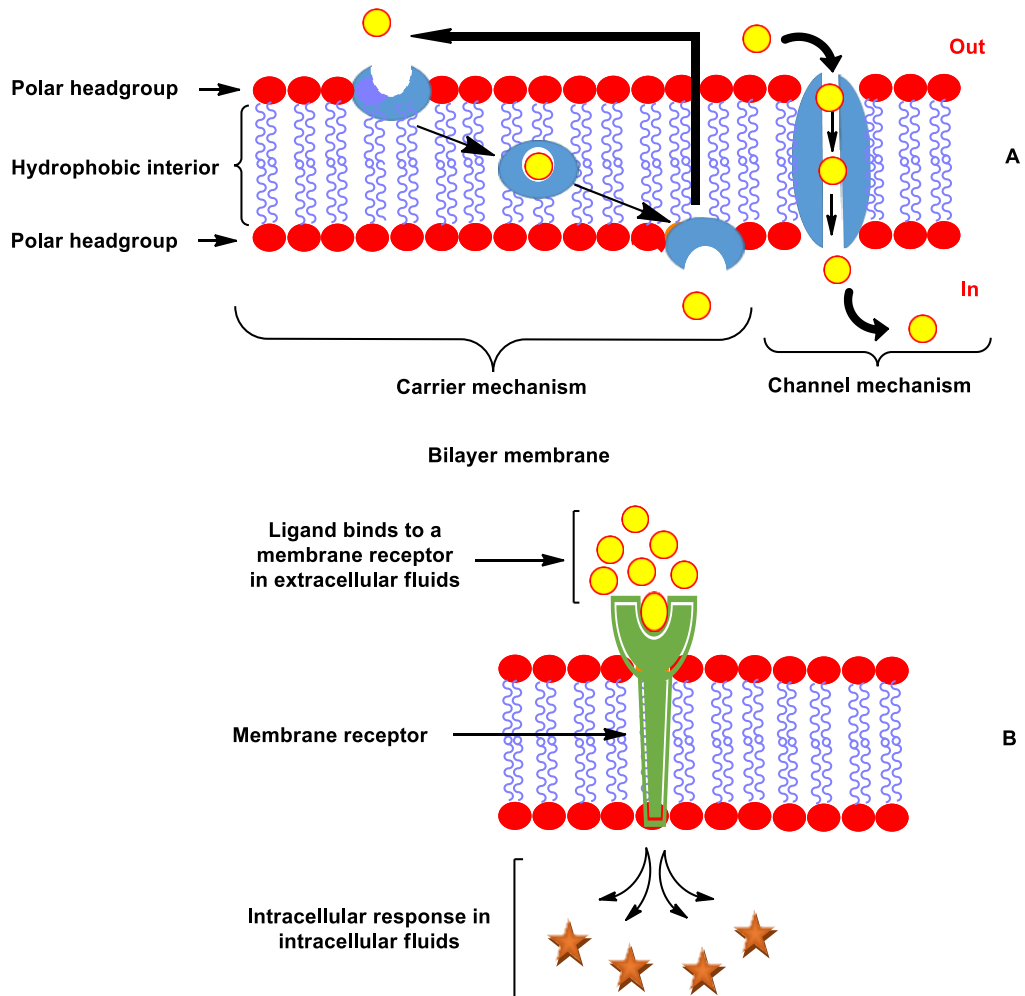
Figure 1-2*: Schematic representation of the mechanism **A**) of ions transport (yellow circles) via ion carriers and ion channels (adapted from ref. 4),[4] **B**) of a signal transduction event in which second messengers (red stars) are released inside a cell upon binding between a receptor (green membrane-spanning object) and a ligand (yellow circles).*

Cell membranes are noncovalent, dynamic, fluid assemblies. Membrane-bound carbohydrates and proteins that regulate many biological membrane processes rely on the membrane fluidity.[5] In these biological signalling processes, the cooperativity can play an essential role. At a membrane surface, the receptors can only move in two dimensions, therefore, it is expected that the binding interactions at membrane interfaces are thermodynamically more favourable than binding interactions in bulk solutions (where movement occurs in three dimensions).[6] Furthermore, the polarity at the membrane interfaces is very different from a bulk solution, and this microenvironment can exert a powerful effect on binding interactions.[7] However, for a number of receptor/ligand

interactions, there is a lack of understanding about how strong the binding affinities are, especially the co-operative binding of receptors restricted to the cell membrane surface.[8] Natural cell membrane receptors frequently fully span lipid bilayers, such as G-protein coupled receptors, and tyrosine kinase receptors which contain seven transmembrane units.[9] Transmembrane receptors are essential for particular functions, for instance, initiating signal transformation pathways. In signal transformation, the messenger attaches to the external portion of the transmembrane receptor on the cell surface. This causes a change in the transmembrane conformation and reorganisation of the receptor. This process leads to the aggregation of the interior receptor sites, thereby stimulating an intracellular response that in turn triggers a signal pathway (cascade) inside the cell.[10] For instance, bacteria chemotaxic receptors, (a family of transmembrane receptors) can detect a very small variation in the concentration of specific chemicals.[11]

1.2   Importance of Bilayer Membranes

The compartmentalisation of aqueous solutions by bilayer membranes can affect reactions in different ways, for example, it can cause a larger local concentration of reactants, accelerating reactions, or may block or decelerate reactions between reactants held in different compartments. Research have shown that compartmentalisation helps some enzymatic reactions by blocking competing reactions (parasitic reactions) that decelerate them.[12,13,14] such as polymerase chain reaction (PCR), which is a method widely used in molecular biology to make several copies of a specific DNA (deoxyribonucleic acid) segment.[13] Furthermore, reactions between lipophilic molecules that are preferentially soluble in the membrane can be improved by the lipid membrane itself.[15] A number of the effects in compartmentalised reactivity are less apparent, however, when researchers study living cells, the effects might be concealed by the complex organisational processes typical of biomolecular systems. These hidden effects might be revealed by the study of simpler compartmentalised systems in the form of lipid vesicles (see Section 1.3). Moreover, some enzymatic reactions that rely on the formation of multimeric enzyme assemblies are favoured by compartmentalization.[16] These are significant effects that are difficult to notice and identify when studying cells but become much clearer in simpler systems.[17] Therefore, it is necessary to be able to identify and predict these effects to:

(i)   enhance the ability to design cell-inspired materials (e.g. micro and nano-reactors for drug delivery and sensing,[18] or the bottom-up approach and assembly of minimal cells with designed functionality.[19]

(ii)   obtaining a better understanding of biogenesis,[19] a process which involves the chemical evolution of non-living matter to cell ancestors (protocells) and then to living cells. The formation of protocells is clearly nature's version of the assembly of a minimal cell, and understanding it could develop the ability to inspire and innovate cell-like de novo systems.[17]

The effect of compartmentalisation on enzyme kinetics are essential, and the impacts of compartmentalisation in nonenzymatic reactions might also be important, particularly for the assembly of extremely simple functional systems with truly bottom-up design, i.e., in the absence of any complicated biomolecules. The destiny of nonenzymatic reactions in compartmentalised systems is particularly important in the context of abiogenesis (i.e., the assembly of the initial protocells), especially when attention is concentrated on the initial steps of protocell evolution, where enzymes would not have existed.[17]

1.3   Biomimetic Membranes: Properties, Importance, and Synthesis

Many synthetic systems have been constructed to mimic the natural membranes of cells and their functions. A good method for functional membrane preparation is the embedding of artificial amphiphiles into a vesicle.[20] Vesicles are dynamic supramolecular structures which consist of bilayer membranes that encapsulate a small amount of water in their interior, and these bilayers can be composed of synthetic amphiphiles, phospholipids, and other components. They have been seen to be biological membranes models that can intensify the reactants then advance chemical reactions.[21, 22] Non-covalent assemblies have a dynamic nature that allows the simple and rapid enhancement of "bio-inspired responsive nanomaterials", which is applied in sensing, catalysis, and molecular recognition (see Section 1.7 molecular recognition). Nonetheless, the complexity that can be attained in synthetic functionalised membranes are still limited and there are challenges such as the analysis of membrane structures and the control of their dynamic properties.[20]

Stable bilayer membranes created from a range of synthetic amphiphiles have been the subject of extensive model studies to obtain insight into physicochemical properties, structure, and biological membrane function.[23] In particular, mixed vesicles of

functionalised amphiphilic molecules and long-chain dialkyl surfactants that have been used in imitating membrane-mediated processes.[24] Functionalised vesicles have also been applied as enzyme models in biomimetic chemistry for illustrating the specificity of natural enzymes and the origin of the catalytic effects.[25] Lipid bilayer systems have been extensively exploited in sensing, drug delivery, and catalysis.[26] Due to the biocompatibility of the vesicles, they can be exploited as drug carriers and are easily functionalized. The reproduction of the transformations occurring within biological systems is the main factor driving the evolution of new applications in the chemistry of vesicles.[20]

1.4 Lipids Properties, Classification, and Shapes

The widely accepted model for the membrane was proposed by Singer and Nicolson in 1972,[27] they suggested that a fluid in which the amphiphilic molecules within the membrane and proteins can move laterally form a fluid mosaic inside the membrane this opposed to what previously suggested models where the proteins were believed to stick to the membrane surface.

The composition of animal cell membranes varies according to the cell's function. However, regardless of function, cell membranes are highly hydrated, as up to 30% of the membrane is water. [28, 29] The dry weight lipid-to-protein ratio 4 to 0.5.[29] The membranes of cells that perform structural functions only have a greater concentration of lipids. As well as saturated phospholipids, there are several other constituents to bilayer membranes.

A main future of the membrane is its **fluidity** (relative mobility), it enables its constituents to move laterally. The first requirement to obtain a fluid membrane is that the ambient temperature must be higher than the fluid **phase transition temperature** (the temperature at which lipids change from the gel phase to the liquid crystalline phase). The structure of lipids changes in these different phases; in the gel phase, lipids are ordered, with the hydrocarbon chains being fully extended and compressed against each other. The liquid crystalline phase is characterised as a disordered state, with the hydrocarbon chains oriented randomly. Membrane fluidity is composed of amphiphilic lipids, though above the transition temperature, fluidity is influenced by other chemical factors, such as the concentration of cholesterol, the length of the alkyl chains and the extent of unsaturation of the alkyl chains. The number of methylene groups in the alkyl chains increases as they engage in van der

Waals interactions.[30] Consequently, as the length of alkyl chains increases s, the membrane fluidity decreases. On the other hand, membrane fluidity increases where the alkyl chains contain one or more unsaturated cis alkenes, causing the chain to kink; this in turn minimises the interactions between neighbouring chains, thereby promoting membrane fluidity.[30] The **cholesterol content** in the membrane ($\approx 40\%$ in animal cells)[22] as stated earlier, membrane fluidity is also affected by the amount of cholesterol in the membrane. The hydroxyl group of cholesterol forms hydrogen bonds with the polar head groups of neighbouring phosphatidylcholines; this causes the non-polar domain of amphiphilic lipids to become more closely packed, resulting in a global reduction in the membrane's stability.

Whilst **cholesterol** is a lipid, its physical characteristics and properties set it apart from phospholipids. The effects of cholesterol in the membrane upon the properties of the lipid bilayer are complex and significant. Cholesterol a single hydroxyl group, providing limited hydrophilicity. Proximal to the hydroxyl group are several fused rings, forming a rigid planar structure; the compound is completed by a short single chain tail, joined to the fused rings at the opposite end of the hydroxyl. The addition of cholesterol to a fluid phase bilayer has long been recognised to minimise the **membrane's permeability to water**.[31,32] Research has established that the mechanism for reducing permeability arises from cholesterol's ability to intercalate with the lipid chains, occupying free space and reducing the chains flexibility.[33] Not only does this reduce the lipid bilayer's lateral diffusion coefficient, but the effect of cholesterol is also to promote the membrane's mechanical **rigidity**. However, the effect of adding cholesterol to gel phase bilayers is quite different. In that situation, the diffusion coefficient is increased as the cholesterol disturbs the local packing order. [34] [35]

The properties of membranes are also modulated by the movement of single lipids within the bilayer. [22] Lipids can move in three ways. It can move laterally in the lipid bilayer; it can rotate on its axis or it can **flip-flop** from one layer to another. The first two of these movements are extremely rapid, with translation occurring every 10^{-7} s and rotation every 10^{-9} s. In contrast, flip-flopping occurs less than once a week in the cell (occurring on average every 10^{5} s).[36]

The flip-flop action of membrane components translocating between the inner and outer leaflets (Figure 1-3) does not present problems if there is homogeneity in the membrane's structure, as the translocation is bidirectional, so components are replaced in a like-for-like manner. Any effect of translocating is nullified. However, membranes are not naturally

homogeneous; rather they are a multi-component system. Introducing a foreign component into one of the membrane's leaflets causes a concentration gradient to arise between the two leaflets. As membranes have a fluid structure, in time, the membrane will adopt a dynamic equilibrium.

Studies using exchange experiments to explore the **flip-flop** phenomenon set the temperature at 50°C. The upper limit was estimated to be approximately 40 min.[37,38] Elsewhere, cationic species are proposed as being a mechanism that reduces the half time required for the flip-flop. Yet demonstrating this has practical implications. If the reaction's progress is examined using a time scale that is comparable to the time scale of an intramembrane flip-flop, the catalyst available to the solution will not have a consistent concentration. The first experiments that sought to confirm the presence of reactivity in a qualitative manner, did not address this aspect.
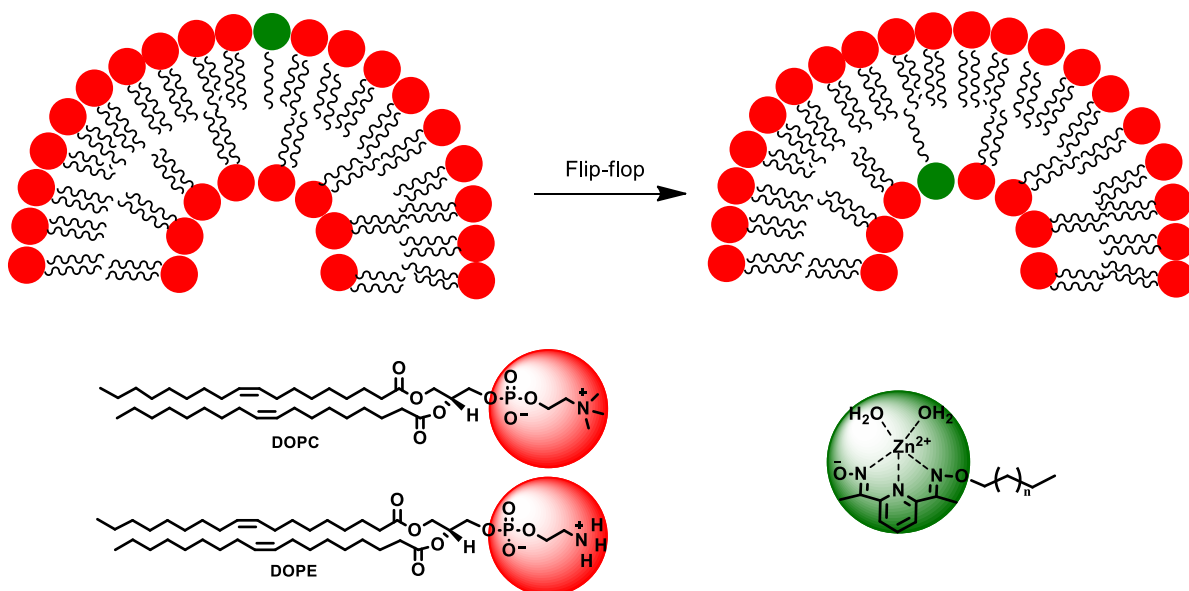
Figure 1-3. Flip-flop movement in the lipid matrix

As stated previously, natural bilayers are not composed of homogeneous lipid molecules; rather they are constructed from multiple lipid components. Typically, the properties of heterogeneous mixtures are intermediate to their components; yet these mixtures also exhibit effects that do not arise in systems composed of a single component. A single homogeneous mixture that forms two discrete phases is known as **phase separation**. This can occur if the components are in different phases at a particular temperature. If some of the components are in the liquid phase and the other are in the gel phase, these two phases can exist as two

distinct populations that are separate in space. Phase separation is key to numerous biochemical events; proteins and other membrane components can separate and accumulate in one or the other phase,[39] from where they can readily be activated.

Despite the name implying that the lipid bilayer is two dimensional, it is in fact a 3D structure, containing multiple and diverse physical features. These regulate protein function and cell signalling. The membrane is exposed to considerable lateral and transverse forces, which vary greatly as membrane components are added, chemically modified or removed, causing the membrane to stretch or distort to accommodate the change. Studies of the structure of the two layers of the membrane have identified differences between the leaflets and between different areas of the bilayer. These different structures and regions work in concert to deform the membrane as required, facilitating peripheral membrane-binding proteins and transmembrane channel activities.[40]

Lipids are essential to life. This ubiquitous and diverse group of compounds undertake significant functions, in beyond forming cell membranes. Lipids are also energy stores and contribute to signalling pathways.[41]

A lipid classification system has been devised by the LIPID MAPS Consortium. The comprehensive system defines lipids as hydrophobic or amphipathic small molecules according to the presence of ketoacyl groups and isoprene groups (Figure 1-4) which are fundamental "building blocks". The mechanisms that create lipids may arise entirely or partially by ketoacyl thioesters undergoing carbanion-based condensations and/or isoprene units undergoing carbocation based condensation. [41]
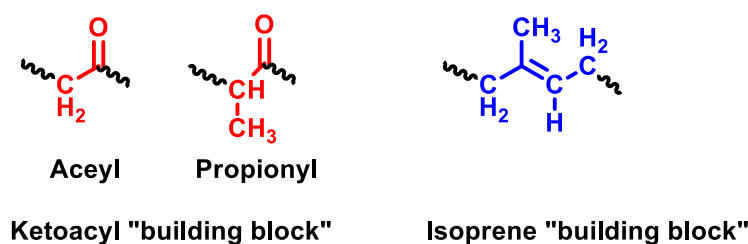
Figure 1-4. The two fundamental "building blocks" of the lipids: ketoacyl groups and isoprene groups

Based on this classification system, lipids have been divided into eight categories: (i) fatty acyls, (ii) glycerolipids, (ii) glycerophospholipids, (iv) sphingolipids, (v) sterol lipids, (vi)

prenol lipids (derived from condensation of isoprene subunits), (vii) saccharolipids and (viii) polyketides (derived from condensation of ketoacyl subunits); (Figure 1-5).[41, 42]
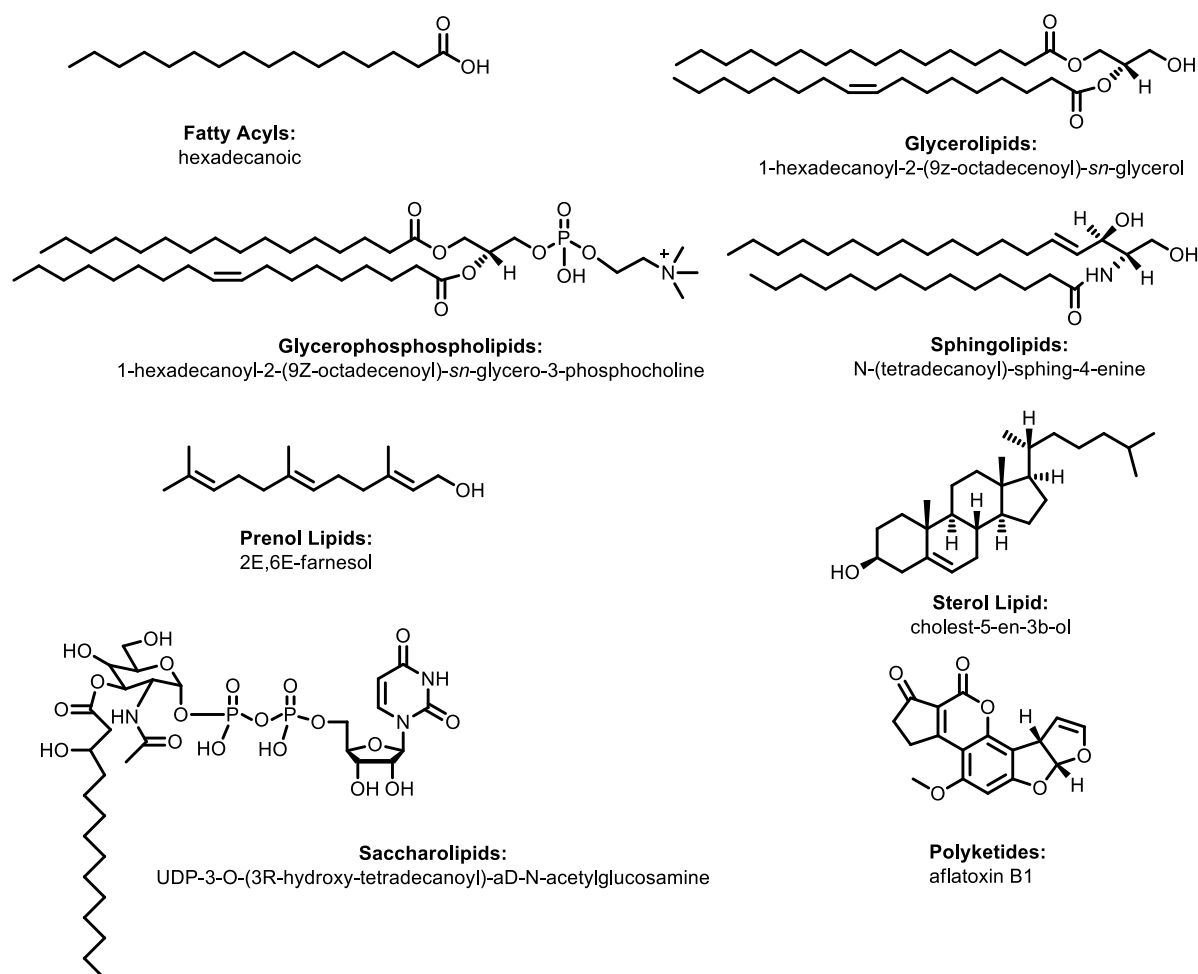
Figure 1-5. *The eight categories of the lipid*

1.5   Spontaneous Curvature and Bending Stiffness of the Lipid

For most membrane components, the hypothesised shape is not flat. Actually, every lipid shape that deviates from a cylinder provides a spontaneous curvature to the membrane.[40,43] Molecules which have an overall inverted conical shape, like detergent molecules, polyphosphoinositides and lysophospholipids, form structures with positive curvatures, such as micelles (Figure 1-6A). Cylindrical-shaped lipid molecules, such as sphingomyelin and phosphatidylcholine, preferentially form flat bilayer structures (Figure 1-6B). Lipid molecules that have an overall conical shape, such as phosphatidylethanolamine and diacylglycerol, with a small hydrophilic cross-section, form structures with negative curvature, such as the inverted hexagonal phase of tubes with headgroups inside and

9

hydrophobic tails outside (Figure 1-6C). The local shape of a membrane depends on which lipids are present and on how they are spatially distributed. Insertion or removal of lipids into the inner or outer leaflet leads to area mismatches that also alter curvature. Membranes resist bending because changing local curvature alters both the headgroup spacing and the entropy of the hydrophobic chains.[40] Different types of lipids take different shapes (Figure 1-6D).
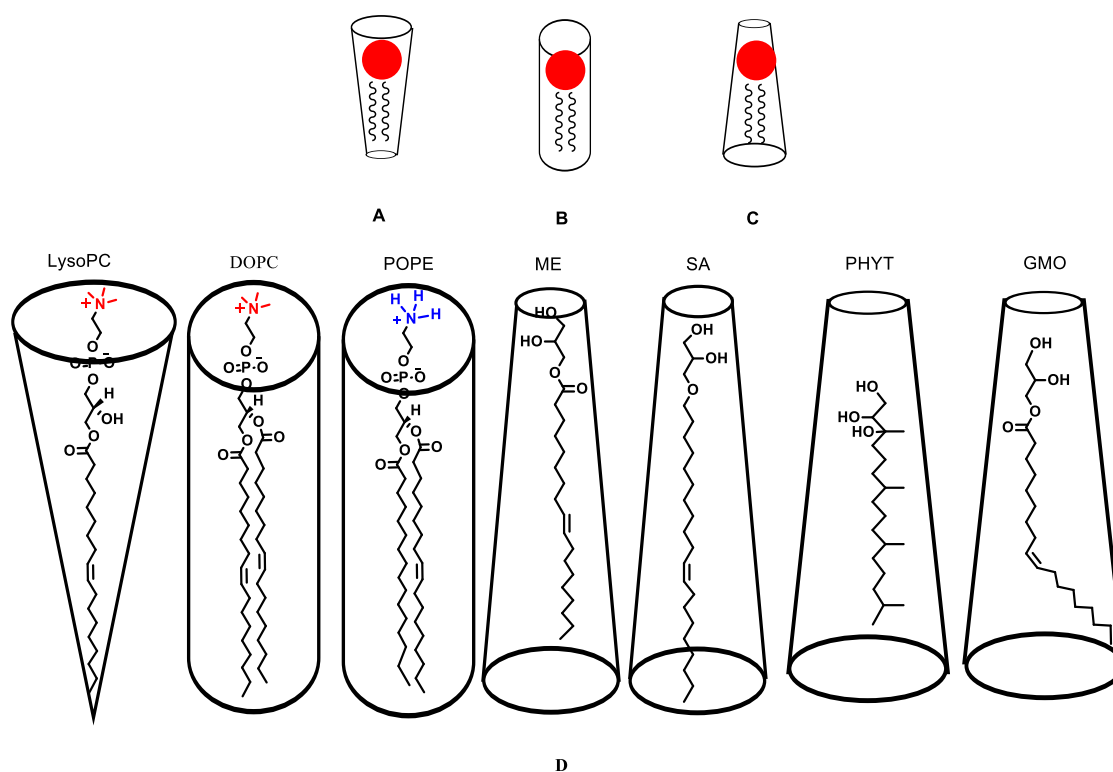
Figure 1-6. *The three possible shapes for the lipids and different lipids shapes with different wedge shapes.* [44]

1.6 Signal Transduction across Lipid Bilayers

Groundbreaking work by Lehn and co-workers demonstrated "electron conduction through a molecular wire spanning a lipid bilayer",[45] but only a limited number of studies have used a receptor that undergoes a conformational change to accomplish transmembrane signalling. Signal transformation through lipid bilayers has been achieved by the dimerisation of a signalling molecule embedded in vesicle membranes, without direct transport of the molecules.[46, 3] A crucial problem with such systems is the difficulty in stopping the reaction in the background completely, which causes the emission of a signal even in the absence of an incoming message. This is because of the high rate of spontaneous dimerisation of the

signal transducer by lateral diffusion. It is essential that the signal-transducing molecule spans the bilayer membrane with signalling units on the inside of the vesicle and sensor units oriented towards the outside.[3]

Artificial approaches to achieving communication through lipid membranes have depended on imitating the direct physical transport of the molecular signal through the membrane. The biological mechanism to transform the signal with proteins is to span the cellular membrane is represented by tyrosine kinase receptors and G-protein coupled receptors; for instance, an external ligand can make tyrosine kinase receptors dimerise; the dimer then autophosphorylates its intracellular domain, which starts a sequence of consecutive events inside the cell.[47] This provides a mechanism for coupling, but separating the chemistry on the interior and exterior of the cell, and in contrast to transport mechanisms, the signal and message can be chemically unconnected and potentially harmful messenger molecules are excluded.[3]

Dijkstra et al.[46] used the membrane-bound receptor (**I**), which contains a fluorescent dansyl ethylenediamine as a headgroup, and cholesterol as a core. When Cu^{2+} was used as a messenger, it coordinated to the ethylenediamine group. They investigated a novel transmembrane spanning receptor (**II**), (Figure 1-7), which mimics the tyrosine kinase receptor, to study the transmission of information through lipid bilayer *via* binding of a receptor to the messenger on the outside of a membrane cell causing a change in the intravesicular receptor.[46]
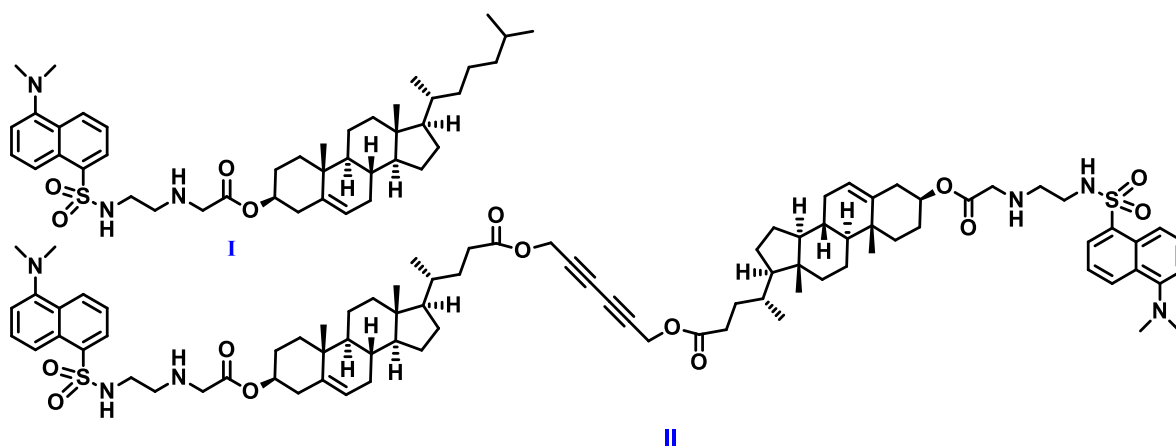
Figure 1-7*: Non-membrane spanning receptor molecule (**I**), and a membrane-spanning molecule (**II**) used to study how the information can be transmitted across lipid bilayers by binding of the messenger to the receptor on the outside of the cell leading to an intravesicular receptor change.*

1.7 Molecular Recognition

The recognition of ions (e.g. metal ions) and molecules at the surface of the cell membrane is important for cell communication.[48,49] Molecular recognition is one of the most significant chemical events occurring in biological systems. Thus, knowledge obtained from research on molecular recognition might provide significant information for the understanding of biological phenomena.[48] In living systems, molecular recognition generally occurs at interfaces such as enzyme reaction sites, membrane surfaces, at or in a DNA double helix, and in antigen-antibody recognition.[50] Investigation of bio-related interfacial molecular recognition has seen much recent progress, and the lipid interfaces provided by vesicle structures have been used extensively in these studies. Another advantage of molecular recognition at assembled media is the possibility of forming sophisticated binding sites upon spontaneous assembly of independent recognition units within confined spaces.[51] The particular interaction between a target molecule and chemical entity is the basis of molecular recognition phenomena. They are predominately complementary in their electronic features and geometric shape.[52] In 1894, Fischer was the first to describe the idea of molecular recognition suggested that the enzymes and substrates join together like ''lock-and-key''.[53] The mechanism of the recognition is mediated fundamentally by supramolecular interactions like ion-pairing, hydrogen bonding, dipolar associations and hydrophobic interactions.[54] Many examples of those mechanisms occur in nature, for example, in ribonucleic acid (RNA) ribosome, deoxyribonucleic acid (DNA) protein and antigen-antibody recognition.[50]

Molecular recognition process was utilised to selective transport of Eu^{3+} ions across the bilayer membrane in the form of functionalised vesicles incorporated with ligands supported with a β-diketone headgroup.[49]

Voskuhl and Ravoo [12] described three approaches to the molecular recognition of vesicles:

- (i) coordination of metals to ligands at a vesicle surface [e.g. Zn^{2+} dipicolylamine (DPA) receptor complex (**II**) to a fluorescent ligand (**I**) at the surface of phosphatidylcholine liposomes], Figure **1-8**a;
- (ii) host-guest interaction of vesicles [e.g. modified cyclodextrins (**III**) form host vesicles to the guest molecule as rhodamine–lissamine (**IV**)], Figure **1-8**b;
- (iii) hydrogen bonding to vesicles, Figure **1-8**c.[12]
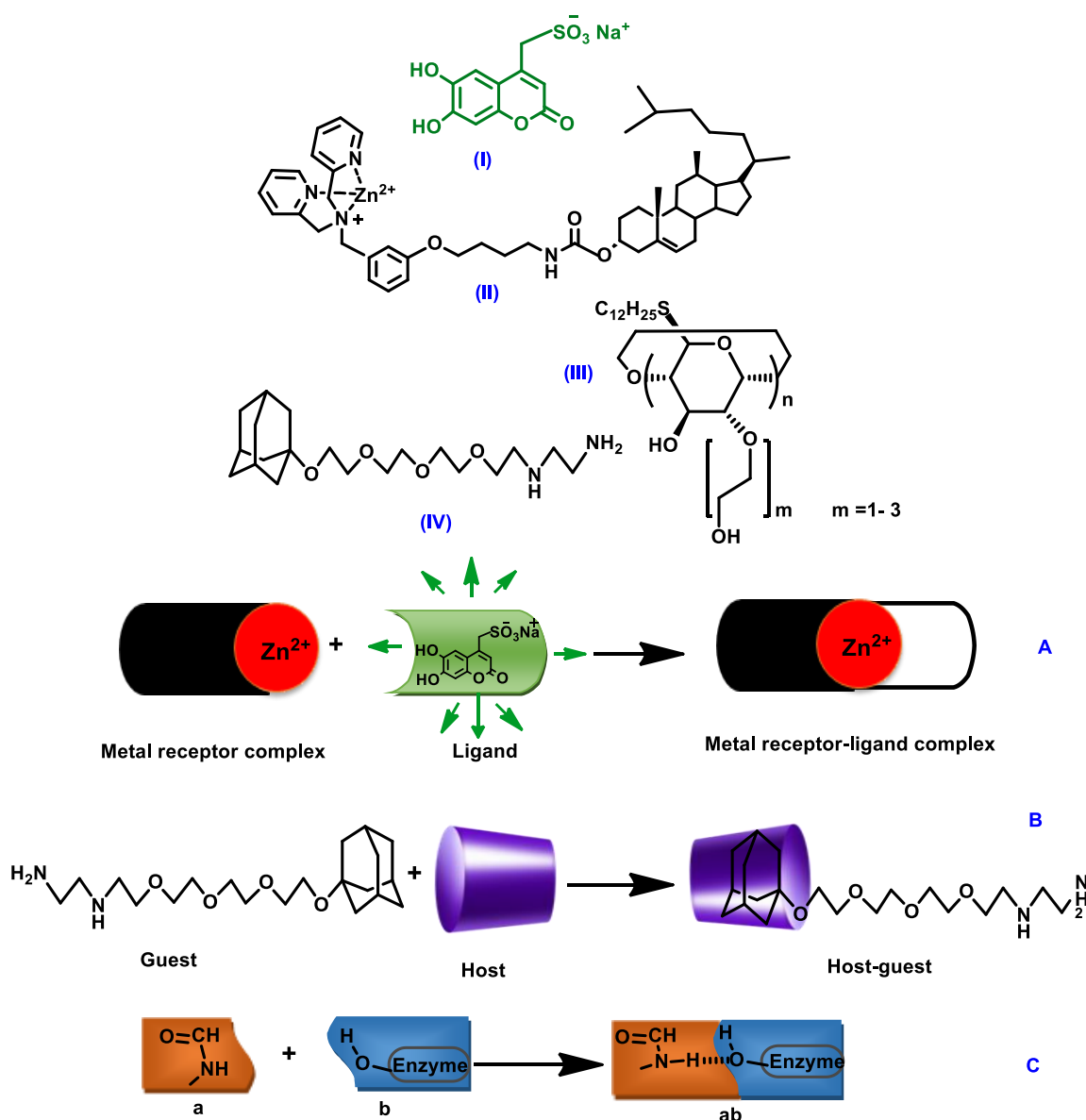
Figure 1-8: *Three approaches to molecular recognition of vesicles (adapted from reference 12).*

Molecular recognition process in biology must occur at physiological conditions of temperature and pH range. Thus, receptors will be able to detect analytes in aqueous or aqueous buffer solutions.

Mainly, there are two types of water-soluble receptors mentioned in the literature:

(i)   neutral non-metallic or positively charged receptors and

(ii) metal complex based receptors.[55,56]

13

The interactions in the first type occur through reversible and weak noncovalent binding forces, such as hydrogen bonding and stacking interactions or electrostatic effects. In the second type, the interactions occur mostly with the analyte *via* charge-charge interactions. The analyte coordinates to the metal centre, imitating many metalloenzymes.[57] A number of metal ions have been utilised as receptors for the recognition of biological phosphates (e.g., PPi, NTP), including those of the main group, transition metals, and lanthanides.[58] König *et al.* functionalised vesicles incorporated with Tb^{3+} complexes and Zn^{2+}-cyclen complexes as receptor-sensitisers to study the molecular recognition of nucleotide triphosphates, uridine-5'-triphosphate (UTP), adenosine triphosphate (ATP), guanosine-5'-triphosphate (GTP) and adenosine diphosphate (ADP) by investigating binding affinities. These are very important targets like phosphates and their derivatives, as they are most abundant in nature, and almost all coenzymes are esters of phosphoric or pyrophosphoric acid. The main reservoirs of biochemical energy are phosphates, and many intermediary metabolites are phosphate esters. Phosphates are prolific in nature, and structures ranging from the cell membranes (phospholipids). However, Zn^{2+} is among the most commonly employed metal centre.[59] Fluorescent and chromogenic Zn^{2+}-based metal receptors binding to biological phosphates are discussed in detail by Jose.[50]

Additionally, unsaturated coordinative metal complexes used as receptors supply binding sites with high affinity for a Lewis base. Numerous important bioanalytes like nucleobases, anions, thiols, amides, esters, and urea are Lewis bases.

Vesicles have been functionalized for bioanalytes recognition; they are commonly seen as closely imitating the membrane of the cell.[22] These characteristics have encouraged the use of vesicles in molecular recognition.[12] The recognition of molecules by membrane-bound receptors (Figure 1-9) is essential in a large number of biological processes.[60] The domains and the clustering of the receptors dynamic formation in fluid membranes perform an important role for instance, in signal transformation followed by specific strong binding of competing for multivalent ligands.[61] Different model systems for biological membranes have been improved to mimic and understand multivalent interactions at interfaces[62] and used for applications in delivery, catalysis and sensing.[63, 20]
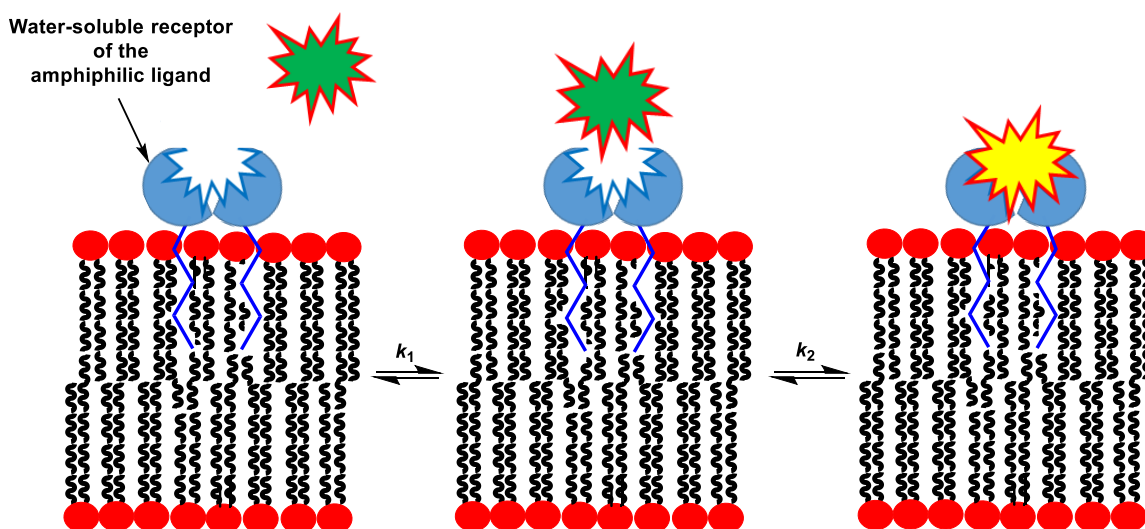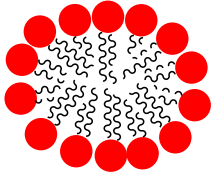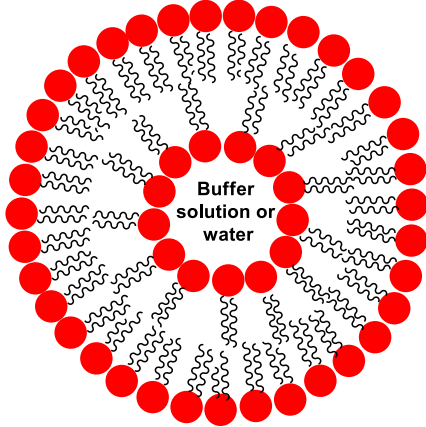
Figure 1-9. *Molecular recognition on the bilayer membrane surfaces*

König. *et al.*[64] have reported how specific peptides recognition can be achieved by energetic interface imprinting of synthetic binding sites of Zn^{2+}–cyclen receptor incorporated in vesicle membranes. The binding sites of amphiphilic metal-complexes are enlisted in the membrane by the target peptide, the result being multivalent interactions and nanomolar binding affinity.[64]

Molecular probes are usually composed of a guest-binding site and a luminescent reporter group that gives useful monitoring of ligand-binding events. The luminescent part can either be a moiety of the actual molecular chemosensor, normally close to the analyte binding site[65] or a separate dye that is first non-covalently linked to the binding site and subsequently replaced by the analyte.[66] Gruber and co-workers prepared luminescent vesicular receptors from bis-zinc cyclen complexes to selectively recognise phosphate anions. They found that the complex with luminescent labels in the homogeneous solution failed to respond to the presence of phosphate anions, but respond when it was incorporated in vesicle membranes as amphiphiles.[67] The luminescent vesicles containing cyclen–Zn^{2+} complexes embedded with a coumarin derivative, showed a strong decrease in fluorescence emission with increasing phosphate anions concentrations, such as pyrophosphate (PPi) or phosphoserine (pSer). The embedded Zn^{2+}–cyclen complexes maintained their anion selectivity, and no emission response appeared when additional amounts of other phosphate anions added.[68]

1.8 Micelles versus Vesicles

	Micelles	Vesicles
Shape		
Definition	Micelle is a structure constituted of a monolayer of amphipathic molecules. In a biological system, the molecules tend to organise themselves in a manner that the inner core of this structure is lipophilic and the outer layer is hydrophilic by self-assembly.[69]	Liposome (vesicle) is composed of a bilayer of amphipathic molecules, the molecules are arranged in two concentric circles. The hydrophilic heads of the outer layer are exposed to the outer environment, and the hydrophilic heads of the inner layer make the inner hydrophilic core. The lipophilic tails are tucked between the two layers.[70]
Formation	Micelles are formed by the aggregation of surfactant, amphipathic molecules in a polar solvent beyond a concentration, known as Critical Micelle Concentration (CMC).[69]	They are formed by the hydration of dry lipid molecules (amphipathic molecules) in an apolar solvent followed by mechanical agitation.[70]
	The formation of both molecules increases considerably beyond a particular temperature.	

	This temperature is known as (Krafft) temperature.	This temperature is known as transition temperature (T_c or T_m).
Nature of Constituent Molecules	Although both are composed of amphipathic molecules, the nature of these molecules is somewhat different.	
	They are preferably formed by surfactant molecules such as detergents, wetting agents, emulsifiers, as well as certain co-polymers.	They are composed of phospholipid molecules, such lecithin, along with cholesterol.
Types	Micelles are formed when the surfactant molecules are dispersed in a polar medium e.g water. In a non-polar medium, they form a different type of micelle known as a reverse micelle.	Depending in the extent of mechanical agitation, or in some cases treatment with a polar solvent, liposomes can be classified as Small Unilamellar Vesicles or SUV (the liposome forms a vesicle of a single bilayer and is of a smaller size), Large Unilamellar Vesicles or LUV (the liposome forms a vesicle of a single bilayer and is of a larger size), Large Multilamellar Vesicles or MLV(the liposome is made of concentric layers of the bilayer), and Multivesicular Vesicles (MVV) (the liposome contains many vesicles of the bilayer that are not arranged in a concentric manner).
Size	They are smaller than vesicles. Their size from 2 - 20 nm.[71]	Depending on the type of the liposome, the sizes: Small Unilamellar Vesicles (SUV): 20 nm - 100 nm[71] Large Unilamellar Vesicles (LUV): 100 nm - 400 nm Large Multilamellar Vesicles (MLV): 200 nm - 3 µm Multivesicular Vesicles (MVV): 200 nm - 3 µm

Nature of Molecules Transported	As these tend to have a hydrophobic core, they are used in the transport of insoluble hydrophobic molecules.	These can carry hydrophobic molecules in their hydrophobic tails (the region between the two layers), and hydrophilic molecules in their hydrophilic core.
In Drug Delivery	Micelles may transiently influence the permeability of the intestinal lining, they are used to administer drugs that are not very soluble, consequently, their absorption will be difficult. (these are administered orally).	Liposomes are usually taken up by organs rich in the reticuloendothelial system; hence, they are used to deliver drugs targeted to these organs.[70] ● Sometimes, they are coated with special polymers so that they can target specific tumour cells only. ● Due to the high cost of making the relative liposomes, these are used only for the treatment of viral infection and killing of tumour cells. ● These drugs are usually administered *via* the parenteral route (routes other than the oral route).
Uses	Micelles have been studied and used extensively because they are capable of encapsulating compounds in solution and because of their ability to mimic biological systems. Properties such as micelle size, shape and permeability have been found to depend sensitively on the amphiphile structure and concentration. A particularly useful tool for	Unilamellar vesicle structures have been used in immunological studies, drug delivery and understanding cellular membrane structure and function. phospholipids are the most commonly used compounds for the formation of unilamellar vesicles, a group of compounds that are the main components of plasma membranes. Vesicle structures can also be formed by simpler amphiphilic compounds, like octanoate, decanoate, and oleate.[71]

	this work has been the investigation of probe molecules by fluorescence spectroscopy (the dynamics of the probe molecule related to the system pressure, the solubility of the probe and the solvent viscosity).[71]	

1.9   Micelles, Metallomicelles, and Metallovesicles

The micelle is an aggregation of surfactants which occurs if the amphiphilic surfactant concentration reaches a particular level that called critical micelle concentration (CMC).[72] The surfactants have the opposing character of the headgroup (hydrophilic) and tail (hydrophobic) moieties lead to a propensity to adsorb at surfaces "surface activity" and the spontaneous formation of rather complex but well-defined structures -"self-assembly".[73] The Stern layer and a hydrocarbon centre with 50–100 molecules and a diameter of 10–28 Å. Generally, in micellar structures, chemical reactions can occur in the Stern layer with selectivities or increase reaction rates.[74]

This enhancement can be considered as a result of

(i)   increase the local concentration of the reactants at the surface or in the interior of the micelle;

(ii)   stabilisation of the reaction transition state due to a favourable interaction with the surfactant molecules;

(iii)   a combined polarity, charge effect, and microviscosity inside the micelle. Namely, by the enriching the substrate in the micelles' Stern layer, where the substrate intermediate or product could be directed and stabilised.

Numerous hydrolytic metalloenzymes have been evolved in nature. They have developed to hydrolyse some of the essential molecules of life such as proteins, DNA, and phospholipids.

Over time, many hydrolytic models of metalloenzyme have been created and studied. Researchers have learned a great deal through careful designs and accurate analyses of uncomplicated enzyme models. Nevertheless, a big difference between these models and natural enzymes is their reactivity. Generally, in enzyme model studies either substrates are very active or they are attached to the catalytic groups which prevent any turnover.[75]

Micelles have frequently been used to mimicking the microenvironments of enzyme active centres over the last decades. In addition to simple micellar systems, researches have included co-micelles, functional micelles, and polymer micelles.[76]
Metalloenzymes perform an essential role in the catalytic hydrolysis of carboxylic acid esters. Many hydrolytically active metalloenzymes exist in nature. In order to create simple artificial hydrolytic metalloenzyme models, metallomicelles (composed of cosurfactants or functionalized surfactants that can effectively chelate metal ions or by mixing non-functional surfactants with metal-lipid complexes), which mimic enzyme in structural and kinetic properties, have been extensively studied.[77,78,79, 80,74,81]

The first report about catalytic hydrolysis reactions using metallomicelles was published in 1978 by Melhado and Gutsche. These researchers investigated metal ion effects in micellar systems for acetyl phosphate (**II**) hydrolysis reactions, they used chelate-forming micelles (**I**) (Figure 1-10), metal-chelated polyamines, amine-ammonium micelles, and polyamides having nucleophilic moieties. The hydrolysis rate could be controlled by optimisation of the pH value.[82]
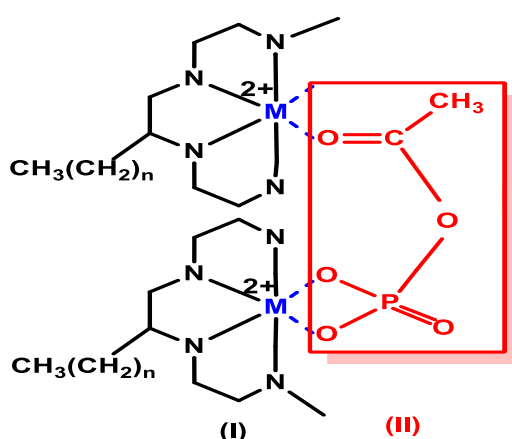
Figure 1-10. The chelates of amines with metal ions, Mn^{2+}, Co^{2+}, Zn^{2+}, Ni^{2+}, and Cu^{2+} to demonstrate the hydrolysis of acetyl phosphate.

In modern metalloenzyme-mimic studies, more attention has been paid to the simulation of the enzyme active centres in structures and functions, whilst the inputs from the microenvironment were normally not taken into account. Furthermore, micelles alone frequently had limited specificity for substrates, low efficiency and so are relatively poor enzyme models. For these reasons, metallomicelles have evolved through the combination of micelles and metalloenzyme models. This kind of aggregate simultaneously has the functions and properties of both metalloenzyme models and micelles. Consequently, these novel supramolecular vehicles not only simulate the enzyme active centre but also mimic hydrophobic microenvironments.[74]

Metallomicelles also mimic the behaviour of phospholipase C enzymes in their catalytic and inhibitory effect on the transesterification of phosphate diesters *via* three important facets:

 (a) active site molecular recognition; (b) recognition at an anion-recognition site, and; (c) interfacial (or hydrophobic) recognition.[83]

Currently, Gemini (a new generation of surfactants are formed by two hydrophilic groups and two hydrophobic groups in one molecule) have attracted great interest.[84] These surfactants have been shown to possess some improved properties, like lower critical micelle concentration (CMC), lower Krafft temperature (minimum temperature to form micelles), greater efficiency in lowering the surface tension, and better solubilisation compared to classic surfactants.[85]

Vesicles are similar to micelles whence they can concentrate the reactants on the interface between water layer and the vesicles' bilayer then accelerate the chemical reactions. Therefore, reactions might be catalysed efficiently as vesicles can adsorb more reactants in comparison with micelles. They have a faster aggregation velocity and a slightly larger specific surface area than micelles.[86, 21]

This has led to novel models for enzymatic catalysis, in other words, metallic vesicles, (metallovesicular systems are aggregates containing lipophilic metallic complexes). Jiang. *et al.*[21] created two types of lipophilic pyridine-containing alkanol ligands and examined the ability of the catalytic hydrolysis of Zn^{2+} complexes of these ligands on *p*-nitrophenyl picolinate (PNPP, Scheme 1-1) in vesicular solutions of cetyltrimethyl ammonium bromide (CTAB) and sodium dodecyl benzene sulfonate (SDBS). The study involved the effects of the alkyl chain length, vesicle concentration, temperature effect, pH effect, and the presence

of Zn^{2+} complexes on the catalytic hydrolytic efficiency. The study demonstrated that the vesicular system itself exhibited no rate enhancing the effect in the absence of metal ions. In comparison, the rate increased around 10-times in the presence of Zn^{2+}-complexes (**a** and **b**, Figure 1-11) and 11-times in the micellar solution. However, it increased 100 fold in the vesicular solution for complexes **a** and **b.**
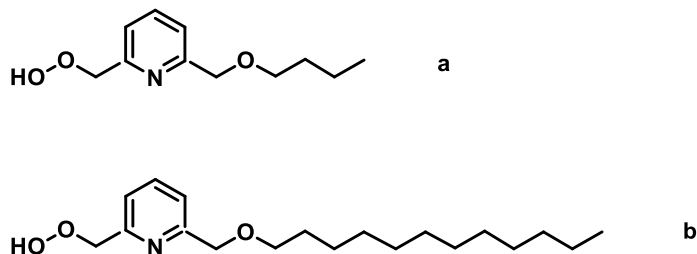
Figure 1-11: Zn^{2+} -complexes with lipophilic pyridine ligands

This exhibits that vesicles can reach a higher catalytic efficiency than micelles. The $k_{obs.}$ of ligand (**b**) is larger than that of ligand (**a**). This denoted that the catalytic efficiency of ligand (**b**) is more effective than that of ligand (**a**), that may be ascribed to the differences in the structure of the two ligands. The longer the alkyl chain of the ligand is the higher the solubility of the complexes in vesicular solution and the higher the catalytic efficiency. At a constant pH, the rate constants are also found to increase with increasing concentrations of complexes. This phenomenon may be attributed to the increase in the collision frequency of the reactants The microenvironment changes may have an impact on the catalytic efficiency.[21]

Scheme 1-1 illustrates the suggested hydrolysis mechanism which involves: [21, 74, 81, 87]

(i)   the formation of a ternary complex (ligand/metallic ion/substrate)

(ii)   the pseudo-intramolecular nucleophilic attack of the activated ligand hydroxyl on the carboxyl group of the ester, resulting in its acylation and the formation of transacylation intermediate

(ii)   the metallic ion-mediated hydrolysis of the acylated intermediate and metal ion promoted and hydrolysis of the intermediate and regeneration of the catalytic species.

22

The product is then formed the catalytic cycle ends.
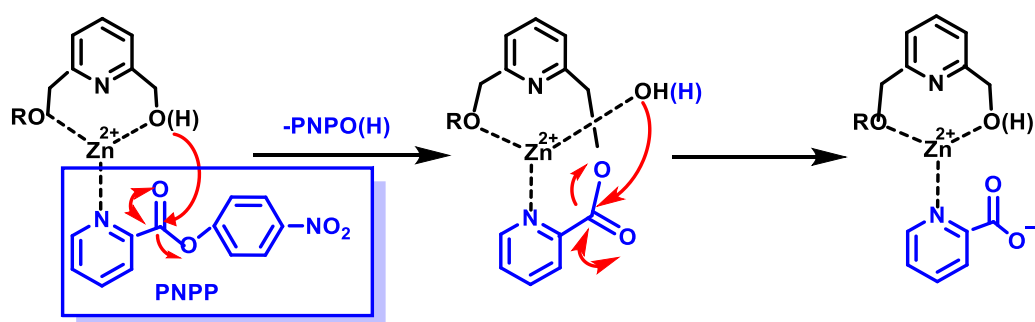
Scheme 1-1: *The hydrolysis mechanism of PNPP in the presence of Zn^{2+} complex*

Jiang *et al.*[21] demonstrated that the metallovesicular system simulates the enzymatic catalysis active centre and effectively mimics the hydrophobic microenvironment. A two-site recognition model can be used to explain the stereoselective and catalytic effects of metallovesicles. In this model, a highly directed ternary complex forms, which results from coordination of the substrate's carbonyl group and the headgroup of the ligand to the metal ion and alignment of the hydrocarbon chains of the substrate and catalyst in the lipophilic micelle's core. The enantioselectivity caused by the metallosurfactants relied on the micellar cosurfactant. Metallovesicles are formed of an amphiphilic ligand, with metal ion coordinated to the lipophobic headgroup which dissolves into the aqueous phase.[88] Model systems for hydrolytic metalloenzymes, Cu^{2+}-containing metallovesicles have been examined as catalysts in the hydrolysis of *p*-nitrophenyl picolinate (PNPP).[89] Engbersen described the catalytic activity and enantioselectivity of amphiphilic ligands toward *p*-nitrophenyl esters of PNPP with N-protected leucine[D(L)-Z-Leu- PNP and D(L)-C,-L~U-PNP] in a vesicular matrix of N-dodecyl-N,N-dimethyl-1-octadecanaminium bromide (**a**) in the presence of divalent metal ions such as Zn^{2+}. Scheme 1-2 represents the complex of Zn^{2+}-1,10-phenanthroline with two long alkyl chains (**b**).[25]

23
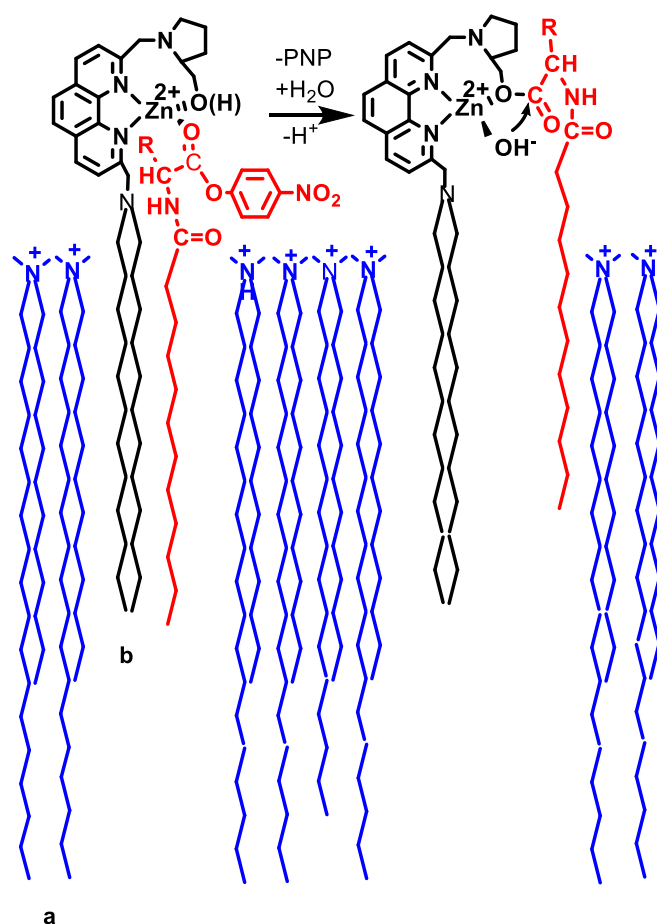
Scheme 1-2. *Metallovesicles composed of lipophilic a ligand containing 1,10-phenanthroline moiety with long alkyl chain and with Zn²⁺ ions embedded in the membrane matrix to study the hydrolysis of long-chain amino acid esters.*

The apolar hydrocarbon parts of the amphiphilic catalyst and substrate are embedded in the lipophilic core of the dialkylammonium bilayer while the polar parts protrude into the aqueous pseudo-phase. Upon complexation with metal ions, the tendency of the headgroup of the catalyst to remain in the aqueous pseudo-phase is enhanced due to the increased hydrophilicity and the electrostatic repulsion between the membrane surface and the chelated headgroup. The ternary complex of substrate and metallocatalyst is formed by coordination of the carbonyl group of the substrate with the metal ion and the association of the hydrophobic parts of substrate and ligand into the apolar core of the membrane. The substrate is hydrolysed by an acylation-deacylation mechanism with metallosurfactants located at both the exo- and endovesicular side of the bilayer membrane.[25]

Catalytic hydrolysis studies of phosphate esters are essential as numerous of the deadly compounds (exposure even to a small quantity is fatal) which are utilised as chemical weapons are organophosphorous compounds (known as nerve agents), such as Soman, Tabun and Sarin.[81] Organophosphorous compounds are repeatedly studied and used as rodenticides, insecticides, pesticides, and other bioactive agents because of their biological importance and environmental degradation and implications.[90] Metallomicellar catalysts have been used widely (due to their obvious similarity with some natural enzymes) for effecting the hydrolysis of a phosphate ester.[91] In 1986 Gellman *et al.* reported the first experiment of metallomicellar catalysis for demonstration the phosphate triester PNPDPP (*p*-nitrophenyl diphenyl phosphate) hydrolysis.[81]

The catalytic hydrolysis of bis(*p*-nitrophenyl) phosphate (BNPP) using complexed metal ligands solubilized within metallomicelles or metallosurfactants incorporated with micelles has been investigated by many researchers,[91] frequently within the structure of the ternary complex kinetic paradigm.

1.10 Metallomicelle-Catalyzed Hydrolysis and How Metallomicelles Help in Hydrolysis Reactions

In metallomicelle systems, there is a common feature, that many ligands containing one or more of hydroxyl groups, and when they form complexes with transition metal ions, the hydroxyl group of the ligand acts as a nucleophilic group.[79, 92, 93] Within the active site, metal ions activate the substrate, stabilize the negative charge, and produce nucleophilic group OH^- under near-neutral conditions.[94] Consequently, there are many studies that reported metallomicelle systems simulating hydrolytic metalloenzymes using metal ions such as transition metal ions for example Cu^{2+}, Co^{3+}, Zn^{2+} and, Ni^{2+} or lanthanides as La^{3+} [95], Ce^{3+} [96, 97] and Pr^{3+} [98] (which they used to hydrolyse bis(*p*-nitrophenyl)phosphate ester) as the active centre. Menger et al. investigated the hydrolysis of bis(*p*-nitrophenyl)phosphate ester) using metallomicelles of Zn^{2+}, Co^{3+}, Cu^{2+}, and La^{3+} and they revealed that La^{3+}-metallomicelle presented the higher catalytic efficacy.[91]

The catalysed hydrolysis of carboxyl acid esters using micelle has been widely studied.[99] As long as the mimetic model of the catalytic function is concerned, the study of Cu^{2+}, Zn^{2+}, Ni^{2+}, and Co^{2+} complexes as hydrolytic metalloenzyme models have been widely reported.[92] They exhibit good catalytic properties to hydrolyse *p*-nitrophenyl picolinate (PNPP). The transition metal ions act an essential role in these hydrolytic processes.[79] Many research groups evolved some binuclear metal complexes that display remarkably higher catalytic activity as a hydrolytic-enzyme like model. In metallomicellar catalysis, ligands contain one hydroxyl groups or more are very effective in the catalytic hydrolysis of carboxylate or phosphate esters. The transition metal ion can activate the hydroxyl group of the ligand and makes it a more effective nucleophile than the chelating water molecule. Using of macrocyclic metal complexes as biomimetic models of hydrolytic metalloenzymes has drawn much attention due to their similarities to the macrocyclic metal complexes that discovered in biological systems, like metalloporphyrin complexes. Some macrocyclic metal complexes demonstrated significant catalytic activity in the hydrolysis of some esters.[74]

Metallomicelles assist in the hydrolysis reactions because the metal ion in the active site coordinates a water molecule and increases the acidity of the bound water by further polarising the H–O bond and leads to enhance the effective nucleophilicity. Therefore, metal

ions perform binary purposes, act as a Lewis acid to bind and activate the carbonyl or phosphoryl bond of the ester/amide or the phosphate substrate, respectively. This makes the "C" carbonyl or "P" phosphoryl more susceptible (liable) to nucleophilic attack. Therefore, they synchronously provide the metal-bound water or HO^- nucleophile to attack the substrate's phosphoryl or carbonyl group during the hydrolysis reaction.

The first and fastest step in many hydrolytic reactions is hastened by metallomicelles and includes the attack onto the substrate by the "catalytic species" that is then chemically affected to give an intermediate species that, in the next step(s), is ultimately hydrolysed to regenerate the catalyst with a rate expressed as the turnover rate or the like. [81]

The understanding of the structure-function relationship of enzymes has motivated extensive research on the design and synthesis of unique metal complexes that miniaturise and imitate enzyme active sites.[100, 101, 102] Number of these studies concentrate on the role of metal complexes toward catalysing hydrolysis reactions of activated esters of carboxylic acid and phosphate esters or amides.[103] The metal ion performs an essential role in the metalloenzyme-based hydrolases. likewise, in a model system that catalyses a hydrolysis reaction, a metal ion like Zn^{2+} or Cu^{2+} should be able to stabilise the tetrahedral transition state (T.T.S.) by which the hydrolysis of an ester or an amide occur. Therefore, the metal ion has to stabilise the T.T.S. *via* coordination with the charged oxyanionic tetrahedral intermediate that of an electrophilic carbonyl carbon is able to interact effectively with a metal ion if there is an O/N on the next atom. This charge stabilisation of the developing negative charge in the T.T.S. and the full negative charge in the intermediate is frequently called electrostatic catalysis. Nearly one-third of all enzymes require metal ions and so such strategy is actually used by many enzymes ever since.[81]

Although the functions of transition metal ions constrained within biological membranes have been an area of intense study for a long time,[104] the research into the interface-bound metals in purely synthetic systems is a recent area of interest in colloid science. In the metallosurfactant amphiphiles, the incorporation of transition metal (d- or f-block) ion into the headgroup gives the molecule chemical functionality, (for example, redox activity and Lewis acidity), besides physical properties such as colour, fluorescence or paramagnetism. This functionality may be restricted at interfaces because of the intrinsic surface activity or self-assembly characteristics of the amphiphilic structure of the metallosurfactant. The definitions of "metallosurfactant" and "metallomicelle" are included "metallated micelles"

in which metal complexes are inserted into standard surfactant micelles by the solubilisation rather than *via* the covalent linking into the surfactant molecular structure itself.[73]

Zeng *et al.*[105] reported the roles of Zn^{2+} ions in the cleavage reaction of 2-hydroxypropyl *p*-nitrophenyl phosphate (HPNP):

(i) Zn^{2+} ions provide as a model so that HPNP is able to coordinate, which make the formation of catalyst–substrate complex easy. Furthermore, Zn^{2+} ions as a Lewis acid activate the HPNP by coordinating P–O− anion and raising the charges density of positive phosphorus atom that acts as a receptor of the nucleophilic C2–oxygen anion of HPNP;

(ii)   another role for Zn^{2+} ions is to reduce the pK_a values of the coordinated water molecule, and supply a higher concentration of the effective intramolecular general base at neutral pH and make the deprotonated process of the C2-hydroxyl of HPNP faster. Consequently, the HPNP hydrolytic cleavage is easily accelerated through a pseudo-intramolecular nucleophilic attack of C2–oxygen anion on phosphorus atoms of the phosphate group of HPNP;

 (iii) the third probable function of Zn^{2+} ions in the hydrolysis of phosphate esters is relevant to the stabilisation of the reaction transition state.[106, 107] In this case, the bivalent zinc ion can stabilise the negative transition state and then reduce the reaction activation energy; consequently, HPNP cleavage is accelerated.

HPNP is extensively used as an RNA model substrate, in nonmicellar systems. In addition, the metallomicelle-catalyzed cleavage of other phosphate diesters, like *p*-nitrophenyl phosphate and bis(*p*-nitrophenyl)- phosphate (BNPP), was examined extensively.[108, 109, 110]

Griffiths *et al.*[73] reviewed applications of metal ions in different metallomicelles systems to catalytic hydrolysis of many species such as amides, esters, phosphate ester, *p*-nitrophenyl diphenyl phosphate, complex thionate ester, *p*-nitrophenyl hexanoate, phosphate monoesters, diesters and triesters, cleave different phosphates (paraoxon), phosphonates, phosphonothioates, and thiophosphates parathion.[73] In addition, Bhattacharya and Kumari[81] reviewed functionalized ligands (e.g. pyridine-based amphiphilic ligands, imidazole-based amphiphilic ligand, triazole-based ligand amphiphiles, phenanthroline-based amphiphilic ligands, and other ligand amphiphiles), as well their metal complexes, and their role in the hydrolysis of different carboxylate and phosphate esters as substrates in organised media. [81]

1.11 Reactivity Enhancement in Micellised Metallosurfactants (Metallomicelles)

Enhancing the catalytic efficiency and obtaining the activity of natural enzymes stays a major challenge faces the researchers. If the catalytic efficiency in such systems is increased, metallomicelles not only imitate the enzymatic active centres of natural enzymes but also simulate their hydrophobic microenvironments.[81] Considerable efforts have been made to acquire synthetic agents in order to reproduce the reactivity of phosphate ester cleaving enzymes.[111] These systems could be suitable for many significant biomedical applications. Some efficient enzymes producing accelerations up to 16 orders of magnitude high than background reaction, predominately contain metal ion in their active sites.[112] Promoting the hydrolytic cleavage of phosphate esters activated by different simple monometallic complexes and metal ions, mainly by Lewis acid catalysis, is well-known, but only modest accelerations have been obtained.[113]

However, if the reaction is achieved in low polarity solvents "impressive" accelerations may occur.[114] Even poorly pre-organized bimetallic complexes produce under these conditions; accelerations rates close to those produced by enzymes. Therefore, it proposed that important elements of nuclease catalysis might be the precise pre-organization of the functional groups participating in the reaction, and the ability to place the negatively charged transition state in an environment with low polarity. The assembly of Zn^{2+} complexes on the surface of monolayer-passivated nanoparticles leads to remarkable cleavage efficiency of phosphate esters because of the cooperation between several identical active species "nanozymes".[115] In this communication, it was reported how by taking full advantage of the modular structure of a nanozyme, which allows the easy modification of the organic coating monolayer. A nanosystem capable of accelerating in water the cleavage of the RNA model substrate (2-hydroxypropyl- *p*-nitrophenyl phosphate, HPNP) more efficiently than any other artificial hydrolytic agent yet reported in this solvent can be obtained.[116]

Most catalytic researches concentrate on the embedding of non-surface active metal complexes onto standard surfactant micelles, but some researches have studied the activity of metal complexes who themselves are capable of forming micelles.[73] A good example is introduced by the work of Menger *et al.*[110] who showed that Cu^{2+} complexes of long-chain derivatives of tetramethylethylenediamine [such as structure (**I**), Figure 1-12] exhibited

considerably enhanced rates of phosphate ester hydrolysis. This work has prompted many subsequent types of research that have concentrated upon phosphate ester hydrolysis in general and more particularly the decontamination of chemical warfare agents (CWAs) like O-isopropyl methylphosphonofluoridate (Sarin).[117]

The metallomicellar hydrolysis is effective not because of the colloidal localisation of a catalytically active metal complex but because of the concentration of substrates in the micellar pseudo phase.[73] In the presence of micellar solutions of CuCl$_2$ and 1-tetra-decyldiethylenetriamine (**II**), the hydrolysis of 2-acetoxy-5-nitrobenzoic acid was found to be comparable to 4-acetoxy-3-nitrobenzoic acid, but faster than both *p*-nitrophenyl acetate (PNPA) and 2-nitrophenyl acetate. The high hydrolysis rate was ascribed to the electrostatic interaction between the cationic metallomicelle surface and the carboxylate anion resulting in the formation of a ternary micelle model (surfactant ligand /metal /substrate complex).[73]

The role of the interface in promoting the complexation was important in the enhancement in the hydrolysis of 2,4-dinitrophenyl diethyl phosphate (DNPDEP), 2,4-dinitrophenyl ethyl methyl phosphonate (DNPEMP) and Sarin by the micellar form of the Cu^{2+} complex of ligand (**I**) Figure 1-12.[46] The presence of cosurfactants like Triton X-100 greatly affected the catalytic activity of the metallosurfactant. At low concentrations of [Cu(**II**)]$^{2+}$, the presence of the cosurfactant enhanced the rate of hydrolysis of 2-acetoxy-5-nitrobenzoic acid and PNPA relative to the simple [Cu(**II**)]$^{2+}$ micelle case through increased solubilisation of the substrate within the micellar phase.[80]

Cu^{2+} and Zn^{2+} complexes of long alkyl pyridyl imine ligands (**III**) and their derivatives with the cationic surfactant cetyltrimethylammonium bromide (CTAB) showed significant rate increase for the hydrolysis of *p*-nitrophenyl picolinate (PNPP) and (PNPA) at 25 °C in the pH range 6.5–8.5. The activated ligand hydroxyl group acts as an effective nucleophilic species in the reactions *via* complexation with the metal ion. The Zn^{2+} complex showed a higher nucleophilicity of the alkoxyl anion compared to the Cu^{2+} complex. Similarly, the catalytic effects upon the hydrolysis of PNPP of metal ions such as Cu^{2+}, Zn^{2+}, and Ni^{2+} complexed with pyridyl glycerol derivatives (structures **IVa–IVd** Figure 1-12) indicate that the metallomicelles formed by pyridine ligands enhanced the hydrolysis of PNPP in the order Cu^{2+} >Ni^{2+} >Zn^{2+}; a stereochemical modification of the complex observed in the CTAB solution was given to account for this seen phenomena .[73]

The long-chain tetraazmacrocyclic complex of ligand (**V**) was found to be more effective as a phosphate ester hydrolysis catalyst in Brij micelles than it non-surface-active analogue (**IVb**) even though the first has a higher pK_a value for the coordinated water molecules. Here, higher-order contributions to the observed kinetics were attributed to the aggregation effect. High stable vesicle from surface-active Xantphos derivatives (structures **VIIa–VIIc** Figure 1-12) ligands with rhodium were found to be recyclable and effective in solubilising substrates (e.g. 1-octene), and enhanced rates of hydroformylation.[73]
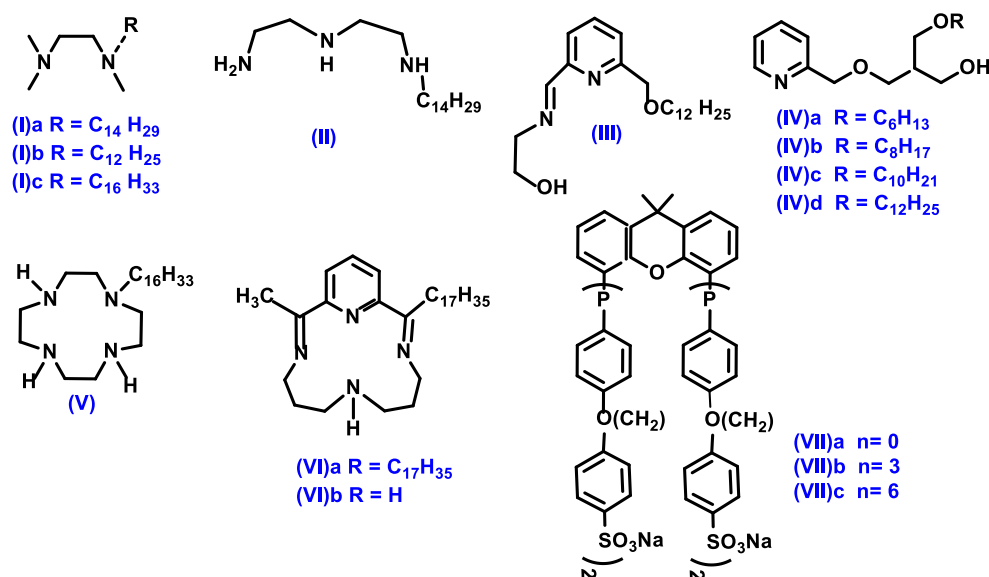
Figure 1-12. Surfactant ligands used in metallomicellar systems with different metal ions

Zeng *et al*. catalysed the hydrolytic cleavage of *p*-nitrophenyl picolinate (PNPP) by imidazole-divalent metal ions complexes (biap:N,N-bis(2-ethyl-5-methylimidazole-4-ylmethyl)aminopropane) complex (M^{2+}L). The result revealed that Zn^{2+} -complex showed a higher hydrolysis rate in micellar solution at a higher pH level, but Cu^{2+} exhibited a higher rate in weak acid medium.[118] In contrast, catalytic system of Zn^{2+}-biap (biap:N,N-bis(2-ethyl-5-methylimidazole-4-ylmethyl)aminopropane) complex (ZnL) (**A**) in micellar solution, this system consisted of a cationic Gemini surfactant 16-2-16 [bis(hexadecyldimethylammonium) ethane bromide] and the Zn^{2+} complex. As a comparison to demonstrate if the Gemini 16-2-16 micelles dominate as a reaction medium in the cleavage reaction of HPNP (Scheme 1-3). Similar experiments of HPNP cleavage were performed by using the same catalyst in a micellar solution of a conventional surfactant CTAB (hexadecyltrimethylammonium bromide), a single-chain analogue of 16-2-16.[105]
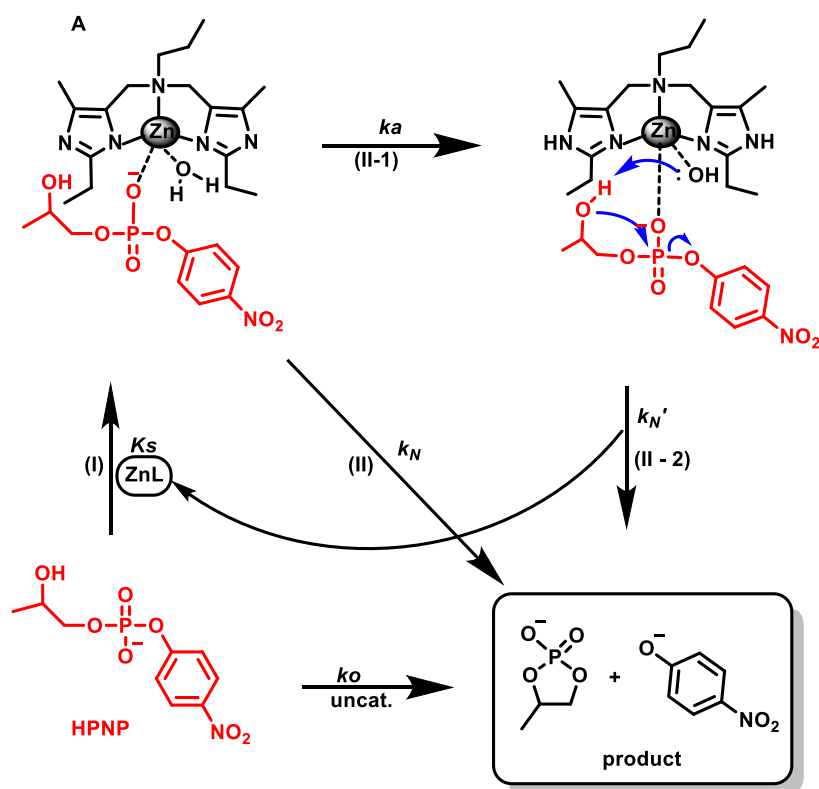
Scheme 1-3: *A suggested mechanism to catalytic cleavage of HPNP by ZnL.*

Compared to CTAB, the results of Jiang *et al.* demonstrated that Gemini 16-2-16 micelles form a more suitable microenvironmental reaction for the HPNP cleavage. Significantly, the HPNP catalytic cleavage rate highly in these new micelles than that in a homogeneous buffer solution, even when HPNP and ZnL are very soluble in water.[105]

Models of micelle-catalyzed reactions as for hydrophobic and electrostatic interaction in biological systems should give information regarding the mechanism of reactions regulation since micelles are structurally simpler and more readily modified than complex biological interfaces.

The HPNP cleavage rate enhanced by Gemini 16-2-16 or ZnL as an individual catalyst is significantly lower. ZnL is not a particularly efficient catalyst for HPNP cleavage.[105] However, in this system, the 16-2-16 /ZnL, the HPNP cleavage rate is about 3 times faster (~2016-fold) than spontaneous HPNP cleavage. The reactivity of HPNP cleavage stimulated by ZnL in Gemini 16-2-16 micelles was increased by an approximately 30-fold or 5-fold increase in hydrolysis rate compare with that obtained by ZnL or 16-2-16, and the rate of HPNP cleavage motivated by the ZnL/CTAB system is 12-fold or 2-fold faster than

that only by ZnL or 16-2-16, respectively. The hydrolytic cleavage of HPNP mediated by ZnL was significantly faster in Gemini surfactant aggregates of 16-2-16 (over 2.5-fold kinetic advantages) than in CTAB micelles. Investigation of the reactivity property of HPNP catalytic cleavage as a function of pH values in the range (6.50-8.50) and catalyst concentration was carried out. It was noticed that k_{obs} values of the HPNP cleavage reaction enhanced with the increase of ZnL concentrations and pH values.[105]

The Zn^{2+}/16-2-16 system shows a higher catalytic power (about a 2016 times rate enhancement). Moreover, the rates of HPNP cleavage in Gemini 16-2-16 micellar solution are faster than those in CTAB micellar solution. This proposes that the maximal rate acceleration of HPNP catalytic cleavage in the ZnL/16-2-16 system is dependent on the unique surface property of Gemini 16-2-16. Mostly, to speed-up the "mass transfer process" in a heterogeneous reaction, surfactants are added to the catalytic system in which the catalyst and the substrate distribute in different pseudo-phases, for example, oil phase and aqueous phase. It is noteworthy, both the substrate HPNP and the Zn^{2+} complex are very good-soluble in water. It is suggested that the HPNP catalytic cleavage in pure aqueous buffers (a homogeneous reaction mode) must be simpler than in a solution of micelles, but the observations were less important. This suggests that Gemini surfactant 16-2-16 or monocationic CTAB micelles may give a particularly favourable microenvironment for the HPNP cleavage reaction. The cleavage of HPNP from pseudo-first-order rate constants (k_{obs}) in various catalytic systems. Under a specific condition of pH 7.00 and [HPNP] = 2.00×10^{-5} M, no trace of uncatalyzed HPNP cleavage in pure aqueous buffer solution has been noticed.[105]

Grochmal and co-workers[17] used a model system which suitably modified amino acids to study the reactivity modulation through the cavity of lipid vesicles, they indicated the residence in the liposomal cavity of one of the building blocks leads to an almost quantitative dipeptide formation while the lipid membrane acts as a catalyzer to condensation reaction.[17]

Metallomicellar systems which contain Gemini surfactants displayed more efficient activity for hydrolysis than those containing the corresponding single-chained conventional surfactant like dodecyl trimethylammonium bromide (DTAB) (**I**). Likewise, the ligand with pendant hydroxyl groups (**II**) Figure 1-13, exhibited higher catalytic activities.[74]
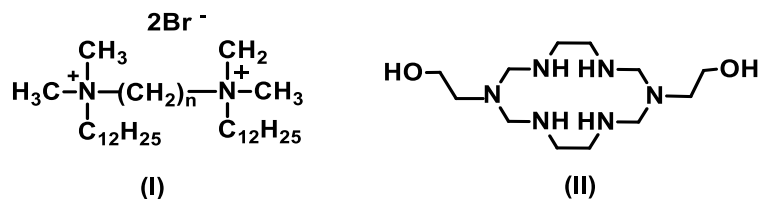
Figure 1-13: Metallomicellar systems containing Gemini surfactants and ligand-bearing pendant hydroxyl groups.

The hydrolysis of (PNPP) catalyzed by Cu^{2+} complexes of a number of triazole-based ligands with hydroxyl groups, 3,5-bis(hydroxymethyl)-1,2,4-triazole in micelles of a cationic Gemini surfactant, 1,2-ethane bis (dimethyl dodecyl ammonium bromide) (12-2-12), were studied kinetically at 25° C. It was noticed that Cu^{2+} complexes of these triazole-based ligands, particularly ligands L3 and L4 (Figure 1-14), revealed effective catalytic activity on the hydrolysis of PNPP. Consequently, imidazole and triazole, and their derivatives and their metal complexes can be chosen to mimic hydrolytic enzymes.[85]
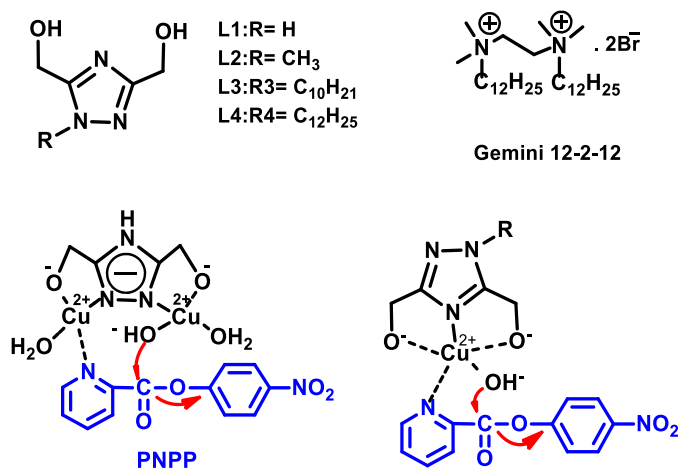
Figure 1-14: Triazole–based ligands with hydroxyl group exploited as metallomicelles for Cu^{2+} ions to PNPP hydrolysis in presence of Gemini 12-2-12.

34

In ongoing work by Poznik and König, they introduced a method to use fluid membranes of vesicles and micelles as support for amphiphilic additives, which collaboratively cleave the bonds of aryl ester. Bis-Zn^{2+} -complex as the membrane-anchored (Figure 1-15) is hydrolytically active and hydrolyses fluorescein diacetate (FDA) and this hydrolysis has a second-order rate constant (k_2) of 0.9 M^{-1} s^{-1}. The activity of hydrolysis is adjusted by co-embedded membrane additives (Figure 1-16), bearing a side chain with functional groups of common amino acid. Therefore, the activity of hydrolysis of the system is enhanced more than 16 fold in comparison with cyclen 1 (k_2 = 14.7 M^{-1} s^{-1}).[119]
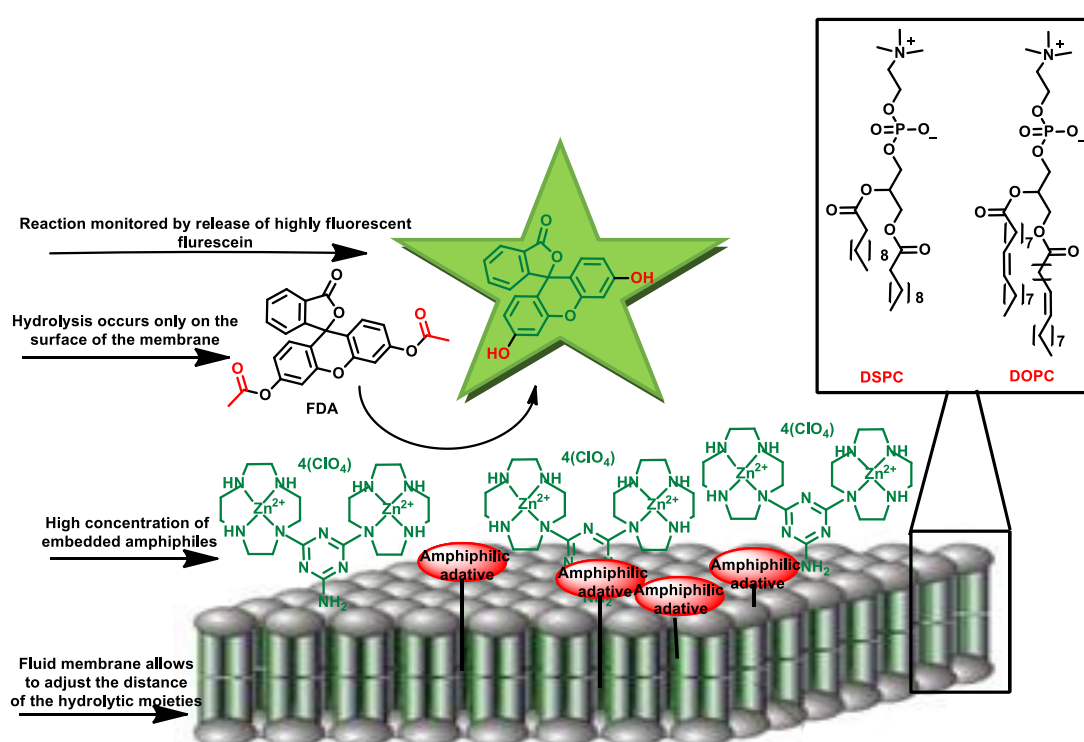
Figure 1-15: *Concept of the proposed membrane hydrolysis using amphiphilic additives (adapted from reference 119).*[119]
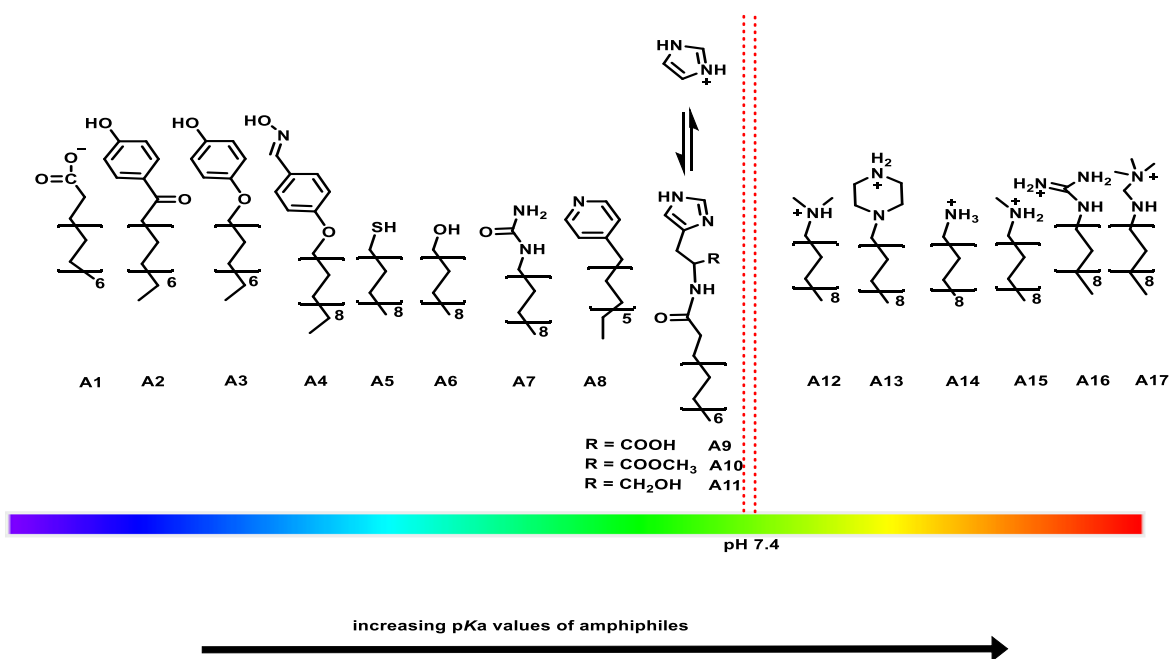
Figure 1-16: Amphiphilic membrane additives utilised to cooperate the hydrolysis in their anticipated protonation state at pH 7.4

It was noted that surfactant with a positive charge such as tetra-ammonium salts, amines doped in vesicles efficiently cleavage *p*-nitrophenol esters in natural pH solution.[120] This effect very probably caused by the high local concentration of the polar functional group on the surface. The active amphiphilic molecules in the membrane are not randomly distributed through the membrane, but they form aggregations or clusters as shown in Figure 1-17.[121]
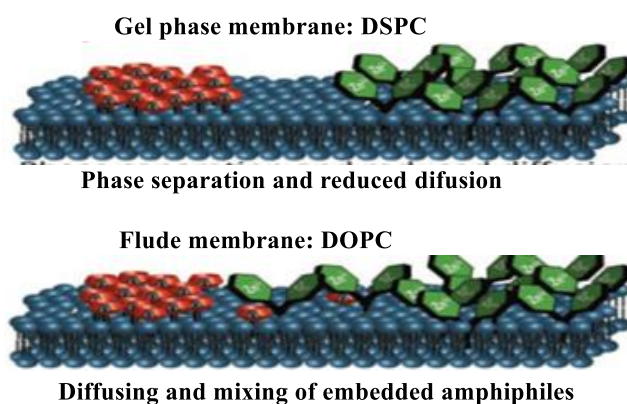
Figure 1-17: Expected patch formation in different phospholipid membranes(adapted from reference 119).

There are two main biological mechanisms for the transformation and amplification of a chemical signal by proteins in bilayer membranes. The initial binding of a ligand to the extracellular region of a membrane-spanning protein receptor induces either (1) an overall conformational change (Figure 1-18A), as represented by the G protein-coupled receptors,[122] or (2) dimerization of two proteins (Figure 1-18B) as observed in tyrosine kinase receptors.[123] These alterations in protein organization stimulate enzyme-catalysed reactions inside cells and cause signal amplification.

Hunter and Williams *et al.*[124, 125, 126] have recently introduced a new mechanism to transduce and amplify a signal across a membrane by using recognition events on one side of the membrane to mobilise a membrane-bound transducer. The transducer can then translocate across the membrane as Figure 1-18C shows. When a catalyst is attached to the transducer, the translocation will display the catalyst to the other side of the membrane, where it can cleave a substrate and generate an amplified signal.
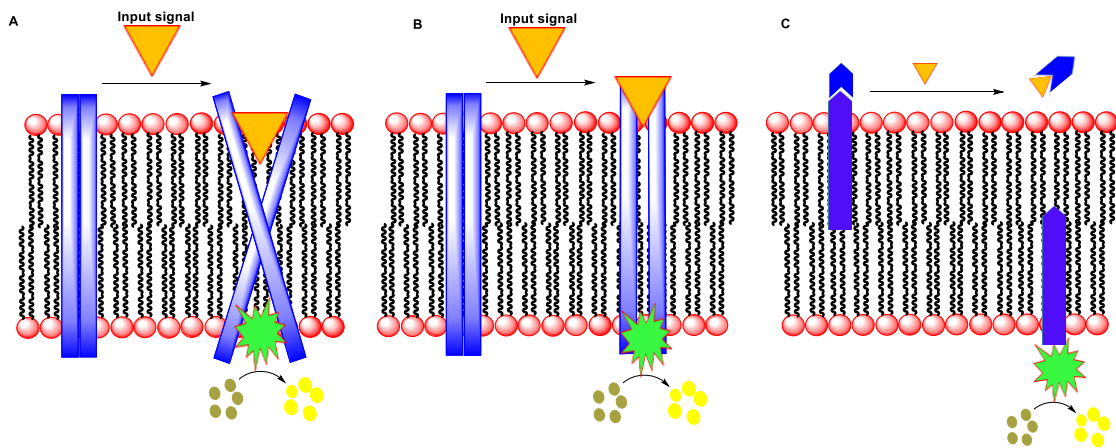
Figure 1-18. The transmembrane signal transduction mechanisms. A) Signal (orange) recognition on the membrane surface stimulates a rearrangement in a transmembrane protein (blue), that produces an active enzyme (green) which turns over the substrate (brown to yellow). B) Recognition of the signal (orange) on the membrane surface leads to dimerization of transmembrane protein (blue) that generates the active enzyme (green) which cleaves the substrate (brown to yellow). C) Translocation leads to the release of the membrane-bound transducer (blue) due to the signal (orange) recognition on the membrane's surface. The active catalyst (green) turns over the substrate (brown to yellow). Adapted from reference 124.

1.12 Metallomicelles-catalyzed Hydrolysis: Kinetic Models

A collaborative effect between the functional groups is an essential feature of efficient enzyme catalysis. In the chemical simulation of enzyme-active centres, the most often used method is to prepare small organic multi-functional molecules and to imitate the catalytic function of the enzyme active centre. Metallomicelles are one of these biomimetic systems; however, studies of their catalytic kinetics and mechanisms are few. The approximate quantitative treatment of metallomicellar catalysis and the establishment of its mathematical model have rarely been reported. A kinetic model of the metallomicellar mimic system of carboxypeptidase (A) was created by Yu et al., and supplies an important way to examine the catalytic processes and mechanisms.[74]

Tagaki *et al.* improved a "binary complex model" for the quantitative treatment of metallomicellar catalytic kinetic study. The model presumes that substrate moiety can weakly interact with the metal ion as a ligand base in aqueous buffer and the metallomicellar catalysis is an intermolecular reaction.[89] In order to find if there is a strong interaction among the metal ion (M), ligand (L) and a substrate (S), Zeng and *et al*. constructed a "ternary complex kinetic model" for metallomicellar catalysis.[127] What follows is a brief introduction to the "ternary complex kinetic model" of the hydrolysis reaction. The "phase separation" model of the micellar system supposes that there are two phases (micellar pseudo-phase and the bulk phase) in micellar solution, and the reaction takes place simultaneously in both micellar pseudo-phase and the bulk phase.[128,129] The following Scheme 1-4 can be used to describe the reaction process:

$$\text{S + Mi} \underset{}{\overset{K_s}{\rightleftharpoons}} \text{MiS}$$

$$\downarrow k_w \qquad\qquad\qquad \downarrow k_m$$

$$\text{P} \qquad\qquad\qquad\qquad \text{P}$$
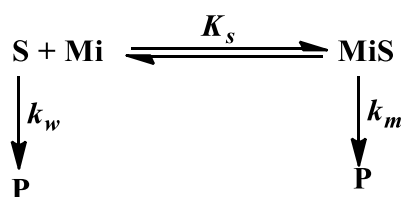
Scheme 1-4. Ternary complex formation by binding the substrate to the metallomicelle complex

S represents a substrate, **Mi** is micelle, *Ks* is the association constant between micelle and substrate, *km* and *kw* are the apparent rate constants for product formation in the micellar phase and in bulk phase.

In the metallomicellar system, mostly there is an equilibrium occurs among a ligand **(L)**, a metal ion **(M)**, and a substrate **(S)**. Based on the phase-separation model of a micelle, the metallomicelle-catalysed reaction can be assumed to exist in the bulk phase and the metallomicellar phase concurrently to give the products **(P)** as illustrated in the following equations.

$$xM + yL \; \underset{}{\overset{K_M}{\rightleftharpoons}} \; M_xL_y + S \; \underset{}{\overset{K_T}{\rightleftharpoons}} \; M_xL_yS \; \xrightarrow{k'_N} \; P$$

$$\Big\downarrow k'_0$$

$$P$$
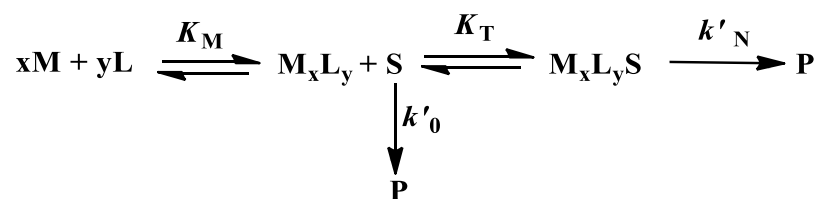
$$k_0' = k_0 + k_m\,[M] + k_L\,[L]$$

Scheme 1-5. *The equilibrium in the metallomicellar system*

Where K_m is the association constant between metal ions and ligands, K_T is the association constant between a binary complex (M_xL_y) and a substrate, k'_N and k'_0 are the apparent first-order rate constants for product formation in the metallomicellar phase and in the bulk phase, respectively. k_0 is the rate constant due to the buffer, k_L and k_M are the second-order rate constants due to the ligand and metal ion alone, [L], [M], and [S] are the concentrations of ligand, metal ion, and substrate in the bulk phase, respectively. [M_xL_y] is the concentration of (x) metal ions or (y) ligands in the metallomicellar phase, and [MxLyS] represents the substrate concentration in the metallomicellar phase.[74]

1.13 pH Effect on Hydrolysis Rate

The pH value performs an essential factor in the hydrolytic reaction. A number of hydrolytic reactions in enzymes require metal ions that are supposed to activate a water molecule acting as a nucleophilic group in a ternary complex. The pH effect can be accounted for by supposing that the dissociated complex anion (T^-) is much more active than the undissociated complex (TH). Where TH is the undissociated complex, T^- is the dissociated complex anion assumed to be the active species in metallomicellar phase, K_a is the acid dissociation constant of the ternary complex, and k_N is the first-order rate constant which is pH-independent.
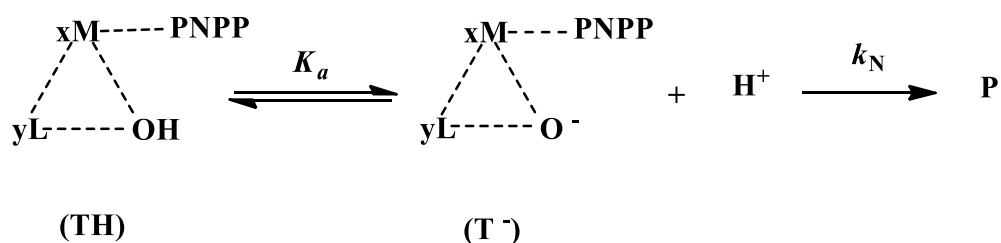
Scheme 1-6. *Tetrahedral transition state (T.T.S.)*

Song *et al*. studied the pH effect on the metallomicelle–catalysed hydrolysis reaction and found that the k'_N and k'_M are pHs dependent as shown in Scheme 1-7.[21]
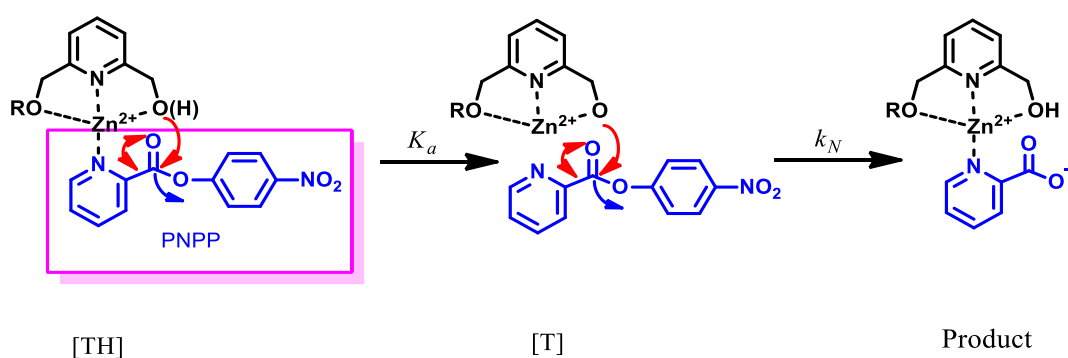
Scheme 1-7: *PNPP hydrolysis by Zn^{2+}-complex in vesicle solution of (CTAB: SDBS) is dependent on the pH value of the medium.*

Jiang *et al* noticed, that when the concentration of the Zn^{2+}-complexes (**a** and **b** Figure 1-11) was held constant, the rate constants for the hydrolysis of PNPP were at first seen to increase progressively with increased pH values. This may be due to the increase in the nucleophilicity of the hydroxyl groups of the complexes, which favours a substrate attack. More increase in the pH values led to a decrease in the rate constants, which may be ascribed to the hydrolysis of Zn^{2+}, which causes a decrease in the concentration of the metallic complexes. The increase in pH values led to a rise in the rate constants of HPNP cleavage. Furthermore, the deactivation of this catalyst was not noticed over the whole pH range; this proves that ZnL complex has higher stability at higher pH.[21]

As shown in Figure 1-19, the pH-rate profile of the hydrolysis of PNPP was catalysed by the metallic complexes in vesicular solution. The inflection points of the curve are at about 7.38 and 7.52 (complex **a** and **b** Figure 1-11, respectively), corresponding to the pK_a of Zn^{2+} in vesicular solution. This denoting that Zn^{2+} ions induce the dissociation of the hydroxyl groups of the ligands to form the active species in the reaction system, increasing the PNPP hydrolysis rates by an effective nucleophilic attack on the substrate.
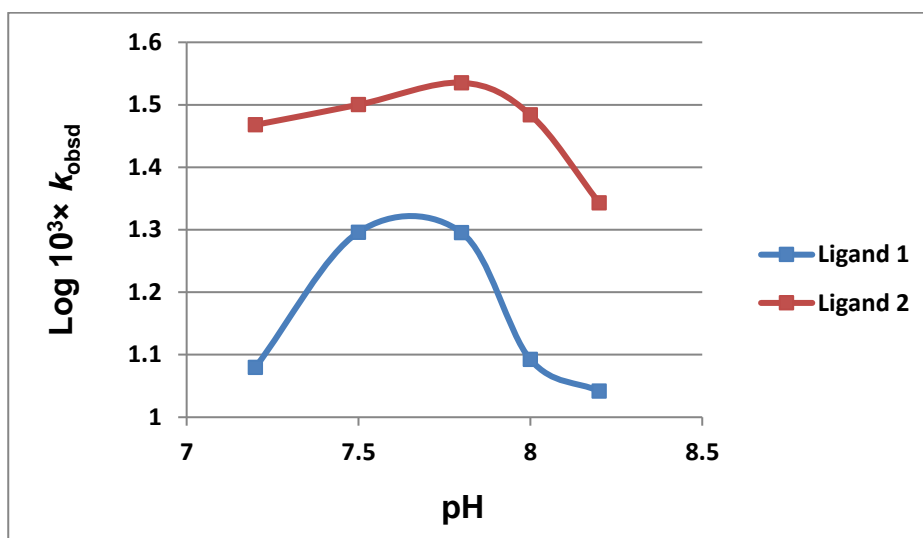
Figure 1-19: *Profiles of k_{obsd} versus. pH for PNPP catalysed hydrolysis by ligands **1** (red curve), **2** (blue curve), and complexes of Zn^{2+} ion in a vesicular system (CTAB:SDBS = 1:4); [SDBS] = [CTAB] = 0.014 M, [L] = [Zn^{2+}] = 1 × 10^{-3} M, [PNPP] = 5 × 10^{-5} M, T = 25°C.*

Qiu and co-workers investigated the pH effect on the hydrolysis of *p*-nitrophenyl picolinate of Cu^{2+} complexes. This kinetic study demonstrated that the apparent first-order rate

constant to form the product in the metallomicellar phase (K'_N), the association constant between the substrate and the binary complex (K_T), and the association constant between the metal ion and the ligand (K_M) increased with an increase in the pH value of the system. With an increase in the hydrocarbon chain length of the ligand, K'_N and K_T increased while k_M decreased at constant pH.[85]

Ni^{2+} and Zn^{2+} complexes with a 6-alkylaminomethyl-2-pyridinealdoxime moiety (structures **A**, Figure 1-20) exhibited a strongly pH-dependent ability to cleave p-nitrophenyl acetate (PNPA) and hexanoate (PNPH) in the presence of CTAB micelles.[79] Cu^{2+}-complexes of lipophilic pyridine ligands (structures **B**, Figure 1-20) form metallomicelles that are catalytically active for the cleavage of p-nitrophenyl esters of acetic, hexanoic, and dodecanoic acids and for p-nitrophenyl diphenyl phosphate. An examination of the rate versus pH profiles indicates that the hydroxyl acts as a nucleophile in the hydrolytic cleavage.[93]

R = C₁₂H₂₅
R = CH₃

A

R = NHC₁₂H₂₅ ; R' =H
R = NHC₁₂H₂₅ ; R' =CH₂OH
R = NHC₁₂H₂₅ ; R' =CH₂OCH₃
R = NHC₁₆H₃₃ ; R' =CH₂OH

B
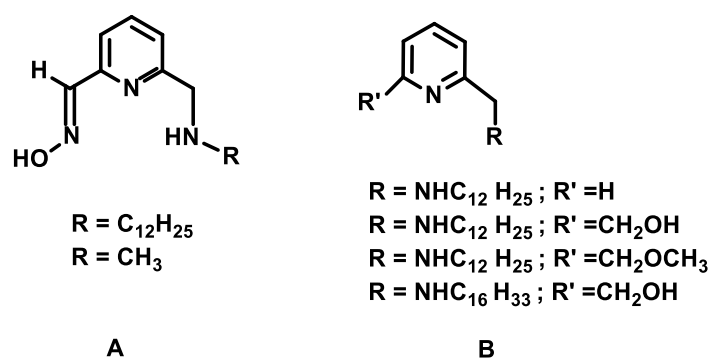
Figure 1-20: Ligands in metallomicelles system with Ni^{2+}, Zn^{2+}, and Cu^{2+} showed high dependence on pH in catalytic efficiency.

Chapter 2 -   The hydrolysis Activity in the Solution

2.1   Aims

The objective of this chapter is to investigate the catalytic activity of a range of short-chain surfactants containing oxime ligands towards the hydrolytic cleavage of carboxylic esters in solution. These surfactants provide a reference set of data for compounds embedded into vesicles (which will have a similar catalytic moiety, Chapter 3).

2.2   Selection of Oximate Ions

Ligands containing one or more hydroxyl groups are significant for the catalytic hydrolysis of phosphate or carboxylate esters. The hydroxyl group of the ligand can be activated by transition metal ions and can act as a more efficient nucleophile than a chelating water molecule.[74] In this study, oximate ions were chosen as ligands for a number of reasons. Oximate anions ($-CH–NO^-$) are strong and powerful nucleophiles, [130,131] and can be used for cleaving phosphoric acid esters, carboxylic or amides.[131] Although not used in natural systems, they have drawn specific interest since the 1950s due to their capacity to act as powerful efficient cholinesterase reactivators[132] and significant applications in the degradation of toxic organophosphorus compounds.[133,90] The oxime's therapeutic activity appears to be directly related to their abnormally high reactivity.[132] Oxime reactivators are valuable implements in biochemical studies, as they have pharmacological applications to treat organophosphorus poisoning.[134] Hence, an important goal was to clarify the factors that control oximate ions reactivity. One of these factors is the α-effect, which is present in nucleophiles that contain unshared electron pairs on atoms adjacent to the nucleophilic centre.[135] These 'α-nucleophiles' often show higher reactivity than other nucleophiles that have a similar pK_a but do not possess the α-effect. Furthermore, it was identified that 'unfavourable solvent effect' is another major factor that affects the oximate ion's nucleophilic reactivity as a representative α-nucleophiles.[132]

Most oximes that have been investigated can be categorised as charged quaternary or uncharged tertiary oximes. The first group possess clinical applications; they can be divided into two groups: bispyridinium and quaternary monopyridinium oximes.[132] The kinetics of phosphate ester and carboxylic acid ester cleavage by oximates has been broadly studied to

optimize their applications and to understand the nature of the above-mentioned α-effect.[130-136] A characteristic feature of the reactivity of oximate anions is a nonlinear Brønsted plot for the oxime pKa versus oximolysis rate constants, revealing a levelling off when the pKa of the oxime reaches around '8'. This behaviour is attributed to the "solvational imbalance effect", which represents a type of transition-state imbalance phenomenon.[137] The solvational imbalance for the nucleophilic substitution reflects the balance of free energy between the desolvation (dehydration in water) of the nucleophile prior to the nucleophilic attack and the benefit of more basic anions. The desolvation energetic cost of more basic oximate anions becomes increasingly higher, leading to the plateau of the rate constant.[138] For high pKa oximate anions, complete solvation by water must become strong enough to compensate for the increase in reactivity. Increasing pKa may also increase the strength of the solvation shell, as hydrogen bond acceptor properties tends to parallel pKa. For lower pKa oximes, solvation may be incomplete and so a nucleophilic site remains available.

Free oximate ligands and their metal complexes are very effective in enhancing PNPA cleavage. However, the reactivity cannot be predicted from the acidity of the oxime function.[131] Neutral oxime ligands have high pK_a values (in the range 10-12), therefore in neutral solutions. The fraction of the reactive deprotonated form is very low, and the expectation is that the pK_a is reduced when coordinated with a metal ion.[136] The oximic ligands complexation causes a noticeable increase in the acidity of the oxime group, following the order $Cu^{2+} > Ni^{2+} > Zn^{2+}$. Both oximates of free ligands and their metal complexes are effective in enhancing PNPA cleavage.

2.3 Selection of Zn^{2+} Ions:

Certain metal ions including transition metals and lanthanides can catalyse diverse organic reactions by participating as a Lewis acid and various kinetic studies have investigated the catalytic roles of these metal ions.[139, 140] Knowledge of the metal ions' role is essential to studying organic and inorganic mechanisms. Moreover, the determination of these roles provides important information about the possible metal ions role in a metalloenzyme.[139]

The main role in a hydrolytic metalloenzymes activity is performed by metal ions (most commonly Zn^{2+}). These metal ions activate the nucleophilic functional group, which may be water molecules or hydroxyl groups, primarily by inducing the deprotonation at physiological values of pH for the reasons noted above. These metal complexes are often used in an effort to mimic the essential roles in the enzyme catalytic models.[131]

2.4 Ester Substrates

Carboxylate esters are more reactive to the hydrolysis compared to phosphate esters, nitriles, and amides. Nevertheless, in most studies of metalloesterase models, esters are found to be either highly labile or covalently connected to diverse metal-binding groups.[75, 141] Using a multifunctional catalysis model, Suh *et al.* investigated the hydrolysis of PNPA catalysed by Zn^{2+} complexes of 2-pyridinecarboxaldoxime or 2-acetylpyridineketoxime. Under their experimental conditions, the reaction progressed exclusively over the formation of the acyl-catalyst intermediate. The oximate ion, the metal ion, hydroxide ion, the metal-bound water molecule and general bases assisted in the multifunctional catalysis of the ester hydrolysis by the $zinc^{2+}$–oximinato ions.[142]

Bidentate oxime ligands (**A**, **B**, **C** and **D,** Figure 2-1)[142, 143] have been used as enzyme analogues in multifunctional catalysis. Ligands **C** and **D** were formed from the acylation of **A** and **B** respectively by the mechanism illustrated in Scheme 2-1.

45

A: R1 = CH$_3$, R2 = H
B: R1 = H, R2 = H
C: R1 = CH$_3$, R2 = CH$_3$CO
D: R1 = H, R2 = CH$_3$CO
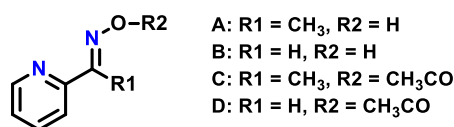
Figure 2-1. *Bidentate oximes used as ligands in the PNPA hydrolysis study.*
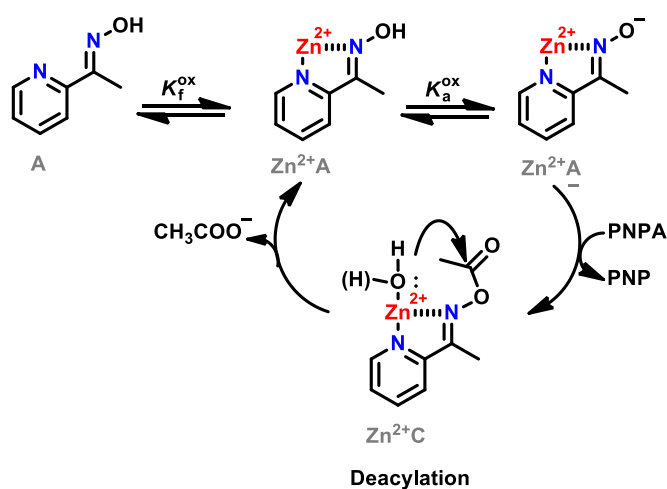
Scheme 2-1. *The acylation-deacylation mechanism of compound A in the presence of Zn^{2+} as a Lewis acid.*

Zinc ions act as Lewis acids to reduce the pH when the oxime group ionises. The complex of oximate anion-metal (**Zn^{2+}A$^-$**, Scheme 2-1) acts as a nucleophile in the acylation step. In the deacylation step, Zn^{2+} ions work as a Lewis acid to enhance the oximate group's leaving ability. Additionally, Zn^{2+} bound water molecules and hydroxide ions of **Zn^{2+}C** can participate as nucleophiles, while the solvent molecules and free hydroxozinc^{2+} ions act as general bases in the deacylation step. In structure **A** (Scheme 2-1), the methyl group increases the rate of acylation by elevating the oximate anion nucleophilicity *via* electronic effects and promotes the deacylation step through steric effects. Rate constants for the acylation (k_A) and the deacylation (k_C) steps are functions of pH, [Zn^{2+}], $K_f{}^{ox}$ and $K_a{}^{ox}$. [142]

Suh and co-workers discovered that in the catalytic hydrolysis of compound **C** by Zn^{2+} ions, the metal-bound water molecules can act as the nucleophilic attack centre [143, 144] (Scheme 2-2). [139]

46
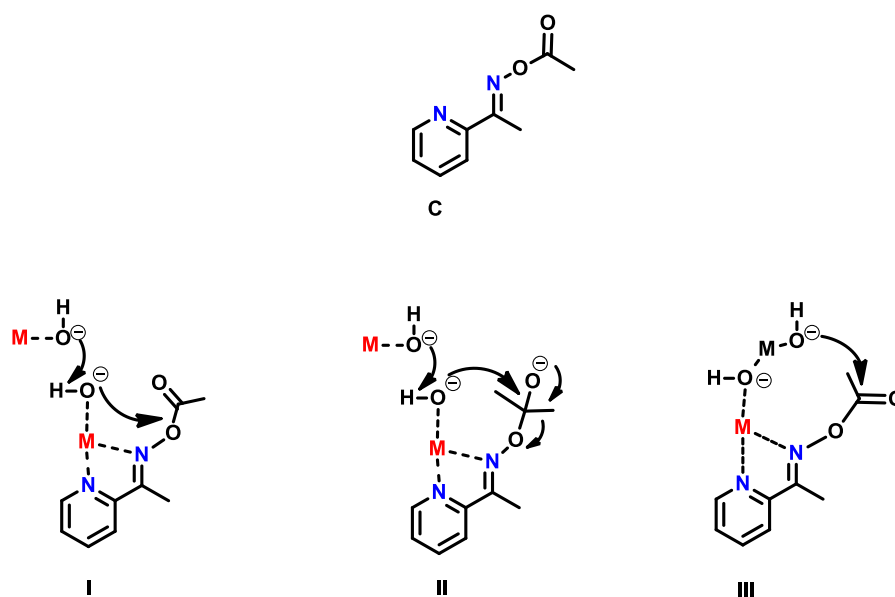
Scheme 2-2. *Possible mechanisms for the hydrolysis of compound **C** using Zn²⁺ ions.*

In the mechanisms, (I) and (II), two hydroxozinc ions are contributing, and only one of them works as a general base in the formation of (I) or in the dissociation or separation (II) of the tetrahedral intermediate. Whereas in (III), the dimer of hydroxozinc ion is involved as a "catalytic unit". Introducing another chelating member to the ring as in compound **E** can create a different effect on the transition state stability.

When Zn^{2+} catalysed the hydrolysis of compound **E,** two different reaction pathways lead to the product. One involves one hydroxide ion and two Zn^{2+} ions in the transition state of the rate-determining step (possible mechanisms shown in the Scheme 2-3). The other pathway involves two hydroxide ions and two Zn^{2+} ions in the transition state of the rate-determining step (similar to the mechanisms shown in a Scheme 2-2).

E

IV

V

VI
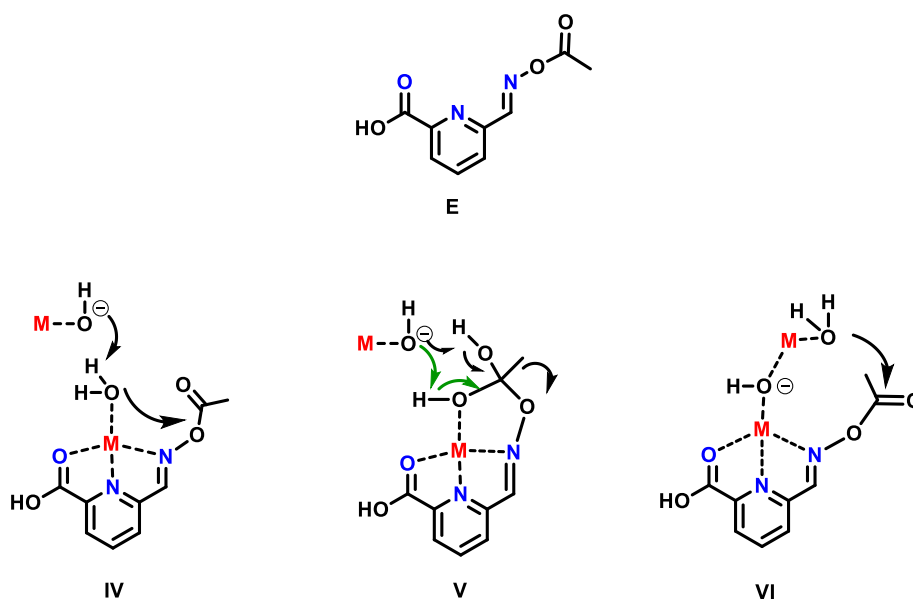
Scheme 2-3. *Possible mechanisms for the hydrolysis of compound **E** using Zn^{2+} ions.*

Yatsimirsky *et al*. reported the hydrolysis rate constant of PNPA by Cd^{2+} and Zn^{2+} complexes with tridentate oxime ligands (Figure 2-2) to be over two orders of magnitude.[130,137] Deprotonated complexes of ligand **F** displayed significant activity for cleaving phosphate triesters and substituted phenyl acetates, but they are unreactive for *p*-nitrophenyl phosphate mono and diesters hydrolysis. These complexes operate as true catalysts through an acylation−deacylation mechanism with reactive substrates.

2

F

G

H

R= H or Me
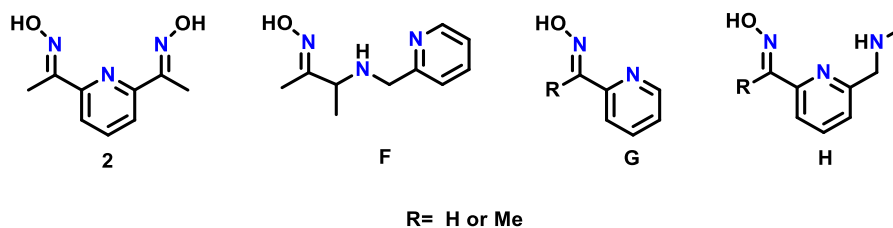
Figure 2-2. *α-Nucleophile oxime ligands that have two adjacent donor atoms used as catalysts after coordination with metal ions for enhancing the reactivity of PNPA cleavage.*

Yatsimirsky *et al.* have suggested two mechanisms (Scheme 2-4) for phenyl acetate cleavage [130] using compound **F**, Figure 2-2.

A

B
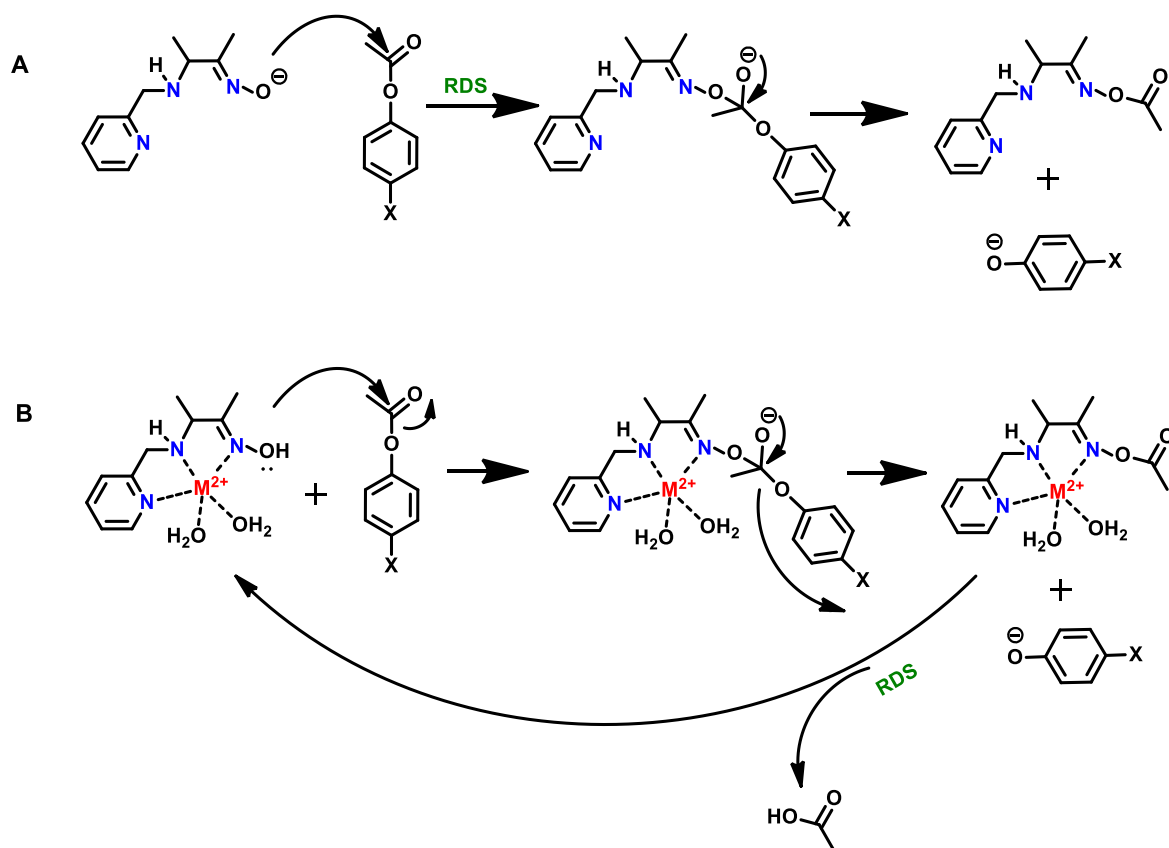
Scheme 2-4. The mechanism and the rate-determining step (RDS) for the PNPA cleavage using the free oximate and the oximate complexes.

In mechanism (**A**), the rate-determining step is the nucleophilic attack of the free oxime on the phenyl acetate, which is why the 'solvational imbalance' plays an important role in the ligand reactivity. In mechanism (**B**), the rate-determining step changes for the oxime-Zn^{2+} or oxime-Cd^{2+} complexes to be the expulsion of the leaving phenolate anion. This describes why the solvational imbalance effect is less important for oximate complexes.

Kinetic studies over a range of pHs showed that the most active form of the complex is $[Zn(Ox)(OH)_2]^-$. This was confirmed by electrospray ionisation mass spectrometry and supported by calculations from density functional theory. The coordinated water in $[Zn(OxH)(H_2O)_2]^{2+}$ deprotonates before the oxime. Yatsimirsky's group addressed important new features of these complexes; they have a very high esterolytic activity even greater than the enzyme catalysed the hydrolysis of aryl acetate ester.

The metal ions perform an essential role in the catalysis of the ester hydrolysis. Zinc ions should be able to stabilise the tetrahedral transition state (T.T.S, see Section 1.10).

2.5 The Approach and the Design

Compounds **2, 4-6** and **9** were prepared starting from the commercially available 2,6-diacetylpyridine (shown in Scheme 2-5).
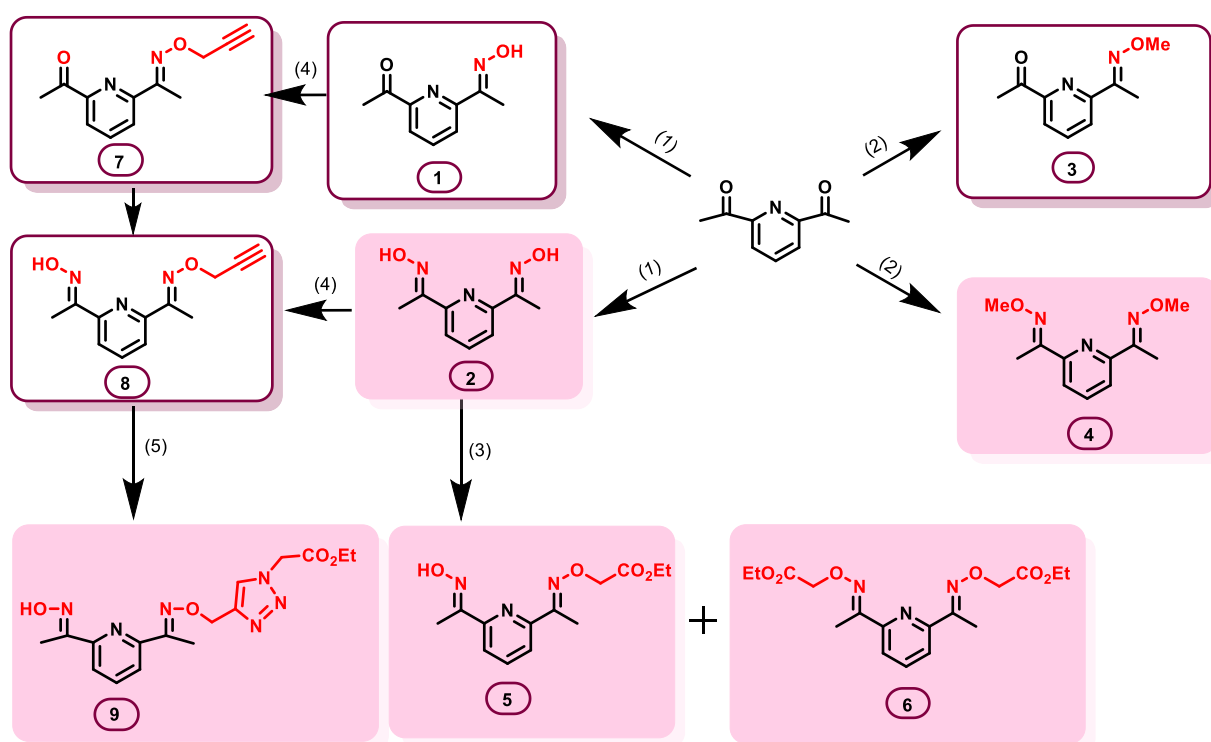
Scheme 2-5*. Synthetic Scheme to show the preparation of the oxime ligands **1-9**. 1) Hydroxylamine hydrochloride, sodium acetate in water at room temperature for 16 hours. 2) Methoxylamine hydrochloride, sodium acetate in water at room temperature for 16 hours. 3) Ethyl bromoacetate, potassium carbonate, in DMF at room temperature for 16 hours.4) Propargyl bromide 80 wt% in toluene, in DMF at room temperature for 16 hours.5) azido ethyl acetate, CuI, DIPEA in DCM for 6 hours.*

Compounds **1** (81%) and **3** (76%) were obtained by reacting 1:1 equivalent ratio of the starting material with the reagents while compounds **2** (85%) and **4** (78%) were obtained from reacting 1:2 starting material to the reagent. Starting from compound **2** to get compound **5** (52%) and **8** (68%) in one step was problematic as the reaction can occur on both sides producing side products such as **6** (yield = 24.%). Thus, to solve this problem the compounds were prepared in two steps starting from **1**.

Complexes of compound **2** with different divalent metal ions have been studied before.[130,137,136] The results of that research revealed that the hydrolysis rate for PNPA by compound **2** at pH 6-8 is enhanced ~ 10^3 fold by the presence of Cd^{2+}, Mn^{2+} and Pb^{2+}, and increased 2-100 times with Hg^{2+}, Ni^{2+}, Zn^{2+} and Pr^{2+}. However, the rate of hydrolysis appeared unaffected by Cu^{2+} and Co^{2+}.[136] Tridentate ligands **4-6** and **9**, have not been studied before. The rationale for this diversity was to see if the linker between the oxime headgroup and the organic chain would affect catalytic activity. It is possible that the triazole group (in compound **9**) could affect the hydrolysis, as it is a good chelating group with Zn^{2+} ions. 1,2,4-Triazole-based amphiphilic ligands have been investigated for their ability to hydrolyse *p*-nitrophenyl picolinate (PNPP) in micelles of CTAB, (compounds are shown in Scheme 2-6). The results revealed that the catalytic activity with the triazole-Cu^{2+} complex is better than the triazole-Ni^{2+}complex.[85] The difference between **4**, **5** and **6** is the group on the left side of the ligand; in **4** and **6** is the ester group on both sides (left and right).
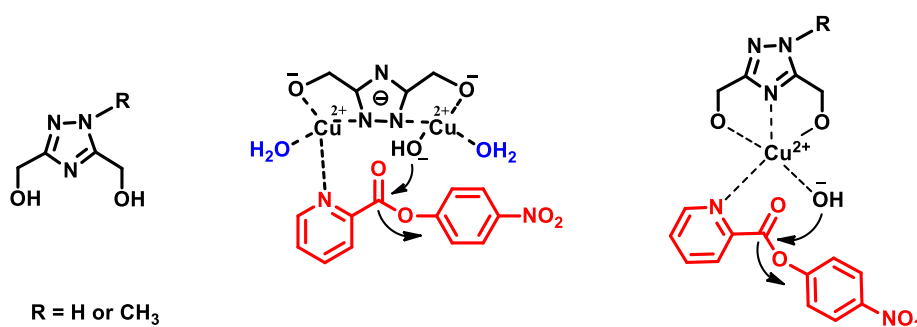
Scheme 2-6*. Complexes from triazole and copper^{2+} used to investigate the hydrolysis of PNPP.*

The reaction, that we are following to assess the nucleophilicity and reactivity of the oximate ions, is the cleavage of two esters with two different leaving groups as shown in Scheme 2-7.
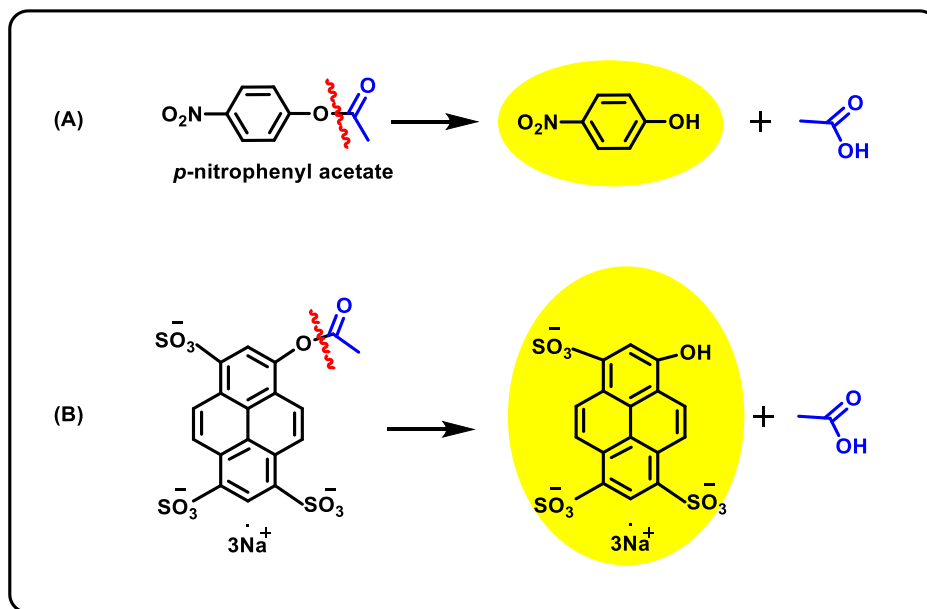
Scheme 2-7. (A). *The cleavage of PNPA ester.* **(B).** *The cleavage of 1,3,6-pyrenetrisulfonic acid, 8-(acetyloxy)-, sodium salt (HPTSA).*

(Scheme 2-7-A and Figure 2-3) show the commercially available ester substrate PNPA, which is organic solvent-soluble and cleaves to give the chromophore, (*p*-nitrophenolate that can be detected easily by UV-Vis spectroscopy (λ_{max} at 400 nm). While in (Scheme 2-7-B) the ester is water-soluble and it releases 8-hydroxypyrene-1,3,6-trisulfonate trisodium salt (HPTS) which can be detected at 450 nm. In both cases (**A** and **B**), the yellow colour of the chromophores is easy to monitor.

2.6 Results and Discussion

2.6.1 Control Experiments

The rate of this hydrolysis reaction can be enhanced by the presence of a base.
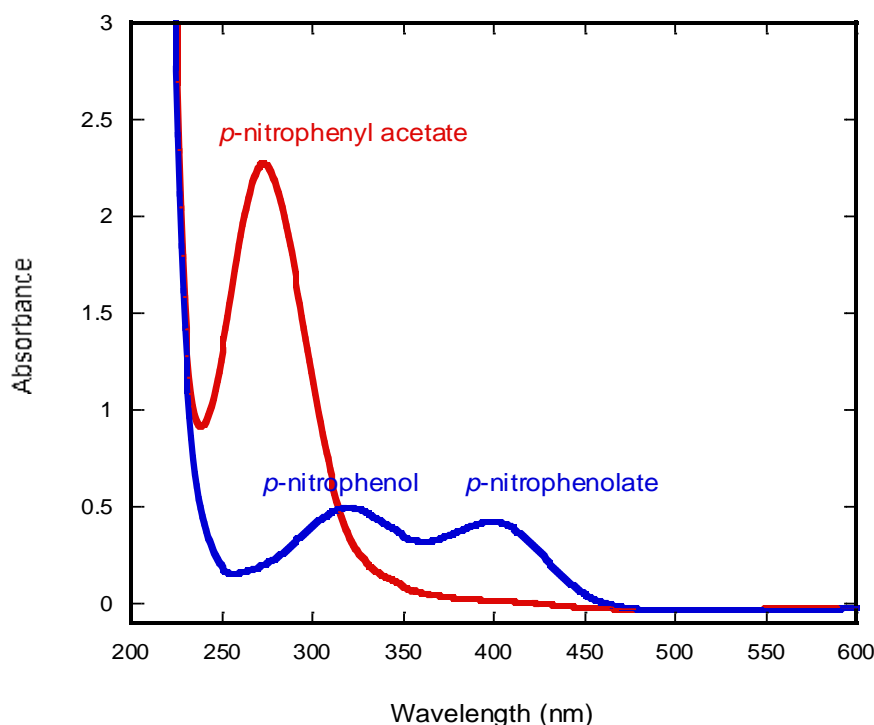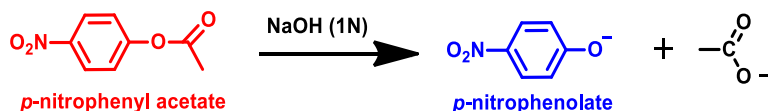
Figure 2-3. The difference in the UV-Vis spectra between PNPA and p-nitrophenol. The red line indicates PNPA (250 µM) in HEPES (100 mM, pH = 7). The blue line indicates p-nitrophenol (250 µM) in HEPES (100 mM, pH = 7). (HEPES) = 4-(2-hydroxyethyl)-1-piperazineethanesulfonic acid

Another substrate that was used in this study to investigate the reactivity in solution was 1,3,6-pyrenetrisulfonic acid, 8-(acetyloxy)-, trisodium salt (HPTSA), which was prepared according to the literature.[145,146] This highly water-soluble substrate hydrolyses to give 8-hydroxypyrene-1,3,6-trisulfonic acid trisodium salt which is easy to monitor at 450 nm (Figure 2-4).
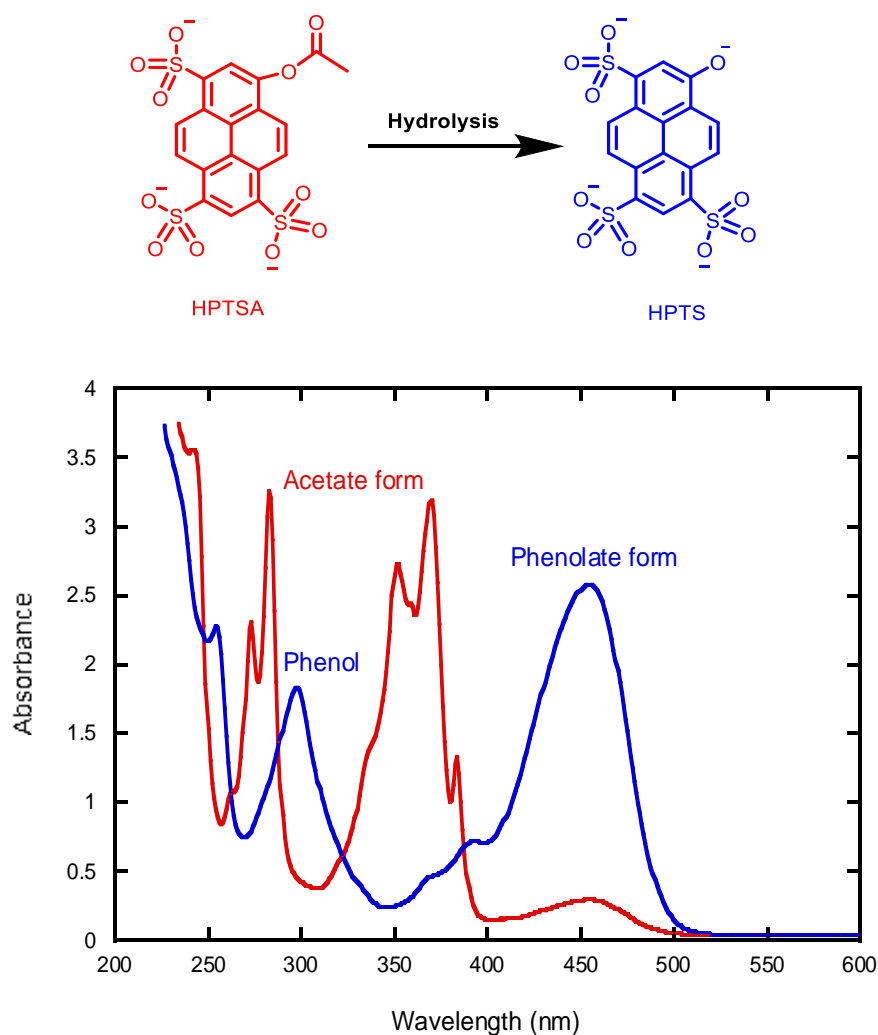
Figure 2-4. *The difference in spectra between HPTSA (250 μM) in HEPES (100 mM, pH = 7) the red line and HPTS (250 μM) in HEPES (100 mM, pH = 7) the blue line.*

The background reaction of the substrates in the buffer 4-(2-hydroxyethyl)-1-piperazineethanesulfonic acid (HEPES) before and after adding the Zn^{2+} (0.04-1.0 mM) was monitored. As no change in absorbance was observed, the substrate was shown to hydrolyse spontaneously too slowly to contribute to any observed reaction under these conditions (see Table of rate constants, Chapter 2 in the appendix).

2.6.2 Investigation of the Effect of Metal Ions on the Substrate Hydrolysis

The results reported by Mancin *et al.*[131] confirmed that complexes of oximes and transition metal ions can enhance the hydrolysis and the structure of the ligand played an important role. Furthermore, the literature reported that many stoichiometric complexations can ocurr[147,148] depending on the ligand structure and the metal ion. To prevent these complications that can arise from the existence of many complexes and to assure the existence of a unique 1:1 species a 10-fold excess of metal ions to the ligand was used.[131] Hence, it was necessary to determine the importance of metal ions on the hydrolysis in the absence of the chelating ligand. Therefore, a set of experiments were completed using different concentrations of Zn^{2+} (Figure 2-5). The increase in the concentration of the product was negligible compared with the experiment devoid of the metal ions. From this observation, we can say there is no catalytic effect from free zinc ions on the hydrolysis rate.
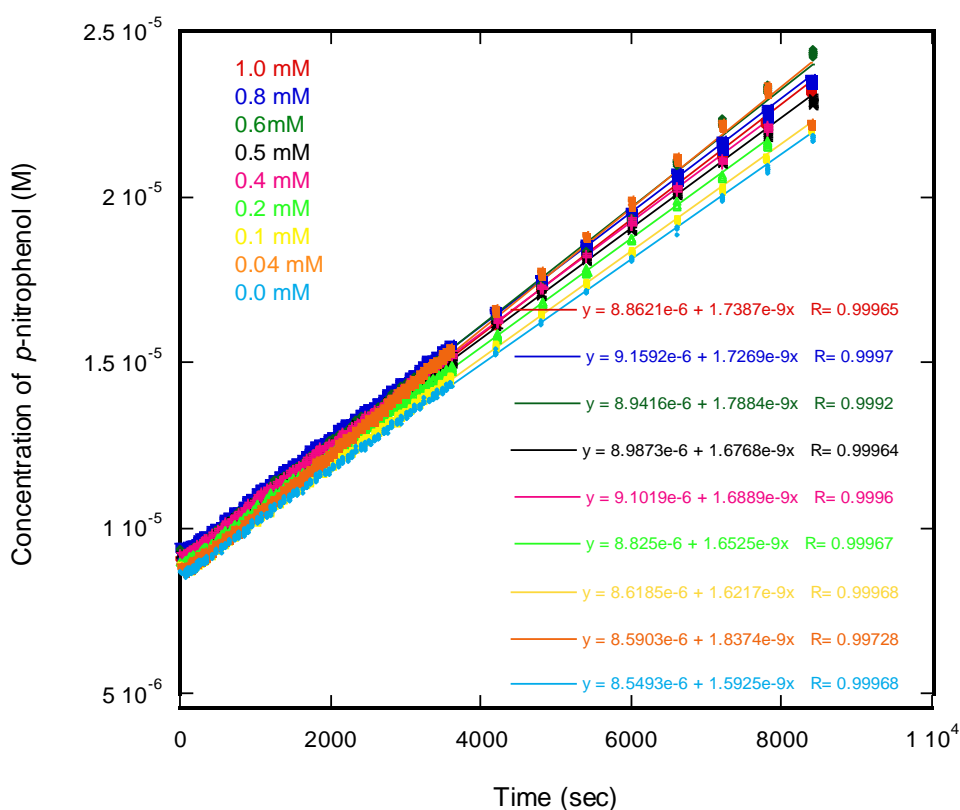
Figure 2-5. Zn^{2+} ions effect on PNPA (0.5 mM) cleavage (these were single measurements).

2.6.3 The Ligand Binding to the Zinc (Titration of Zn^{2+} into the Ligand)

Various concentrations of Zn^{2+} (0.1 - 0.7 mM) were titrated into the oxime ligands **2**, **4-6** and **9** (0.2 mM) at room temperature, pH $\approx$ 7. Figures 2-6 to 2-8 show the titration results of the reference ligand **2** and ligands **5** and **9** with zinc. As the zinc concentration was increased, there was a change in the absorbance spectrum at around the region 300-400 nm and 250-280 nm for compounds **2, 5** and **9**. For ligand **5**, the change in absorbance was much less defined suggesting weak binding between the ligand **5** and the metal ion. Compounds **4, 6** were prepared to examine the activity in a solution similarly to compounds **2, 5** and **9**. Different concentrations (0.2 - 0.002 mM) of compounds **4** and **6** were prepared to investigate the activity of these compounds. At 0.2 mM, precipitation occurred, this is likely to be due to the bulky organic structure. Lower concentrations did not show significant enhancement in the hydrolysis rates. For this reason, they were not used any further. This indicated that these compounds have solubility limits in the solution. This follows the hypothesis that ligands possessing hydroxyl groups are more effective than those that do not have hydroxyl in the active side. Another attempt to enhance the solubility of the compound was to form a complex of the compound by increasing the concentration of zinc in the solution, but this too did not improve the activity.
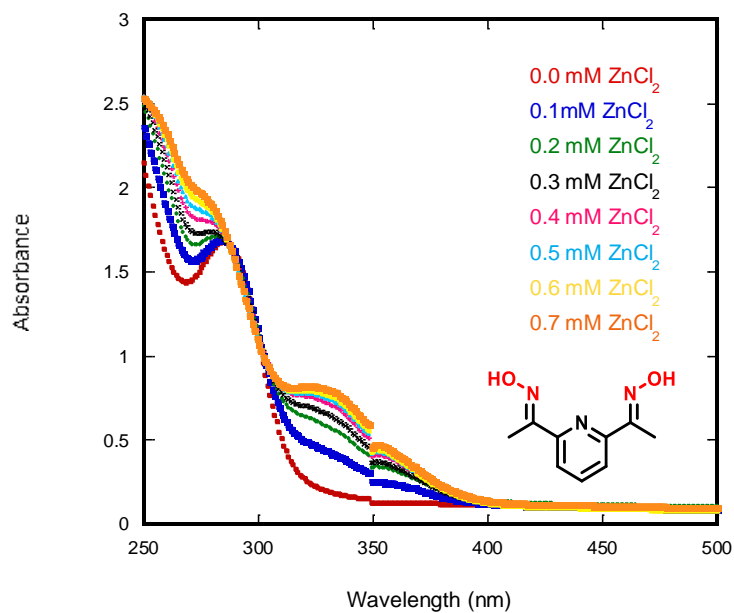
Figure 2-6. The differences that Zn^{2+} ions make to the UV-Vis absorbance during binding ligand *2* (0.2 mM) in HEPES (100 mM, pH 7). The disconnect at 350 nm is due to changing the spectrometer lamp, (these were single measurements).
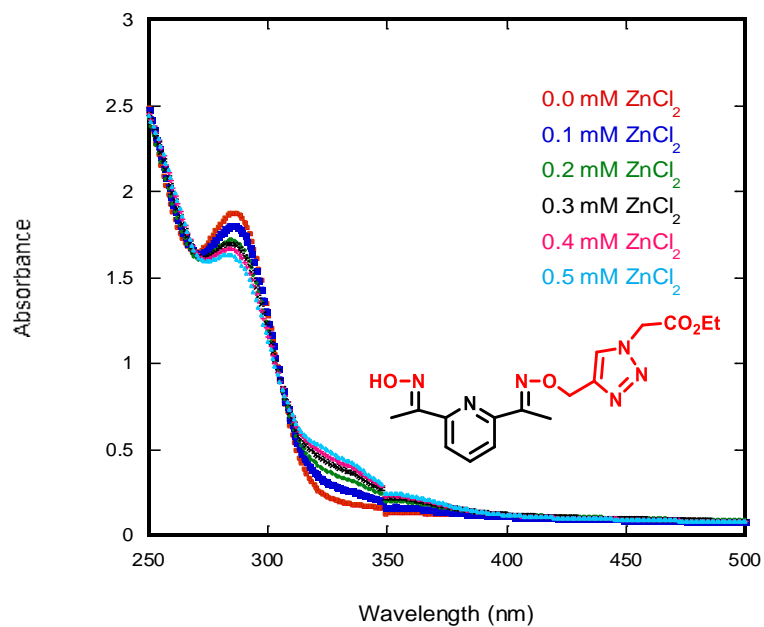
Figure 2-7. The differences that Zn^{2+} ions make to the UV-Vis absorbance during binding ligand *9* (0.2 mM) in HEPES (100 mM, pH 7). The disconnect at 350 nm is due to changing the spectrometer lamp, (these were single measurements).
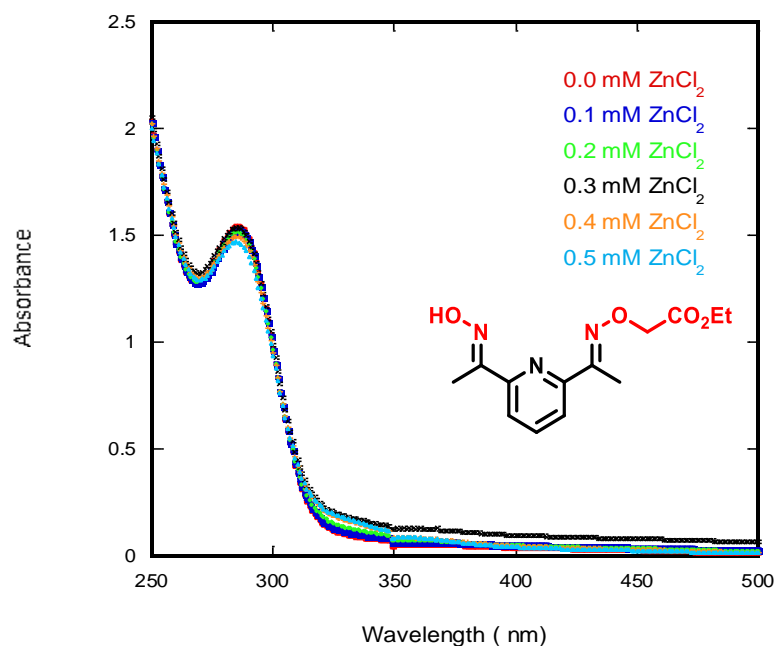
Figure 2-8. *The differences that Zn²⁺ ions make to the UV-Vis absorbance during binding ligand **5** (0.2 mM) in HEPES (100 mM, pH = 7.0. The disconnect at 350 nm is due to changing the spectrometer lamp; (these were single measurements).*

2.6.4 Stability of the Metal-Ligand Complexes

To investigate the stability of the ligands **2, 5** and **9** complexed with the Zn^{2+} ions, the UV-Visible spectra of the reaction solutions ([buffer] = 100 mM, [ligand] = 0.2 mM, [Zn^{2+}] = 1 mM, pH = 7, at 25 °C) were observed over time. For the zinc complex of compound **2**, which does not contain an ester group, no change in the spectrum was observed even after a day as Figure 2-9 shows. Similarly, with compound **9**, which has an ester group as well as a triazole did not show a significant change in the absorbance spectrum (Figure 2-10). This result is contrary to that observed for compound **5,** which displayed a remarkable change in the UV-Vis spectrum even after 1 hour as Figure 2-11 shows. The pHs of the solutions were determined after a day and the values were consistently around 7.0.
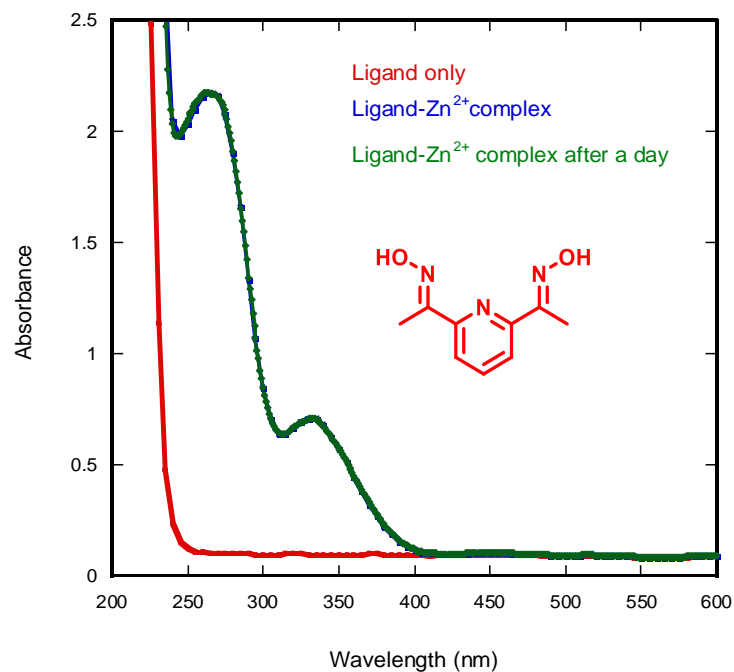
Figure 2-9. *Red curve indicates ligand **2** (0.2 mM) in HEPES (100 mM, pH = 7.0), blue curve indicates ligand **2** (0.2 mM) treated with 1 mM Zn^{2+} and the scan taken, green curve; ligand **2** (0.2 mM) treated with 1 mM Zn^{2+} and the scan taken, green line after a day.*
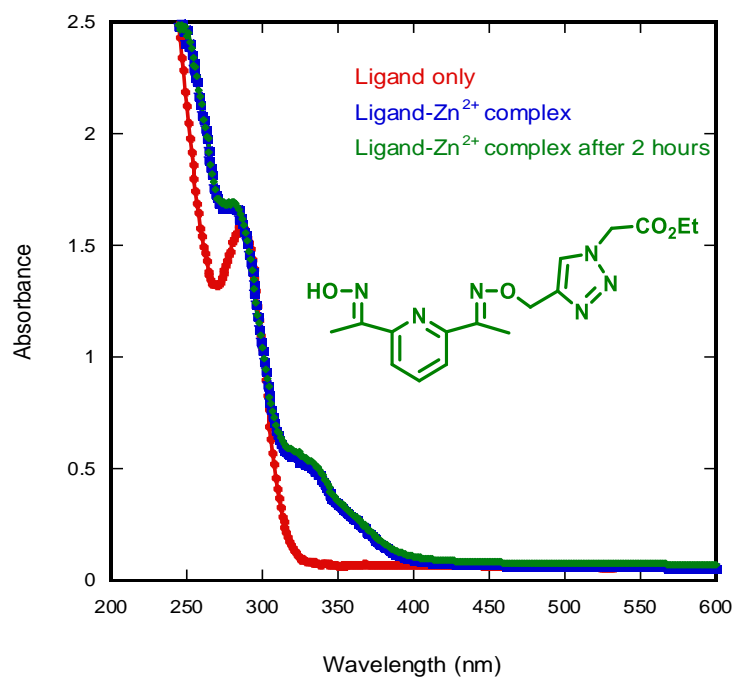
Figure 2-10. *Red curve indicates ligand **9** (0.2 mM) in HEPES (100 mM, pH = 7.0), blue curve indicates ligand **9** (0.2 mM) treated with 1 mM Zn^{2+} and the scan taken, green curve; ligand **9** (0.2 mM) treated with 1 mM Zn^{2+} and the scan was taken, green line after 2 hours.*
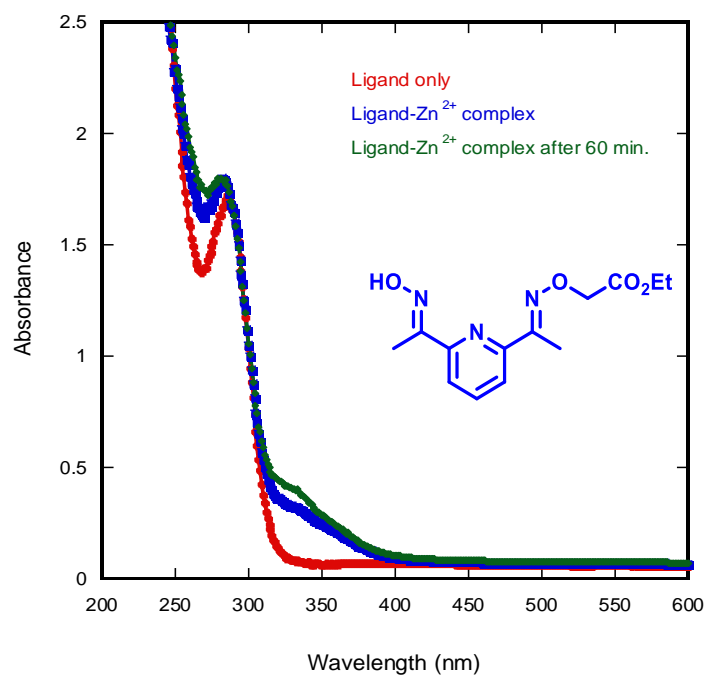
Figure 2-11. Red curve indicates ligand **5** (0.2 mM) in HEPES (100 mM, pH = 7.0), blue curve indicates ligand **5** (0.2 mM) treated with 1 mM Zn^{2+} and the scan taken, green curve; ligand **5** (0.2 mM) treated with 1 mM Zn^{2+} and the scan taken, green line after an hour.

2.6.5 Dependence of the Reaction Rate on the Zn^{2+} Concentration in the Presence of Ligands 2, 5 and 9

After determining which compounds (ligands and the substrates) were to be used in this study, the reaction conditions, such as the buffer (HEPES) pH 7 (was chosen to keep the background reaction as slow as possible and similar to the biological media range), and the reaction temperature is 25 °C, the rate constants for the reaction could be measured. To determine the best ligand–metal ratio for promoting the hydrolysis rate, a series of experiments were carried out with a variety of different ligand and zinc concentrations.

2.6.6 The Hydrolysis Rates to Cleave Ester Substrate Using Complexes of Compounds 2, 5 and 9

Figures **2-12** and **2-13** show the relationship between the $ZnCl_2$ concentration and the rate constants for the cleavage of the substrates. From the results, it is clear that the three ligands **2**, **5**, and **9** behave similarly in the hydrolysis of both substrates PNPA and HPTSA. The hydrolysis follows the first-order rate reaction and all the data were fitted to first-order rate equation (Equation 2-1). Compound **9** revealed the highest rate constant values and compound **5** showed the lowest values. While compound **2** exhibited strong binding to the metal at 0.2-1.0 mM concentration. It is noticeable that the three compounds behave similarly towards the two substrates.

$$A = A_0e^{-kt} \qquad \qquad \text{Equation 2-1}$$
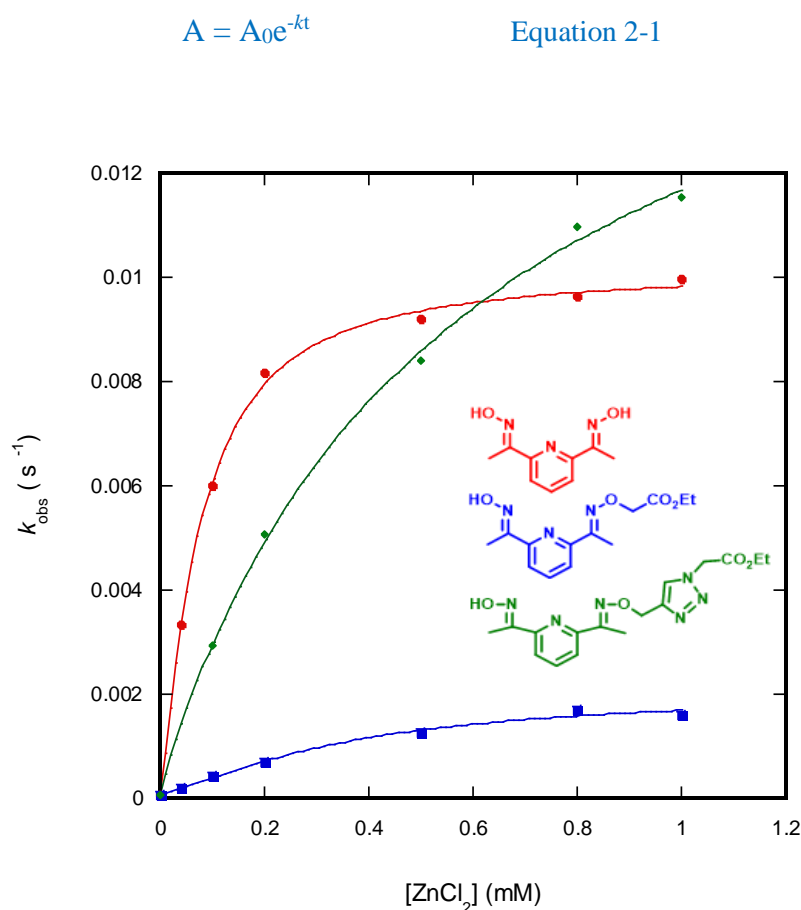
Figure 2-12. *Hydrolysis rate constants for HPTSA hydrolysis versus various concentrations of $ZnCl_2$ using compounds **2**, **5** and **9** (0.2 mM) in HEPES (100 mM, pH 7) at 25 °C (the experiment for compound **9** was repeated twice and the average was taken, see the data in the appendix).*

It was noticed that with compounds **5** and **9** the rate of 1,3,6-pyrenetrisulfonic acid, 8-(acetyloxy) hydrolysis was raised as the $ZnCl_2$ concentration increased, while with compound **2** the hydrolysis rate increased constantly until the concentration of $ZnCl_2$ reached 0.3 mM, then it plateaued and no further increase. This may be because compound **2** binds most tightly but **9** reaches a higher rate when there is enough Zn^{2+}.

Another point to note was that the three compounds behaved similarly but 10-times slower towards the hydrolysis of PNPA under the same conditions of [compound], [$ZnCl_2$], [substrate], [buffer], pH value, and temperature as shown in Figure 2-13.
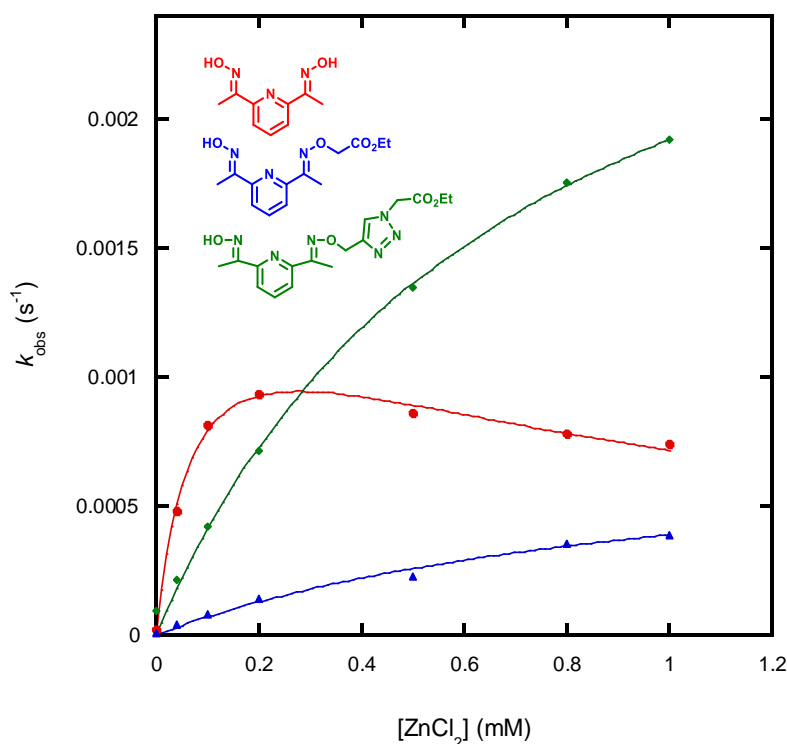
Figure 2-13. *The observed rate constants for the PNPA cleavage by complexes of compounds **2**, **5**, and **9** (0.2 mM) with different concentrations of $ZnCl_2$ (0.04-1 mM) in 100 mM HEPES at 25 °C. Data for compound **2** taken as average from two experiments (the experiment for compound **2** was repeated twice and the average was taken, see the data in the appendix).*

The overall conclusion of the effect of varying the concentration of $ZnCl_2$ with the ligands (0.2 mM) can be summarised as that the maximum hydrolysis rate of both substrates 1,3,6-pyrenetrisulfonic acid, 8-(acetyloxy) trisodium and PNPA follows this order:

<div align="center">

Compound **9** > compound **2** > compound **5**

</div>

An issue that should be considered is the various forms of complex that can be formed as the ratio of metal ion to ligand varies. The possibilities are shown schematically in Scheme 2-8. In this Scheme, it is anticipated that increasing the Zn^{2+} ion concentration will facilitate the formation of the simple mononuclear complex, which can act on the substrate. Thus, the change in activity with increasing metal ion concentration is explained by saturation of ligand with metal ions. However, it is possible that this increase is affected by dimerization of the complex to form an inert dimer–inert because the hydrazone OH would be involved in bridging two Zn^{2+} ions and become an ineffective nucleophile. This would lead to lower observed activity, depending on the dimerization constant. Similarly, at low concentrations of metal ions, it is possible for two ligands to coordinate a single ion. This would lead to lower reactivity at low concentrations of added Zn^{2+} ions, but there is no observable sign of this.
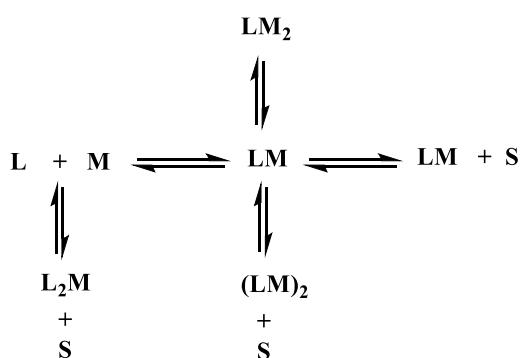
Scheme 2-8. *A chemical Scheme indicating binding interactions between the metal (M) and the ligand (L) to form the catalyst and potentially inert species.*

The above findings confirmed that as the metal concentration increased (5-times) this led to an increase in the catalyst concentration. A surprising observation is that the hydrolysis rates of PNPA using the Zn^{2+}-compound **2** complex decreased (after reaching a maximum at about 1:1 ratio) as the concentration of zinc increased. This might suggest that a second Zn^{2+} ion binds weakly to the complex to inhibit its activity, but it is difficult to see how this can occur with the structures involved. The phenomenon might be related to the nature of the substrates–one is anionic and the other neutral, but again, a ready explanation is not apparent.

The suggested mechanism for the hydrolysis of the ester substrate by a 1:1 ZnL complex is shown below in Scheme 2-9 and the steps are:

Step 1: The deprotonation of the oxime ligand by the metal ions to form the oximate anion

Step 2: The nucleophilic attack of the oximate anion to the ester substrate to form the tetrahedral intermediate

Step 3: The collapse of the tetrahedral intermediate and release the phenolate anion

`
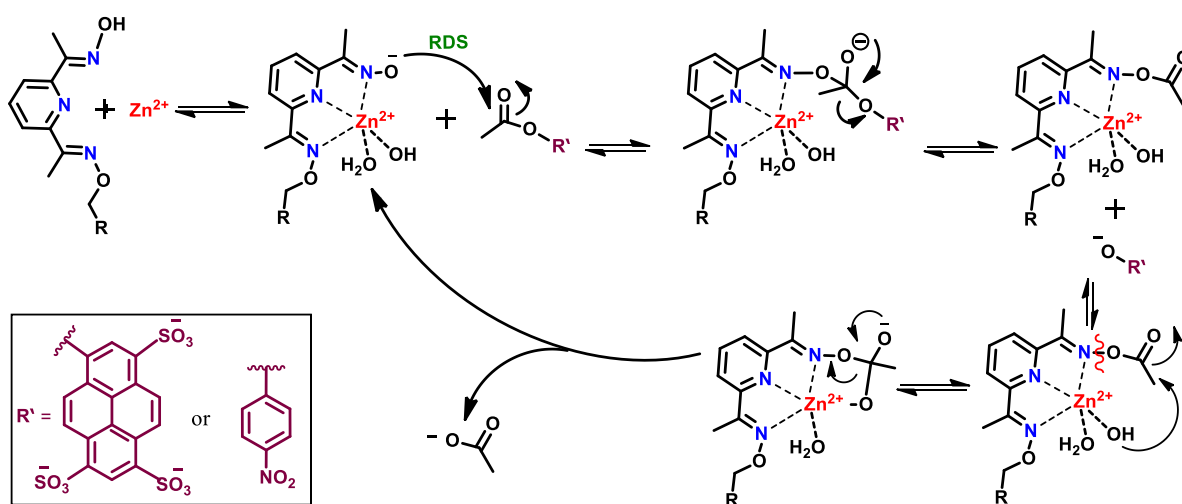
Scheme 2-9. *The suggested mechanism for the ligand-metal binding and hydrolysis of the substrate in the solution.*

2.6.7 Effect of Ligand Concentration

The effect of varying the concentration of ligand was investigated using different concentrations of compounds **2**, **5** and **9** (0.2 mM-0.02 mM) and a constant concentration of Zn^{2+} (0.2 mM). A first-order rate equation was fitted to the change in absorbance with time to generate observed rate constants for each reaction. The data and curve fits are shown in Figures 2-14 to 2-16.
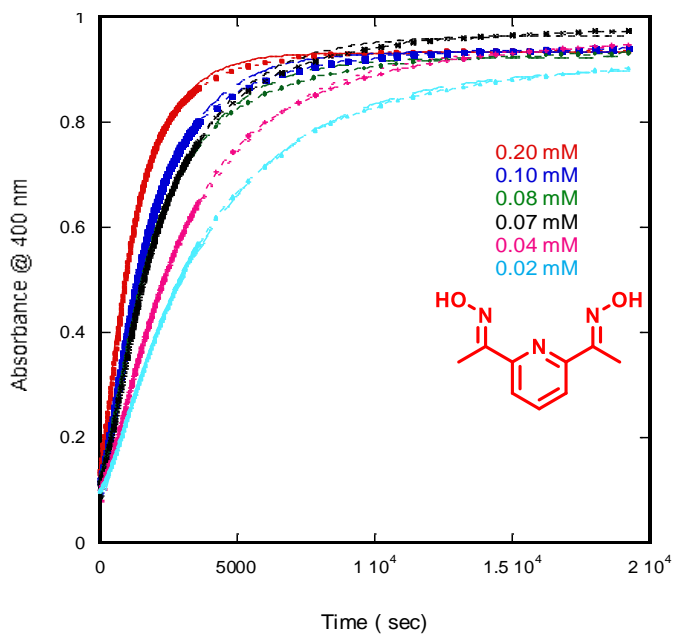
Figure 2-14 *Reaction progress with variation in compound **2** concentration: HEPES (100 mM), ZnCl₂ (1 mM), PNPA (0.1 mM), the pH of the reaction mixtures were measured before and after the reactions, it was ≈ 7.1, experiment temperature 25°C.*
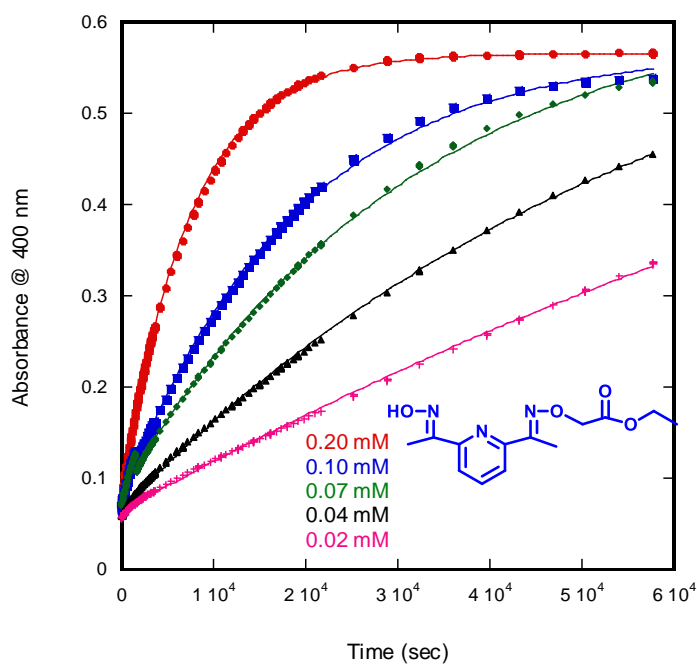
Figure 2-15. *Reaction progress with variation compound **5** concentration: HEPES (100 mM), ZnCl₂ (1 mM), PNPA (0.1 mM), the pH of the reaction mixtures were measured before and after the reactions, it was ≈ 7.1, experiment temperature 25°C.*
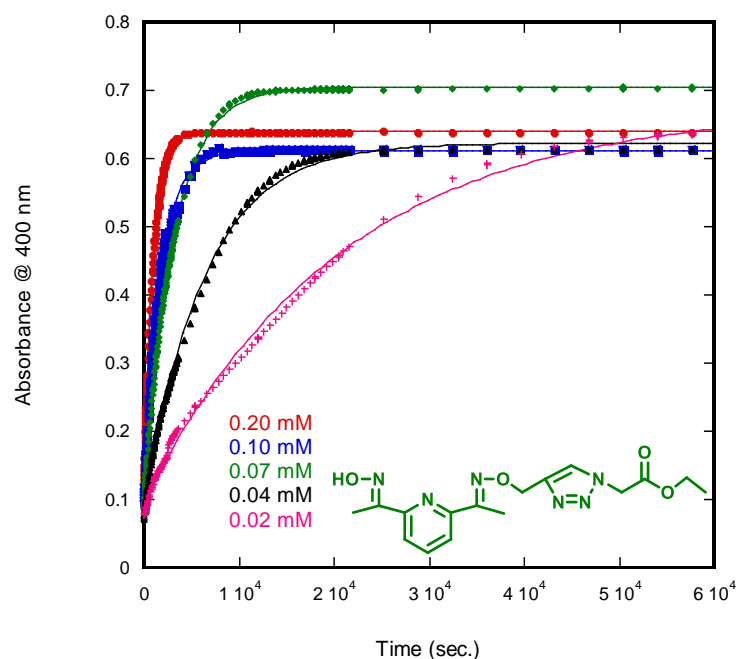
Figure 2-16. *Reaction progress with variation compound* **9** *concentration: HEPES (100 mM), ZnCl₂ (1 mM), PNPA (0.1 mM), the pH of the reaction mixtures were measured before and after the reactions, it was ≈ 7.1, experiment temperature 25°C.*

The observed rate constants are plotted against the change in ligand concentrations in Figure 2-18. Under these conditions, both **5** and **9** show a reasonably linear relationship ($5.19\pm0.210 \times 10^{-3}$ mM^{-1} s^{-1} for compound **9** and $6.19\pm0.427 \times 10^{-4}$ mM^{-1} s^{-1} for compound **5**) and between the observed rate constants and ligand concentrations that goes through the origin, but a similar fit for the data for **2** leads to a significant positive intercept. This suggests that the increase in the concentration of active species is non-linear and based on previous reports in the literature, it is likely that the complex can form an inert dimer as shown in Scheme 2-8 and Figure 2-18. This Scheme leads to Equation 2-2, which was fit to the data for compound **2** to give K = 2000 ± 8000 mM^{-1} and $k = 0.3\pm2 \times10^{-7}$ mM^{-1} s^{-1}.

$$[\text{ML}] = \frac{-1+\sqrt{1+8K[\text{ML}]_{\text{T}}}}{4K} \qquad \text{Equation 2-2}$$

66

Reports in the literature[136] consider the possibility of compound **2** forming a dimer when the concentration of the complex increases and the proposed structures are shown in Figure 2-17.
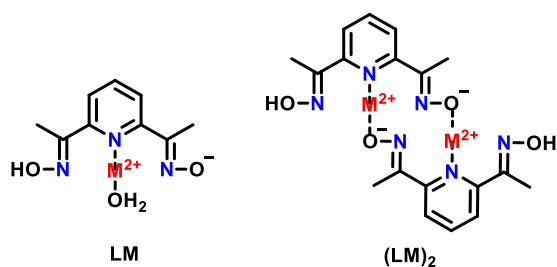
Figure 2-17. *Monomeric and dimeric complex structures that may form in the solution.*
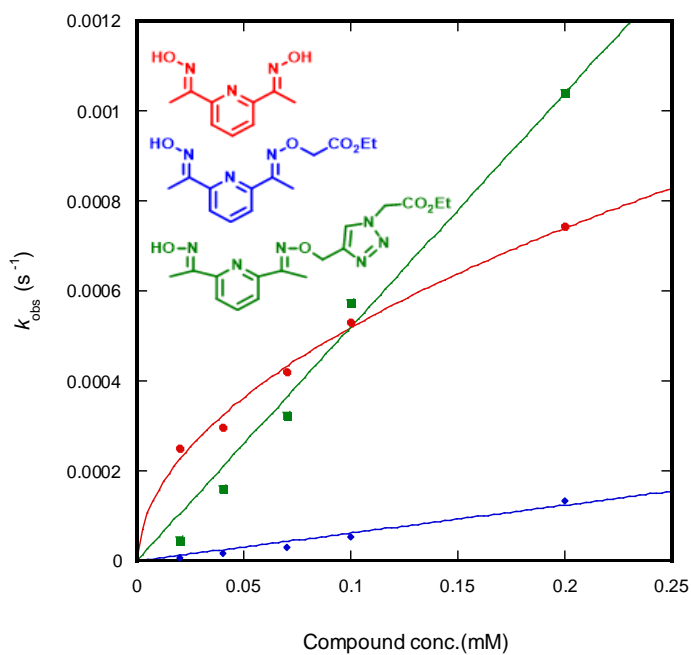
Figure 2-18. *Relationship between the observed rate constants for PNPA cleavage with the concentrations of compounds 2, 5, and 9 (0.02-0.2) using ZnCl$_2$ (1 mM), in HEPES (100 mM, pH 7) at 25 °C (these were single measurements see the data in the appendix).*

67

These rate constants show that the change in ligand structure has a significant effect on the reactivity towards PNPA. As compound **2** has two nucleophilic sites, the rate constant needs to be corrected for this statistical effect to compare the intrinsic reactivity of the oxime within each complex. The difference between **5** and **9** may reflect their capacity to coordinate Zn^{2+} effectively, with the triazole group in **9** providing a more effective coordinating group than the ester in **5**. The additional coordination group may also prevent the formation of inactive dimers for these compounds. The lower coordination number in **2** may lead to a more reactive complex, although usually this also leads to a lower complexation constant for the Zn^{2+} ion.

2.6.8 pH Effect on the Hydrolysis Rate:

Two different concentrations (0.2 and 0.02 mM) of compound **9** were used to investigate the pH effect on the hydrolysis rate of PNPA over a pH range of 7.2-8. The findings showed that the hydrolysis rate increases only slightly over this pH range, and so the catalysed reaction is not very sensitive to the pH of the solution. Equation 2-3, which assumes that the complex needs to be ionised to be active, was fitted to both sets of data as shown in Figure 2-19 and provides pKa values for the complexes (7.4). As these are the same within error, suggesting that this complex does not undergo any significant dimerisation under these conditions. Similarly, the limiting rate constants (0.0003 and 0.003 for 0.02 and 0.2 mM respectively) show a satisfactory first-order dependence, consistent with the data described above.

$$\log k_{obs} = \log\left(k \; \frac{10^{-pka}}{\left(10^{-pka} + [H^+]\right)} \right) \qquad \textbf{Equation 2-3}$$
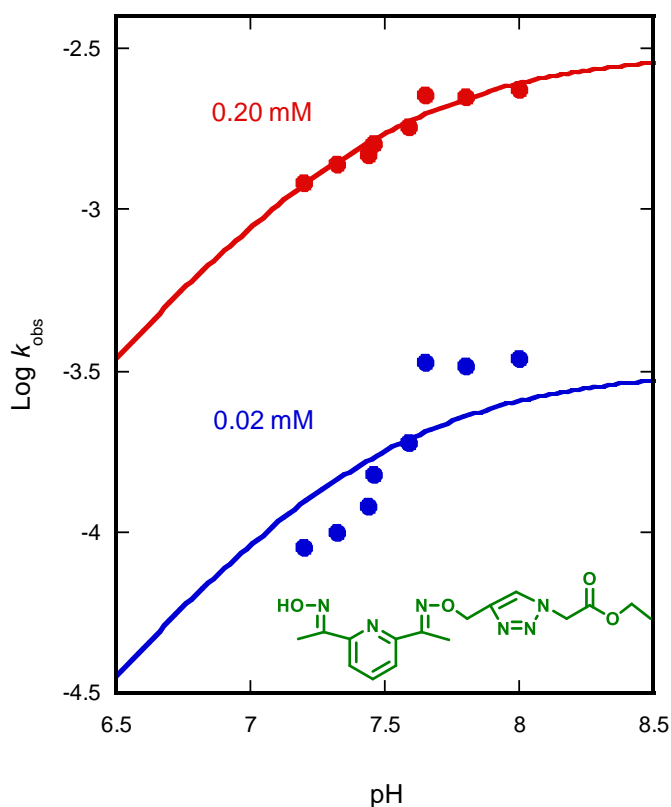
Figure 2-19. *Variation of the pH to investigate its effect on the reactivity of compound **9** (0.2, 0.02 mM) in the presence of ZnCl₂ (1 mM) during the PNPA hydrolysis (these were single measurements, see the data in the appendix).*

2.7 Conclusion:

The aim of this investigation was to assess the oxime-Zn^{2+} complex as a headgroup that can be attached to the lipophilic moiety and find the best conditions (concentrations and the pH value) to enhance the hydrolytic reaction. The findings from this study make some contributions to the previous literature.[136, 137]

From these experiments, a number of conclusions can be made. This study has shown that metal ions do not enhance the hydrolysis of the substrates in an aqueous solution in the absence of the ligand. Furthermore, the ligands do not suffer from the hydrolysis in the presence of the metal ions (Zn^{2+}). This can be attributed to two reasons: the first is that the oxime headgroup and the ester in the ligand are separated by a methylene group. The second reason is that the intermediate that forms after binding the metal ions to the ligand will be more efficient in the catalytic hydrolysis of the substrate ester group than the ligand itself as mentioned in the literature.[139]

The complexes of the oxime containing ligands with short organic arms (**2**, **5**, **9**) lead to increased hydrolysis rates compared to the background reaction. As expected from precedent in the literature [79,92,93] the hydroxyl group in these complexes (**2**, **5**, **9**) plays a key role. The complex of compound **2** revealed high hydrolysis rates compared to the complexes of compounds **5** and **9,** which they have one hydroxyl group on their sides enabling their participation in the catalytic ring. The complex of ligand **9** showed slightly better reactivity, this could be attributed to the rise in the electronic effect due to the ligand structure. Increasing the oxime concentration from 0.02 to 0.2 mM led to enhanced hydrolysis rates, this also was apparent when the pH of the medium was changed (Figure 2-19). With 0.2 mM the data fitted to Equation 2-3 more properly than 0.02 mM. Moreover, increasing the concentration of Zn^{2+} in the solution caused a significant increase in the reaction rates. To avoid dimerisation, the concentration of metal ions must be more than the ligand concentration. If the concentration of the metal ions is less than the ligand concentration, this will lead to form (LM)$_2$ complex, instead of LM (Figure 2-17).[136] The results of this chapter show that these complexes are satisfactory catalysts for the hydrolysis of the activated esters and provide a solution benchmark that can be compared with the membrane-embedded analogues.

Overall, this study strengthens the idea that the ligand structure plays an important role in the catalytic reactions.

2.8   Kinetic Measurements

The reaction progress was monitored at 400 nm for *p*-nitrophenolate and 450 nm for (HPTS) with a Cary 300 Bio UV-Vis spectrophotometer with a Cary temperature controller set at 25 °C. pH measurements were carried out with a Mettler Toledo pH meter.

HEPES was used as the buffer (stock solution of 250 mM, pH was adjusted to 7 using NaOH, 1N). The stock solution of PNPA (10 mM) was prepared in dry acetonitrile and the reaction mixtures for kinetic studies contained 4% (v/v) acetonitrile. A stock solution of the oxime ligands **2**, **5** and **9** (10 mM) were prepared in dimethyl sulfoxide, 17 µL-50 µL volumes were taken to mix with the metal solution in a buffer (the sample contains 2% (v/v) dimethyl sulfoxide). The required volumes of the metal solution and the ligand were mixed in HEPES buffer and the substrate was added finally to give the final volume 2.5 mL. The observed rate constants for the reactions were calculated using KaleidaGraph 4.5.0 programme by fitting a first-order rate equation to the data.

Chapter 3 -   Bilayer Membranes

3.1 Aims

This study aim was to prepare an artificial bilayer membrane containing different embedded ligands and to investigate the catalytic efficacy of a hydrolysis reaction of ester substrates. The research also aimed to control the reactivity of this metallovesicular system and increase the catalytic efficiency of the reaction. Moreover, we sought to demonstrate the role of zinc metal ions in the catalytic hydrolysis, using kinetic studies to follow the rate of reactions.

Instead of the membrane transducer molecules that were used (Figure 3-1B),[124,125,126] we used a ligand with one headgroup (shown in Figures 3-4 and 3-5). The essential idea was to investigate the catalytic reaction on the surface of the vesicle and to compare it with the short surfactants in a solution and with the previously designed systems. The differences between the transducer system and the proposed system are illustrated in Figure 3-2.
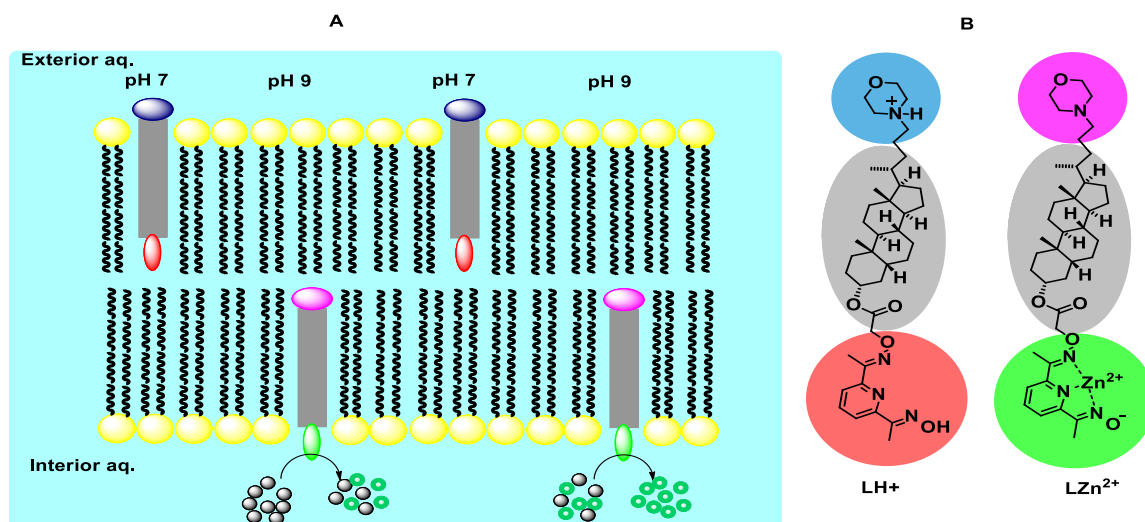
Figure 3-1. A) The transducer that is incorporated in a lipid membrane can translocate when it has two headgroups. One of the headgroups is polar (blue) and prefers to stay in the aqueous layer. The other one is nonpolar (red) prefers to sit in the membrane. When the output signal is added (base) the polar headgroup will deprotonate and becomes nonpolar (purple) then enters the membrane. This enables the nonpolar headgroup (red) represents a pro-catalyst to reach another side of the membrane and to bind the cofactor (Zn^{2+} ions). B) Synthetic transducer molecules, LH$^+$ represents Off state and LZn^{2+} represents On state (figure is adapted from ref. 124).

There are some important differences between the transducer system and the one headgroup system. In the transducer system, the reaction occurs inside the vesicles and it cannot be triggered without an input signal outside the vesicle, affecting the other end of the transducer. The reaction is catalysed inside the vesicle (an encapsulated reaction). On the other hand, in the one headgroup system, it is not possible to use an encapsulated reaction as described above, as the reaction starts during the synthesis of the vesicle. Therefore, we use the fact that the one headgroup that faces the outside is able to catalyse the reaction after it binds the metal ion (which can be added to the outer phase of the vesicles). In this case, the reaction occurs in a much larger volume; the comparison is shown in Figure 3-2.
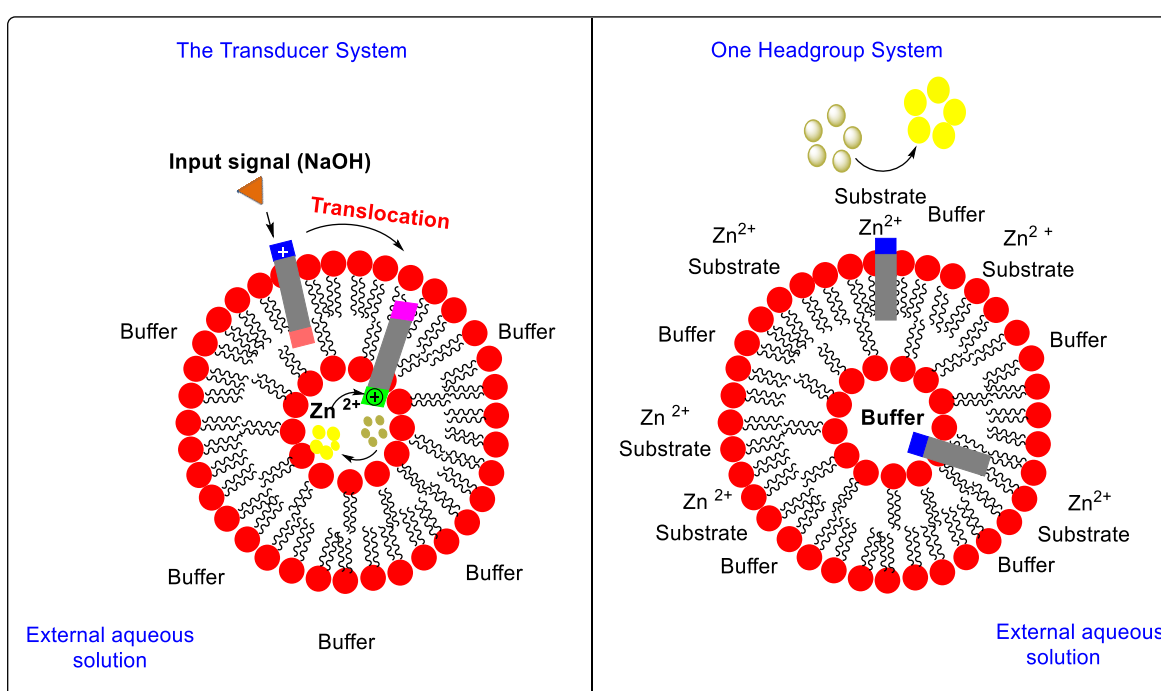
Figure 3-2. The previous transducer system (left) and the one headgroup amphiphilic ligand (right) orientated in the membrane.

The merit of the one headgroup system is that it does not need the control or input signal as for the transducer system, and components can be added after the vesicles have been created. In Chapter 2, different ligands were examined to identify the best headgroup and the proper conditions for the hydrolysis reaction. In this chapter, the same type of ligands are used but with longer hydrophobic tails to allow them to be embedded into membranes.

3.2   The Approach and the Design

The molecules need to be amphiphilic ligands, which include two moieties; one hydrophilic and the other hydrophobic. There are some requirements for the selection of the components of these membrane embedding molecules:

- The tail must be hydrophobic and long enough to insert in the membrane (a long aliphatic tail allows the ligand to embed easily into the membrane).

- The molecule must be rigid and cannot loop or twist back to form U-shaped as in Figure 3-3 (if it is flexible it will be lost from the membrane).

- The headgroup should be a chelating agent that can bind metal ions to become active for catalysing the hydrolysis of activated esters.
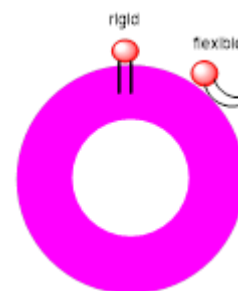
Figure.3-3. *U-shape molecule and rigid molecule orientation in the membrane*

Complexes that are formed from ligands containing oxime derivatives and Zn^{2+} ions will be used as headgroups (as described in Chapter 2), while cholesterol or lithocholic acid acts as a membrane-anchor.

3.3   The Selection of Membrane-Anchor

Cholesterol is a good membrane-anchor as it is a natural fundamental element of many cell membranes.[3, 46, 149, 150, 151, 152] Similarly, bile acids (lithocholic acid among them) have been utilised as the main building blocks to design artificial hosts for molecular recognition in different systems (organic, solid-state or aqueous).[153] Cholesterol is able to penetrate freely the bilayers perpendicular to the membrane plane.[151] It is a reasonably planar, rigid molecule and binds strongly to the membrane bilayer.[151] Cholesterol molecules are around 17 Å long[154] (a lithocholic acid molecule has a similar length), approximately half of the bilayer membrane thickness (40 Å)[155], which provides a good substructure for incorporation into the membrane.

To investigate the reactivity of the catalysts at the membrane interface, we decided to choose different lipophilic membrane-anchors. Besides cholesterol and lithocholic acid, an aliphatic chain that is either saturated or unsaturated was chosen. The aim was to discover whether

there is any difference in the activity that is obtained when the membrane-anchor is changed. The linker between the hydrophilic and lipophilic moieties is a simple ester, as shown in compounds **10-15** (Figure 3-4). Aliphatic chains are much less bulky and less rigid than cholesterol as a membrane anchors.

Compounds **10-15** (Figure 3-4) were prepared as shown in Scheme 3-1:

Step 1: Preparation of the hydrophobic tail ester,
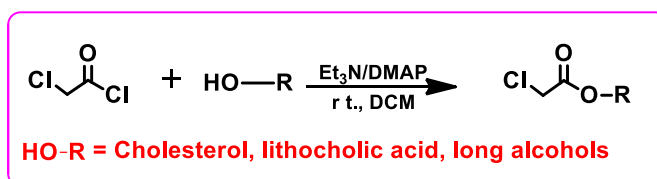
Step 2: Preparation of the headgroup,
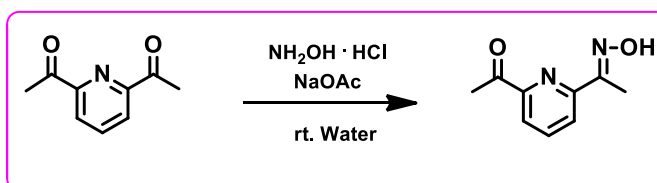
Step 3: Join the headgroup with the tail,
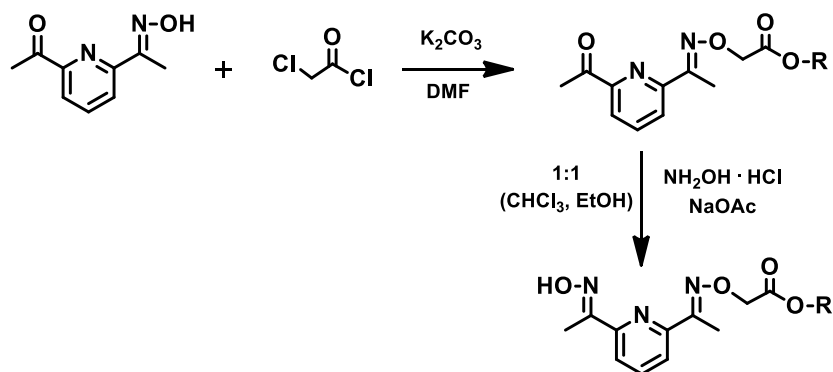
Scheme 3-1: *Schematic to prepare the membrane ligand* **10-15** *in three steps.*
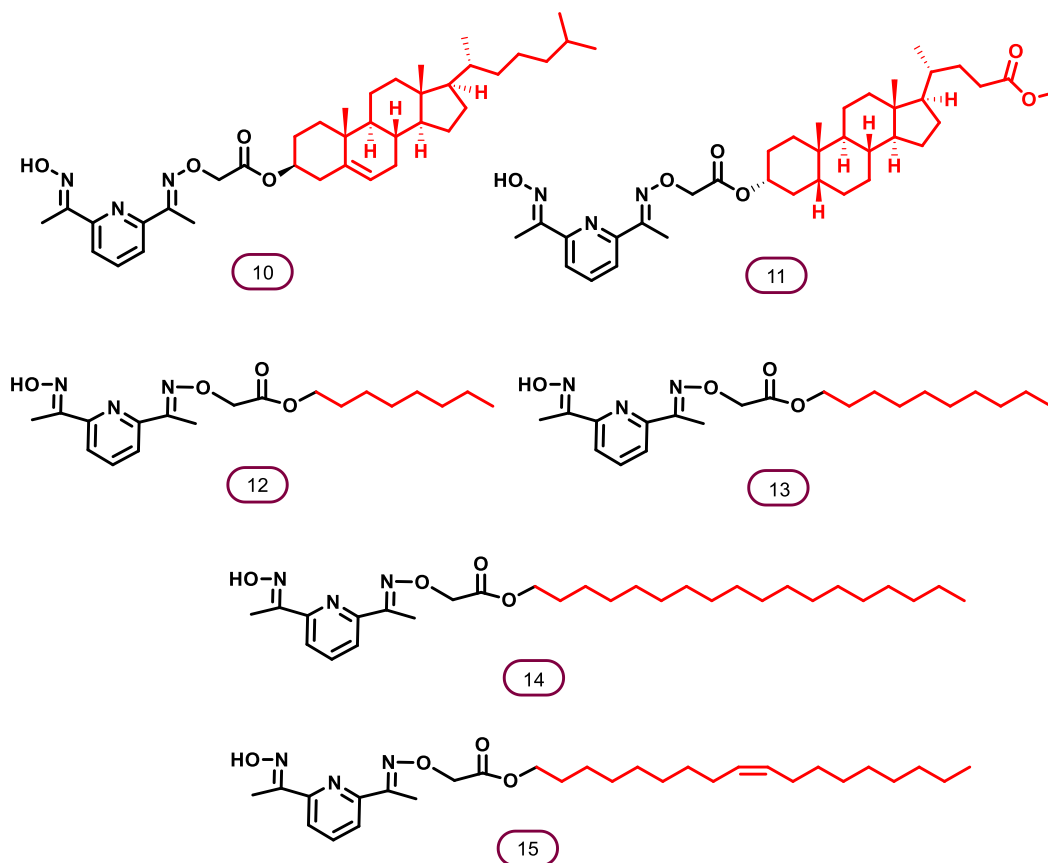
Figure 3-5. Synthetic amphiphilic ligands 10-15 with different lipophilic tails for the membrane catalysis reactions, prepared as shown in Scheme 3-1.

It is also of interest to determine the effect of changing the nature of the linker, from one without a binding site (as shown in the linkers of compounds **10-15**), to one with an extra binding site (in the form of a triazole moiety, as shown in the linkers of compounds **16-23** (Figure 3-5). The compounds were prepared as shown in Scheme 3-2. The triazole group was chosen as it is a common functional group created in the course of click reactions. The consequences and potential limitations of using this process to combine molecular modules are important to understand. This adds an extra comparison by changing the length of the linker as this would change the distance between the headgroup and the lipophilic moiety as in compounds **16-19** (the difference between **16** and **17** is the linker between the headgroup and the tail; it is similar to that between **18** and **19**). This length in the linker may give the headgroup more flexibility so that it can project further into the aqueous layer, and may alter the way the ligands interact with the metal ion.

Steps 1 and 2: Preparation of the hydrophobic tail
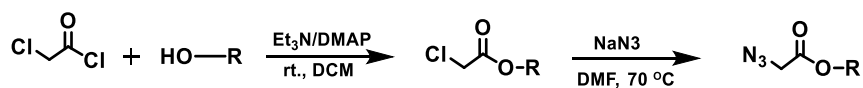
HO-R = Cholesterol, lithocholic acid, long alcohols

Step 3, 4 and 5: preparation of the headgroup
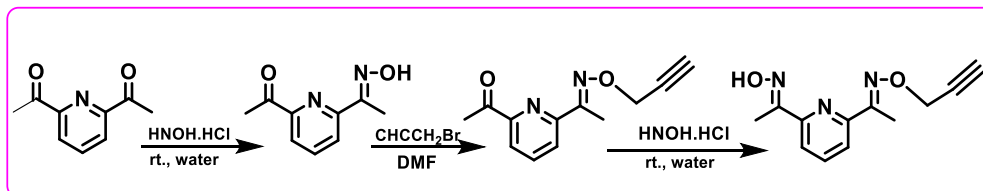
Step 6: Join the headgroup with the tail by click reaction,
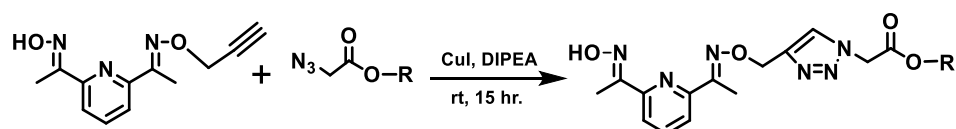
Scheme 3-2. *Schematic to prepare the membrane ligand **16-23** from click reaction by six steps.*
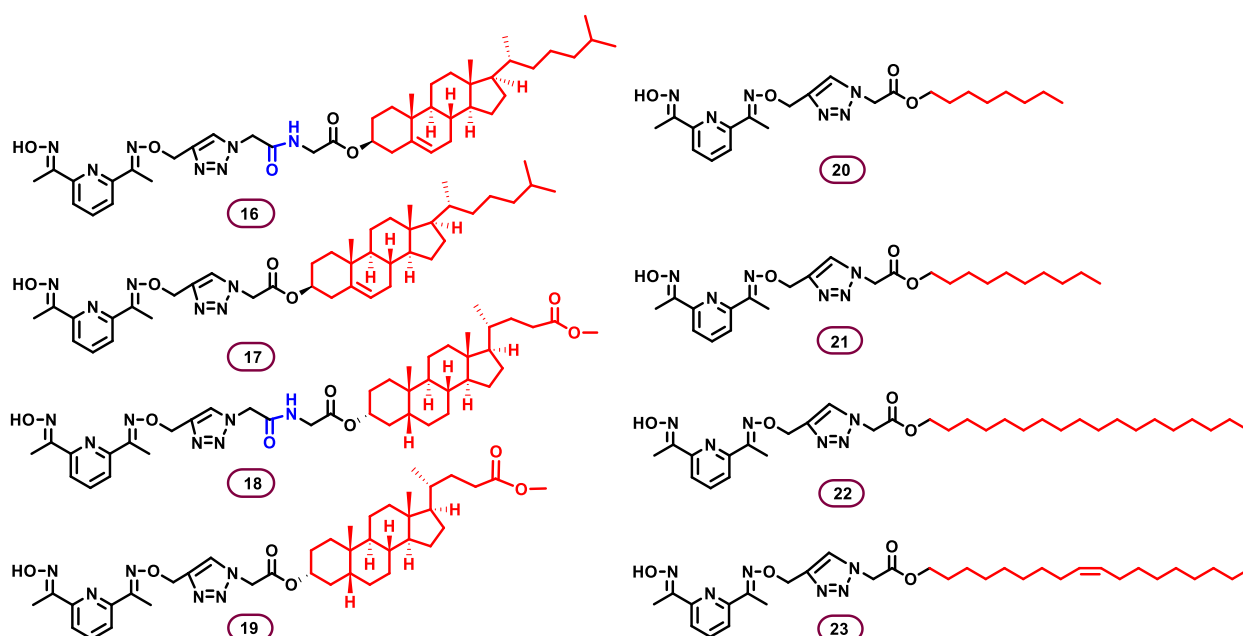
Figure 3-5. *Synthetic amphiphilic ligands **16-23** with different lipophilic tails for membrane catalysis reactions, each prepared using a click reaction.*

3.4 Bilayer Membrane Matrix

One of the main requirements for these bilayer membrane systems is that the molecules reorganise in the membrane rapidly (see Chapter 1, molecular recognition section). Therefore, the lipid needs to be in a fluid phase at room temperatures to allow the incorporated molecules to be diffuse freely within the membrane. Egg yolk phosphatidylcholine (EYPC) is a commercially available lipid which is provided with a mixture of saturated and unsaturated alkyl groups with different chain lengths (C14 - C20)[156], Figure 3-6. EYPC forms vesicles spontaneously when it is mixed with a buffer solution or water. The structure of the phospholipid molecule generally consists of two hydrophobic fatty acid "tails" and a hydrophilic "head" consisting of a phosphate group as Figure 3-6 illustrates schematically.
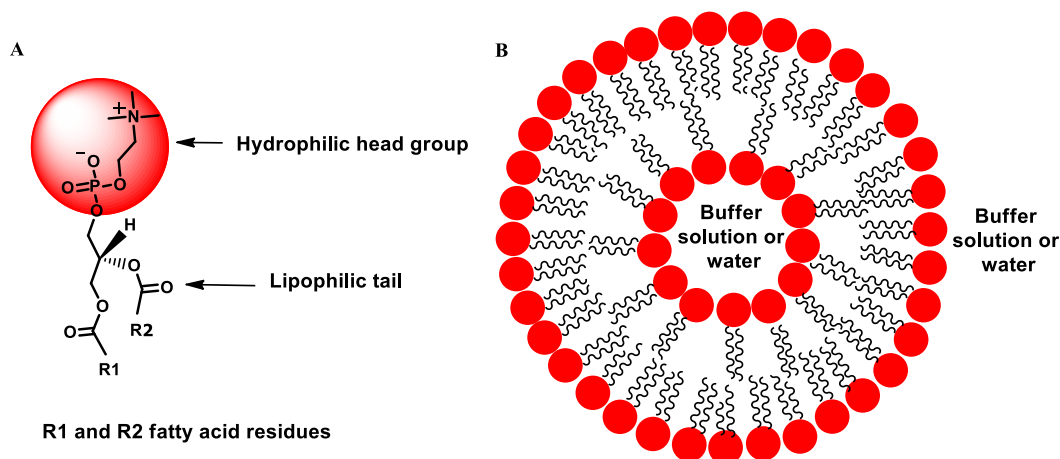
Figure 3-6. Vesicles as a cell membrane-like model.

Another lipid mixture chosen for this study was 1,2-dioleoyl-sn-glycero-3-phosphocholine (**DOPC**) and 1,2-dioleoyl-sn-glycero-3-phosphoethanolamine (**DOPE**) with a ratio of 3:2, as described by Hunter *et al.* [124, 125] The specific ratio was chosen in order to maintain a pH gradient between the outside and the inside the vesicles.[157, 158] However this is not essential for our experiments due to the unchanged pH that we used inside and outside the vesicles. The use of this mixture helps to link the obtained data with the previously published data with similar complexes and to discover whether the nature of the lipid makes significant differences in the activity of the complexes. Figure 3-7 demonstrates the structure of the lipids.
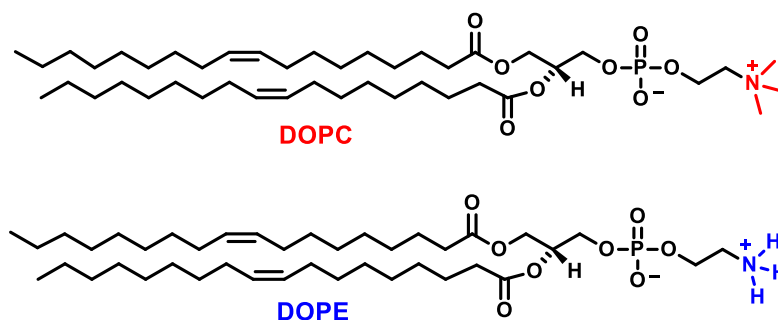
Figure 3-7. DOPC and DOPE lipids basic unit structure.

In the present system, the chosen vesicles were unilamellar vesicles (200 nm) doped with ≈ 2.5 % ligand as described by Hunter *et al.*[124, 125] This size was obtained using a standard manual extruder "LipoFast" (Figure 3-8). The vesicle solutions were only stable for a few days (2-3 days) if the solution was kept at a low temperature (4 °C); however, König and Jose[159] claimed that the stability is dependent on the concentration of the vesicle solution. High vesicle concentrations are more unstable compared with dilute solutions, which can be stable for more than three months if they are stored at 4 °C. In all cases, the vesicle size had to be confirmed by dynamic light scattering (DLS).
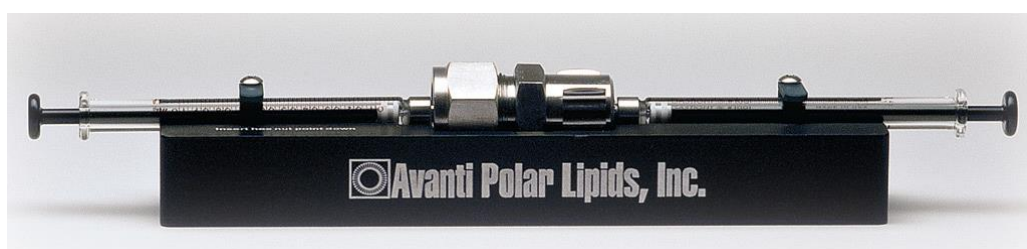
Figure 3-8. Avanti mini extruder to prepare large unilamellar vesicles (image from https://avantilipids.com/divisions/equipment-products*).*

The vesicles are encapsulated a small amount of buffer solution; the metal ions and the substrate were added to the bulk solution outside the vesicles. Hence, the metal ions would bind to the oxime headgroup and catalyse the substrate hydrolysis.

In this chapter, the same reactions were used as discussed previously in Chapter 2, and which are reproduced in Scheme 3-3.
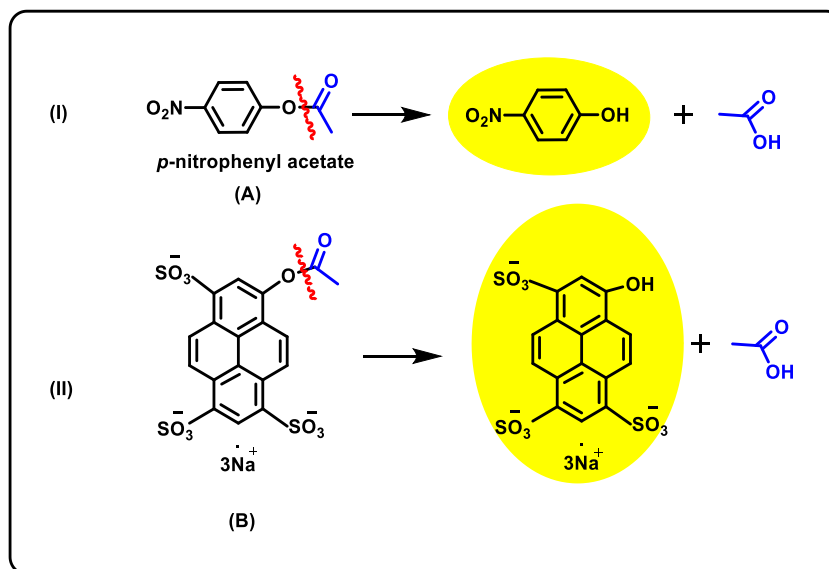
Scheme 3-3. *The two hydrolysis reactions that were used in this study.*

The difference between the two substrates is their solubility in an aqueous phase (**B** is highly charged when the pH is neutral and prefers to sit in the aqueous layer and does not permeate the membrane),[124, 125, 126] whereas **A** is neutral and it can readily cross the membrane and reach the interior of the vesicle as well as the bulk solution phase. We have already shown that the zinc-oxime complexes can hydrolyse these substrates, the reaction can be followed spectrophotometrically by the release of *p*-nitrophenol at 400 nm and 8-hydroxypyrene-1,3,6-trisulfonate trisodium salt at 450 nm.

3.5   Reactions at Vesicles versus Reactions in Solutions

An increase in reaction rates in membranes has been attributed to the strong binding between the reagent and the bilayer, which produces higher local concentrations. Other reasons for the raised reactivity implicate the changes in the local environmental conditions as well as binding to the bilayer. Many systems described involving one fixed component

in the vesicular interface, either it is incorporated into an inactive bilayer or forming the bilayer itself if it is an effective surfactant. The second component is usually added after the vesicle is formed. Systems, where both components are constrained in the vesicle, have also been examined, and in these instances, the rate acceleration was also attributed to the enhanced local concentration.

Menger *et al*. explored the vesicle/vesicle reaction when a nucleophilic amphiphile was inserted into phospholipid vesicle and the electrophilic amphiphile was inserted in another phospholipid vesicle (both the nucleophile and the electrophile contain the same lipophilic moiety) as illustrated in Figure 3-9, A and B. The researchers found that the reactivity and the rates are dependent on the exposure of the membrane-bound functionalities to the external water.[160] They also studied the vesicle-to-vesicle transfer process by collision (Figure 3-9, D). A shorter half-life (0.75 min) for the reaction was observed when **B** (not embedded into vesicles) was added to the vesicles solution of **A**. The researchers' explanation was that the electrophilic ester was transferred into the vesicles bearing the nucleophile followed by fast intravesicular hydrolysis and that direct reaction between the two functional groups, when embedded in different vesicles, was slow.[161]
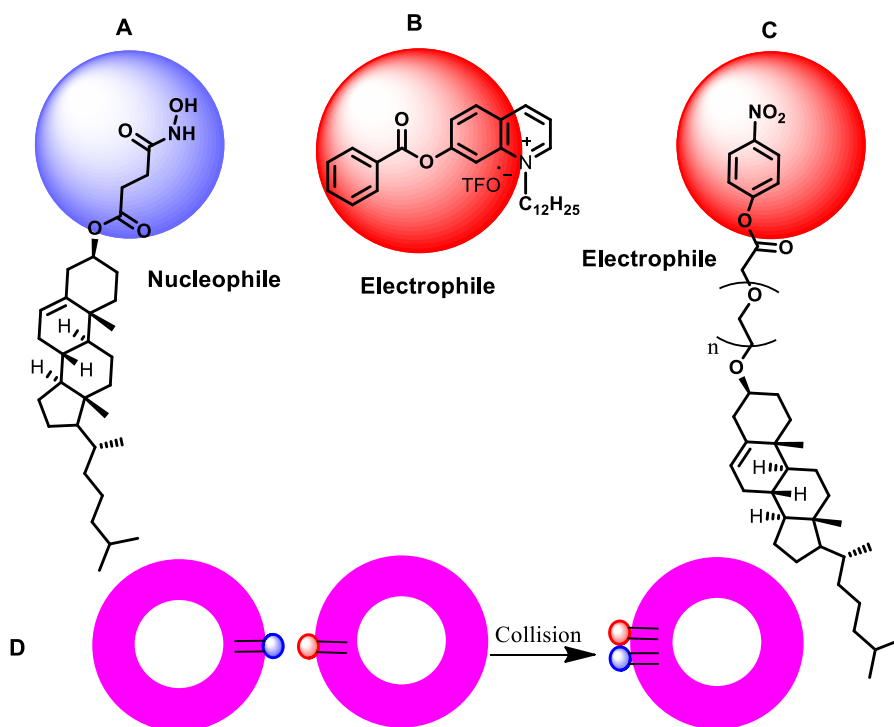
Figure 3-9. *Vesicles-vesicles collision model*

König *et al*. [67, 162] created artificial bilayer membrane systems to be used as catalytic systems that operate more efficiently than their solution counterparts. They investigated the effect of membrane incorporation on amphiphilic ligands for **ruthenium** (II) as photosensitizer and water oxidation catalysts (Figure 3-10) to study the efficiency of photocatalytic water oxidation, compared to the oxygen evolution of a homogeneous aqueous solution containing photosensitizer.[162] This mimics photoactive membranes in biology and allows photocatalytic water oxidation using very low concentrations of the catalyst (500 nM) which cannot be accomplished in a homogeneous solution system.
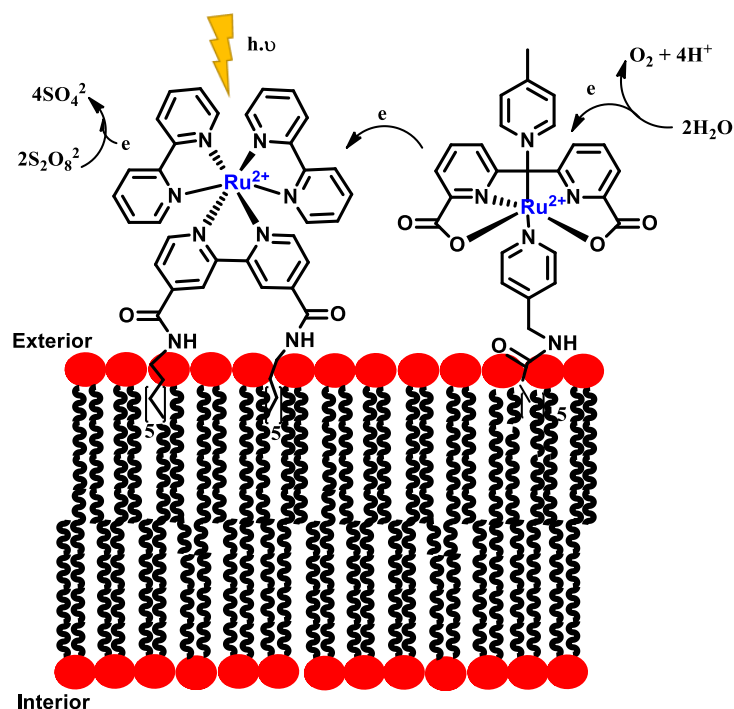
Figure 3-10. *Schematic reaction mechanism of photocatalytic water oxidation using amphiphilic water oxidation catalyst and amphiphilic photosensitizer embedded into vesicles.*

Bizzigotti's [163] system showed a remarkable decrease in the rate when both components were bound to the bilayer. However, in this case, the components were in close proximity and they were both able to react with a second reactant that is not embedded (the system described in Chapter 4)

3.6   Results and Discussion

The findings presented in Chapter 2 show that it is not convenient to use bulky compounds (such as cholesterol functionalised with different ligands) in solution even when a very low concentration of the ligand was used. Therefore the activity of ligands with membrane anchors that were embedded in vesicles could not be compared directly with the same compounds in bulk solution. The statistical distribution of the transducer in the interior and exterior sides of the bilayer membrane is 50:50.[124, 125, 126] Consequently, half of the ligand concentration will have the catalytic oxime group-oriented to the inside of the vesicles. The other half will have the recognition group facing towards the outside the vesicles (Figure 3-11). Thus, we already know that the reactivity in the bilayer membrane, which we designed, will be less than that for the same total concentration of complex in bulk solution (where all the molecules will be active because of the absence of internal and external phases).
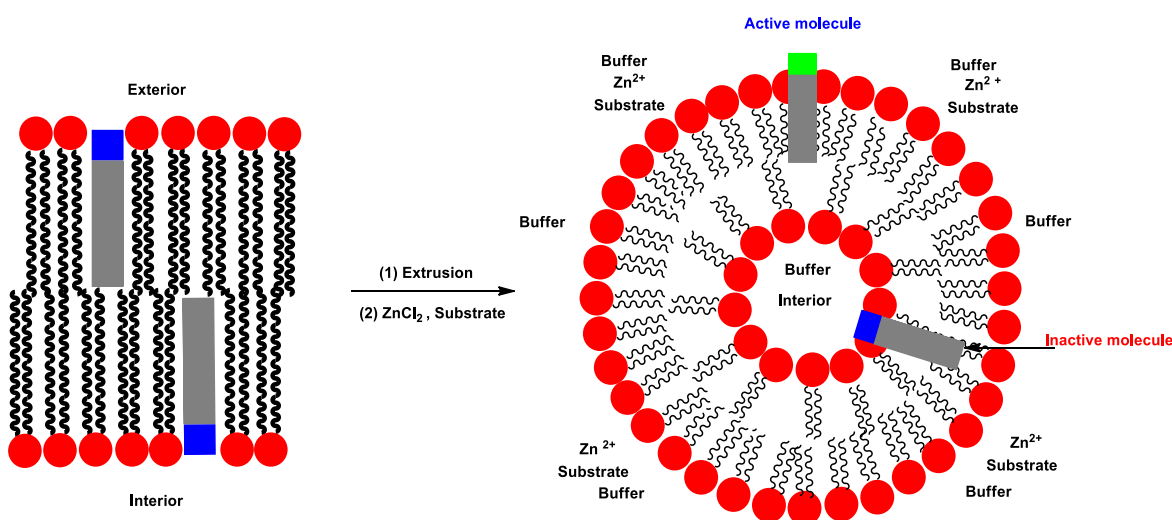
Figure 3-11. *The orientation of the ligand molecules in the bilayer membrane.*

The data have been collected from the UV-Vis measurements were fitted nicely into the burst equation (Equation 3-1) as they are not fitted to first-order as Figure 3-12 shows.

$$P = \frac{k_2 k_3 \, e_0 t}{k_2 + k_3} + \frac{k_2^2 e_0 \{1\text{-}\exp[-(k_2 + k_3)\,t]\}}{(k_2 + k_3)^2} \qquad \text{Equation 3-1}$$

k_2, k_3 the hydrolysis rate, t = time, e_0 = initial catalyst concentration, P = the product. This indicates that the rate-determining step in the membrane reaction is different from what occurs in the solution. In solution, burst kinetics are not clearly observed, although, at the lowest concentrations used, deviations from the first-order behaviour might be evident (Figures 2-16 and 2-17). Under these conditions, it may be that the first-order rate constant for the hydrolysis of the acylated intermediate becomes the rate-limiting step as the lowered concentration of complex leads to a slower second-order reaction between the complex and substrate.
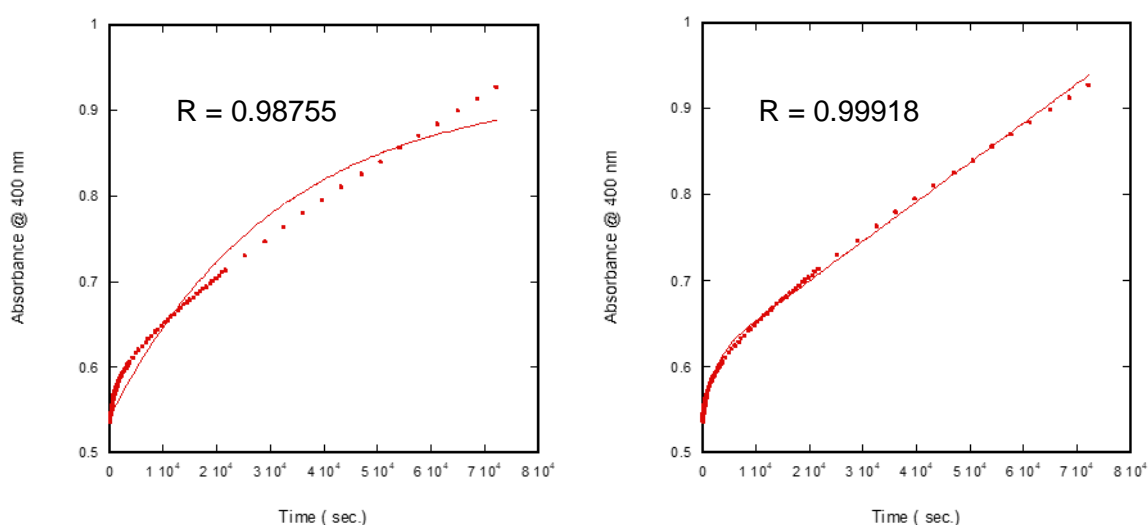
Figure 3-12. *compound **11** (50 μM) embedded into vesicles (2 mM), ZnCl₂ (250 μM) and PNPA (250 μM) were added to outside the vesicles. The experiment was run in HEPES buffer (100 mM, pH 7) at 25 °C. On the left, fitted to the first-order equation, on the right, fitted to the burst equation, R = goodness of fit. These were single measurements.*

The reformation of the complex is the RLS, then the burst, the burst expected to occur when $k_2 \gg k_3$ and when $k_3 \gg k_2$ no burst will occur (k_2 is the rate constant for acylation the ligand, and k_3 is is the rate constant for deacylation).
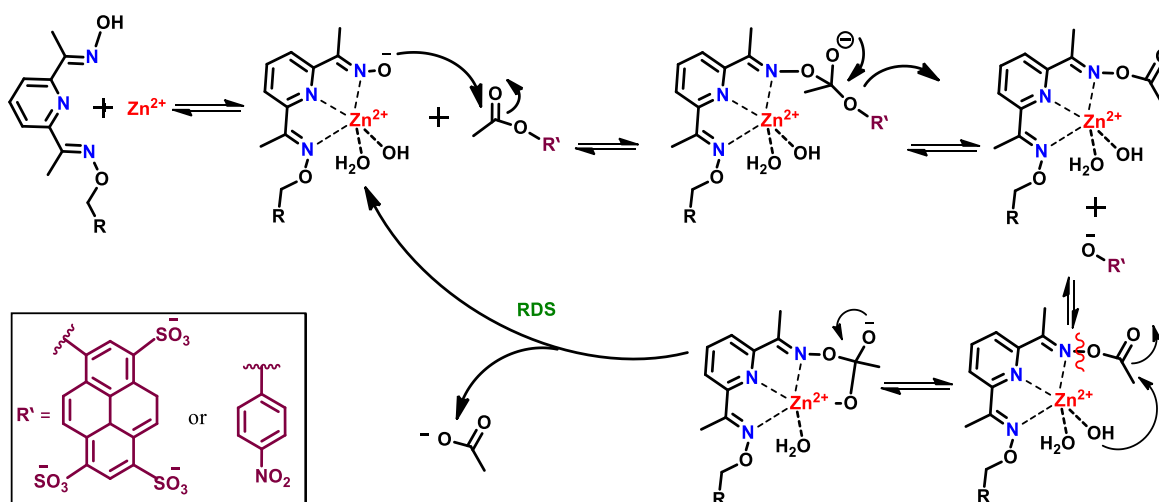
Scheme 3-4. *The suggested mechanism for the ligand-metal binding and hydrolysis of the substrate in the membrane.*

3.6.1 Varying the Concentration of the Embedded Ligand

Increasing the concentration of the ligand in the presence of the same concentration of lipid increases the bulk and local catalyst concentration and this might be expected to lead to enhancing the hydrolysis rate. The experiments results are shown in Figures 3-13 and 3-14.
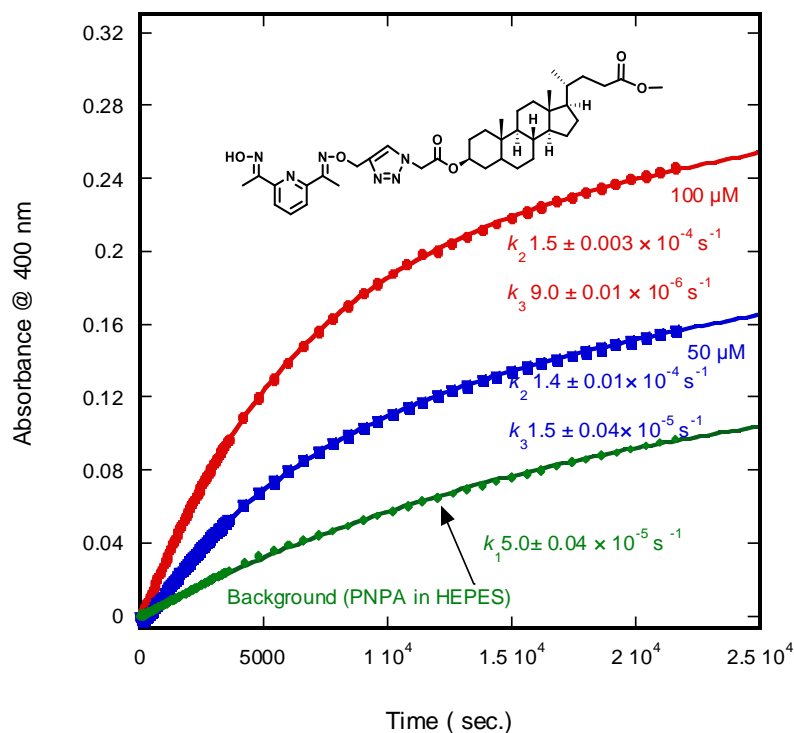
Figure 3-13. *Ligand concentration effect, red curve; (100 μM) and blue curve; (50 μM) of ligand 19 embedded into lipid (2 mM). $ZnCl_2$ (250 μM) and PNPA (250 μM) were added to outside the vesicles. Green curve only PNPA (250 μM) in HEPES buffer (100 mM, pH 7), the experiment was run at 25 °C, these were single measurements.*

The results showed a slight increase in k_2 value (acylation) and decrease in k_3 value (diacylation) of the rate hydrolysis for PNPA when the ligand (compound **19**) concentration increased (Figure 3-13). While the results showed a slight decrease in both k_2 and k_3 for HPTSA hydrolysis when the concentration of compound **16** increased from 50 μM to 100 μM (Figure 3-14).

86
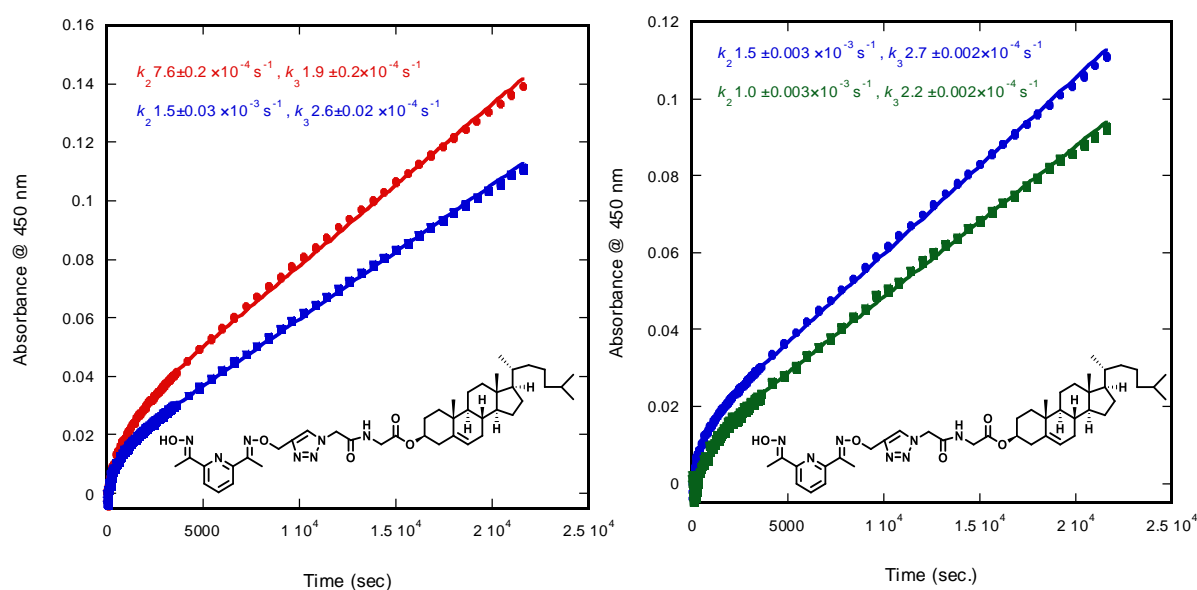
Figure 3-14. *Ligand concentration effect, red curve (100 μM) and a blue curve (50 μM) of ligand 16 embedded into lipid (2 mM). ZnCl₂ (250 μM) and HPTSA (250 μM) were added to outside the vesicles the experiment was run in HEPES buffer (100 mM, pH 7) at 25 °C. The green curve, vesicles (2 mM) of lipid only, ZnCl₂ (250 μM), HPTSA (250 μM) and ligand 16 (50 μM) were added to outside the vesicles. These were single measurements.*

An attempt was made to increase the local concentration of lipid and ligand, which will lead to a greater catalytic surface, the vesicles concentration and the incorporated ligand were increased. The vesicle lipid concentration was increased from 2 mM to 4 mM and the ligand that was embedded into the vesicles was increased from 50 μM in 2 mM vesicles to 200 μM in 4 mM vesicles.

Increasing both the catalyst and lipid means that the bulk concentration increases; however, the local concentration in the membrane remains constant. The results of Figure 3-16 showed that there is a small decrease in the k_3 value when the ligand concentration was increased from 100 μM in 2 mM vesicles ($k_2 = 3.7 \pm 0.2 \times 10^{-4}$ s^{-1}, $k_3 = 2.2 \pm 0.1 \times 10^{-4}$ s^{-1}) to 200 μM ($k_2 = 2.4 \pm 0.04 \times 10^{-4}$ s^{-1}, $k_3 = 1.2 \pm 0.01 \times 10^{-4}$ s^{-1}) and when the vesicles concentration increased from 2 mM to 4 mM including the ligand concentration of 300 μM (the ratio is 2 mM vesicles:150 μM ligand); the hydrolysis rate ($k_2 = 4.2 \pm 0.04 \times 10^{-4}$ s^{-1}, $k_3 = 1.7 \pm 0.01 \times 10^{-4}$ s^{-1}) is slightly enhanced. These values allow us to assume that when the ligand concentration increased more than 150 μM in the vesicle, the catalyst is inhibited from performing its job

87

due to forcing the molecules to exist close to each other and to form a cluster structure similar to that in Figure 3-15 below.
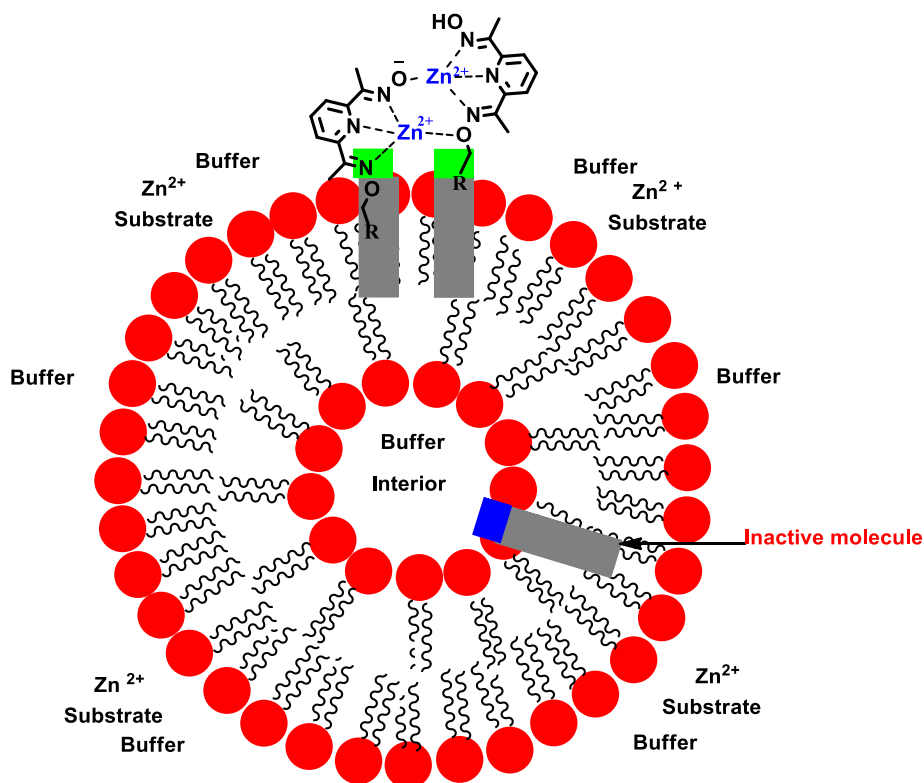
Figure 3-15. *Formation of the complex cluster due to aggregation of the ligand at the vesicles*

This process is similar to what can occur in solution when the ligand concentration is higher than the metal ion concentration. The problem in the vesicle solution is that even if the metal concentration is higher than the ligand concentration, this will not prevent inhibition because the ligand is constrained in the bilayer membrane of the vesicle and it cannot move or change its orientation. To reach high hydrolytic activity with metal complexes it is very important to retain their positive charge in the complex and to open coordination sites for binding with the substrate.

This study is unable to demonstrate how the ligand is distributed and directed in the vesicles. A plausible explanation for this might be that the increase in the ligand concentration and the metal concentration leads to aggregation on the vesicle surface. Accordingly, every two complexes close to each other will hinder the catalyst from hydrolysing the substrate. Lithocholic acid is one of the cholic acids which they are known to aggregate in the presence

of trivalent lanthanide ions[164,165] or some transition metal ion such as Zn^{2+}.[166] If this can occur in our system it will inhibit the hydrolysis somewhat.
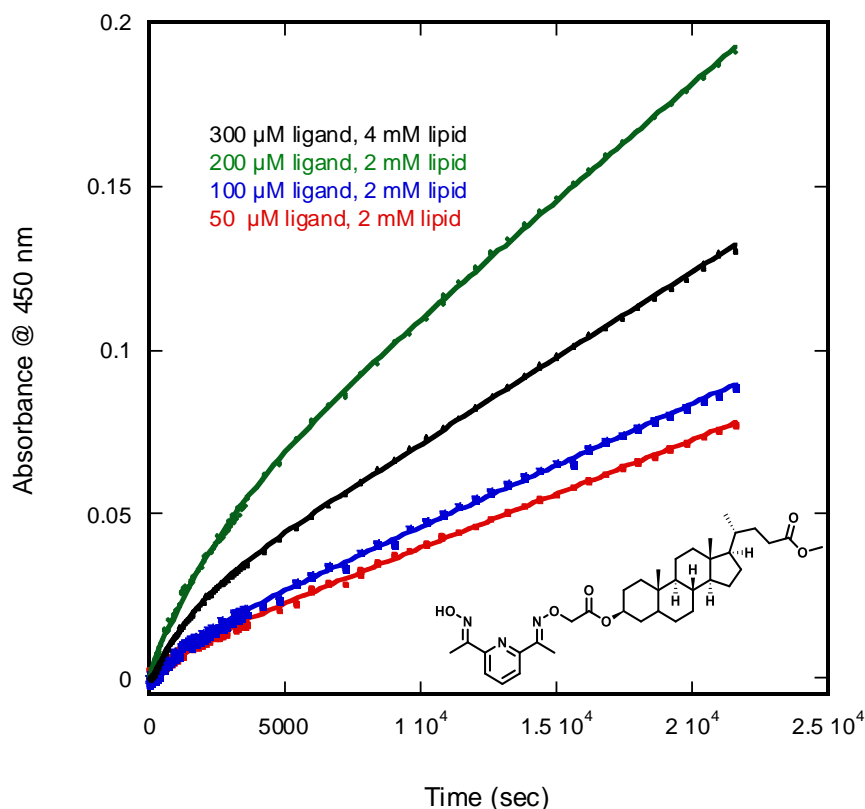
Figure 3-16. *Ligand concentration effect, green curve (200 μM), blue curve (100 μM) and red curve (50 μM) of ligand **11** was embedded into lipid (2 mM). ZnCl₂ (250 μM) and HPTSA (250 μM) were added to outside the vesicles, the experiment was run in HEPES buffer (100 mM, pH 7) at 25 °C, these were single measurements.*

The effect of the linker (the structure and the length) was investigated in this study with both steroid lipids, cholesterol and lithocholic acid tail. Compounds **16-19** were embedded into vesicles, ZnCl₂ and substrate were added to outside the vesicles. Figure 3-17 and Table 3-1 show there is no consistent effect for the glycin linker. Compound **17** which does not have glycin linker showed the higher k_2 value followed by compound **19**, and compound **19** exhibited the higher k_3 value between the selected compounds.
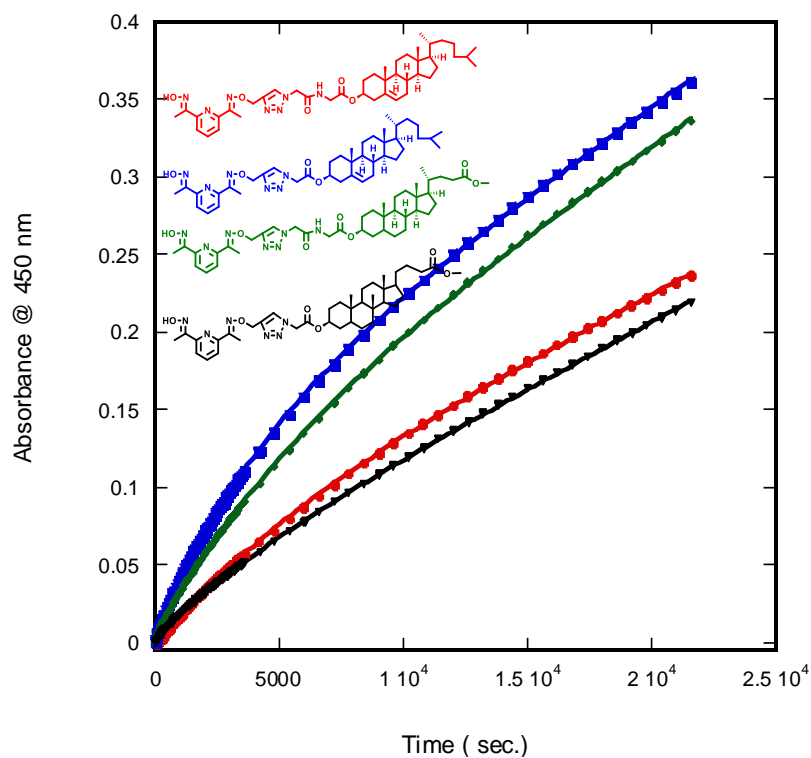
Figure 3-17. *Ligands **16** (red curve), **17** (blue curve), **18** (green curve), and **19** (black curve) in 100 μM concentration was embedded into vesicles (2 mM). ZnCl$_2$ (250 μM) and HPTSA (500 μM) were added to outside the vesicles, the experiment was run in HEPES buffer (100 mM, pH 7) at 25 °C, these were single measurements.*
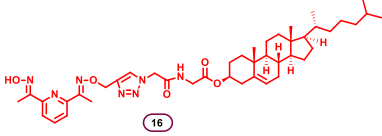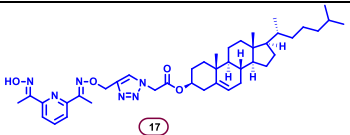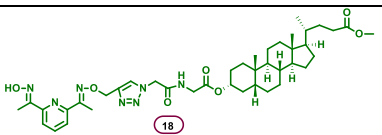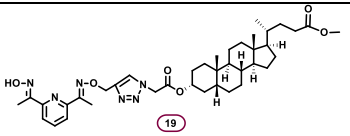
Compound structure	k_2 s^{-1}	k_3 s^{-1}
	$1.04 \pm 0.01 \times 10^{-4}$	$7.8 \pm 0.1 \times 10^{-5}$
	$1.7 \pm 0.01 \times 10^{-4}$	$7.0 \pm 0.1 \times 10^{-5}$
	$1.2 \pm 0.01 \times 10^{-4}$	$7.1 \pm 0.1 \times 10^{-5}$
	$1.2 \pm 0.02 \times 10^{-4}$	$1.3 \pm 0.02 \times 10^{-4}$

Table 3-1. *The hydrolysis rate constants for HPTSA (500 μM) hydrolysis in the presence of vesicles (2 mM) incorporated with ligands **16-19** (50 μM), ZnCl₂ (250 μM). The experiment was run in HEPES buffer (100 mM, pH 7) at 25 °C.*

3.6.2 Preparing the Catalytic Complex before Adding the Substrate

In order to be confident of the best way to prepare the systems, a comparison between two ways of preparing the metallovesicles was made. The formation of the hydrophilic complex from the headgroup (which is originally hydrophobic) and Zn^{2+} ions rather than inserting the ligand into the bilayer membrane was prepared in the normal way as shown in Figure 3-18– A. The $ZnCl_2$ and the substrate were added after preparing and purifying the vesicles, just before taking the measurements. In a slightly different approach, the dried bilayer film from the ligand which is incorporated in lipid was hydrated with $ZnCl_2$ solution; the GPC columns were already washed with $ZnCl_2$ solution. After purification, the vesicles were purified using a GPC column in the presence of more $ZnCl_2$ (250 µM) with the substrate (Figure 3-18– B). (Kinetic data are shown in Figure 3-19).
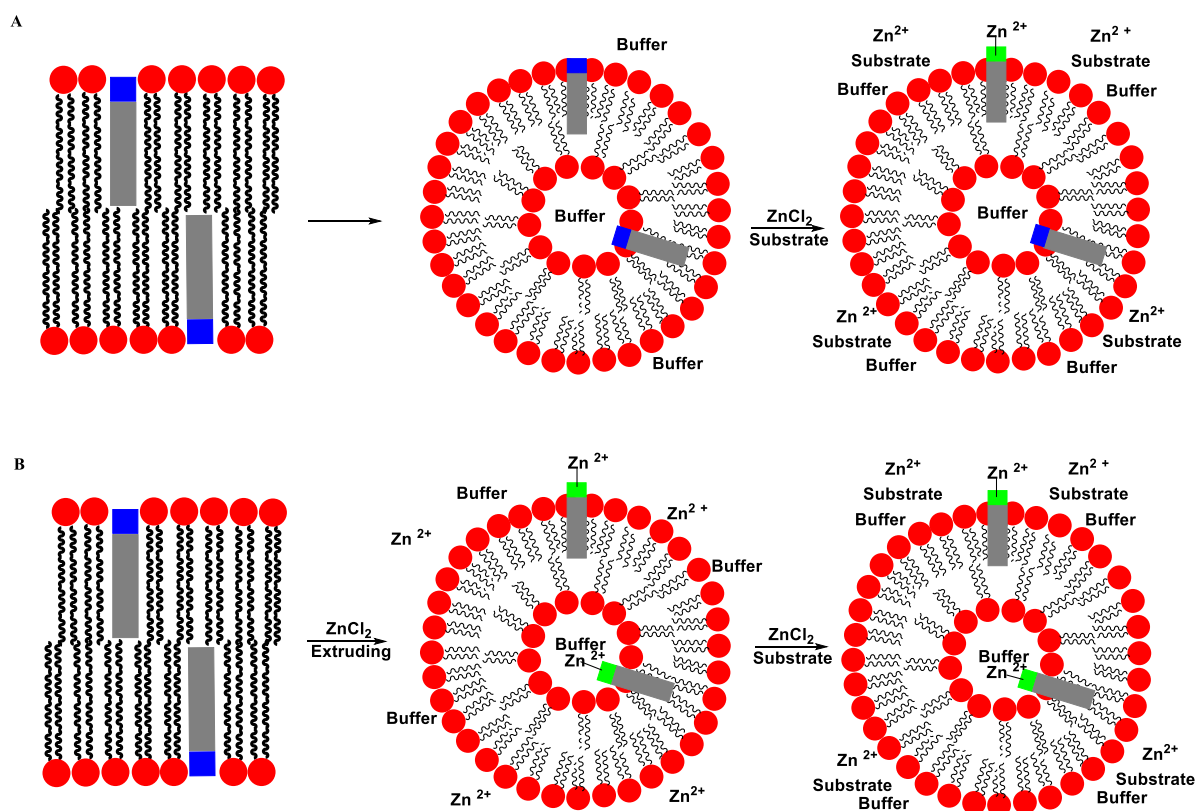
Figure 3-18. *The two possible ways to prepare the catalyst within the vesicles*

$k_2\ 7.2 \pm 0.3 \times 10^{-5}\ s^{-1}$, $k_3\ 3.4 \pm 0.3 \times 10^{-5}\ s^{-1}$

$k_2\ 1.4 \pm 0.04 \times 10^{-4}\ s^{-1}$, $k_3\ 6.4 \pm 0.2 \times 10^{-5}\ s^{-1}$

$k_1\ 6.7 \pm 0.08 \times 10^{-6}\ s^{-1}$
Background reaction
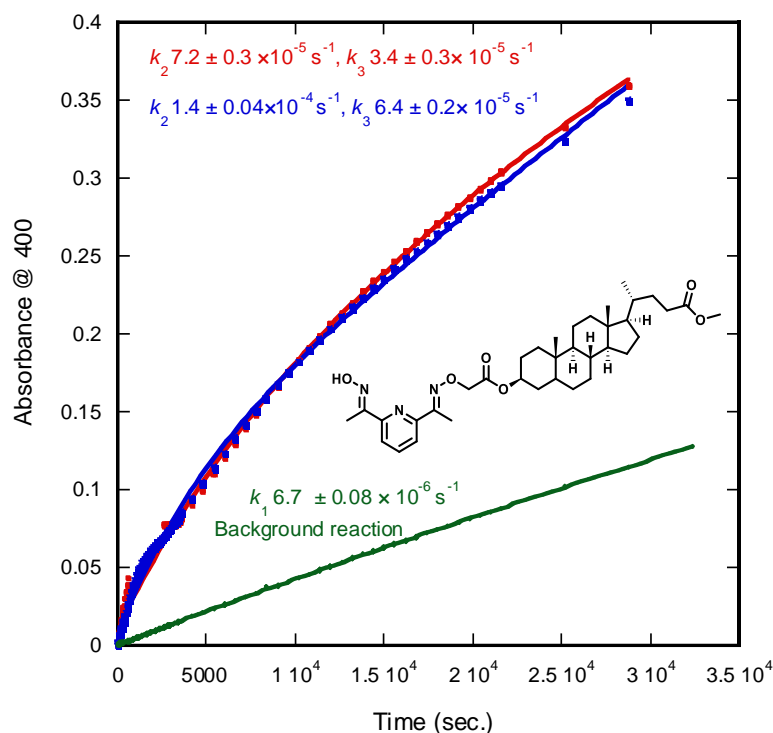
*Figure 3-19. The effect of the way of adding the Zn^{2+} ions. Ligand **11** (100 μM) is embedded into vesicles (2 mM). The red curve; $ZnCl_2$ (250 μM) was added to the vesicles solution before the purification using GPC column then $ZnCl_2$ (250 μM) was added to outside the vesicles with PNPA (250 μM) in HEPES buffer (100 mM) at 25 °C. The blue curve; when $ZnCl_2$ (250 μM) was added to outside the vesicles with PNPA (250 μM) in HEPES buffer (100 mM). Green curve; $ZnCl_2$ (250 μM) with PNPA (250 μM) in HEPES buffer (100 mM, pH = 7), these were single measurements.*

Data were collected from kinetic studies of this experiment (Figure 3-19) showed that there is no big difference between the two procedures (**A** and **B**), however, procedure (**A**) showed a slightly higher hydrolysis rate than (**B**). This suggests both substrate and Zn^{2+} ions cross the membrane rapidly.

Reported in the litruture[30] that the length of the alkyl chains, the degree of unsaturation of those chains and the cholesterol content are parameters affect the fluidity of the membrane. The alkyl chains have Van der Waals interactions that increase with the number of methylene groups.[30] Hence the longer the chains are, the more it decreases the membrane fluidity when the alkyl chains contain one or several cis alkenes unsaturation, they possess kinks that decrease the interactions between adjacent chains and thus increase the membrane fluidity.[30] The cholesterol content in the membrane is the last variable that affects membrane fluidity.

In order to investigate the effect of different aliphatic chains, saturated and unsaturated lipophilic moieties were chosen from stearyl and oleyl alcohols. These two alcohol types are quite similar in the structure and molecular weight except for the double bound in the middle of oleyl alcohol. Figure 3-20 reveals the differences in observed rates between two ligands, one including a stearyl group and another one including an oleyl group.

An experiment was carried out using three samples, one from vesicles incorporated with compound **21,** and one with compound **22** and third sample vesicles incorporated with compound **23**. The three samples were prepared according to the same procedure at the same time and under the same conditions of [vesicles], [ligand], [buffer], [ZnCl$_2$] and [substrate]. The three samples were run together with background reaction including vesicles not incorporating any ligand and ZnCl$_2$ with the substrate were added to the vesicles solution, the reaction progress is shown in Figure 3-20.
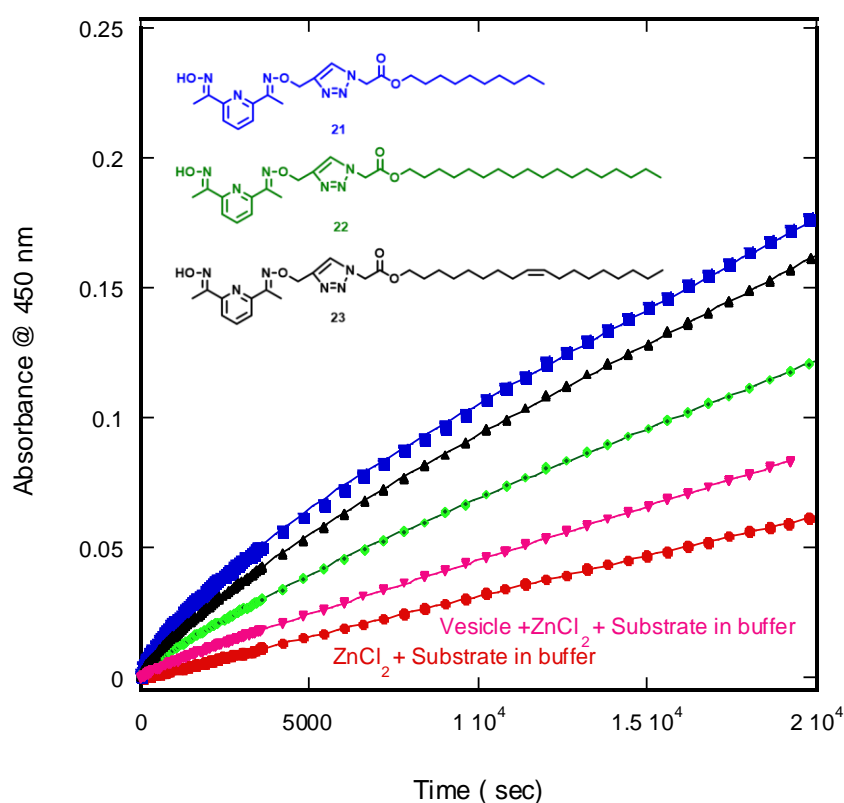
Figure 3-20. *Vesicles (2 mM) incorporated with amphiphilic ligand (50 µM) in HEPES (100mM, pH 7), red curve; no compound was embedded in the vesicles. Blue curve ZnCl$_2$ (250 µM) and HPTSA (250 µM) in buffer solution. Green curve; compound **21**, black curve compound **22**, pink curve compound **23**. ZnCl$_2$ (250 µM) and HPTSA (250 µM) were added to outside the vesicles, these were single measurements.*

Figure 3-21 shows the difference in the absorbance progress versus the time for compounds **16-23** compared with the background reaction. It is clear that there are differences between them as it is shown from the k_{obs} values in Table 3-2.

The conditions (concentrations of Zn^{2+}, substrate, HEPES buffer, vesicles and ligand) which were used in this experiment for the kinetic studies are the same as those specified by the system designed by Hunter *et al.* [124, 125]
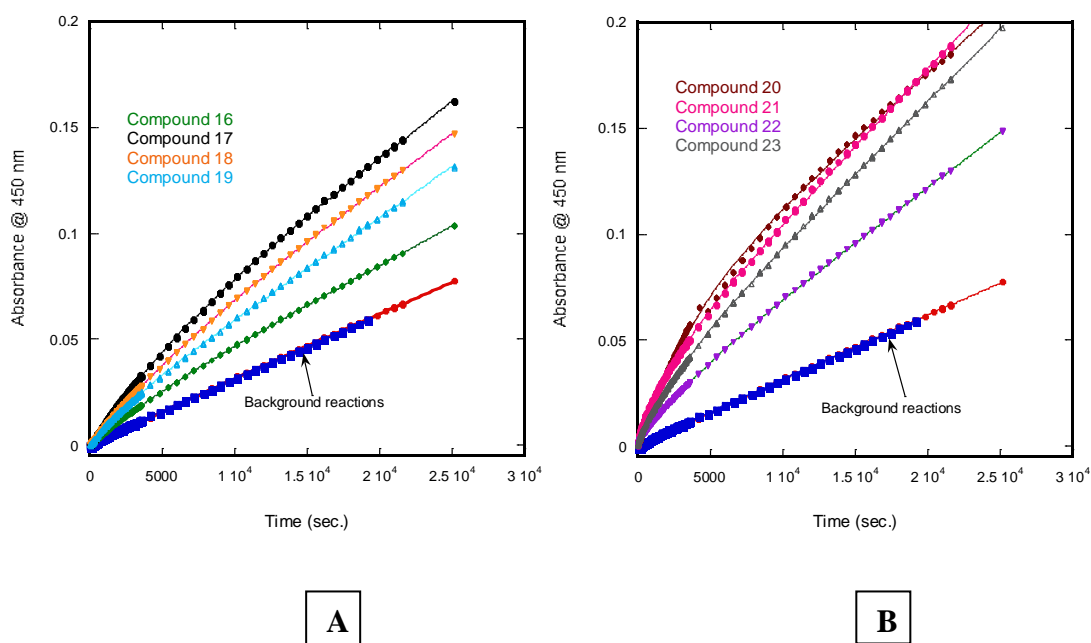
Figure 3-21. *Absorbance versus time for hydrolysis rate of HPTSA (250 µM) in the presence of vesicles (2 mM) incorporated with a ligand, A). 16-19, B). 20-23 (50 µM), then ZnCl₂ (250 µM) was added to outside the vesicles. The experiment was run in HEPES buffer (100 mM, pH 7) at 25 °C (the reaction after 7 hours), these were single measurements.*
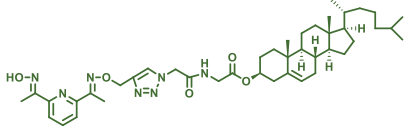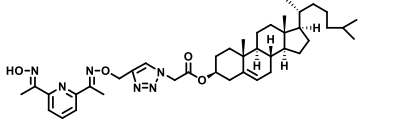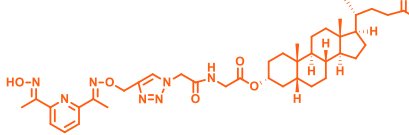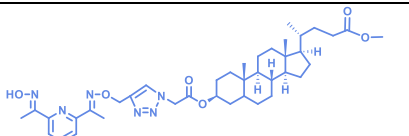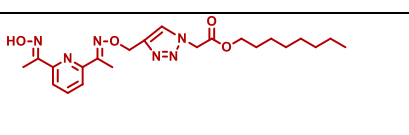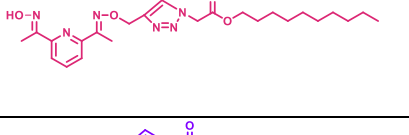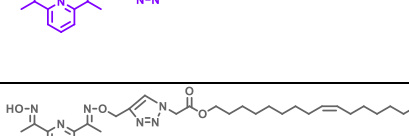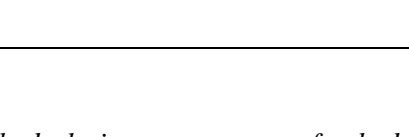
Compound No.	Compound structure	$k_2 \, \text{s}^{-1}$	$k_3 \, \text{s}^{-1}$
Background	Substrate (250 µM) + ZnCl$_2$ (250 µM) in HEPES	$k \quad 4.1\pm0.1\times10^{-6}$	
	Pure vesicles + ZnCl$_2$ (250 µM) + Substrate (250 µM) in HEPES	$k \quad 7.9\pm0.3\times10^{-6}$	
16		$8.6\pm0.2\times10^{-5}$	$1.3\pm0.02\times10^{-4}$
17		$8.3\pm0.01\times10^{-5}$	$7.9\pm0.01\times10^{-5}$
18		$6.3\pm0.08\times10^{-5}$	$8.2\pm0.1\times10^{-5}$
19		$1.3\pm0.003\times10^{-4}$	$1.8\pm0.02\times10^{-5}$
20		$1.9\pm0.003\times10^{-4}$	$7.9\pm0.1\times10^{-5}$
21		$2.4\pm0.003\times10^{-4}$	$1.6\pm0.002\times10^{-4}$
22		$1.1\pm0.001\times10^{-4}$	$1.4\pm0.001\times10^{-4}$
23		$1.5\pm0.02\times10^{-4}$	$1.5\pm0.01\times10^{-4}$

Table 3-2. *The hydrolysis rate constants for hydrolysis of HPTSA (250 µM) in the presence of vesicles (2 mM) incorporated with ligands **16-23** (50 µM), ZnCl$_2$ (250 µM). The experiment was run in HEPES buffer (100 mM, pH 7) at 25 °C. The reaction after 7 hours.*

The data from Figure 3-21 and Table 3-2 showed that compound **21** catalysed the hydrolysis of HPTSA faster (higher k_2 and k_3 values) than other compounds (containing click linker) followed by compound **20**. Both these compounds including a simple and short saturated aliphatic chain. The conceivable reason for that is they were flexible in their movement in the solution while they are embedded into the membrane. Therefore they can reach the metal ion and the substrate molecules easier and faster than other compounds that they embedded into the membrane in a rigid way. Compound **18** showed the lowest k_2 value and **19** showed the lowest k_3 value (both compounds containing a lithocholic acid as lipophilic moiety).

The concentration of the ligand was increased 4-fold more to investigate the effect of the catalyst concentration, which can be formed. The data exhibited in Figure 3-22 and Table 3-3 do not show a significant increase in the hydrolysis rate constants using vesicles incorporated with compounds **10** to **15**. Compound **14** showed the higher k_2 and k_3 values while compound **12** showed the lowest k_2 value and compound **15** exhibited the lowest k_3 value.
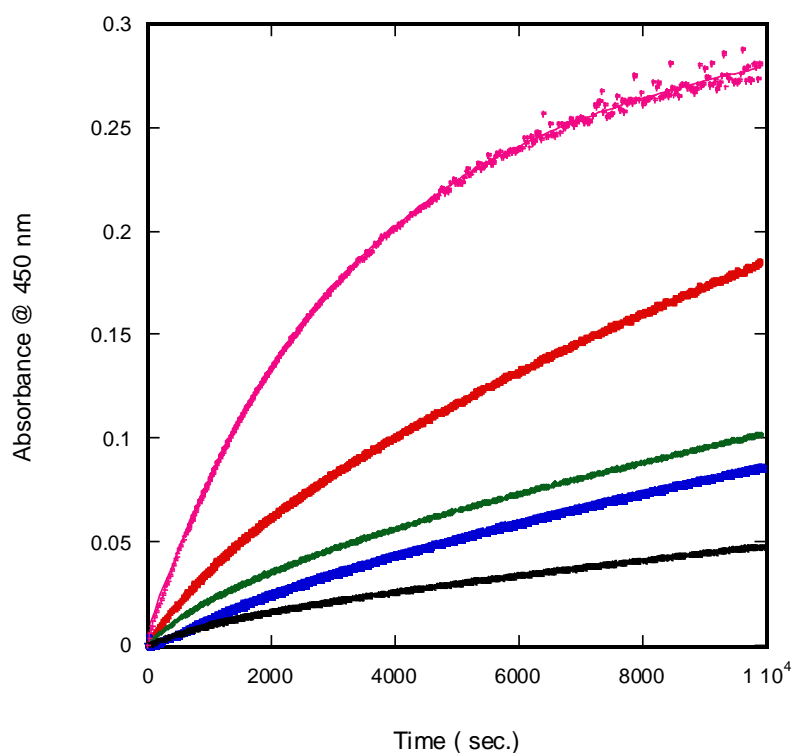
Figure 3-22. *Vesicles (2 mM) incorporated with amphiphilic ligand (200 μM) in HEPES (100 mM, pH 7), the* red *curve; compound* **10***,* blue*; compound* **12***,* green*; compound* **13***,* **black***; compound* **14***,* pink*; compound* **15**. *ZnCl_2 (250 μM) and HPTSA (250 μM), these were single measurements.*
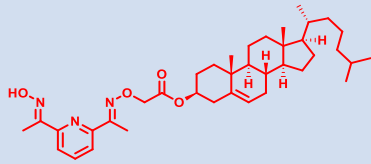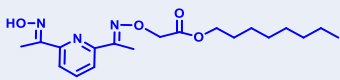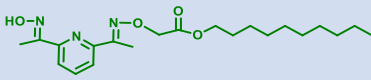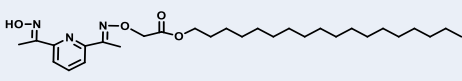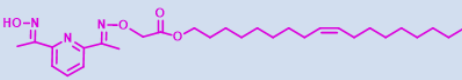
Compound No.	Compound structure	k_2 s^{-1}	k_3 s^{-1}
10		$2.9\pm0.02 \times 10^{-4}$	$1.5\pm0.01 \times 10^{-4}$
12		$2.3\pm0.02 \times 10^{-4}$	$1.6\pm0.01 \times 10^{-4}$
13		$3.4\pm0.02 \times 10^{-4}$	$1.6\pm0.01 \times 10^{-4}$
14		$4.0\pm0.04 \times 10^{-4}$	$2.0\pm0.01 \times 10^{-4}$
15		$3.2\pm0.02 \times 10^{-4}$	$1.4\pm 0.01 \times 10^{-5}$

***Table 3-3**. Vesicles (2 mM) incorporated with amphiphilic ligand **10** and **12-15** (200 µM) in HEPES (100 mM, pH 7),. ZnCl$_2$ (250 µM) and HPTSA (250 µM) were added to outside the vesicles.*

3.7 The Encapsulation Reaction

To investigate the ligand ability to inserted in the membrane and catalyses the hydrolysed inside the vesicles, the substrate with zinc ions were encapsulated in the vesicles then a solution of the ligand in THF was added to the vesicles solution. The result showed there is hydrolysis for HPTSA, $k_2 = 8.8 \times10^{-4}\,s^{-1}$, $k_3 = 2.2\times10^{-4}\,s^{-1}$ (Figure 3-23) similar to that when the same ligand with the same concentration was incorporated with the vesicles before adding the metal ions and the substrate $k_2 = 1.5 \times10^{-4}\,s^{-1}$, $k_3 = 2.7\times10^{-4}\,s^{-1}$ (Figure 3-14). This suggested that the ligand can reach inside the vesicles and binds the metal ion then hydrolyses the substrate, or both the metal ions and the substrate permeate the membrane to the outside phase.
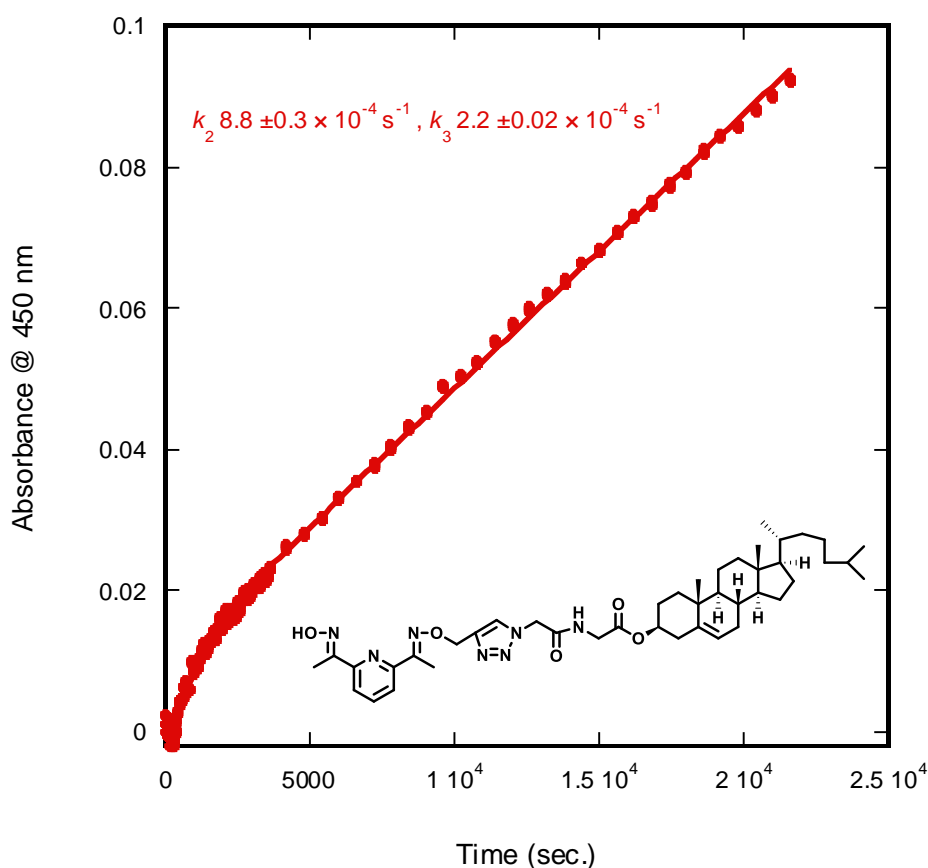
Figure 3-23. Encapsulation reaction. ZnCl$_2$ (250 μM) and HPTSA (250 μM) were encapsulated inside vesicles (2 mM), then compound 16 (50 μM) was added to outside the vesicles, these were single measurements

Zn^{2+} concentration was increased from 0.25 mM to 1.0 mM, similar to the approach applied for the solution experiments. Figure 3-24 shows the difference between the two concentration of Zn^{2+} on the hydrolysis rate of the HPTSA using the same concentration of vesicles incorporated with compound **11**.
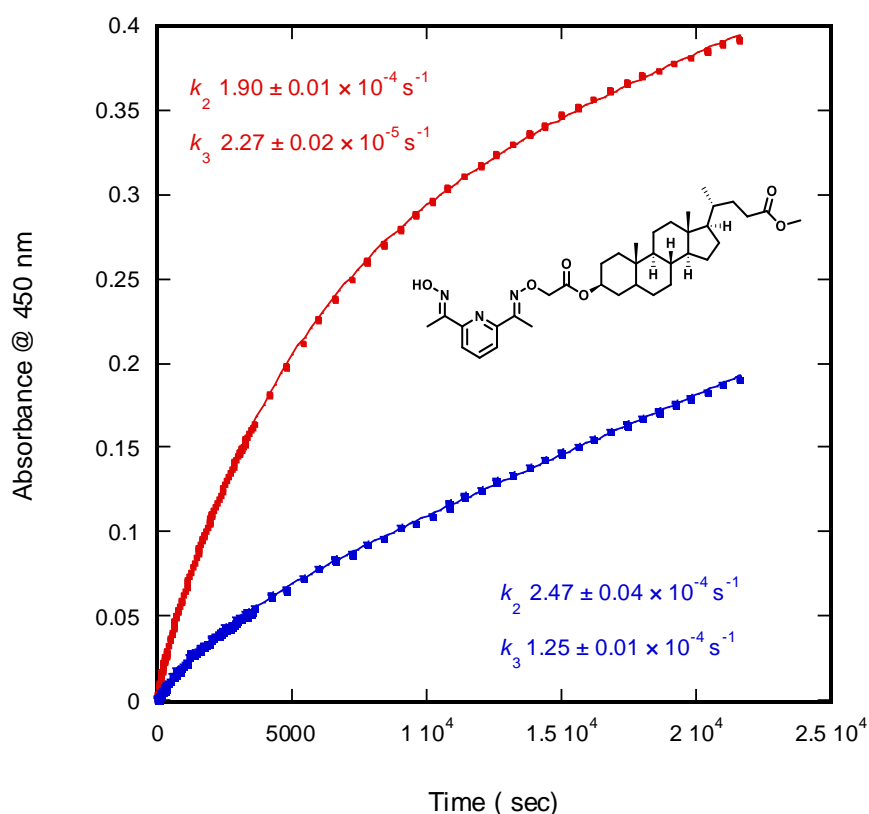
Figure 3-24. ZnCl$_2$ concentration effect on the hydrolysis rate of HPTSA (250 μM), in the presence of ligand 11 (200 μM) embedded into vesicles (2 mM). The red curve with 1 mM ZnCl$_2$, blue with 0.25 mM ZnCl$_2$, HEPES (100 mM, pH 7), these were single measurements.

Increasing the Zn^{2+} concentration did not enhance the rate constant but the absorbance increased significantly. As the data fitted to the burst equation: This experiment needs to be repeated or fitting differently as the sample with more Zn^{2+} shows a higher absorbance compering with another one with 3-times less Zn^{2+}.

3.8 Conclusion

The aims of this study were; firstly, to investigate the catalytic efficacy of artificial bilayer membrane incorporating different catalysts designed to hydrolyse ester substrates and secondly to enhance this efficiency by changing the structure and the concentration of the catalyst. The present study also was designed to determine the effect of changing the hydrophilic moiety. The additional aim of this study was to explore the impacts of the linker between the headgroup and a hydrophilic moiety.

In the transducer system, the hydrolysis reaction occurs inside the vesicles in a small volume, where the embedded complex provides a locally high concentration of complex to the interior. In one headgroup system, where the reaction is involved a much larger volume and therefore is expected to be slower than the reaction inside the vesicles, as shown in Figure 3-2, 3-25.

2% of the solution volume is inside the vesicles and reacts 50-times faster than 98% outside the vesicles as the concentration of the complex is 50-times higher. Furthermore, if the substrate can cross the membrane rapidly, the rate will be twice as fast as if it can't (as can reach 100% catalyst instead of 50%).

$$[\text{catalyst}]_{\text{outside}} = [\text{catalyst}]_{\text{inside}}$$

$$\text{Rate} = k_2[\text{catalyst}]_{\text{outside}} \ [\text{substrate}]_{\text{outside}} + k_2[\text{catalyst}]_{\text{inside}} \ [\text{substrate}]_{\text{inside}}$$

$k_{\text{obs.}}$ for outside reaction ≈ 0.02 for inside

$$\text{Rate} = k_2[\text{catalyst}]_{\text{outside}} \ 0.98[\text{substrate}]_{\text{total}} + k_2 \ [\text{catalyst}]_{\text{outside}} \times (49 \times 0.02) \ [\text{substrate}]_{\text{total}}$$
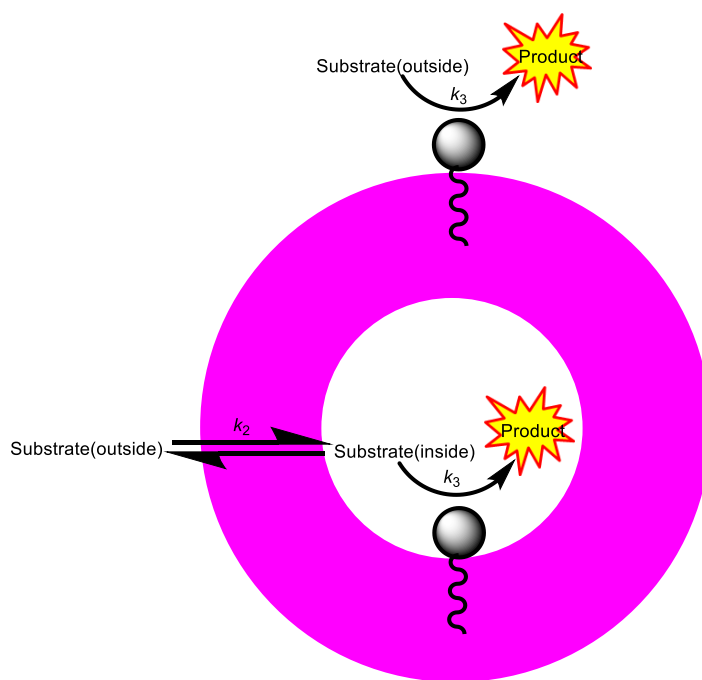
***Figure 3-25.** The difference in the volume between the inside and outside vesicles affects the catalytic hydrolysis reaction rate.*

Increasing the ligand concentration leads to an enhanced rate of hydrolysis as the experiments in the solution showed. Increasing the ligand concentration in the vesicles did not display similar behaviour, this may be attributed to forming complex clusters as shown in Figure 3-15, which inhibited binding of the substrate. The same event occurred when the vesicle concentration was increased from 2 mM to 4 mM meaning the vesicles were doped with a low concentration of the ligand. The case was shown to be more complicated in the vesicles and it produced a very cloudy solution with increased concentration of vesicle.

Increasing the zinc concentration led to a precipitate of the complex over time. One needs to prepare the catalytic complex before adding the substrate, to ensure that the headgroup is in the aqueous layer and it is ready to catalyse the substrate; rather than it is buried in the membrane (which did not improve the hydrolysis rate).

Generally, all the ligands in the membrane behaved similarly and there was no significant difference between them towards the hydrolysis of the substrates in HEPES buffer at pH 7. Another conclusion is that the second step (releasing the phenolate anion or HPTS) was the determining step in these hydrolysis reactions.

The problem that could have affected the measurement of the vesicles solution absorbance is that the increase in the vesicle concentration causes more scattering of the light. Furthermore, it is unfortunate that the study did not include evidence on how to direct the ligand in the vesicles; therefore one or several physicochemical methods (transmission electron microscopy, dye encapsulation, and capillary electrophoresis) is needed to characterise and to determine the shape of the vesicles.

3.9 Experimental

Stock solutions of the lipids 1,2-dioleoyl-sn-glycero-3-phosphocholine (**DOPC**, 13 mM) and 1,2-dioleoyl-sn-glycero-3-phosphoethanolamine (**DOPE**, 13 mM) were prepared and mixed (3:2) in a solution of chloroform/ethanol (1:1). The solution kept at – 5 °C until required. Stock solutions of the synthetic ligands **10-23** (5 mM) were prepared in chloroform, dichloromethane, or tetrahydrofuran (according to the solubility).

The required ligand and lipid were mixed in a solution (ratio 1 – 2.5%), such that the final lipid concentration was 1.5 – 4.0 mM, taking into account the dilution during the vesicles extrusion and purification. The solution was prepared in a dry round-bottomed flask (5 mL); solvents were removed under reduced pressure for at least 2 hours before use. The dry film was then hydrated with HEPES buffer (2.5 mL). In the metallovesicles preparation experiment, $ZnCl_2$ solution (250 µM) was mixed with the buffer to hydrate the film. A stock solution of HEPES buffer (250 mM, pH = 7) was prepared in deionized distilled water, its pH value was adjusted by adding analytical sodium hydroxide solution (1 N).

The lipid-ligand mixture was then suspended in the buffer using a vortex mixer for 1 minute. The resulting cloudy suspension of the bilayer membrane (from lipid-containing a ligand) was subjected to 5 rounds of freeze-thaw (in a dry ice bath) before the solution was warmed to ~ 40 °C. The resulting unilamellar vesicles were extruded using mini extruder (Figure 3-9). The solution was pushed 25 times through polycarbonate membrane (200 nm) to get the selected size. The vesicles were diluted ~1.4 x (if the original volume was 2.5 mL, the collected volume was ~2.4 mL).

The vesicle solution was purified (to remove any small particles) using the pre-packed gel permeation chromatography (GPC) column (GE healthcare Sephadex PD-10 desalting column) which washed 6 times (3.5 mL each time) with HEPES buffer before use. The vesicle size was determined by dynamic light scattering technique (DLS) at 25 °C, 5 runs in 10 min, the cell path length was 10 mm, wavelength = 660 nm. The solution was considered as water, with viscosity = 0.890 cP, reflex index = 1.330.

Fresh stock solutions of the substrates, PNPA (10 mM) and HPTSA (10 mM) in dry acetonitrile and in water, respectively were prepared on the day of use. A stock solution of zinc chloride ($ZnCl_2$, 50 mM) was prepared in deionized distilled water.

104

Chapter 4 -   Activation of the Papain

4.1 Aims

One of the aims of this chapter was to see if a synthetic molecule (containing a thiol group) which had been embedded in a lipid bilayer membrane of a vesicle could be used to activate an inhibited enzyme in the aqueous phase surrounding it. Another aim was to investigate whether this would provide the system with the potential to be completely inactive in the 'off' state if used in a membrane translocation system for signal transduction. As enzymes are more efficient catalysts than synthetic equivalents, a less active substrate can be used. It was envisioned that this would decrease the likelihood of spontaneous decomposition of substrate molecules as observed previously.[124] It was also investigated whether the enzyme was capable of amplifying a signal once activated. Finally, a further aim was to see if a transducer molecule with a polar headgroup could be made, similar to the one in Figure 4-1, which could be held with the enzyme-activating moiety held inside the vesicle membrane until a primary signal was inputted. This could then be used in a similar system to that shown in Figure 4-1.
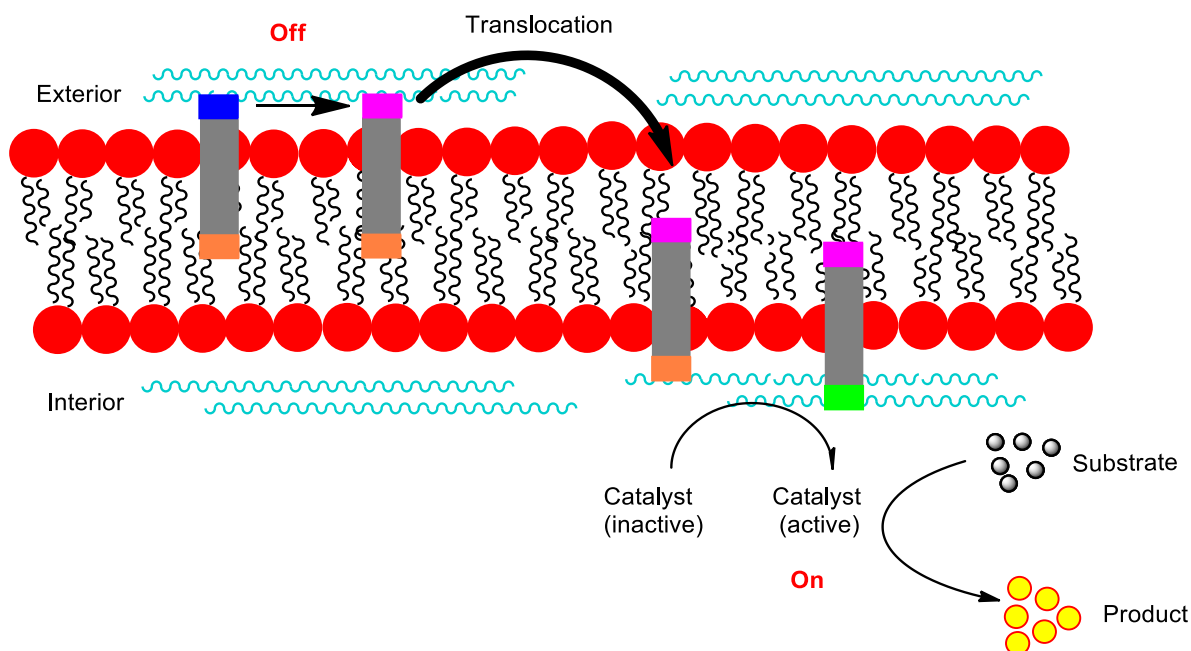
Figure 4-1. *Membrane translocation mechanism as a method of signal transduction*

Hence, we decided to use thiol-disulphide exchange reactions as the starting point for our studies, due to the precedent for such reactions occurring in vesicles, and such reactions have pivotal functions in biology.[167] For a long time, thiol-disulphide exchange was thought to only have a protein-stabilizing structural purpose, but it is now evident that this exchange is also responsible for the various dynamic functional properties of many enzymes.[167] Disulphides are also the major products of thiol oxidation. The kinetics of thiol-disulphide interchange reactions are pH-dependent, because of the much stronger nucleophilicity of the thiolate compared to the thiol. The difference in the nucleophilicities is so dramatic that in many cases the reaction proceeds via the thiolate even when it is a minor species (i.e., at pH values far below the thiol pK_a).[167]

Some previously reported example systems have used thiol-disulphide exchange reactions. Bizzigotti[163] attributed the retardation in the thiol-disulphide exchange processes in the bilayer to the strong binding of both components (thiol-functionalised surfactants and disulfide) to the vesicles; the reaction and the structures are shown in Scheme 4-1. The second step was the determining-rate step, and it was speculated that the membrane environment conformationally restricted the surfactant head groups, inhibiting their reaction with each other.
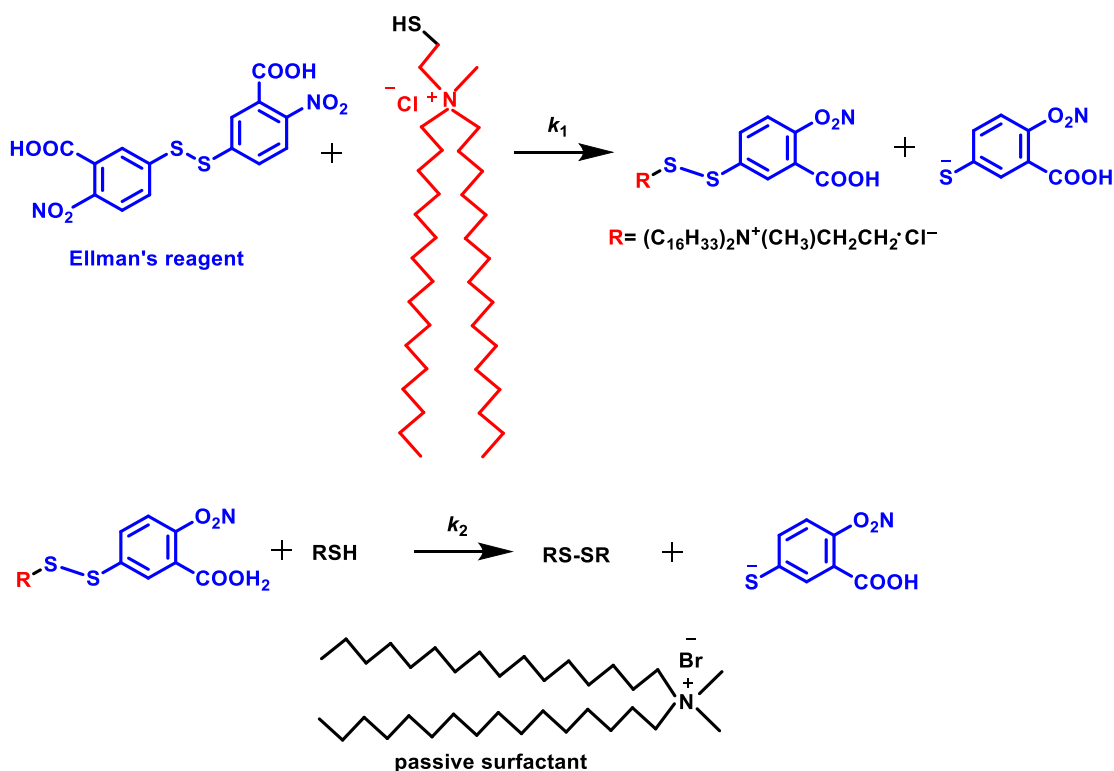
Scheme 4-1. *Thiol-functionalised surfactants to study thiol-disulphide exchange reaction in vesicles solution (Bizzigotti model).*

Potter[156] used cysteine as a thiol-functionalised charged headgroup and a pyridine-2-thiol leaving group, attached to the target thiol as a disulphide. Furthermore, he studied the linker effect on the intravesicular reactivity using more flexible linker (ethylene glycol) as shown in Figure 4-2.
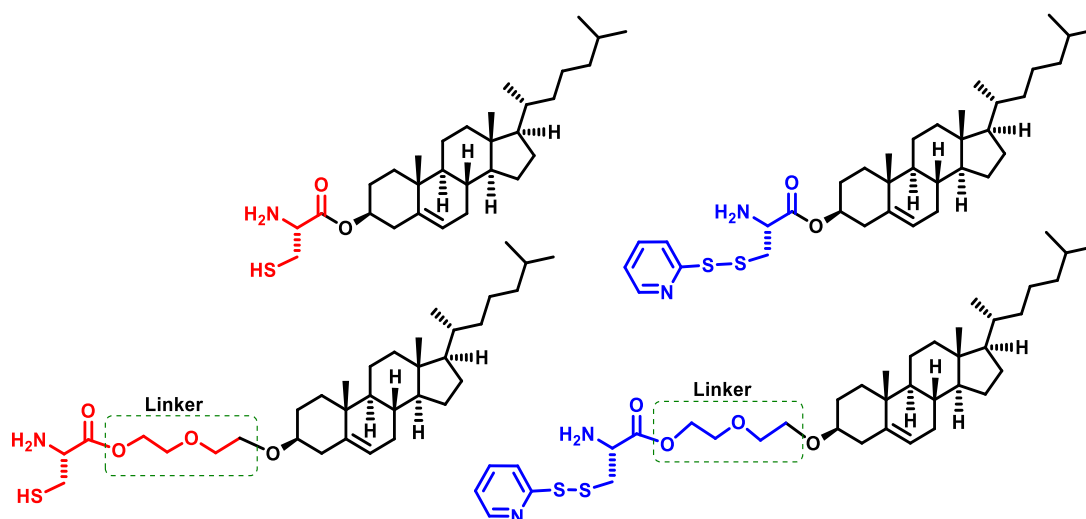
Figure 4-2. *Molecular structures to investigate the intervesicular reactivity by thiol-disulphide exchange*

4.2 The Approach and the Design

Aiming to investigate the reactivity of similar systems, we used simple model compounds (Figure 4-3). Compound **24** is based on cholesterol and **25** on lithocholic acid, for studies on reactivity in the membrane, and **26** is isopropyl 3-mercaptopropionate, to use for control experiments in the solution.
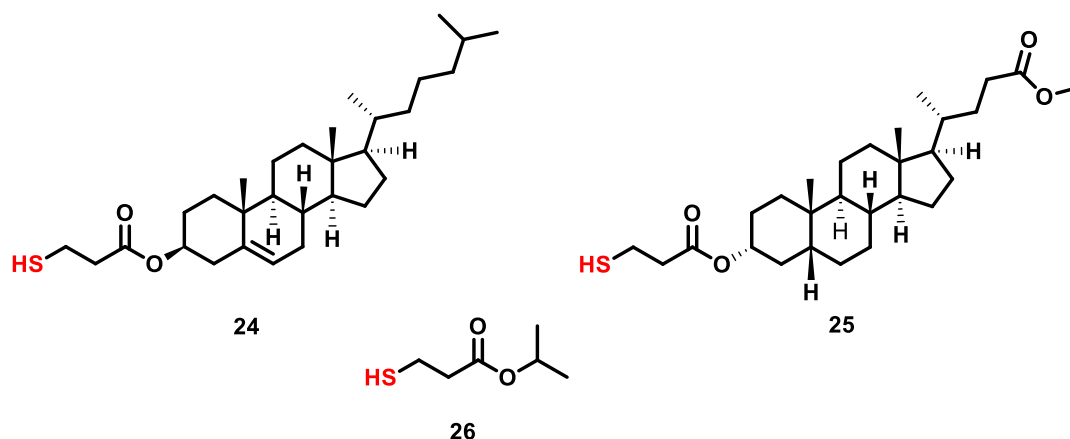
Figure 4-3. Structures of thiol-functionalised compounds to be used to activate an enzyme in thiol-disulphide exchange reactions

Therefore, the first task was to synthesise a molecule that could be embedded in a lipid bilayer membrane in a way that presented a thiol group on the end of the molecule to the aqueous media surrounding the membrane. The lipid bilayer would be in the form of vesicles. We chose cholesterol and lithocholic acid molecules as membrane anchors (in **24** and **25** respectively) since these steroidal molecules are known to partition into artificial lipid bilayers in aqueous solutions and have been used in chapter 3. Cholesterol has been shown to embed in an orientation that is perpendicular to the plane of the bilayer, parallel with the fatty acid molecules, with the alcohol pointing out of the membrane and the alkyl chain orientated towards the centre of the bilayer.[168]

The 3-mercaptopropionic acid substructure provides the thiol-functionalised headgroup that can be readily attached to the hydrophobic tail. Thiols are less polar than alcohols, so are less soluble in aqueous media. However, they are more polar than the alkyl chain on the cholesterol, so by attaching a thiol to the alcohol end of cholesterol, it was envisaged that the synthesised molecule would embed in the same orientation as the parent steroid (Figure 4-4).
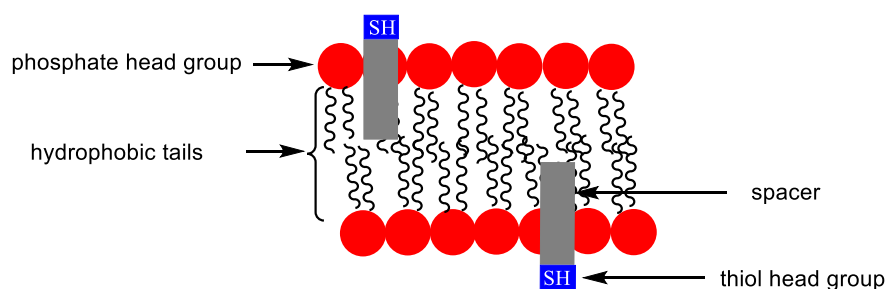
Figure 4-4. The expected orientation of the synthesised molecules in a lipid bilayer

The thiol part of the transducer molecule (blue block) should, therefore, be available to react with the enzyme (inhibited by blocking an essential catalytic cysteine residue as a disulphide). The transducer thiol group will, therefore, react in a disulphide exchange to activate the enzyme. The enzyme papain, which is commercially available, was chosen for this study; it has a thiol at its active site that is essential for catalytical activity (Scheme 4-2). It can be purchased in this form and converted to a disulphide, which is the inactive form. The inactive enzyme is activated by thiols, which reacts with the disulphide to free the active site thiol. The papain's activity can be measured using $N\alpha$-benzoyl-L-arginine, p-nitroanilide (L-BAPNA), a chromogenic papain substrate. This colourless substrate allows easy detection; its hydrolysis by active papain gives highly coloured (dark yellow) p-nitroaniline. Hence, L-BAPNA will be present in the aqueous surroundings along with inactivated papain. Activation of papain will then be detected when it cleaves L-BAPNA to release p-nitroaniline (a chromophore that can be monitored using UV/Vis spectrometry at a wavelength of 410 nm). The reaction is shown in Scheme 4-2.
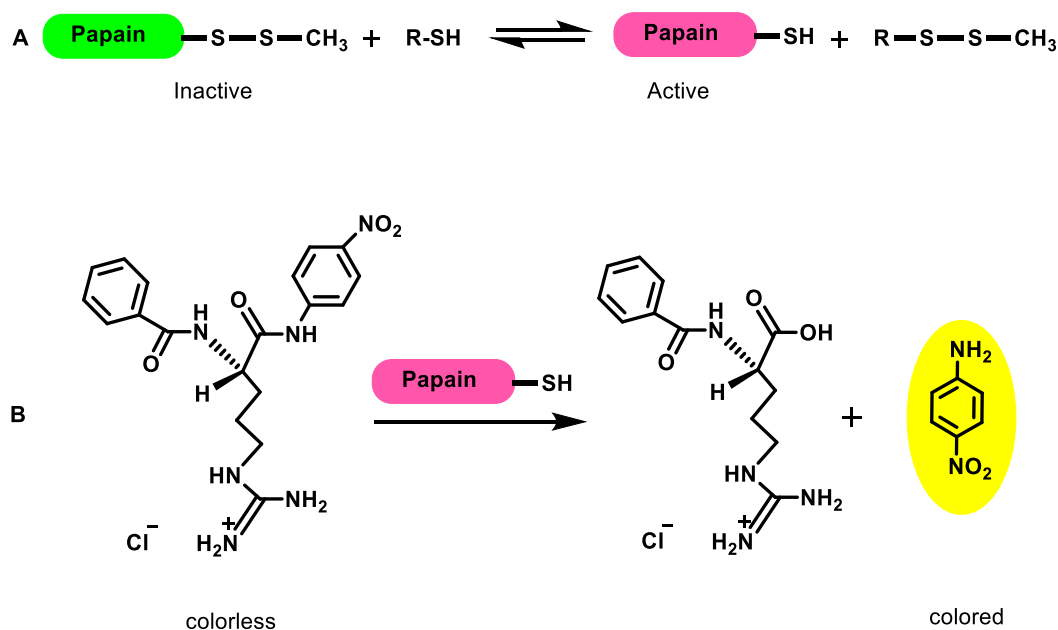
Scheme 4-2. (A) Activation of papain at Cys25 by disulphide exchange. (B) Hydrolysis of L-BAPNA by the enzyme releases the strongly-coloured p-nitroaniline product

4.3 Papain Enzyme

Papain is a thiol protease, which occurs naturally in the latex of *Carica papaya*. This enzyme displays wide proteolytic activity, and due to a number of applications is of high research interest.[169] The mature papain protein has seven cysteine residues; six are in the form of three internal disulphide bonds. The remaining reactive thiol group (-SH), Cys25, is essential for activity and participates in the catalytic mechanism by forming acyl intermediates with substrates.[170 171 172]

Kinetic studies of papain-catalyzed hydrolysis of α-*N*-benzoyl-L-arginine-*p*-nitroanilide,[173] α-*N*-benzoyl-L-arginine ethyl ester and α-*N*-benzoyl-L-argininamide,[174] carbobenzoxyglycylglycine (CGG), benzoylglycinamide (BGA), carbobenzoxy-L-histidinamide (CHA),[175] suggest that the hydrolysis of the substrate proceeds *via* the formation of an acyl-enzyme intermediate:

$$\mathbf{E + S} \underset{k_{-1}}{\overset{k_1}{\rightleftharpoons}} \mathbf{ES} \overset{k_2}{\longrightarrow} \mathbf{ES'} \overset{k_3}{\underset{H_2O}{\longrightarrow}} \mathbf{E + P_2} \qquad \textbf{(Equation 4-1)}$$
$$+ \\ \mathbf{P_1}$$
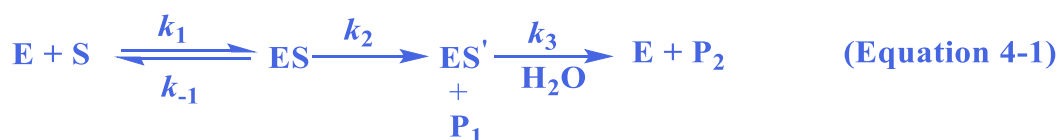
where **E** is the enzyme, **S** the substrate, **ES** is a bound complex and **ES′** is the acyl-enzyme intermediate. The most suitable substrates for papain are those which possess an arginyl or lysyl residue; i.e., they have a strongly cationic group on the side chain. Papain can hydrolyze synthetic substrates, which possess an ester or thiol ester bond, as well as those with amide bonds or peptide.[176]

The pH effect on the catalytic hydrolysis of CGG, BGA and CHA by papain has been investigated.[175] Lowe and Yuthavong[177] studied the pH effect on hydrolysis of *N*-acetyl-L-phenylalanylglycine *p*-nitroanilide, and found that the equilibrium binding constant, K_s, is independent of pH between 3.7 and 9.3, whereas the acylation constant, k_2, shows bell-shaped pH-dependence with apparent pK_a values of 4.2 and 8.2. This tells us any pH value between these numbers is sensible to use in our experiments.

4.4 Deactivation and Activation of Papain Enzyme

Papain is activated by compounds such as cysteine, sulphides, sulfite, and is reversibly inactivated in the presence of air and low concentrations of cysteine. The inactivation is improved in the presence of Cu^{2+} and Fe^{2+} ions and is reduced by EDTA (ethylenediaminetetraacetic acid). The strongest activation occurs using thiol compounds such as cysteine with EDTA.[178] Research of divalent metal ions showed that Cd^{2+} and Zn^{2+} have a stronger inhibitory effects with papain compared cysteine.[178] Cu^{2+}, Fe^{2+}, Pb^{2+}, and Hg^{2+} showed no (or a small) preference between binding papain over cysteine.[178] Studies using labelled cysteine (cysteine-^{35}S) showed that the reversibly dominant inactive form is a mixed disulphide of the enzyme and cysteine, and this cysteine is isolated on activation.[178] Studies recorded by Klein and Kirsch[179] confirmed this result.
Sluyterman's[178] results showed that the inactivation of papain (PSH) by the dimerization, as the following equation shows, is either very slow or absent.

$$2\ PSH + \tfrac{1}{2}\ O_2 \longrightarrow PS\text{-}SP + H_2O \qquad \textbf{(Equation 4-2)}$$

The suggested steps to the inactivation are: air oxidation catalyzed by heavy metal ions of cysteine (SH) to cystine (S-S) as follows:

$$2\ CysSH + \tfrac{1}{2}\ O_2 \longrightarrow CysS\text{--}SCys + H_2O \qquad \textbf{(Equation 4-3)}$$

Then the inactivation of papain by thiol-disulphide exchange:

$$PSH + CysS\text{--}SCys \rightleftharpoons PS\text{--}SCys + Cys \qquad \textbf{(Equation 4-4)}$$

Of course, a more direct inactivation is possible according to:

$$PSH + CysSH + \tfrac{1}{2}\ O_2 \longrightarrow PS\text{-}SCys + H_2O \qquad \textbf{(Equation 4-5)}$$

The inactivation of active papain can be achieved in different ways. Kanazawa *et al*.[180] used Cu^{2+}-ascorbic acid in presence of air and found the degree of inactivation was dependent on the decrease in the enzyme's thiol group 'SH' content.[180]

Potter[156] attempted to activate papain-$SSCH_3$ which was encapsulated inside the vesicles using a membrane-bound to transmembrane signalling compounds as shown in Figure 4-5. Potassium ferricyanide was used to oxidise the external thiols, which caused a transmembrane signalling event, releasing pyridine-2-thiol inside the vesicles. This

performs deprotection of the active side and activation of the papain, which hydrolyses the L-BAPNA. However, it was unclear whether the membrane-embedded molecule activated the papain directly.
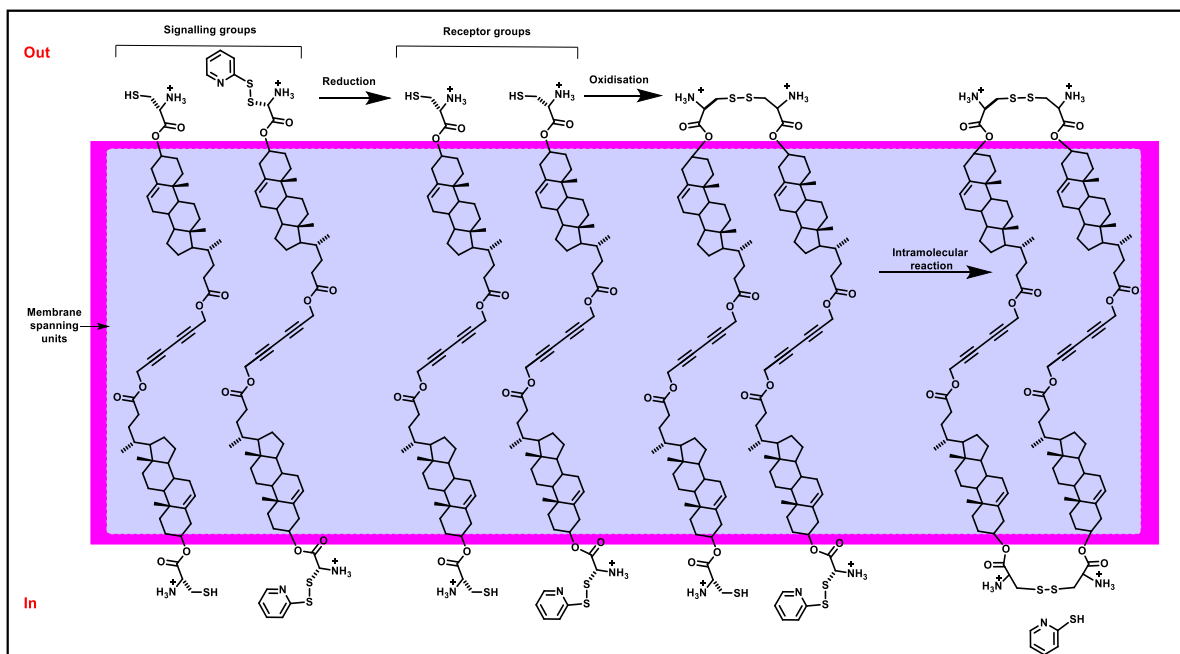
Figure 4-5. *The transmembrane signalling through dimerization of spanning membrane molecules with thiol and disulphide headgroup on the exterior of the vesicles.*

Contrary to this covalent approach, Schrader *et al.*[181] established a noncovalent prototype system using a recognition concept between transmembrane-building blocks with thiol and disulphide headgroups and adrenaline as a primary messenger. They successfully reduced the disulphide to thiol using 10 equivalents of triphenylphosphine-3,3,3-trisulfonic acid trisodium salt to release 2-thiopyridine (monitored at 343 nm) as a secondary messenger; Figure 4-6 shows the mechanism.
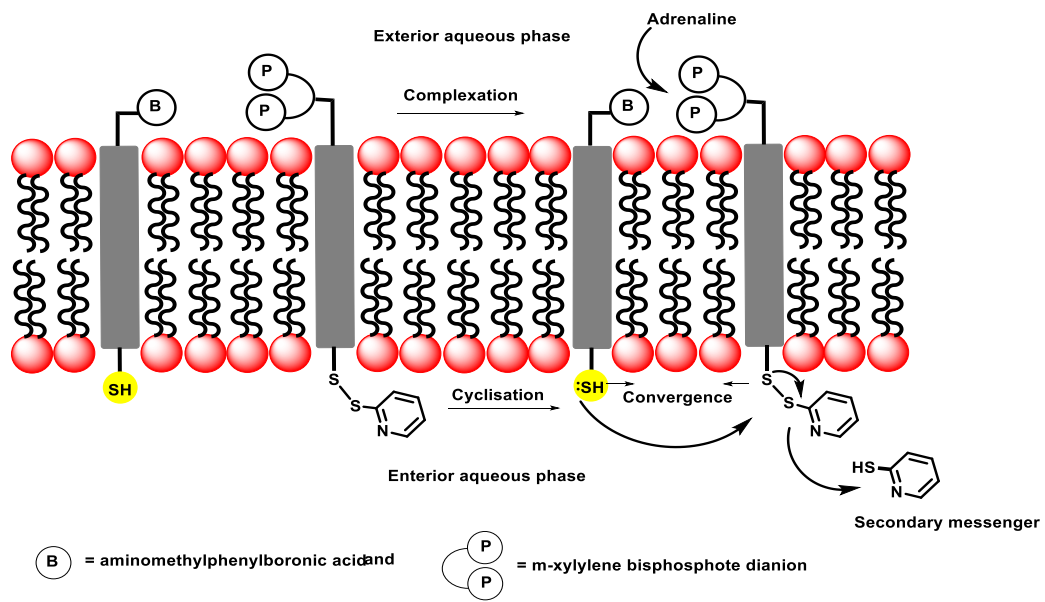
Figure 4-6. *A noncovalent approach to transfer an artificial signal across the bilayer membrane.*

4.5 Results and Discussion

4.5.1 Reactivity Studies

The reaction in vesicular media is the key reaction of interest, but to establish convenient conditions, similar reactions were first studied in solution. These reactions are a point of reference for the rates in a bilayer. The reaction with isopropyl-3-mercaptopropionate **26** was chosen as a reference reaction to study in solution. Compounds **24** and **25** cannot be used as they are insoluble in aqueous solution even in low concentrations, even in the presence of a high volume of water-miscible solvents [THF (tetrahydrofuran), dioxane].

The progress of the L-BAPNA hydrolysis reaction was followed by UV/Vis absorbance spectroscopy, monitoring of the release of *p*-nitroaniline (coloured) at 410 nm. The complete UV/Vis spectrum was recorded before and after each reaction to confirm the presence of a peak at 410 nm corresponding to the release of *p*-nitroaniline. The changes in the absorbance were monitored as a function of time at 25 °C using a Cary 300 UV/Vis spectrometer.

4.5.2 Control Experiments in Solution

Control experiments were performed in a solution using short thiol ester compound **26** to show that the thiol compounds (with similar local structure) can activate the enzyme. The individual components present in each reaction were monitored over time, to ensure that only the anticipated reaction was going to occur; the results are shown in Figure 4-7. In the control reactions where one reactant was excluded from the reaction, the same volume of the buffer was substituted to ensure the concentrations and conditions were as close as possible to those used in the final experiments. For example, in the control experiments where the enzyme was excluded, buffer B (see Experimental Section) was added, and when thiol was excluded, 60 μL of THF was added in its place because compound **26** was dissolved in THF.
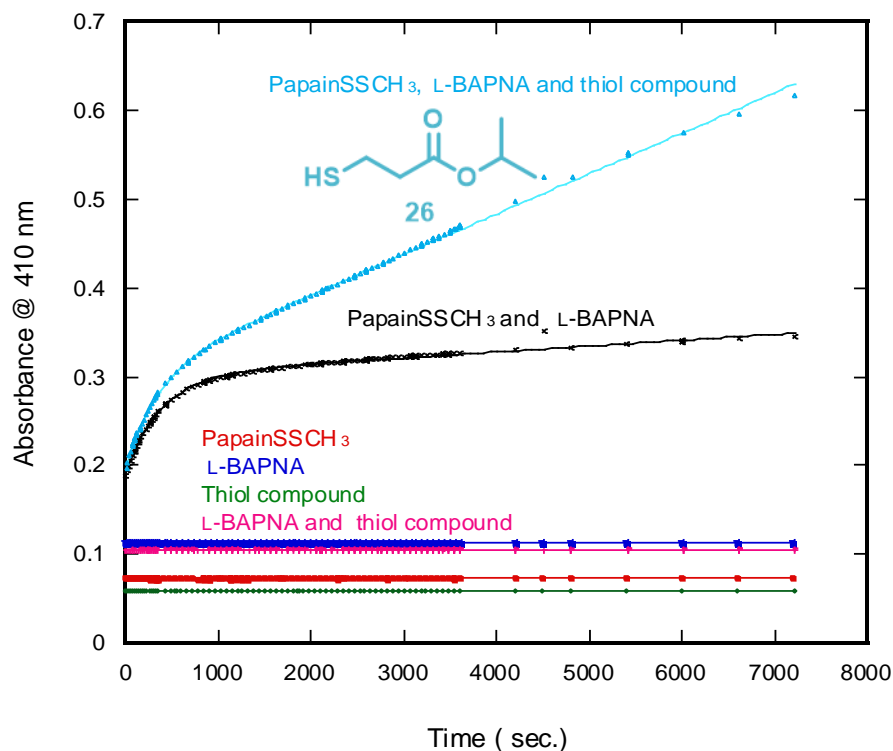
Figure 4-7. Absorbance versus time of all the possible combinations of reagents present in the solution, papainSSCH₃ (26 μM), L-BAPNA (2.4 mM), compound 26 (26 μM), control experiments at 25 °C, pH of the solution ≈ 6.5, the experiment was repeated twice.

These control experiments demonstrate that no spectral response at 410 nm is observed after timescale of 2 hours with the enzyme, the substrate or a solution of both of them in the absence of thiol compounds.

Mixing two of the reactants at a time, in all three possible combinations, showed a small change in absorbance of 0.2 over 2 hours. This was mostly due to a rapid increase at the start, with the absorbance increasing by 0.2 in the first 15 minutes. The result was unexpected for the control experiment, as it was assumed no change in absorbance at 410 nm would be seen. The reason for the slight change in absorbance could have been due to the thiol reacting with the papainSSCH₃, as it was expected to do.

The reaction involving papainSSCH₃ and L-BAPNA showed a significantly higher increase in absorbance (0.3) over the reaction time-scale than the other control experiments. The change in absorbance was due to the release of *p*-nitroaniline, caused by the reaction between active papain and the substrate. The result indicated that the papainSSCH₃ sample used was not completely pure, and some active papain was present in the reaction. This interpretation is supported by the absence of any change in absorbance in the presence of

115

only L-BAPNA. The change in absorbance only occurs when L-BAPNA is in the presence of papainSSCH$_3$, implying that decomposition of the substrate was not the cause.

The reaction with isopropyl-3-mercaptopropionate **26** was used as a control to see if a thiol would activate the inhibited papain in the absence of vesicles. Short thiol, compound **26** was prepared in buffer (5 mM solution sodium acetate, 50 mM NaCl, 0.5 mM EDTA, pH 4.7, see experimental, page 131), and had a similar structure to the thiol, with the isopropyl carbons next to the ester in the same hybridisation as the corresponding carbons in cholesterol or lithocholic acid. Therefore, it was assumed that it would give a reliable indication of whether cholesterol or lithocholic acid would be able to react with the disulphide in the inhibited enzyme.

There are likely two steps to release the product. The first one is a reaction between the enzyme **(E)**, and thiol compound (RSH) to activate the enzyme, the reaction summarised in Equation 4-6:

$$\textbf{ES–SR}' + \textbf{RSH} \rightleftharpoons \textbf{ESH} + \textbf{RS–SR}' \qquad \textbf{(Equation 4-6)}$$

Secondly, the active enzyme will hydrolyse the substrate **(S)** as shown in the following Equation 4-7, to release the products **(P$_1$, P$_2$)**:

$$\textbf{ESH} + \textbf{S} \underset{k_{-1}}{\overset{k_1}{\rightleftharpoons}} \textbf{ES} \xrightarrow{k_2} \textbf{EQ} + \textbf{P}_1 \xrightarrow{k_3} \textbf{E} + \textbf{P}_2 \qquad \textbf{(Equation 4-7)}$$

Where **ESSR**, **RSH**, **ESH**, **S** are the inhibited enzyme, the thiol compound, the active enzyme and the substrate respectively, **P$_1$** and **P$_2$** are products released subsequently.

This will happen if the final step is the rate-limiting, so k_3 will be small compared with k_1, k_{-1}, then the enzyme exists almost entirely as **EQ** in the steady-state. **P** can be released before **EQ** is formed as following:

$$\textbf{(Equation 4-8)}$$

The standard mechanism to the substrate hydrolysis during the formation of thiol ester intermediate is shown in Scheme 4-3.

Scheme 4-3. *The mechanism of the L-BAPNA hydrolysis using papainSH.*

The formation of **ES** is enhanced by the ionic interaction between the enzyme and the substrate, which formed due to the ionized enzyme's β-carboxyl group and the cationic group in the substrate.

PapainSH which was purchased from Sigma showed a significantly lower reactivity than expected for active papain, as illustrated in Figure 4-8. When compound **26** was added, which would activate the enzyme, the reactivity increased, suggesting that the 'active' papain, still contained an inactive enzyme, because of this result, the enzyme was modified as described in Section 4.5.3.
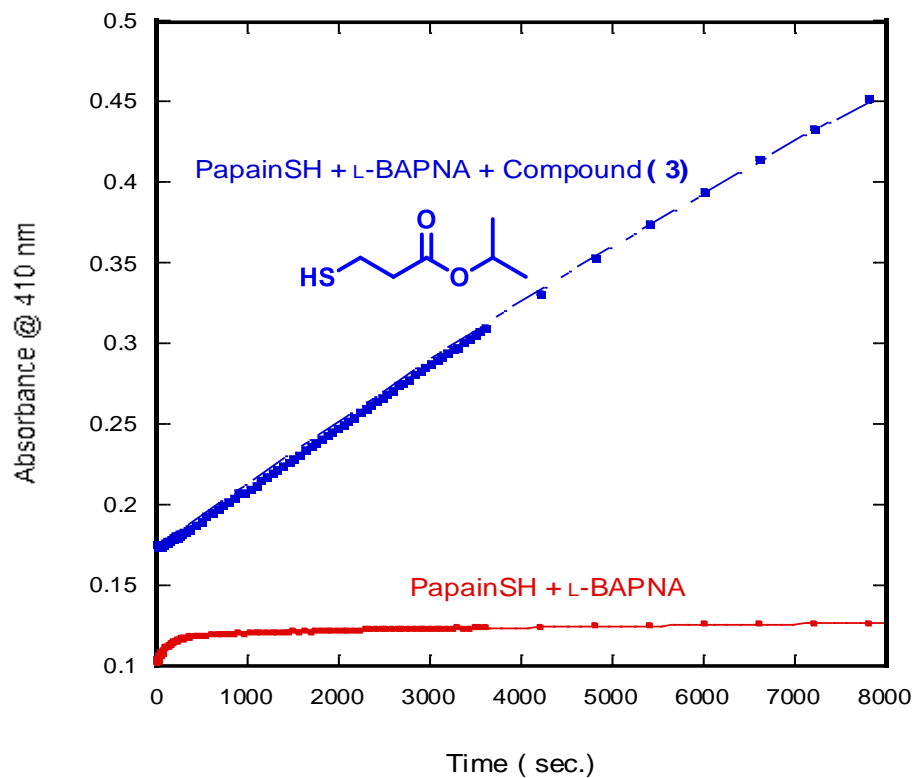
Figure 4-8. *The hydrolysis of L-BAPNA (0.98 mM) with active papain (10.4 μM), with and without compound **26** (98 μM), at 25 °C, pH of solutions ≈ 6.5, the experiment was repeated twice.*

4.5.3 Deactivation the Native Papain

The inactive enzyme was prepared according to the literature using either **(A)** Aldrithiol™-2 (2,2′-Dithiodipyridine) or **(B)** *S*-methyl methanethiosulfonate,[22] as shown in Scheme 4-4.
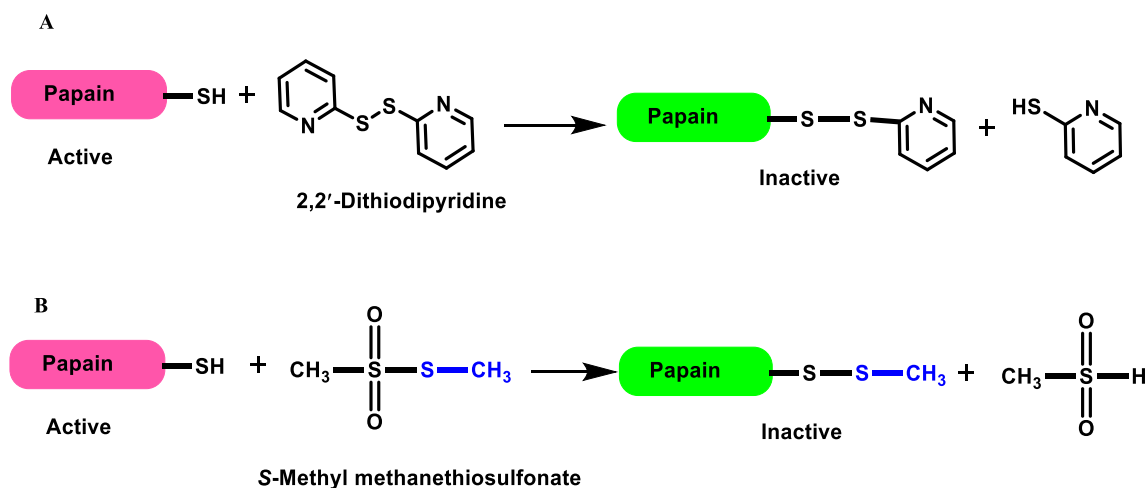
Scheme 4-4. *The reaction of the active enzyme with* **A***) Aldrithiol or* **B***) S-Methyl methanethiosulfonate to give the inactive form.*

As a result of the successful inhibition of the enzyme, when the reaction was examined with an inactive enzyme, no absorbance change was noticed over a long timescale. In contrast, adding the thiol compound to the solution containing an inhibited enzyme and the substrate caused a large change in the absorbance due to the enzyme activation, and the consequent substrate hydrolysis rate enhancement as shown in Figure 4-9.
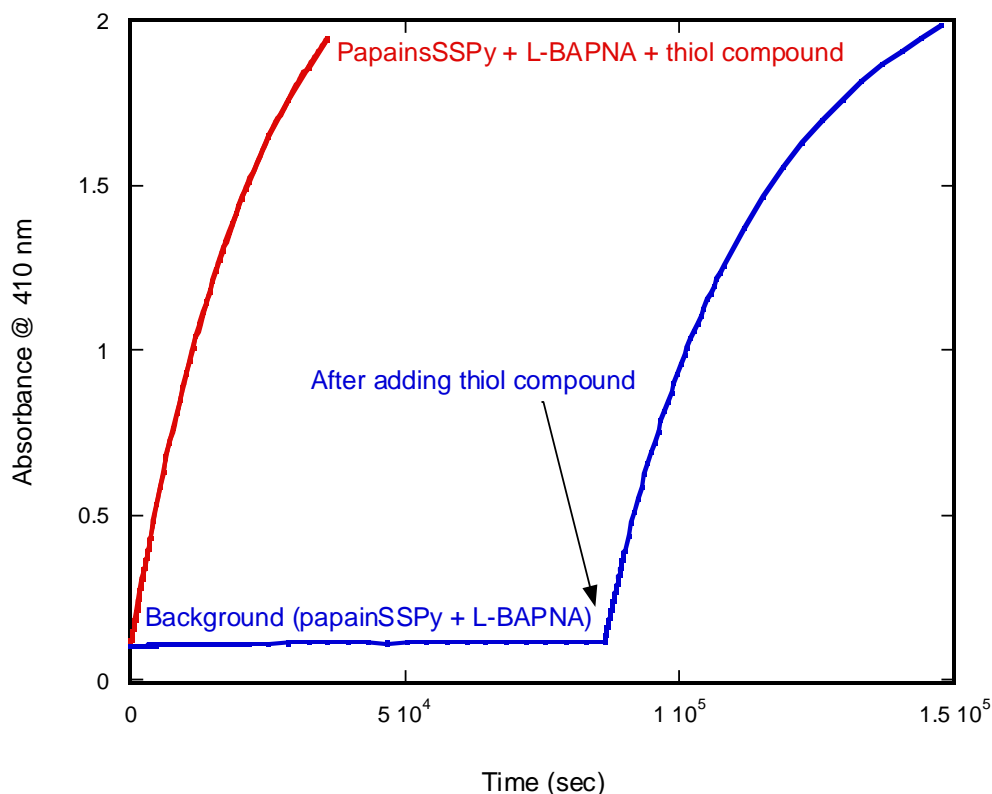
Figure 4-9. Investigate the enzyme activity after adding the thiol compound. Red curve; activation of papainS-SPy using compound 26, enzyme (10.4 µM), L-BAPNA (0.98 mM) in the presence of compound 26 (0.2 mM). The blue line is background where is no thiol then compound 26 was added, at 25 °C, pH of solutions ≈ 6.5, the experiment was repeated twice

4.5.4 pH Effect on the Hydrolysis Rate

Papain has its maximum activity in the pH range between 4 and 8. In order to confirm this a series of samples was prepared to contain the same concentration of papainS-SCH$_3$, L-BAPNA, and thiol compound **26**. Then the different volumes of NaOH (1 N) were added to each sample, the pH was measured using litmus paper (a normal pH probe was not used to avoid damage to the probe due to reaction with the thiol). The hydrolysis rate increased with increasing the pH from 2-7, as Figure 4-10 illustrates and, at high pH (> 8) the hydrolysis rate increased immediately by the base catalysis rather than enzyme catalysis. Because of these results, a consistent pH of 6-7 was used throughout, although these data show that the enzyme-catalysed reaction is not sensitive to pH over a wide range.
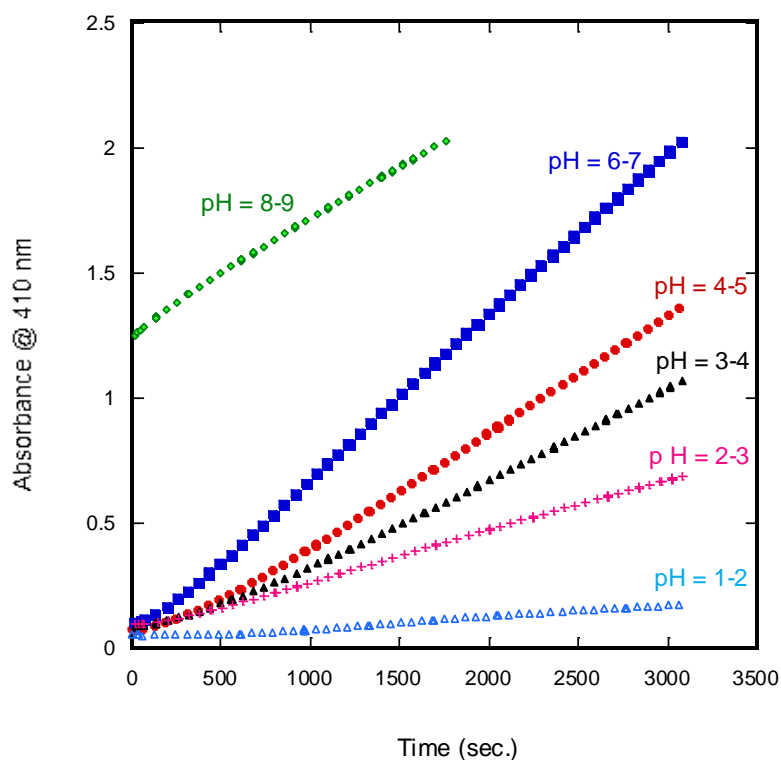
Figure 4-10. *Effect of changing the pH on the papain activity. PapainSSCH$_3$ (10 μM), L-BAPNA (98 μM), thiol compound **26** (0.2 mM), the experiment was repeated twice.*

4.5.5 Isopropyl-3-mercaptopropionate Concentration Effect

The effect of isopropyl-3-mercaptopropionate concentration was investigated (compound **26**) in a buffer solution. Different concentrations (0.02, 0.05, 0.1, 0.2, 0.4, 0.6 mM) of thiol compound **(26)** were used to activate the enzyme at pH 6-7 and hydrolyse the substrate. We indicated that using low concentrations of thiol, there is no significant effect on the hydrolysis within a short time-scale (2 hours). At higher thiol concentrations (over 0.1 mM) the hydrolysis rate increased dramatically. It seems that the concentrations up to 0.1 mM led to faster activation of the inactive enzyme, Figures 4-11 and 4-12 show how compound **26** enables enzyme activation; moreover, a comparison was made between two water-miscible solvents (THF and dioxane). Using dioxane showed that increasing the thiol concentration led to gradual enhancement in the hydrolysis rate.
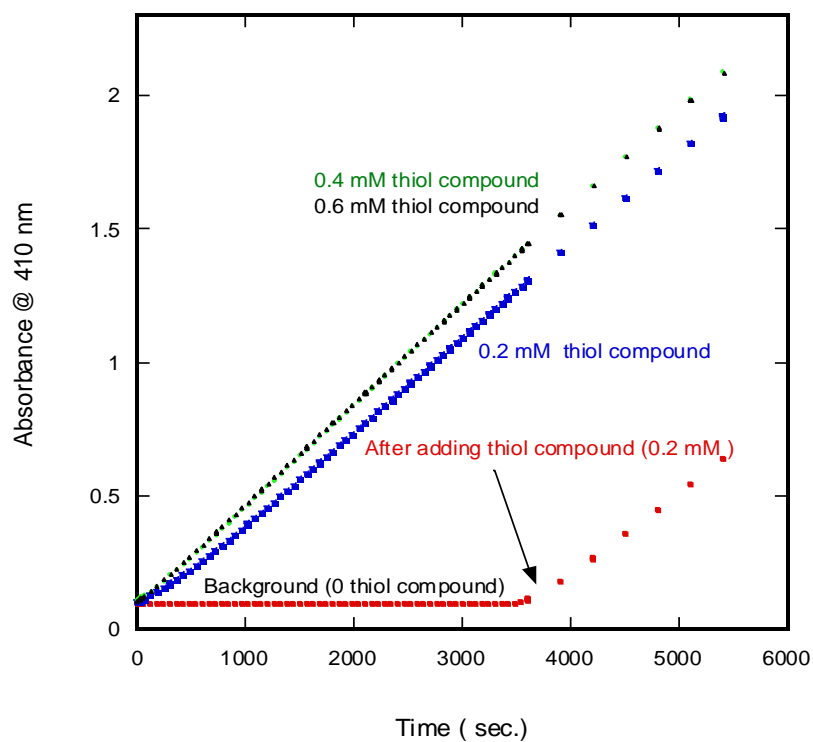
Figure 4-11*: Effect of thiol concentration on the hydrolysis of L-BAPNA. PapainSSCH₃ (10.4 µM),
L-BAPNA (0.98 mM) compound **26** was dissolved in THF, pH 6-7, at 25 °C.*
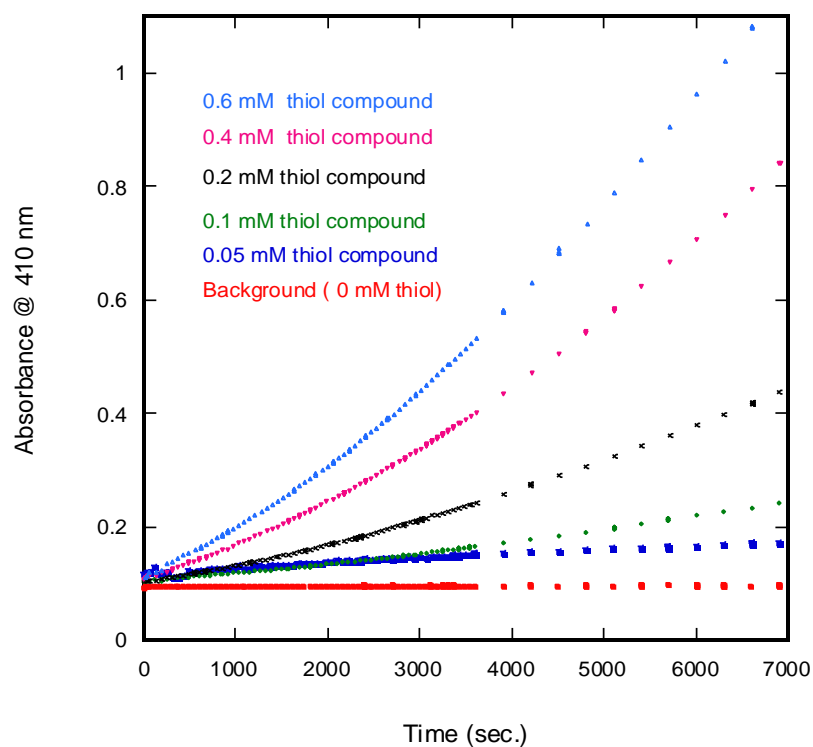
Figure 4-12*. Effect of thiol concentration on the hydrolysis of L-BAPNA. PapainSSCH₃ (10.4 µM),
L-BAPNA (0.98 mM) compound **26** was dissolved in dioxane, pH 6-7, at 25 °C.*

The reactivity of the long thiol compounds **24** in solution was investigated and compared with compound **26**. Background reactions were run at the same time with two samples containing the same concentration of papainSSCH₃, L-BAPNA; one of them contained compound **24**, the other contained compound **26**. Figure 4-13 shows that the active enzyme in the background reaction cannot hydrolyse the substrate; this suggests the enzyme has oxidised and turned to an inactive form. Adding compound **26** triggered the L-BAPNA hydrolysis, while compound **24** which was dissolved in THF [compound **24** and **25** not soluble in alcohols, trifluoroethanol, DMSO (dimethyl sulfoxide) or acetonitrile] caused a decrease in the absorbance over a long time-scale. Varying the concentration of compounds **24** or **25** in the solution did not show any reactivity, due to precipitation (even if they were dissolved in THF or dioxane). Hence, examining the reactivity of compounds **24** and **25** in solution was not possible.
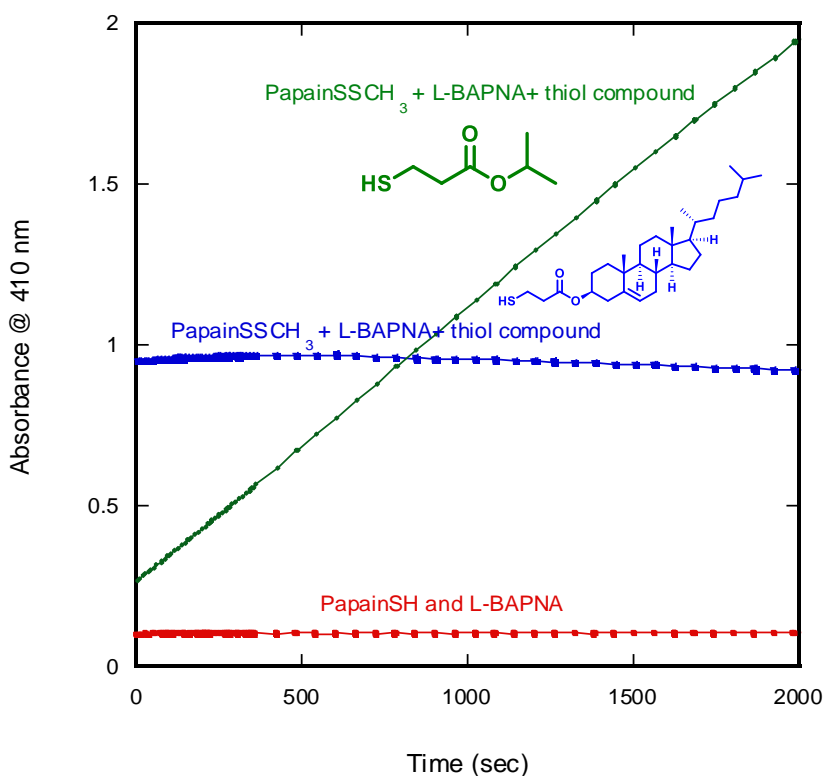
***Figure 4-13**. A comparison between compound **24** and **26** in the solution. The red line; is the background reaction containing papain (12 μM) and L-BAPNA (1.1 mM), the green line is reaction including papainSSCH₃ (12 μM), L-BAPNA (1.1 mM) and thiol compound **26** (0.2 mM) with the same and the blue line including papainSSCH₃ (12 μM), L-BAPNA (1.1 mM) and compound **24** (0.2 mM).*

4.5.6 Reactivity in the Bilayer Membrane (Vesicles)

Mixing organic solutions containing phospholipids and the synthetic thiol molecules **24** and **25** will form a vesicle where the thiol orients approximately 50% of the thiol outside and 50% inside (due to the flip-flop mechanism) as shown in Figure 4-14. From the above data, it was shown that they can activate the inactive papain that added to the bulk solution outside the vesicles due to release *p*-nitroaniline, which gives a strong absorption at 410 nm. While no change in the absorption was noticed when no enzyme or no substrate is present in the surrounding aqueous phase. Hence embedding the thiol into the vesicles caused a clear change in the absorption.
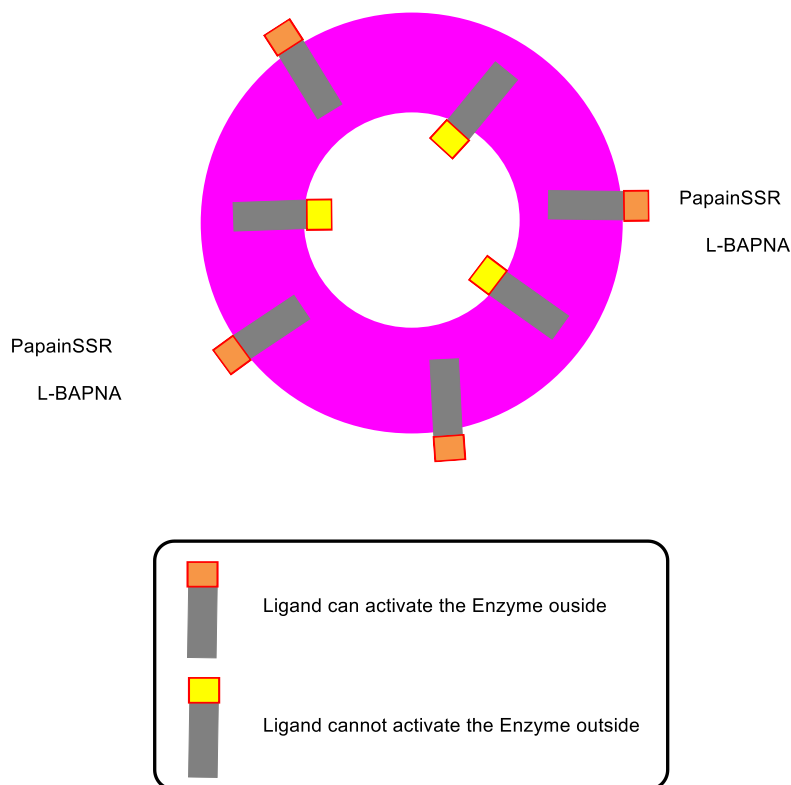
Figure 4-14. Thiol compound orientation in the vesicles when mixing their organic solvent together

4.5.7 Effect of the Thiol Concentration

Two different concentrations of vesicles (1.3 mM and 0.7 mM) incorporating different concentrations of compound **24** (16 µM, 31 µM, 62 µM) were prepared. The aim was to establish the relationship between the concentration of the vesicles, their loading with compound **24** and papain activation. Figures 4-15 and 4-16 show that increasing the vesicle and compound **24** concentrations led to an increase in the hydrolysis rate.
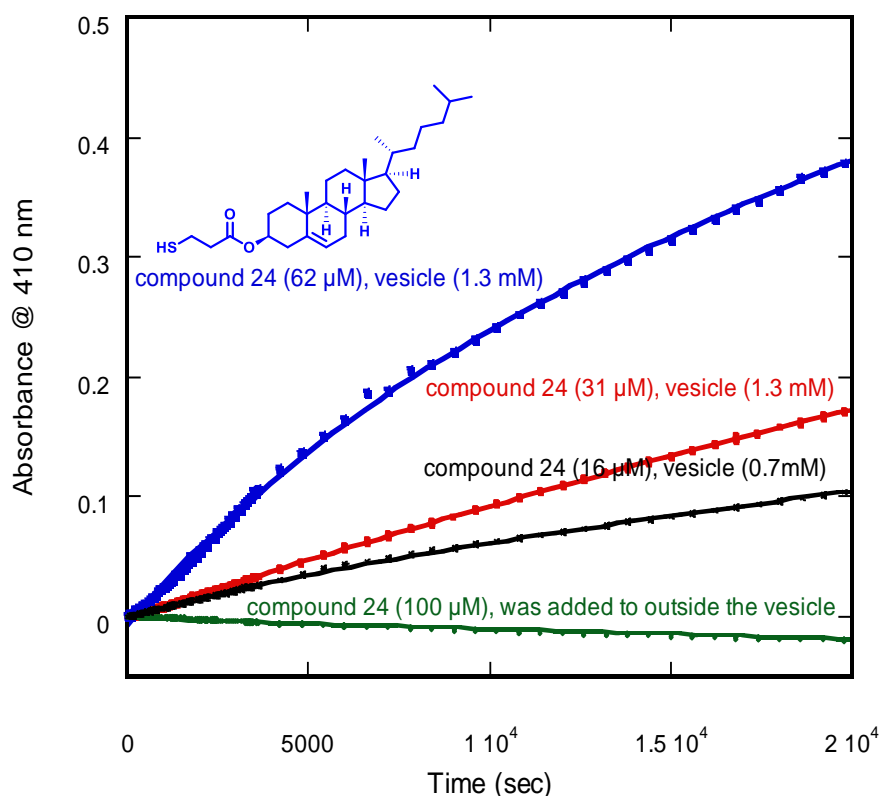
Figure 4-15. *Variation the concentration of vesicles and the incorporated thiol compound. Concentrations; [Vesicles] =1.3 mM and 0.7 mM,, [compound **24**] = 62 µM 31 µM, and 16 µM [papainSSCH₃] = 5 µM, [L-BAPNA] = 0.9 mM. The green line; [compound **24**] = 100 µM was added to outside the vesicles, papain and L-PABNA inside encapsulated in the vesicles.*

Different concentrations of compound **24** were embedded into a certain concentration of vesicles, and high concentrations were used (160 and 120 µM) showed higher activity than the lower concentrations (80 and 40 µM) as Figure 4-16 shows. The curvature (bend) at the beginning of the curves can be attributed to the binding between the inactive enzyme and

the thiol compound until the enzyme becomes activated similar to what explained in Equation **4-6** and **4-7** (Section 4.5.2).
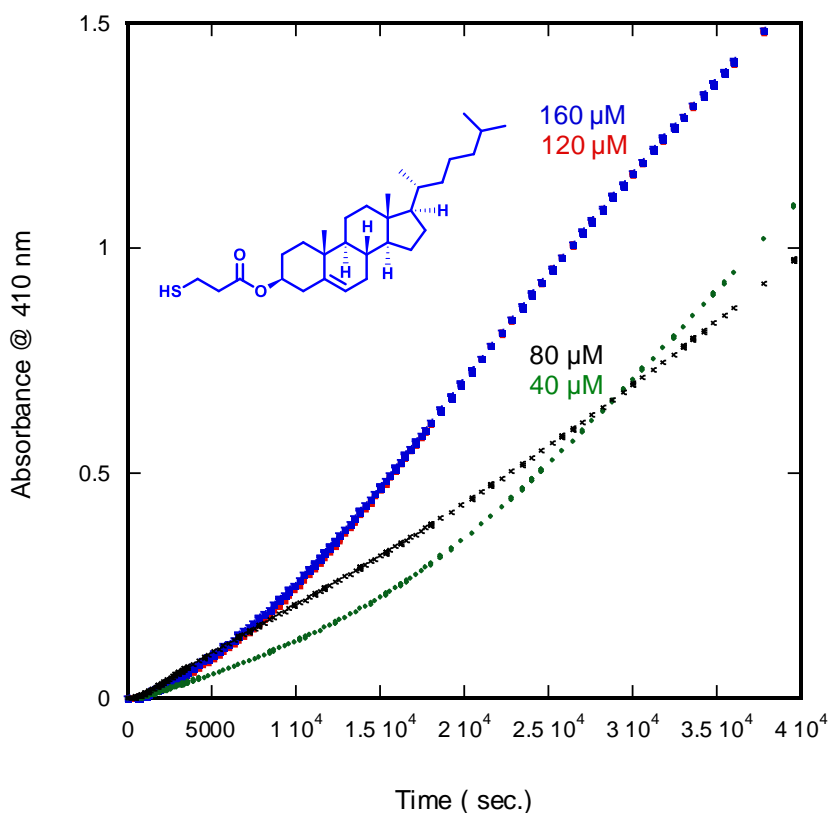
Figure 4-16. *Variation the concentration of compound **24** at a fixed concentration of vesicles (1.6 mM). Vesicles were embedded with different concentrations of compound **24** and vesicles with less concentration of **24** had pure cholesterol added to keep the structure of the vesicle the same in each case. PapainSSCH₃ (10.4 µM), L-BAPNA (0.98 mM) were added to outside the vesicles.*

The results show that there is no difference between thiol concentrations 160 and 120 µM which they are embedded into vesicles and the change between these concentrations and less concentrations (80 and 40 µM) appears after long time-scale of the reaction. It seems that the different concentrations of thiol in vesicles can affect the rate of activation. Nevertheless adding the thiol afterwards did not increase the rate significantly; and that adding cholesterol did not effect from changing the concentration of thiol.

Compounds containing different sterols, cholesterol and lithocholic acid (**24** and **25** respectively) were compared. Thiol compounds **24** and **25** were incorporated in vesicles then the inactive enzyme and L-BAPNA were added to the bulk solution. These experiments showed a good absorbance change over time. The two compounds were mixed with lipid mixture in the same concentration and same ratio (1:13, thiol compound: lipid),.and the data

showed there is no significant difference in the absorbance using the two compounds (**24** and **25**) over a time-scale of 7 hours, (Figures 4-17).
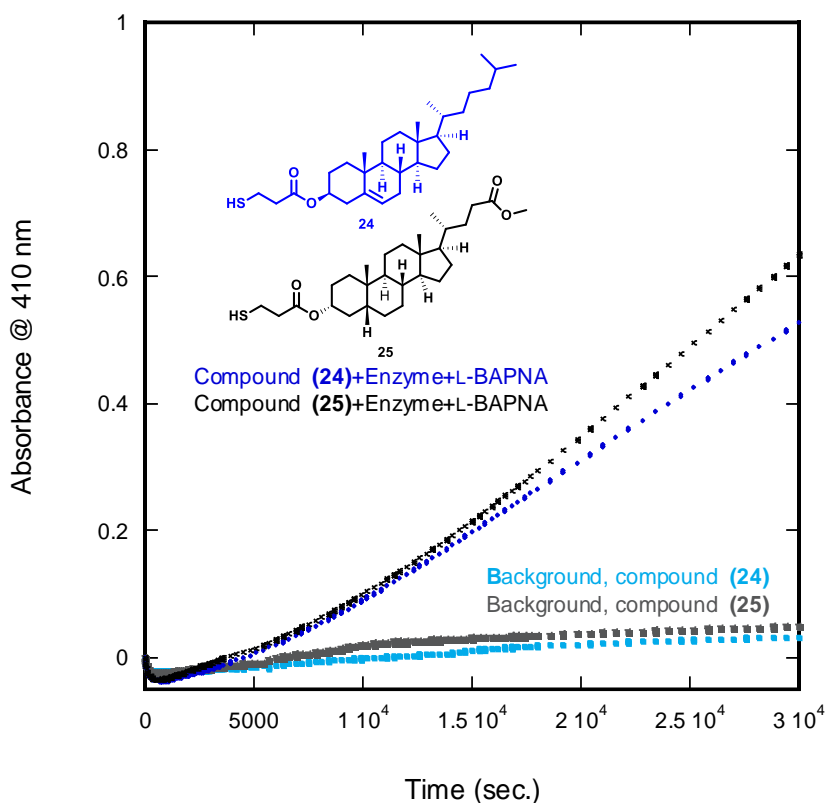
Figure 4-17. Compound 24 or 25 (120 μM) were embedded into vesicles (1.6 mM), L-BAPNA (0.98 mM), papainSSCH₃ (10.4 μM) were added to outside the vesicles. Background reaction does not include an enzyme.

4.5.8 Comparison between Reaction in Solution and in Vesicles

On the assumption that the thiol embedded into vesicles will orient into two ways (outward and inward, Figure 4-14), this means only half of the total thiol concentration will be able to activate the enzyme compared with the whole thiol concentration in the solution. Furthermore, the interaction between the thiol compound and the enzyme to form the active enzyme which catalyses the substrate later is more facile in a solution because the thiol can move easily in three dimensions. Figure 4-18 presents a comparison between two reactions, one of them in a solution and another one in vesicles incorporated with the thiol compound.
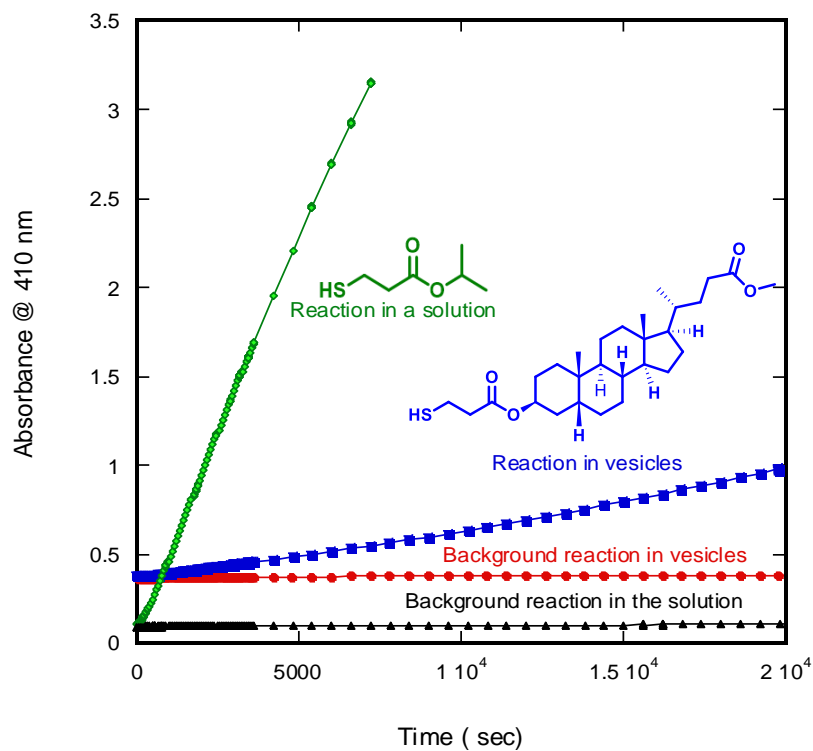
Figure 4-18. *Vesicles versus solution, the* *red* *and* *blue* *lines; thiol compound* **25** *(120 μM) was embedded into vesicles (1.6 mM), L-BAPNA(0.98 mM), the* *red* *line; no enzyme was added. The* *blue;* *papainSSCH₃ (10.4 μM) was added to outside the vesicles. The* **black** *without thiol and* *green* *with thiol* **26** *(200 μM) in the solution and the same substrate and enzyme concentrations were added. The experiments were run at 25 °C, pH 6-7.*

4.5.9 Encapsulation Experiments

Isopropyl-3-mercaptopropionate (**26**) is probably capable of crossing the membrane and therefore activates the enzyme both outside and inside of the vesicles. To prove that the thiol molecule was crossing the membrane and reaching the interior phase where the inactive enzyme and the substrate are, encapsulation experiments of the papainSS-CH$_3$ and L-BAPNA on the interior of vesicles were undertaken. This was achieved by preparing vesicles in the usual way, but instead of adding only buffered solution, solutions of an inactive enzyme and L-BAPNA were added to be encapsulated inside the vesicles. After the extrusion, the enzyme and L-BAPNA were both inside and outside the vesicles. In order to remove the substrate and the enzyme from outside, the vesicle solution is purified by gel permeation column (GPC, PD-10, convenient to separate proteins and other large molecules $>$ 5000 M$_r$), and the substrate is separated according to size. As the vesicles have a very large molecular weight, these are eluted first when the buffered solution is applied.

***Figure 4-19.** Molecules separate according to the size using gel permeation column.*

Compound **24**, **25** or **26** in THF or dioxane was added to the bulk solution (outside the vesicle). With compounds **24** and **25** precipitation occurred and the absorbance decreased. Short thiol compound **26** led to a significant absorption change over the course of an hour after adding L-BAPNA to outside the vesicles.

This indicates that there is some of papainSSCH$_3$ still outside the vesicle after the purification (Figure 4-19) and after adding the thiol compound and the substrate the reaction starts as illustrated in Figure 4-20.

Figure 4-20. *The reactivity in encapsulation experiments shows there is no reactivity even for long time-scale to compound **24**. (50 µM)   The red line; compound **24** was added to the outside the vesicles. The blue curve; compound **26** (50 µM) was added to the outside the vesicles (the experiment was repeated twice).*

4.5.10 Investigation of the Location of Thiol Compounds

It was noticed that the absorbance was stable for 45 minutes before adding anything but, adding the thiol compound **24** or **25** in THF or dioxane led to a sharp increase then decrease in the absorbance while this did happen with the short thiol compound.

To find in which way the thiol compound can orient in the vesicles solution, experiments with Ellman's reagent were undertaken. Ellman's reagent was used as it can react with thiol compounds as shown in Scheme 4-5. It was hypothesized there are two ways for the thiol compounds to orient as illustrated in Figure 4-21.
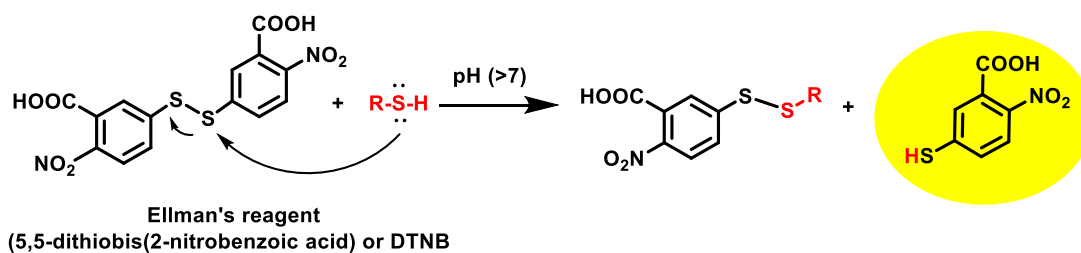
Scheme 4-5. *The mechanism for the reaction of Ellman's reagent with thiol compounds in basic medium.*
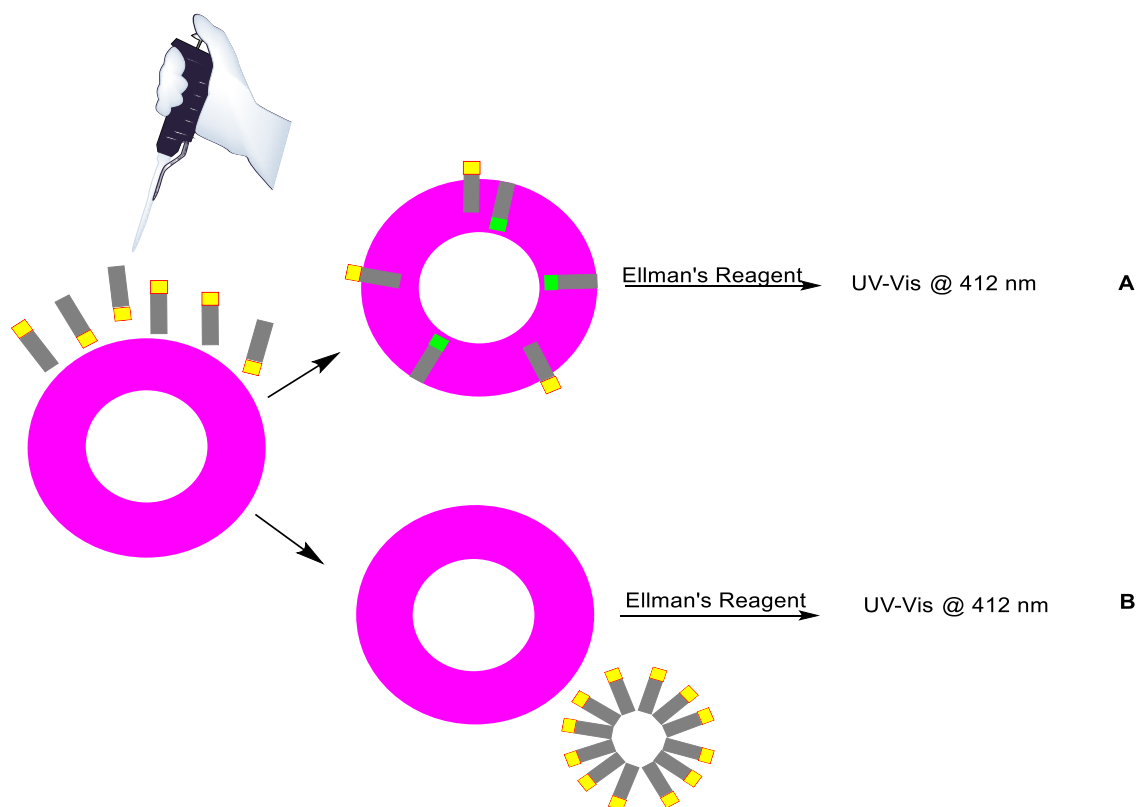
Figure 4-21. *The possible locations of the thiol compounds in the vesicle solution.*

The long thiol compounds **24** and **25** have two possible orientations **A** and **B** (Figure 4-21) in the vesicle solution. In **A** the compound will insert in the vesicles and directed inward and outward of the vesicles and the 50% (outward) will react with Ellman's reagent (5,5-dithiobis(2-nitrobenzoic acid) or DTNB as in Figure 4-21. In **B** the thiol may have self-assembled outside the vesicles by forming micelle and this led to decrease the absorbance

(with the reverse micelle there would not be any signal at 412 nm due react the Ellman's with the thiol because the headgroups will orient inside).

Pure vesicles (no thiol compound incorporated), papainSSCH$_3$ and L-BAPNA (inside the vesicles) were mixed. Then the thiol compound was added to the exterior vesicular phase (pre-formed vesicles). It was assumed that due to its lipophilicity and known insolubility in aqueous buffered that it would insert into the vesicle bilayer. However, it is well known that oxidation of thiols compounds is extremely facile (the compounds were generally stored under argon and in the fridge). Our compounds showed high stability against oxidation; this was confirmed by deliberate oxidation of the compounds using potassium ferricyanide and confirmation using NMR spectroscopy (see the appendix for the compounds' spectra).

An interesting question here is if the headgroups face the outside and they react with Ellman's why did not activate the enzyme?

In order to investigate this, 1.6 mM pure vesicles (from lipid only) were made and purified then compound **24** was added to outside the vesicles. Part of the sample was purified again using a GPC column to remove the thiol compound, as these are much smaller than the vesicles. As illustrated in Figure 4-22 the UV/Vis data showed there is absorbance at 412 nm this means there is a reaction between the thiol and Ellman's reagent. The blue line refers to the vesicles solution and 120 µM compound **24** in dioxane was added to outside the vesicles then the solution left to equilibrate for 30 minutes then purified again using GPC column. The red line refers to the same vesicle solution and 120 µM compound **24** in dioxane was added to the outside and left without second purification. Then to each sample was added Ellman's reagent, which reacts with any free thiol group.
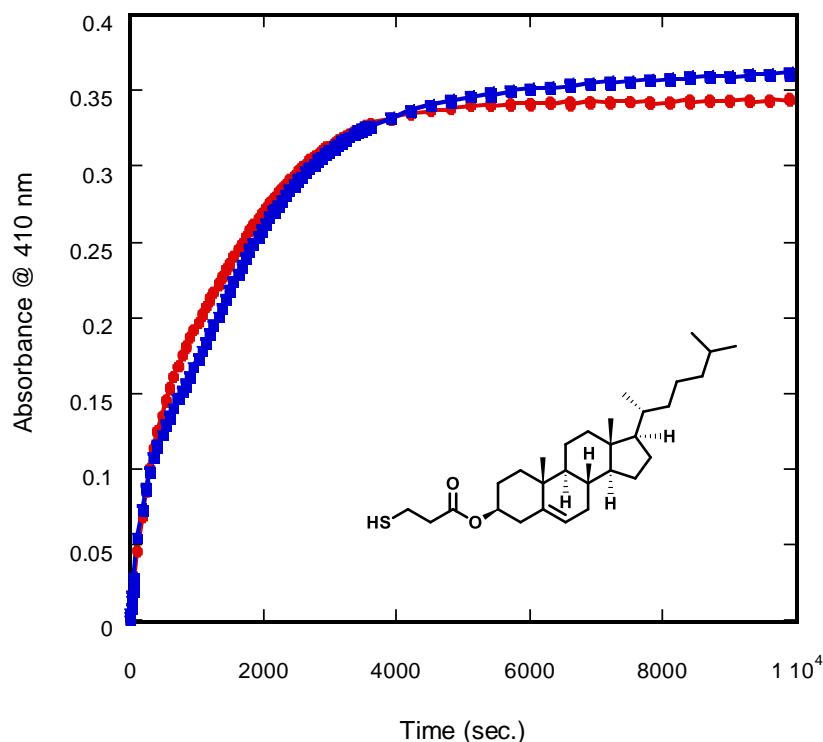
Figure 4-22. *Ellman's reagent was added to outside the vesicles to indicate the thiol. Pure vesicles (~2 mM), compound **24** in dioxane (0.1 mM) was added to outside then after 30 minutes the solution purified again and Ellman's (10 μL of 100 mM) was added, (the experiment was repeated twice).*

The conclusion from this experiment is that thiols are present and are not removed by GPC, so either they are incorporated into the vesicles, or aggregate and are not separated by GPC.

4.5.11 Dynamic Light Scattering (DLS)

A comparison was implemented using the DLS technique to see if the thiol can insert into or permeate the vesicles and reach the internal aqueous layer where the inactive papain and the substrate are located. The particle size of the pure vesicles of lipid only was measured, then long thiol compound **24** or **25** (in dioxane) was added to the external aqueous layer. The measurements were done again after equilibration for 15 minutes and obvious size changes were noted, suggesting that the thiol compounds especially compound **24** had inserted into the bilayer membrane (vesicles). In order to see if the compounds inserted into the vesicles or just were attached outside the vesicles, a second purification of the vesicles solution (using the GPC column) was performed. The vesicle size was similar to the size it was before adding compound **25**. As this result did not occur with compound **24**, this may

133

be because that compound **24** inserted into the vesicles while compound **25** did not. Table 4-1 shows the size of the vesicles before and after the second purification.
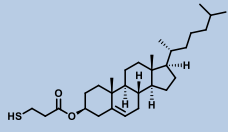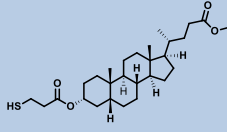
Experiment	Vesicles size (nm)	
	Thiol compound **24**	Thiol compound **25**
Before any addition	181.4 ± 1.8	181.4 ± 1.8
After adding 0.2 mM thiol	266.4 ± 11.7	233.9 ± 1.3
After purifying the vesicle solution again	244.2 ± 5.8	182.0 ± 5.2

Table 4-1. *The DLS findings to the pure vesicles, vesicles size after adding compound **24** or **25**, and vesicles size after the second purification after thiol addition.* see the appendix.*

4.5.12 Investigation of the Suitability of the GPC Column to Separate or Purify the Large Molecules Such as PapainSSCH₃

In this part, pure vesicles from lipid only were prepared, then papainSSCH$_3$ in buffer **B**, (40 mM sodium phosphate, 2 mM EDTA, pH 7.6, see the experimental part) and bis-tris buffer (instead of the substrate) were added. After this, the final volume (3 mL) was purified again using the GPC column, but only 2.5 mL was collected (not 3.5 mL) which was then separated into two cuvettes. To one of the cuvettes was added a concentration of compound **24** and to another one has added the same concentration of compound **26**. We observed that adding the L-BAPNA triggered the reaction in the presence of compound **26** and a significant absorbance change occurred, which proved that there is some papainSSCH$_3$ still outside the vesicle solution even after purification using the GPC column. The case was different with compound **24** as Figure 4-20 shows because the absorbance did not increase with a long time.

To investigate where the absorbance signal belongs to the lipid itself, to the buffer solutions, or maybe to Ellman's reagent in the buffer, a control experiment was run with each possible composition in a buffer (pH = 7.6) and the absorbance monitored. A pure vesicle solution in a buffer (pH = 7.6) that was treated with Ellman's did not show any absorbance change as illustrated in Figure 4-23. The sample of vesicles solution without thiol where papainSSCH$_3$ and L-BAPNA were added to the outside did not show any increase in the absorbance. Meanwhile, another sample containing vesicles incorporated with thiol compound **24** showed progress in the absorbance. The one reaction could not monitor was that including thiol compound **26** and Ellman's (0.4 mM) in a buffer (pH = 7.6); the reaction started immediately (the colour turned from colourless to dark yellow quickly).
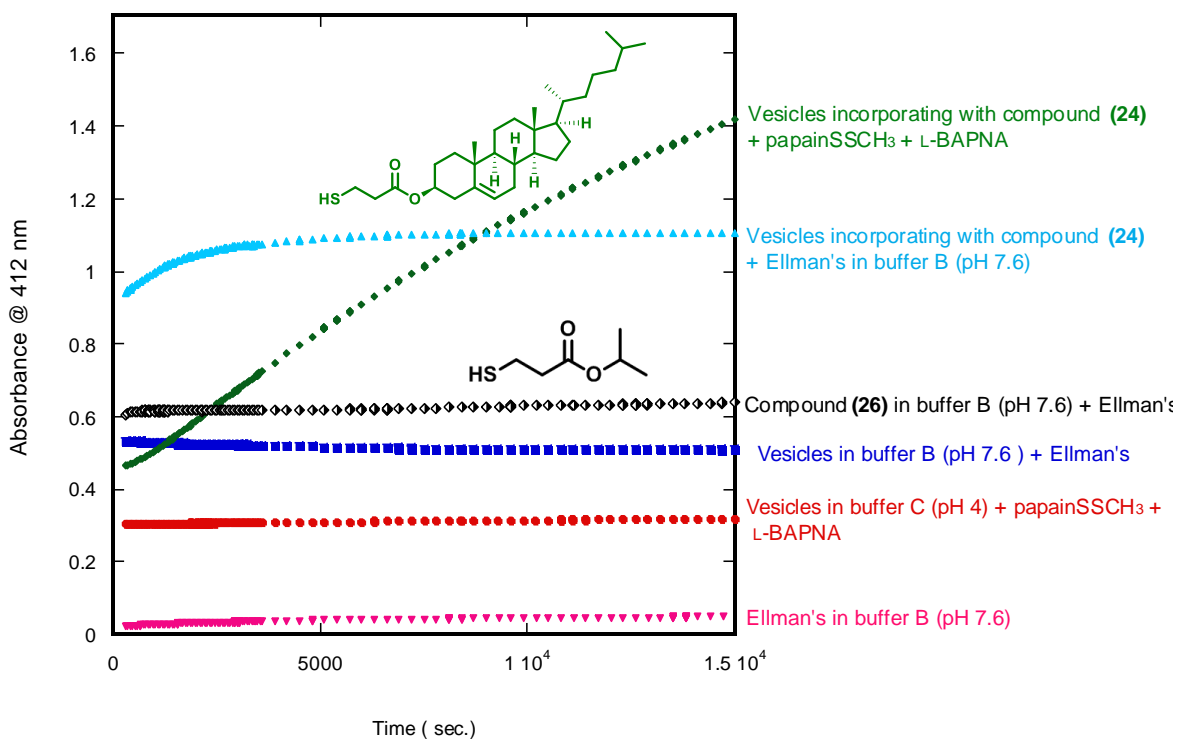
Figure 4-23: Indicates thiol reactivity using Ellman's reagent, concentrations are: [vesicles] =1.6 mM,[compound 24] =120 μM, [papainSSCH$_3$]=10.4μM, [L-BAPNA] = 0.98 mM, [compound 26] = 0.05 mM), [Ellman's] = 0.4 mM (the experiment was repeated twice).

4.5.13 On-Off System

The experiments described above lead to the conclusion that the embedded thiols **24** and **25** are capable of activating papain that has been inactivated. The activation appears to be less effective than for simple thiols in solution but does occur on a comparable time scale.

Knowing that this type of compound can show this activity, we needed to investigate whether the activity can be turned off. If this can be achieved, then this will open up the prospect of creating a transducer that can exploit the efficiency of enzyme catalysis.

In order to find an answer to the final aim of the project, another transducer molecule needs to be synthesised, bearing a polar headgroup, on the opposite end to the thiol, which can be switched between polar and non-polar groups (Figure 4-1). This would allow the enzyme activation mechanism to be implemented in signal transduction as part of a larger system analogous to that found in the literature.[124,182] The applications of such a system would be broad, such as in catalysis, nanotechnology and drug delivery.[124 182, 3, 183,184, 181.]

The proposed transducer with two polar headgroups was prepared from lithocholic acid (Scheme 4-6) by protecting the carboxylic acid group with ^{t}BuOH first, then adding 3-(tritylmercapto) propanoic acid to the alcohol. In the last step, both functional groups were deprotected.
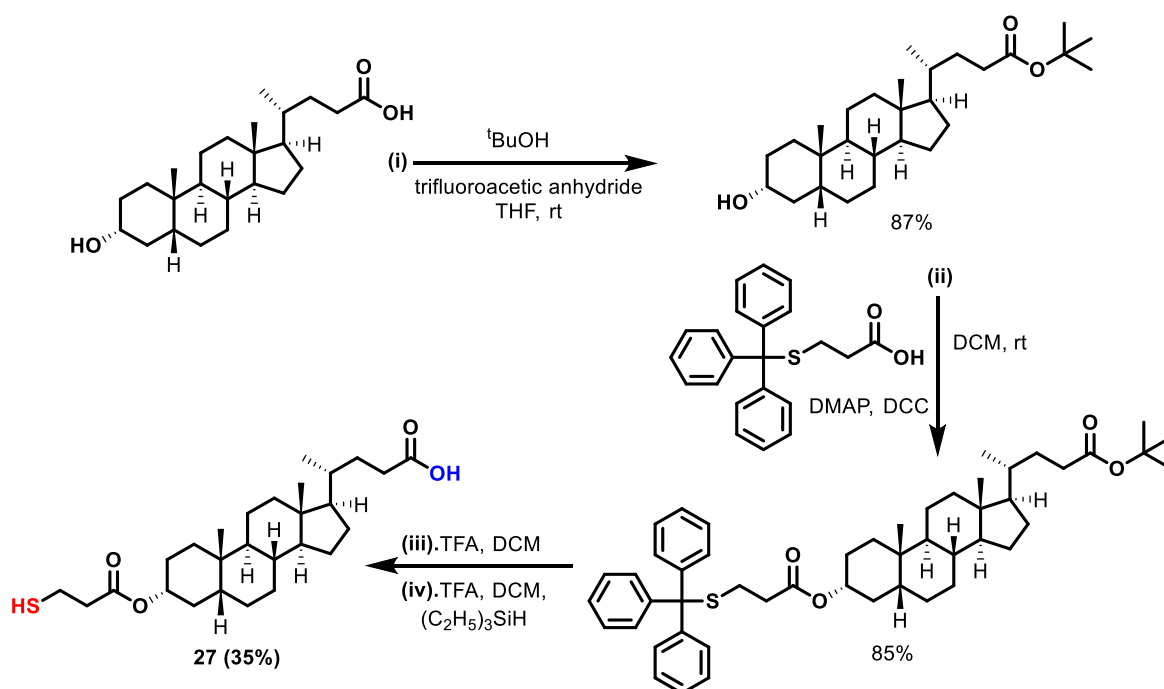
Scheme 4-6. *Preparation of the ligand with two polar headgroups*

To control the activity of the transducer, the aim is to change the pH and turning the acidic COOH group at another end of the molecule (Figure 4-24). In this case, if the pH (> 7) the COOH will deprotonate to COO$^-$ then it will prefer to sit in the aqueous layer. Therefore, this will pull the thiol head in the membrane more than in the exterior aqueous layer.
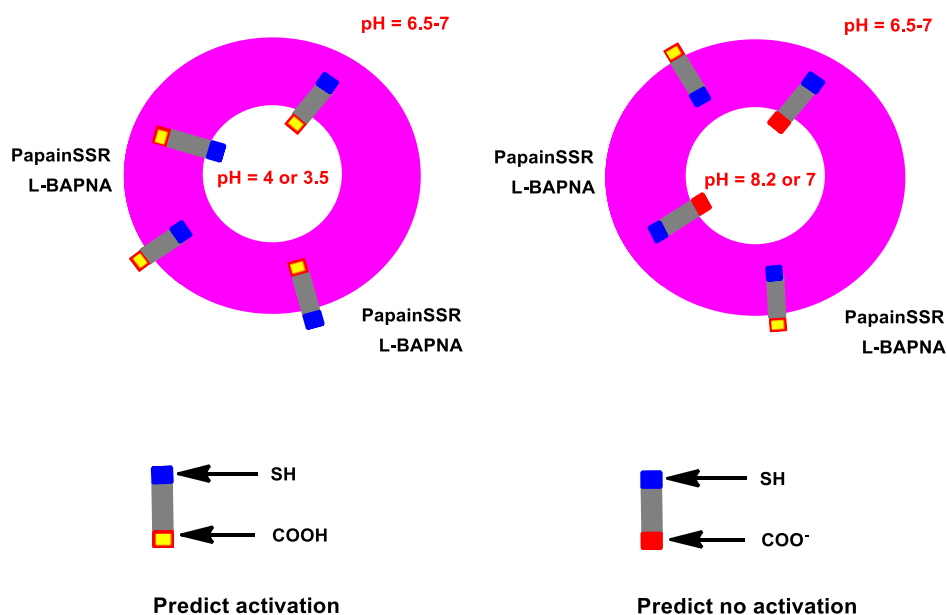
Figure 4-24. *The pH effect on the acidic headgroup*

On changing the pH inside the vesicles to slightly basic (pH = 7.7 or 8.2) and keeping the pH outside as usual (pH 6-7) showed very similar activity to when the pH inside equal 4 (vesicles encapsulated with buffer, pH = 3.5 or 4) as Figure 4-25 displays.
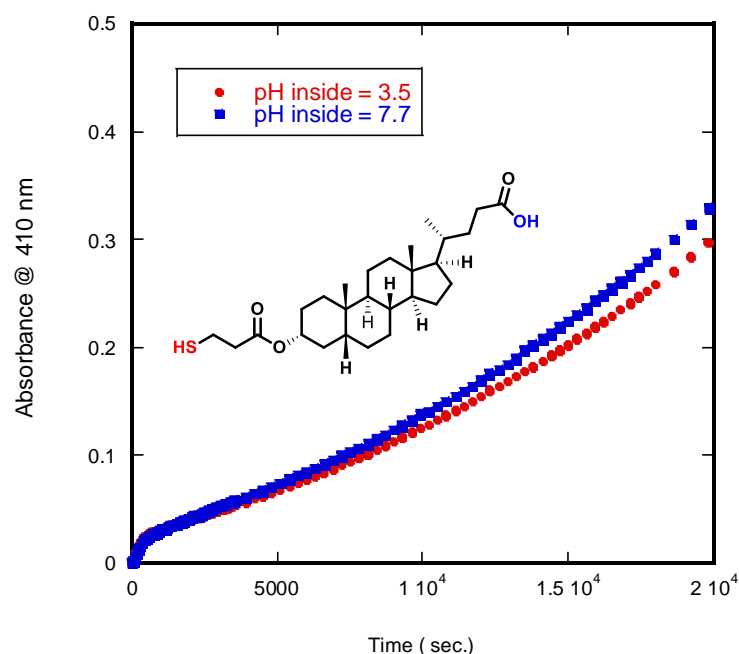
Figure 4-25. *Vesicles (1.6 mM) were embedded with compound **27** (0.12 mM), papinSSCH₃ (10.4 uM) and L-BABNA (0.98 mM) were added to outside the vesicles. The red curve; pH inside the vesicles is 3.5, the blue curve the pH inside is 7.7 and pH outside the vesicles is 6-7.*

137

Thiols are more acidic than alcohols (pK_a for thiol ~10, pK_a for alcohol ~16); therefore, the pK_a of the thiol compounds must be taken into account as the pK_a for compound **27** will decrease to around 5 for the carboxylic acid group. When the reaction environment is basic (high pH) the thiol will ionise and be prone to oxidation to disulphides, therefore the pH of the reaction is better kept below 8.

As a direct comparison, the two lithocholic derivatives **25** and **27** were used in experiments where the pH inside the vesicles was 7 and outside was 6-7. The UV/vis data disclosed that both ligands (ending with a carboxylic acid or methyl ester group) behaved similarly, activating the enzyme outside the vesicles. This led us to say that the carboxyl group was not polar enough to control the position of the transducer in the membrane layer.

4.6 Conclusion

The first aim was to see if a ligand molecule embedded in a membrane could be used to activate an inhibited enzyme. This was investigated using papain, which was inhibited by a disulphide formed with the critical thiol in its active site. Ligand molecules based on cholesterol **24** and lithocholic acid **25** were successfully synthesised and embedded in vesicles. L-BAPNA, a substrate for papain, was added to vesicles containing these molecules in the presence of inhibited papain. This led to an increase in the absorbance at 410 nm correlating to the release of *p*-nitroaniline. This indicated that the thiol of **24** or **25** had successfully activated papainSSCH$_3$, leading to hydrolysis of the substrate. This is strong evidence that the thiol embedded in the membrane was reacting with the disulphide bond inhibiting the papain. Incorporation the long thiol compounds **24** and **25** in the vesicles showed good reactivity using a low concentration of papain and a large concentration of L-BAPNA, which indicates that this enzyme undergoes multiple turnovers, which leads to the amplification of each deprotection event.

In order to activate the enzyme inside the vesicles, translocation of the thiol ligand to the interior phase is the key requirement, along with ensuring that the thiol and inhibited enzyme do not come into contact with each other. This requires that the thiol is added after the enzyme is encapsulated, so that the thiol only reaches the enzyme if it is allowed to cross the membrane. Due to the low solubility of the ligands (**24** and **25**) in aqueous solvents, adding the compounds to pre-formed vesicle was not possible.

The second aim was to investigate whether the system had the potential to be in a completely inactive 'off' state. To test whether activation could be prevented, a molecule with two polar headgroups (compound 2**7**, Scheme 4-6) was synthesised to establish a translocation system. This required the reaction to be carried out inside the vesicles rather than at the outside surface. The results showed that there is difficulty in controlling the position of this molecule in the membrane when the pH was changed. This may be attributed to the polarity of the headgroup (OH) and the acidity of the thiol group (pK_a).

The outcome of the control reaction (papain and L-BAPNA in solution, no vesicles) ruled out the possibility under the conditions used.

The results of the research suggest the system did have the potential for signal amplification, the overall aim. As the investigation into the first aim showed that the thiol embedded in the

membrane was capable of activating the protecting papain, it can be assumed that amplification is possible. One molecule of **(25)** was assumed to activate one enzyme active site, in a stoichiometric reaction. As enzymes are efficient catalysts, it was assumed that one papain molecule had the potential to convert all substrate molecules.

Different concentrations of substrate and papainSSCH$_3$ should be investigated to see if the output signal could be changed. However, the key problems that need to be solved are the successful encapsulation of the inhibited enzyme, removing any enzyme that has not been encapsulated, and a method to introduce the transducers to the outer leaflet of the fully formed vesicles.

4.7 Experimental

4.7.1 Preparation of the Buffer Solutions According to the Thiol and Sulphide Quantitation Kit[185]

Buffer A: 5 mM solution sodium acetate, 50 mM NaCl, 0.5 mM EDTA, pH 4.7

Sodium acetate (41 mg) and NaCl (292 mg) were dissolved in deionised water (80 mL). EDTA (1 mL of 50 mM, pH 8.0) was added, then the pH was adjusted to 4.7 with 1 M HCl. Sufficient deionised water was added to bring the volume to 100 mL.

Buffer B: 40 mM sodium phosphate, 2 mM EDTA, pH 7.6

NaH_2PO_4 (0.55 g) was dissolved in deionised water (80 mL). EDTA (4 mL of 50 mM, pH 8.0) was added, and the pH was adjusted to 7.6 with 1 M NaOH. Sufficient deionised water was added to bring the volume to 100 mL.

Buffer C: 5 mM sodium acetate, pH 4.0

Sodium acetate (41 mg) was dissolved in deionised water (80 mL). The pH was adjusted to 4.0 with 1 M HCl. Sufficient deionised water was added to bring the volume to 100 mL.

Bis-Tris/EDTA buffer, pH 6.3

Bis-Tris (50 mM) and EDTA (1 mM), the pH was adjusted to 6.3.

All buffer solutions were degassed thoroughly before use.

4.7.2 The Substrate Solution

A 4.9 mM stock solution of *N*-benzoyl-L-arginine, p-nitroanilide (L-BAPNA) was prepared by first dissolving the L-BAPNA (55 mg) in DMSO (1.5 mL) The solution was sonicated briefly to help solubilize the L-BAPNA and then of Bis-Tris/EDTA buffer (24.5 mL) was added. The solution was stable for up to six months at 4 °C.

4.7.3 Deactivation of Papain Enzyme

Papain-S-S-CH$_3$ was prepared according to Singh and co-workers procedure with some modifications.[186] Papain from papaya latex lyophilized powder (3.6 mg) was suspended in 3 mL buffer B, pH 7.6. To this solution was added S-methyl methanethiosulfonate (10 µL) or aldrithiol-2 (2,2'-dipyridyldisulphide) (5 mg). The reaction mixture was stirred at 4 °C for 90 min. The enzyme was then purified using G25, P-10 column (Sephadex anion exchange column, convenient to separate proteins and other large molecules > 5000 M$_r$). To prepare papain working solution; the above solution was mixed in the reaction day with the same volume of buffer C.

4.7.4 Thiol Compounds

The thiol compound solutions (5 mM in THF or DCM) were prepared freshly on the reaction day to avoid any oxidisation, however, the compounds did not oxidise and they are stable (evidence comes from leaving the compounds exposed to the air for 5 days then repeat the NMR, see the appendix).

4.7.5 Vesicle Preparation

Phospholipids used for vesicle preparation must generate membranes that are capable of maintaining a pH gradient so that the pH on the outside and inside of the vesicles can be changed independently. In addition, the vesicles must be impermeable to the substrate, the product, and the buffer. A mixture (3:2) from 1,2-dioleoyl-**s**n-glycero-3-phosphocholine (DOPC) and 1,2-dioleoyl-sn-glycero-3 phosphoethanolamine (DOPE) lipids was found to perform this function effectively.

A stock solution of DOPC and DOPE in a 1:1 mixture of chloroform and ethanol (10 mL, 13 mM) was made (solution 1). A stock solution of cholesterol mercaptopropanoate **(24)** or Me-lithocholic mercaptopropanoate **(25)** in THF (2mL, 5 mM) was also made (solution 2). Buffer **A** was made as mentioned previously.

To a clean, dry 5 cm^3 a round-bottomed flask was added lipid stock solution (770 µL, 13 mM) and cholesterol mercaptopropanoate (**24**) or Me-Lithocholic

mercaptopropanoate (**25**) stock solution (50 μL-150 μL, 5 mM), and the solvents were evaporated under high vacuum for 2 hours to afford a thin film on the wall of the flask. This was hydrated in buffer **A** (2.5 mL) and vortexed for 30 seconds. The solution was extruded through a polycarbonate membrane with 200 nm pores, using an Avestin "LipoFast" extruder apparatus, 27 times, before purification using Sephadex G-25 in PD-10 Desalting Columns with 3mL buffer **A** to give 200 nm diameter vesicles in a solution of buffer **A**. The final concentration of lipid was ≈ 2 mM and final transducer concentration was 100 μM (≈ 5%, 1:20 loading of transducer in vesicles). The diameter of the vesicles was confirmed by dynamic light scattering (DLS).

Chapter 5 -   Final Conclusion and Future Work

This study set out to investigate the ability of oxime-Zn^{2+} complexes to work as efficient catalysts to hydrolyse ester substrates with good leaving groups and compare the activity in bulk solution with that in the bilayer membrane. A complementary aim was to explore the activation of an inhibited enzyme by membrane-embedded activating groups.

The findings of this investigation complement those of earlier studies with compound **2** (used as a reference compound) and confirmed the activity of a Zn^{2+}-complex of this compound. Subsequently, ester substrate hydrolysis rates catalysed with compound **5** were relatively slower than compounds **2** and **9**. The findings of the control experiments in the solution provided a benchmark to compare with analogues that were used in the bilayer membrane studies.

Embedding the ligand into vesicles has the potential to present a range of questions such as determining the best concentration of the ligand and best concentration of the metal. Embedding high concentration of the ligand may lead to the formation of an aggregate of the ligand on the surfaces of the vesicles, which will inhibit the catalyst functioning efficiently. Moreover adding a high concentration of Zn^{2+} may lead to form zinc hydroxide which is only slightly soluble in water solution and leads to precipitation. Ligand structure can play an important role in solubility and binding with the metal ion.

The transducer system showed a higher hydrolysis rate because it occurs inside the vesicles (in a small volume), where the embedded complex provides a locally high concentration of complex to the interior. While the one headgroup system is slower than the reaction inside the vesicles. The hypothesis for that is, the hydrolysis rate depends on the reaction volume and area, so it will decrease in the one headgroup system as the volume will increase then the local concentration will decrease.

This study needed evidence of the structural characterisation of the vesicles, as there was limited information on how the ligand oriented and embedded in the vesicles. Thus physiochemical methods such as AFM, DSC, TEM [187] and domain formation by spectroscopic methods are needed to confirm the distribution and the shape of the vesicles.

It is difficult to carry out encapsulation experiments (all the reactants inside the vesicles) with membrane-embedded ligands that do not have an "**off**" state as the reaction will start immediately during making the vesicle solution. Thus, the reactions were studied outside the vesicles, which revealed different behaviour to related reactions reported on the inside

of vesicles (using transducers which contain two head groups). The apparent decrease in activity could be rationalised by considering the different relative concentrations and overall reaction limits. These experiments revealed a different balance of rate-limiting step compared to previous data and compared to reactions in solution. Embedding the ligands appears to lead to rate limiting deacylation (the burst expected to occur when $k_2 \gg k_3$, and when $k_3 \gg k_2$ no burst will exist) of an intermediate in the catalytic cycle.

Catalyst + Substrate $\xrightarrow{k_2}$ **Catalyst-Substrate + Product 1**

k_3

Product 2
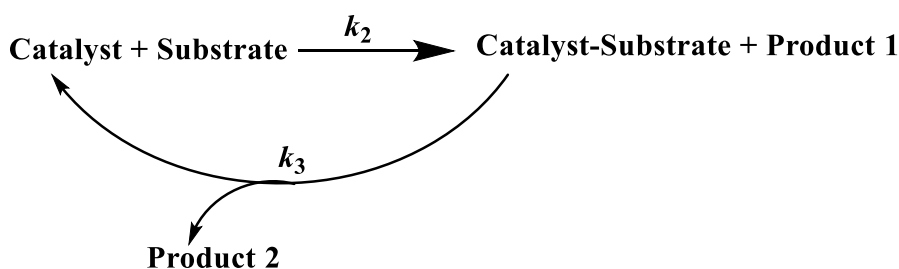
Adding the ligand to outside the vesicles to allow the initiation of the reaction after forming the vesicles led to unclear behaviour, with either precipitation of the ligand, the formation of micelles or dissociation of the ligand from the metal leaving zinc hydroxide.

Activation of covalently inhibited papain enzyme using a thiol attached to a steroid moiety embedded into a membrane was successfully achieved by exploiting a thiol-disulfide exchange reaction. The following challenge in this work was to achieve activation of the enzyme inside the vesicles which requires controlling the system from off to on by translocating the thiol from the outside to the inside of the vesicles. Furthermore, the relatively large size of the enzyme prevented the encapsulation being achieved successfully, as some of the enzyme remained outside the vesicles, so special kind of the GPC column is required to separate the vesicles from the enzyme.

Further investigation that will extend this work would be to try and investigate the direction of the ligand in the membrane and to explore whether the rate-limiting step for ester hydrolysis on the membrane surfaces can be increased so that initial attack becomes the rate-limiting step. Moreover, using an amphiphilic substrate and incorporating it in vesicles.

Chapter 6 -   Experimental Procedures

6.1   Instruments and Tools:

Analytical HPLC was carried out using a Waters Alliance 2695 system with a UV-visible wavelength detector (model 2487) and a Phenomenex Kinetex XB-C$_{18}$ 100 Å 5 µm column, 250 x 4.6 mm.

Preparative HPLC employed a Varian Prostar system comprising a model 410 autosampler, model 320 UV-visible detector, two model 210 pumps and a model 701 fraction collector. A Waters Xbridge OBD 5 µM C-18, 19 x 250 mm column, was used.

Particle Sizing was performed using a Brookhaven ZetaPALS system with the following settings:

Size Range 2 nm – 3 µm

Diffusion Coefficient Range 10^{-6}- 10^{-9} cm^{2}s^{-1}

Accuracy ±1-2% (monodisperse sample)

Reproducibility ±1-2% (dust-free sample)

30 mW 660 nm solid state HeNe laser

Temperature 6-74 °C

Sample Volume 0.5-3.0 mL

Measurement Time Typically 1-2 minutes

Fixed Angles 90° (particle sizing) &15° (zeta potential)

Detection Avalanche Photodiode

Detector Count Rate 2-500 kcps (recommended)

Cell Path Length 10 mm

Reference Polystyrene latex reference material

Nuclear Magnetic Resonance Spectra

^{1}H NMR spectra were recorded on a Bruker Avance 400 (400 MHz), a Bruker Avance III HD (400 MHz) or a Bruker Avance III HD (500 MHz) spectrometer as indicated, using the residual solvent as the internal reference in all cases. In the assignment of ^{1}H NMR spectra,

the chemical shift information (δ_H) for each resonance signal is given in units of parts per million (ppm) relative to trimethylsilane (TMS) where δ_H TMS = 0.00 ppm. The number of protons (n) for a reported resonance signal are indicated as nH from their integral value and their multiplicity represented by the following abbreviations:

br–broad, s–singlet, d–doublet, dd–double doublet, td–triple doublet, t–triplet, q–quartet, and m–multiplet.

Mass Spectra

Mass spectra were recorded on:

LC-MS analysis

LC instrument – Agilent 1260 Infinity

MS instrument – Agilent 6530 Q-ToF

Mobile Phase – Solvent A, 0.1% formic acid, Solvent B, Acetonitrile/ 0.1% formic acid

Gradient – 5%B to 95% B in 10 minutes

Column – Phenomenex Aeris Widepore 3.6u XB-C18 50 mm x 2.1 mm

Injection volume – 1.0 uL

Flow – 0.4 mL/min

MS mode ESI +ve

Source parameters – Drying Gas temperature 350 ℃, 11 L/min, Nebuliser 45 psig, Capillary voltage 4000 v

All spectra were run by Mr. Simon Thorpe, or Ms. Sharon Spey, who are technicians at the University of Sheffield Mass Spectrometry Service.

UV-Visible Spectroscopy

Was carried out using either Cary 100 Bio or Cary 300 Bio UV-spectroscopy instruments, using temperature-controlled sample compartments.

6.2 Chemicals:

All chemicals were purchased from commercial sources (Sigma, Alfa Aesar, Fisher scientific) and used as supplied without further purification unless otherwise stated.

6.3 Solvents

Solvents were obtained from commercial sources (Sigma-Aldrich and VWR) and were used as supplied except for:

Dry dichloromethane and tetrahydrofuran, which were obtained from an in-house Grubbs solvent purification system at the University of Sheffield. In addition, ethanol and methanol were dried before use with molecular sieves.

6.4 Chromatography

TLC analyses were performed using Merck 60 F_{254} nm silica-coated aluminium sheets and visualised under UV light (256 or 365 nm) or with alkaline aqueous $KMnO_4$. Preparative flash column chromatography was achieved using silica gel (SiO_2), 40-60 µm, 60 Å (Fluorochem).

6.5 Oxime Ligands Synthesis

6.5.1 1-{6-[(1E)-N-Hydroxyethanimidoyl]pyridin-2-yl}ethan-1-one

1

$C_9H_{10}N_2O_2$
Mwt = 178.19
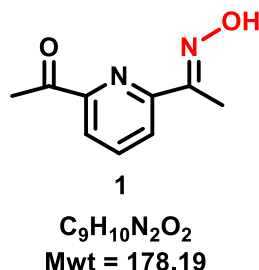
The compound was prepared according to the reported method.[124]

2,6-Diacetylpyridine (1.80 g, 11.03 mmol, 1 eq.), hydroxylamine hydrochloride (0.69 g, 9.93 mmol, 0.9 eq.) and sodium acetate (0.05 g, 0.61 mmol) were placed in a round-bottomed flask. Distilled water (40 mL) was added, and the suspension was refluxed at 100 °C for 1 hour, then left to stir at room temperature for 16 hours. The white precipitate was collected by filtration and washed with water to remove the sodium acetate. After drying the product under high vacuum, it was purified using column chromatography (SiO_2, 0-50% ethyl acetate in dichloromethane) to yield the title compound as a white solid (1.60 g, 8.98 mmol, 81%).

^{1}H NMR (400 MHz, acetone-d_6) δ 10.80 (s, 1H), 8.13 (m, 1H), 7.97 – 7.92 (m, 2H), 2.70 (s, 3H), 2.39 (s, 3H).

^{13}C NMR (101 MHz, acetone-d_6) δ 198.9 (C=O), 154.9 (C=N), 154.18, 152.5, 136.9, 123.2, 120.6, 24.6, 9.2.

HPLC: A compound was found as one peak at 15.012 min., the method was run as 5-95% acetonitrile (ACN) in water over 30 minutes followed by isocratic elution for a further 30 minutes. Data was recorded at 275 nm, and 0.01% v/v TFA was added to both mobile phase solvents.

6.5.2 N,N'-{Pyridine-2,6-diyldi[(1E)eth-1-yl-1-ylidene]}dihydroxylamine

2

$C_9H_{11}N_3O_2$

Mwt = 193.21
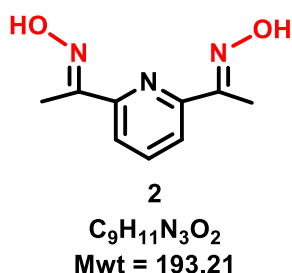
This synthesis is a modification of the reported method.[188] 2,6-diacetylpyridine (1.0 g, 6.13 mmol, 1 eq.), hydroxylamine hydrochloride (0.86 g, 12.38 mmol, 2 eq.) and sodium acetate (0.045 g, 0.55 mmol) were mixed in a round-bottomed flask. Distilled water (40 mL) was added and the suspension was refluxed at 100 °C for 1 hour, then left to stir at room temperature for 16 hours. The white solid product was filtered and washed with water to remove the sodium acetate. After drying the product under high vacuum, the product was washed with cold dichloromethane to remove any residual starting material. The title compound was obtained as a white solid (1.0 g, 5.18 mmol, 85%). mp 234 - 238 °C (mp: 236–238).[188]

¹H NMP (400 MHz, acetone-d_6) δ 10.59 (s, 2H), 7.88 (d, J = 7.7 Hz, 2H), 7.74 (t, J = 7.8, 7.3 Hz, 1H), 2.36 (s, 6H).

¹³C NMR (101 MHz, acetone-d_6) δ 155.0, 153.7, 136.3, 119.3, 9.2.

IR (FTIR), cm⁻¹: 3500-2500 (-NOH), 2939 (CH), 1699 (C=N), 1571 (C=C), 1458.

6.5.3 1-{6-[(1E)-N-Methoxyethanimidoyl]pyridin-2-yl}ethan-1-one
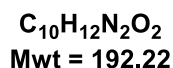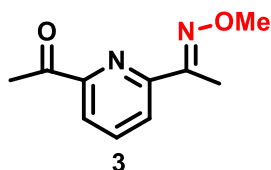
C$_{10}$H$_{12}$N$_2$O$_2$
Mwt = 192.22

2,6-Diacetylpyridine (0.50 g, 3.06 mmol, 1 eq.) was reacted with methoxylamine hydrochloride 27 wt.% (5 N) solution in water (0.70 mL, 0.26 g, 3.08 mmol, ≈ 0.9 eq.), sodium acetate (0.024 g, 0.29 mmol) and distilled water (20 mL) were added. The mixture was refluxed at 100 °C for 1 hour then left to stir at room temperature for 16 hours. The white solid product was filtered off and washed with water, dried under high vacuum then purified using column chromatography (SiO$_2$, 14% ethyl acetate in petroleum ether 40-60%) to yield a white solid (0.45 g, 2.34 mmol., 76%).

^{1}H NMR (400 MHz, CDCl$_3$) δ 8.13 (dd, *J* = 7.9, 1.1 Hz, 1H), 8.00 (dd, *J* = 7.7, 1.1 Hz, 1H), 7.81 (t, *J* = 7.8 Hz, 1H), 4.06 (s, 3H), 2.75 (s, 3H), 2.39 (s, 3H).

^{13}C NMR (101 MHz, CDCl$_3$) δ 200.0, 155.2, 153.5, 152.3, 136.9, 123.7, 121.2, 62.4, 25.4, 10.7.

HPLC: The compound was found as one peak at 21.932 min., the method was run as 5-95% ACN in water over 30 minutes followed by isocratic elution for a further 30 minutes. Data recorded at 275 nm and 0.01% v/v TFA was added to both mobile phase solvents.

6.5.4 (1E,1'E)-1,1'-(Pyridine-2,6-diyl)bis(N-methoxyethan-1-imine)
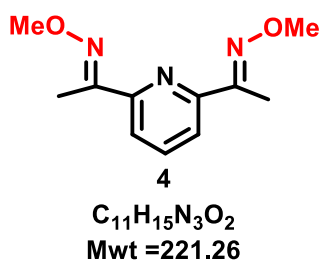
4
$C_{11}H_{15}N_3O_2$
Mwt =221.26

2,6-Diacetylpyridine (0.50 g, 3.06 mmol, 1 eq.) was reacted with methoxylamine hydrochloride 27 wt.% (5 N) solution in water (1.4 mL, 0.52 g, 6.2 mmol, ≈ 2 eq.), sodium acetate (0.045 g, 0.55 mmol) and distilled water (20 mL) was added. The mixture was refluxed for 1 hour and left to stir at room temperature for 16 hours. The white solid product was filtered off and washed with water, dried under high vacuum. Then purified using column chromatography (SiO$_2$, 10% ethyl acetate in petroleum ether 40-60%) to give the title compound (0.53 g, 2.40 mmol, 78%).

^{1}H NMR (400 MHz, CDCl$_3$) δ 7.89 (d, *J* = 7.8 Hz, 2H), 7.65 (t, *J* = 7.8 Hz, 1H), 4.05 (s, 6H), 2.36 (s, 6H).

^{13}C NMR (101 MHz, CDCl$_3$) δ 155.8, 153.4, 136.3, 119.6, 62.4, 10.9.

HRMS calculated for C$_{11}$H$_{15}$N$_3$O$_2$ (M+H)$^+$: 222.1237, found: 222.1241.

HPLC: The compound was identified at 26.951 minutes as one single peak. The method was run as 5-95% ACN in water over 30 minutes followed by isocratic elution for a further 30 minutes. Data were recorded at 275 nm., 0.01 % v/v TFA was added to both mobile phase

6.5.5 Ethyl{[(E)-(1-{6-[(1E)-N-hydroxyethanimidoyl]pyridin-2-yl}ethylidene)amino] oxy} acetate

5

$C_{13}H_{17}N_3O_4$

M wt = 279.30
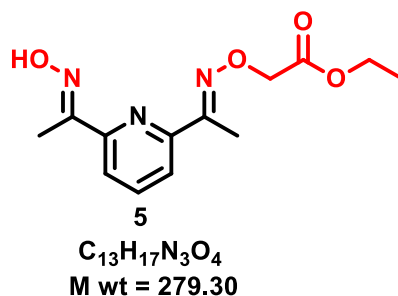
A round-bottomed flask containing potassium carbonate (1.10 g, 7.96 mmol, 2.6 eq.) was cooled to 0 °C in an ice bath before a solution of compound **2** (0.60 g, 3.11 mmol, 1 eq.) in DMF (5 mL) was added. The mixture was stirred for an hour at room temperature, and then cooled again to 0 °C, and a solution of ethyl bromoacetate (0.045 g, 0.03 mL, 0.43 eq.) in DMF (2 mL) was added, and the mixture was allowed to stir at room temperature overnight. The reaction mixture was diluted with dichloromethane and washed with water, brine, and then the organic layer was separated, dried with $MgSO_4$ and evaporated under reduced pressure. Purification using column chromatography (SiO_2, 5% methanol in dichloromethane) afforded the title compound (0.45 g, 1.61 mmol, 52 %, **R**$_f$. 0.84). A sample of the disubstituted ligand **6** (0.27 g, 0.74 mmol, 24%, **R**$_f$. = 0.6) was also obtained.

¹H NMR (400 MHz, CDCl₃) δ 9 (s,1H), 7.87 (d, J= 7.6 Hz, 1H), 7.79 (d, J = 7.7 Hz, 1H), 7.65 (t, J = 7.8 Hz, 1H), 4.80 (s, 2H), 4.28 (q, J = 7.2 Hz, 2H), 2.46 (s, 3H), 2.42 (s, 3H), 1.32 (t, J = 7.2 Hz, 3H).

¹³C NMR (101 MHz, CDCl₃) δ 170.2, 157.6, 156.8, 152.9, 152.7, 136.4, 120.8, 120.1, 71.1, 60.9, 14.1, 11.3, 10.5.

HRMS calculated for $C_{13}H_{17}N_3O_4$ (M+H)⁺: 280.1292, found: 280.1292.

HPLC: The compound was observed as one peak at 20.262 min in good purity and no major impurities were observed. The method was run as 5-95% ACN in water for 30 minutes followed by isocratic elution for a further 30 minutes. Data was recorded at 275 nm, and 0.01% v/v TFA was added to both mobile phase solvents.

6.5.6 Diethyl2,2'-(((1E,1'E)-(pyridine-2,6-diylbis(ethan-1-yl-1-ylidene))bis (azanylylidene)) bis(oxy))diacetate

6
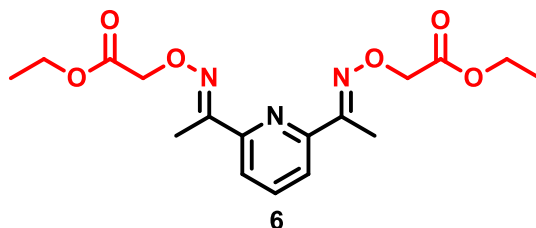
$C_{17}H_{23}N_3O_6$

Mwt = 365.39

The title compound is a by-product formed during the synthesis of the previous compound. The compound was isolated as 0.27 g, 0.74 mmol, 24%.

¹H NMR (400 MHz, CDCl₃) δ 7.86 (d, *J* = 7.8 Hz, 2H), 7.63 (t, *J* = 7.8 Hz, 1H), 4.76 (s, 4H), 4.27 (q, *J* = 7.1 Hz, 4H), 2.45 (s, 6H), 1.32 (t, *J* = 7.1 Hz, 6H).

¹³C NMR (101 MHz, CDCl₃) δ 170.0, 157.6, 152.6, 136.3, 120.6, 71.0, 60.8, 14.4, 11.3.

6.5.7 (E)-1-(6-(1-((Prop-2-yn-1-yloxy)imino)ethyl)pyridin-2-yl)ethanone

7

$C_{12}H_{12}N_2O_2$

Mwt = 216.24
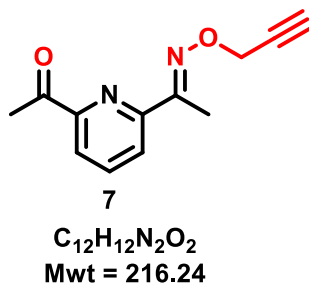
A round-bottomed flask was charged with potassium carbonate (0.70 g, 5.06 mmol, 3 eq.) and placed in an ice bath at 0 °C. A solution of compound **1** (0.30 g, 1.68 mmol, 1 eq.) in DMF (5 mL) was added, the mixture was warmed to room temperature and stirred for an hour before re-cooling to 0 °C. Another solution of propargyl bromide (80 wt.% in toluene, 0.30 mL, 0.40 g, 2.7 mmol, 1.6 eq.) was added, and the final mixture was stirred for 16 hours. The solvents were evaporated under high vacuum, and then the residue was partitioned between dichloromethane (50 mL) and brine (50 mL). The organic layer was separated, dried with MgSO₄ and the solvent removed to give compound **7** as a white solid (0.34 g, 1.57 mmol, 93%).

¹H NMR (400 MHz, CDCl₃) δ 8.16 (dd, *J* = 7.9, 1.1 Hz, 1H), 8.02 (dd, *J* = 7.7, 1.1 Hz, 1H), 7.83 (t, *J* = 7.8 Hz, 1H), 4.86 (d, *J* = 2.4 Hz, 2H), 2.76 (s, 3H), 2.53 (t, *J* = 2.4 Hz, 1H), 2.44 (s, 3H).

¹³C NMR (101 MHz, CDCl₃) δ 200.2, 156.5, 153.4, 152.4, 136.9, 123.8, 121.4, 79.6, 74.4, 61.9, 25.6, 10.9.

6.5.8 (E)-1-(6-((E)-1-(Hydroxyimino)ethyl)pyridin-2-yl)ethanone o-prop -2-yn-1-yl oxime

8
$C_{12}H_{13}N_3O_2$
Mwt =231.26
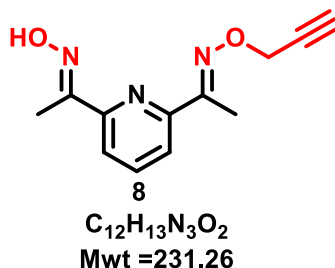
Compound **7** (0.30 g, 1.39 mmol) was reacted with hydroxylamine hydrochloride (0.13 g, 1.87 mmol) in the presence of sodium acetate (0.040 g, 0.54 mmol). The solvent was a mixture of chloroform:ethanol:distilled water (10:10:1, 21 mL). The reaction mixture was stirred at 60 °C for 16 hours. The solvents were evaporated under high vacuum. The product was purified using column chromatography (SiO$_2$, 0-5% methanol in dichloromethane) to offer the product as a white solid (0.22 g, 0.95 mmol, 68%).

¹H NMR (400 MHz, DMSO-*d*) δ 11.57 (s, 1H), 7.96 – 7.72 (m, 3H), 4.85 (d, *J* = 2.4 Hz, 2H), 3.52 (t, *J* =2.4 Hz, 1H), 2.31 (s, 3H), 2.25 (s,3H).

¹³C NMR (101 MHz, DMSO-*d*) δ 156.8, 154.6, 154.2, 152.4, 137.6, 120.4, 120.3, 78.1, 62.2, 11.5, 10.6.

IR (FTIR) cm⁻¹: 3263. (CCH, stretch), 2942. (CH, stretch), 2117 (-CC-, stretch), 1571. (N=C, stretch), 1008. (C-N).

HRMS calculated for $C_{12}H_{13}N_3O_2$ (M+H)⁺: 232.1081, found: 232.1079.

6.5.9 Ethyl2-(4-(((((E)-(1-(6-((E)-1-(hydroxyimino)ethyl)pyridin-2-yl) ethylidene)amino)oxy)methyl)-1H-1,2,3-triazol-1-yl)acetate

$C_{16}H_{20}N_6O_4$
Mwt = 360.37

9
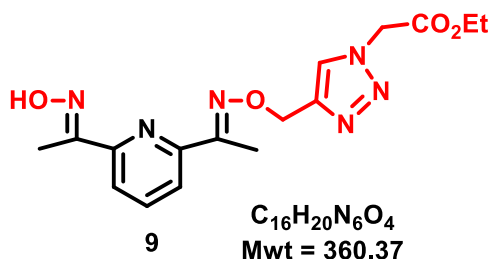
To a covered and an evacuated round-bottomed flask containing a mixture of compound **8** (0.10 g, 0.43 mmol, 1 eq.) ethyl azidoacetate (0.06 g, 0.47 mmol, 1.1 eq.), and copper (I) iodide (0.17 g, 0.87 mmol, 2 eq.), dry dichloromethane–DIPEA (as 8:2, 10 mL) was added. The mixture was stirred at room temperature overnight, the dark green-brown solution was treated with EDTA (20 mL, 0.1 M, pH = 8) to remove the copper (the aqueous layer changed colour from colourless to azure colour). The solution was then diluted with dichloromethane (50 mL), and the product was extracted to the organic layer, dried with MgSO₄, and the crude product was purified using column chromatography (SiO₂, 20% ethyl acetate in hexane) to yield compound **9** (0.15 g, 0.42 mmol, 96%).

¹H NMR (400 MHz, CDCl₃) δ 9.60 (s, 1H), 7.88 – 7.82 (m, 1H), 7.80 – 7.72 (m, 2H), 7.64 – 7.55 (m, 1H), 5.39 (d, *J* = 2.6 Hz, 2H), 5.15 (s, 2H), 4.23 (q, *J* = 7.1 Hz, 2H), 2.39 (s,3H) , 2.36 (s, 3H), 1.27 (t, *J* = 7.0, 3H).

¹³C NMR (101 MHz, CDCl₃) δ 166.3, 156.9, 153.3, 153.0, 145.3, 136.4, 124.5, 120.4, 120.3, 120.2, 67.7, 62.5, 50.9, 14.0, 11.2, 10.5.

HRMS calculated for C₁₆H₂₀N₆O₄ (M+H)⁺: 361.1619, found: 361.1619.

IR(FTIR) cm ⁻¹: 1738 (CO).

6.6 Alcohol Esters Synthesis
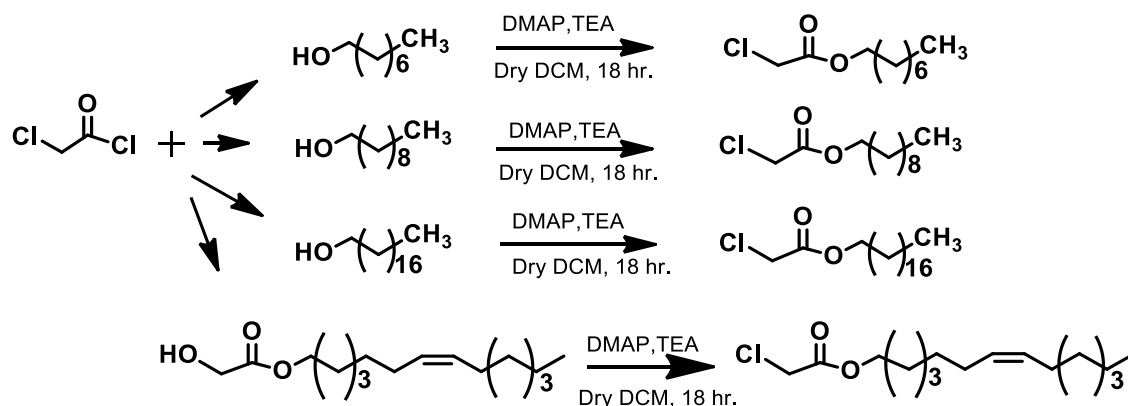
Octyl chloroacetate and decyl chloroacetate are previously reported compounds that were prepared using different procedures.[189, 190]

6.6.1 Octyl 2-chloroacetate
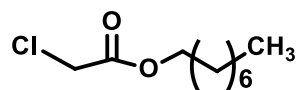
1-Octanol (2.0 g, 2.42 mL, 15.4 mmol, 1 eq.) and 4-dimethylaminopyridine [DMAP (0.90 g, 7.37 mmol) were placed in a round-bottomed flask. The round was covered and evacuated, then dry dichloromethane was added (50 mL) followed by triethylamine (1.76 mL, 1.28 g, 1 eq.). After 5 minutes, chloroacetyl chloride (1.58 mL, 2.24 g, 19.83 mmol) was added, the reaction mixture was stirred for 18 hours at room temperature. Then the solution was treated with diluted HCl (1N) and washed with water (25 x 2 mL) then brine (25 mL), and the compound was extracted to the organic layer. The crude compound was dried with MgSO$_4$ and the solvent was evaporated. The crude product was purified by column chromatography (SiO$_2$, 3% methanol in dichloromethane) to afford a yellowish oily product (3.0 g, 14.51 mmol, 95%).

^{1}H NMR (400 MHz, CDCl$_3$) δ 4.15 (t, J = 6.7 Hz, 2H), 4.03 (s, 2H), 1.68 − 1.58 (m, 2H), 1.41-1.23 (m, 10H), 0.85 (t, J = 6.9 Hz, 3H).

^{13}C NMR (101 MHz, CDCl$_3$) δ 167.4, 66.4, 40.9, 31.7, 29.1, 28.4, 25.7, 22.6, 14.0.

IR(FTIR) cm $^{-1}$ 1739 for (C=O).

6.6.2 Decyl 2-chloroacetate
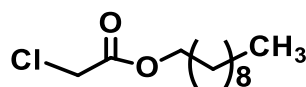
1-Decanol (2.0 g, 2.41 mL, 12.64 mmol, 1 eq.) and 4-dimethylaminopyridine (0.90 g, 7.37 mmol) were placed in a round-bottomed flask, and the round was covered and evacuated then dry dichloromethane was added (50 mL) followed by triethylamine (1.76 mL, 1.28 g, 1 eq.). After 5 minutes, chloroacetyl chloride (1.55 mL, 2.20 g, 19.50 mmol) was added, the reaction mixture was stirred for 18 hours at room temperature. Then the solution was treated with diluted HCl (1M) and washed with water (25 x 2 mL) then brine (25 mL), and the compound was extracted to the organic layer. The crude compound was dried with $MgSO_4$ and the solvent was evaporated. The crude product was purified by column chromatography (SiO_2, 3% methanol in dichloromethane) to afford a yellowish oily product (2.90 g, 12.35 mmol, 98%).

^{1}H NMR (400 MHz, CDCl$_3$) δ 4.17 (t, J = 6.8 Hz, 2H), 4.05 (s, 2H), 1.69 – 1.60 (m, 2H), 1.38 – 1.20 (m, 14H), 0.87 (t, J = 6.9 Hz, 3H).

^{13}C NMR (101 MHz, CDCl$_3$) δ 167.5, 66.5, 40.9, 31.9, 29.5, 29.3, 29.2, 28.4, 25.7, 22.7, 14.1.

IR(FTIR) cm $^{-1}$ 1737 for (C=O).

6.6.3 Stearyl 2-chloroacetate: or Octadecyl 2-chloroacetate
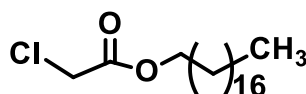
1-Octadecanol (2.0 g, 7.39 mmol) and 4-dimethylaminopyridine (0.90 g, 7.37 mmol) were placed in a round bottomed flask. The round was covered and evacuated, then dry dichloromethane was added (50 mL) followed by triethylamine (1.76 mL, 1.28 g, 1 eq.). After 5 minutes, chloroacetyl chloride (1.43 mL, 2.00 g, 17.70 mmol) was added, the reaction mixture was stirred for 18 hours at room temperature. Then the solution was treated with diluted HCl (1M) and washed with water (25 x 2 mL) then brine (25 mL) and the compound was extracted to the organic layer. The crude compound was dried with $MgSO_4$ and the solvent was evaporated. The crude product was purified by column chromatography (SiO_2, 3% methanol in dichloromethane) to afford the product (2.5 g, 7.21 mmol, 97%) as a white solid.

^{1}H NMR (400 MHz, CDCl$_3$) δ 4.21 (t, J = 6.7 Hz, 2H), 4.08 (s, 2H), 1.72 – 1.64 (m, 2H), 1.35 – 1.25 (m, 30H), 0.90 (t, J = 6.8 Hz, 3H).

^{13}C NMR (101 MHz, CDCl$_3$) δ 167.4, 66.4, 40.9, 31.9, 29.7, 297, 29.6, 29.6, 29.5, 29.4, 29.2, 28.5, 25.8, 22.7, 14.1.

IR(FTIR) cm $^{-1}$ 1749 for (C=O).

6.6.4 (9Z)-Octadec-9-en-1-yl chloroacetate
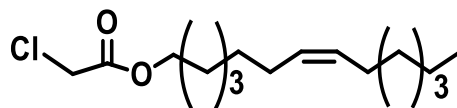
Oleyl alcohol (2.0 g, 7.45 mmol) and DMAP (0.90 g, 7.37 mmol) were placed in a round-bottomed flask. The round was covered and evacuated, then dry dichloromethane was added (50 mL) followed by triethylamine (1.76 mL, 1.28 g, 1 eq.). After 5 minutes, chloroacetyl chloride (0.65 mL, 0.91 g, 8.06 mmol) was added, the reaction mixture was stirred for 18 hours at room temperature. Then the solution was treated with diluted HCl (1M) and washed with water (25 x 2 mL) then brine (25 mL), and the compound was extracted to the organic layer. The crude product was dried with $MgSO_4$ and the solvent was evaporated and purified by column chromatography (SiO_2, 3% methanol in dichloromethane) to afford the product (2.0 g, 5.80 mmol, 78%) as a white solid.

¹H NMR (400 MHz, CDCl₃) δ 5.43 – 5.31 (m, 2H), 4.18 (t, *J* = 6.7 Hz, 2H), 4.05 (s, *J* = 4.2 Hz, 2H), 2.05 – 1.92 (m, 2H), 1.70 – 1.58 (m, 2H), 1.35 – 1.24 (m, 22H), 0.87 (t, *J* = 6.8 Hz, 3H).

¹³C NMR (101 MHz, CDCl₃) δ 167.4, 130.0, 129.8, 66.4, 41.0, 32.6, 31.9, 29.8, 29.7, 29.7, 29.5, 29.4, 29.3, 29.2, 29.2, 28.5, 27.2, 27.2, 25.8, 22.7, 14.1.

IR(FTIR) cm⁻¹ 1740 for (C=O), 1761.

6.6.5 Cholest-5-en-3-yl chloroacetate or Cholesteryl 2-chloroacetate

$C_{29}H_{47}ClO_2$
Mwt =463.14
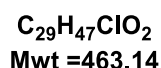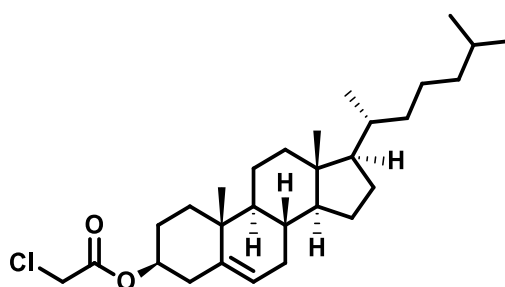
Prepared according to Deck *et al.*[191] and modified from the procedure of Zhang *et al.*[192] Cholesterol (2.00 g, 5.17 mmol), triethylamine (1.45 mL, 1.05 g, 10.4 mmol), and chloroacetyl chloride (0.64 mL, 0.99 g, 8.05 mmol) were combined in dichloromethane (50 mL). The reaction was allowed to stir overnight at room temperature after which time TLC indicated complete disappearance of the starting material. The dichloromethane reaction mixture was first washed twice with diluted HCl (10 mL), then twice with saturated sodium chloride (50 mL) and dried with $MgSO_4$. The mixture was then filtered, and the solvent was removed by rotary evaporation. The resulting solid was purified on a SiO_2 column. Elution with dichloromethane gave a white solid (1.92 g, 4.15 mmol, 80%), mp: 161-164 °C.

¹H NMR δ 0.65-2.48 (m, 43H), 4.02 (s, 2H), 4.68 (m, 1H), 5.37 (t, *J*, = 6 Hz 1H).

¹³C NMR (101 MHz, CDCl₃) δ 166.7, 139.2, 123.1, 76.2, 56.7, 56.1, 50.0, 42.3, 41.2, 39.7, 39.5, 37.9, 36.9, 36.7, 36.2, 35.8, 31.9, 31.8, 28.2, 28.0, 27.6, 24.3, 23.8, 22.8, 22.6, 21.0, 19.3, 18.7, 11.9.

HRMS calculated for $C_{29}H_{47}O_2NaCl$ 485.3162 (M+Na)⁺, found: 485.3157.

IR (FTIR) cm⁻¹: 1751 cm⁻¹ (C=O).

6.6.6 Methyl 3-hydroxycholan-24-oate (Methyl 3α-hydroxy-5β-lithocholan-24-oate)

$C_{25}H_{42}O_3$
Mwt= 390.61
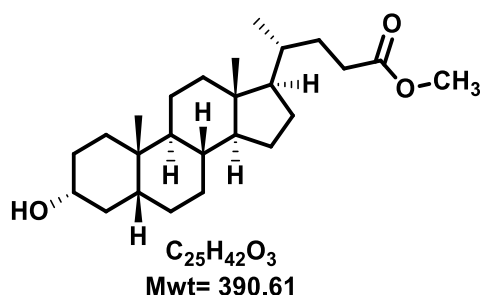
The compound was prepared according to literature procedures [193,194].

Lithocholic acid (3.77 g, 10.0 mmol) was dissolved in anhydrous methanol (50 mL), then concentrated hydrochloric acid (5 mL) was added. The reaction mixture was then stirred for 14 hours at room temperature. After completion of the reaction, the solvent was evaporated under reduced pressure and the reaction mixture was diluted with ethyl acetate (50 mL). The organic layer was then washed with sodium bicarbonate (2 x 20 mL) and brine (2 x 10 mL). The organic phase was dried with $MgSO_4$ and then concentrated to obtain the pure compound without more purification as a white solid (3.79 g, 9.70 mmol, 97%).

¹H NMR (400 MHz, CDCl₃) δ 3.65 (s, 3H, −CO-OCH₃), 3.59 (m, 1H), 2.45-2.25 (m, 1H), 2.28 – 2.15 (m, 1H), 2.01 – 0.94 (m, 27H), 0.95 – 0.87 (m, 6H), 0.63 (s, 3H).

¹³C NMR (101 MHz, CDCl₃) δ 174.8, 71.8, 56.5, 56.0, 51.5, 42.7, 42.1, 40.4, 40.2, 36.5, 35.8, 35.4, 35.4, 34.6, 31.0, 30.5, 28.2, 27.2, 26.4, 24.1, 23.4, 20.8, 18.3, 12.0.

HRMS (ESI): m/z = [M+Na]⁺: calculated for $C_{25}H_{42}O_4Na^+$ 413.3032, found: 413.3026.

IR (FTIR) cm ⁻¹: 3517 (OH), 1712 (C=O).

6.6.7 Methyl 3α-chloroacetyloxy-5β-lithocholan-24-oate

$C_{27}H_{43}ClO_4$
Mwt= 467.09
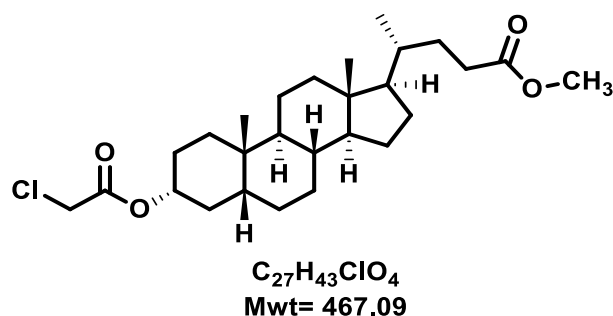
The procedure to prepare the compound was modified from literature procedures[194, 193]

To a solution of methyl 3α-hydroxy-5β-lithocholan-24-oate (2.0 g, 5.12 mmol) and DMAP (0.63 g, 5.16 mmol) in dry dichloromethane (60 mL), triethylamine (0.75 mL, 0.55 g, 5.38 mmol) was added dropwise. After 5 minutes, the solution placed in an ice bath and chloroacetyl chloride (0.45 mL, 0.64 g, 5.65 mmol) was added; the colour changed from colourless to yellow. The mixture was stirred overnight, then filtered, the solvent was evaporated and the product was purified using the column chromatography (SiO$_2$, 0-10% methanol in dichloromethane) to give a white solid (1.50 g, 3.21 mmol, 63%).

^{1}H NMR (400 MHz, CDCl$_3$) δ 4.90 – 4.75 (m, 1H, CH), 4.04 (s, 2H, −CO-CH$_2$-Cl), 3.68 (s, 3H, −CO-O-CH$_3$), 2.42 – 2.29 (m, 1H), 2.28 – 2.16 (m, 1H), 2.03 – 0.98 (m, 27H, CH$_2$), 0.98 – 0.88 (m, 6H), 0.66 (s, 3H).

^{13}C NMR (101 MHz, CDCl$_3$) δ 269.8, 174.6, 166.8, 76.7, 56.5, 56.0, 51.5, 42.7, 41.9, 41.3, 40.4, 40.1, 35.8, 35.4, 34.9, 34.6, 32.0, 31.0, 28.2, 27.0, 26.5, 26.3, 24.2, 23.3, 20.8, 18.3, 12.0.

HRMS (ESI): m/z = [M+Na]$^+$: calculated for $C_{27}H_{43}ClO_4Na^+$ 489.2742, found: 489.2742.

IR (FTIR) cm^{-1}: 1751(C=O), 1733(C=O).

6.6.8 Cholest-5-en-3-yl N-(tert-butoxycarbonyl)glycinate
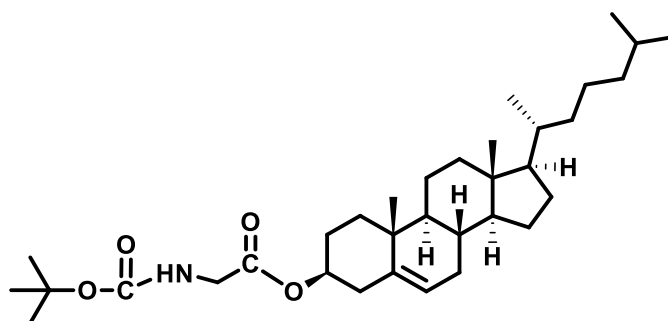
$$C_{34}H_{57}NO_4$$
$$Mwt = 543.83$$

The compound was prepared according to literature procedure.[195]

Cholesterol (1.0 g, 2.59 mmol, 1 eq.) was dissolved into anhydrous dichloromethane (10 mL) together with N-t-Boc-glycine (0.5 g, 2.854 mmol, 1.1 eq.) and DMAP (0.08 g, 0.645 mmol, 0.25 eq.). Subsequently, the reaction mixture was stirred at 0 °C for 10 hours after the addition of dicyclohexylcarbodiimide DCC (0.58 g, 2.81 mmol, 1.1 eq.). The dicyclohexylurea (DCU) was filtered off and the filtrate was concentrated *in vacuo*. The product was purified using column chromatography (SiO$_2$, 1:1 hexane: diethyl ether) to afford a white solid (1.2 g, 2.21 mmol, 85%). mp. = 82-87 °C.

^{1}H NMR (400 MHz, CDC$_{l3}$) δ 5.40 (d, *J* = 3.9 Hz, 1H), 5.02 (s, 1H), 4.77 – 4.63 (m, 1H), 3.90 (d, *J* = 5.3 Hz, 2H), 2.34 (t, *J* = 11.2 Hz, 2H), 2.07 – 1.79 (m, 6H), 1.46 (s, 9H) ,1.71 – 0.84 (m, 32H), 0.70 (s, 3H).

Mass Spectra (ES$^+$) m/z = 566.4 [M+Na]$^+$, (ES$^+$) m/z = 582.4 [M+K]$^+$.

6.6.9 Cholest-5-en-3-yl glycinate

$$C_{29}H_{49}NO_2$$
Mwt = 443.72
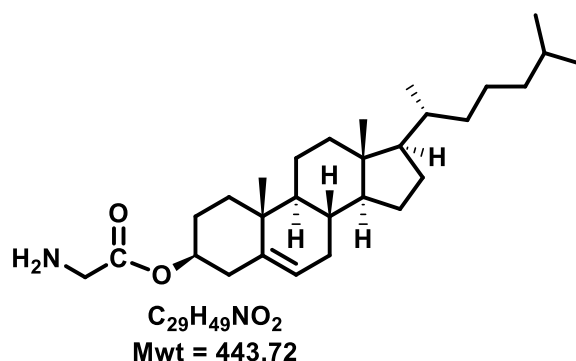
The compound was prepared according to the literature procedure.[195]

For the removal of the t-Boc group, cholesterol-t-Boc-amino acid ester (1.0 g, 1.84 mmol was treated with a mixture of CH_2Cl_2/TFA (40 mL, 1:1, v/v). The reaction mixture was stirred at $0^{\circ}C$ for 3 hours and then was poured onto ice and a precipitate appeared. The mixture was filtered off and evaporated to dryness without any further purification.

¹H NMR (400 MHz, CDCl₃) δ 6.94 – 6.85 (s, 2H), 5.40 (d, J = 4.9 Hz, 1H), 4.78 – 4.60 (m, 1H), 4.12 (d, J = 4.9, 2 H), 2.11 – 0.81 (m, 40H), 0.69 (s, 3H).

¹³C NMR (101 MHz, CDCl₃) δ 167.7, 139.0, 123.3, 76.4, 56.7, 56.1, 50.0, 42.3, 41.6, 39.7, 39.5, 37.9, 36.8, 36.6, 36.2, 35.8, 31.9, 31.8, 29.7, 28.2, 28.0, 27.6, 24.3, 23.8, 22.8, 22.6,

6.6.10 Cholest-5-en-3-yl N-(chloroacetyl)glycinate

$C_{31}H_{50}ClNO_3$
Mwt= 520.20
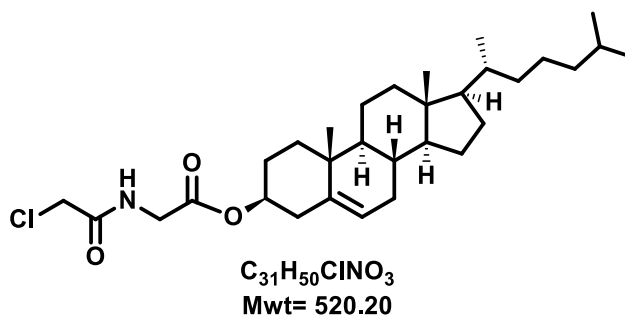
Cholest-5-en-3-yl glycinate (1.0 g, 2.25 mmol) was reacted with chloroacetyl chloride (0.36 g, 0.25 mL, 3.14 mmol) in the presence of DMAP (0.07 g, 0.57 mmol) and an excess of triethylamine (0.44 g, 0.6 mL, 4.31 mmol) in anhydrous dichloromethane (50 mL). The basicity of the medium was checked using litmus paper. The reaction was run at 0 °C, then left at room temperature for 18 hours. The resulting solid was treated with hydrochloric acid (1 N) until neutralisation. Then the crude product was extracted to the dichloromethane layer and purified using the column chromatography (SiO_2, 5% methanol in dichloromethane) to give the pure product as white solid (0.77 g, 1.48 mmol, 66%).

^{1}H NMR (400 MHz, $CDCl_3$) δ 7.13 (t, J = 7.5, 1H), 5.40 (d, J = 3.9 Hz, 1H), 4.77 – 4.62 (m, 1H), 4.15 – 4.01 (m, 4H), 2.36 (δ, J= 7.8 Hz, 2H), 2.10 – 0.80 (m, 38H), 0.69 (s, 3H).

^{13}C NMR (101 MHz, $CDCl_3$) δ 168.6, 166.2, 139.2, 123.1, 75.8, 56.7, 56.1, 50.0, 42.4, 41.8, 39.7, 39.5, 38.0, 36.9, 36.6, 36.2, 35.8, 31.9, 31.8, 28.2, 28.0, 27.7, 24.3, 23.8, 22.8, 22.6, 21.0, 19.3, 18.7, 11.9.

HRMS (ESI): m/z = [M+Na]$^+$: calculated for $C_{31}H_{50}ClNO_3Na^+$ 542.3371, found: 542.3368.

IR (FTIR) cm^{-1}: 1743 (C=O, ester), 1646 (C=O, amide).

6.6.11 Methyl 3-{[N-(tert-butoxycarbonyl)glycyl]oxy}cholan-24-oate

$C_{32}H_{53}NO_6$
Mwt= 547.78
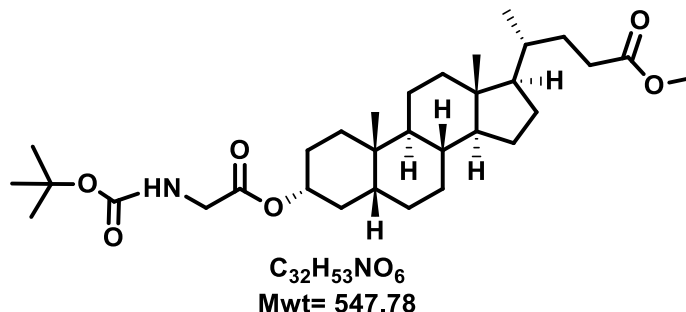
Methyl 3α-hydroxy-5β-lithocholan-24-oate (2.0 g, 5.12 mmol, 1 eq.) was dissolved into anhydrous dichloromethane (30 mL) together with N-t-Boc-glycine (1 g, 5.71 mmol, 1.1 eq.) and DMAP (0.18 g, 1.47 mmol, 0.25 eq). Subsequently, the reaction mixture was stirred at 0 °C for 10 hours after the addition of DCC (1.15 g, 5.57 mmol, 1.1 eq). The dicyclohexylurea (DCU) was filtered off, and then the filtrate was concentrated in *vacuo* at room temperature. The resultant solid was purified using column chromatography (SiO$_2$, 0-10% methanol in dichloromethane) to afford the product (2.7 g, 4.93 mmol, 96%).
R$_f$= 0.5 (1:1, diethyl ether: hexane).

^{1}H NMR (400 MHz, CDCl$_3$) δ 5.05 (s, 1H), 4.86 – 4.72 (m, 1H), 3.86 (t, *J* = 6.4 Hz, 2H), 3.66 (s, 3H), 2.35 (ddd, *J* = 15.3, 10.2, 5.1 Hz, 1H), 2.27 – 2.14 (m, 1H), 1.96 (d, *J* = 11.6 Hz, 1H), 1.91 – 1.50 (m, 9H), 1.47 – 1.43 (s, 9H), 1.43 – 0.97 (m, 16H), 0.91 (dd, *J* = 12.2, 5.8 Hz, 6H), 0.64 (s, 3H).

^{13}C NMR (101 MHz, CDCl$_3$) δ 174.8, 169.8, 155.7, 79.8, 75.6, 56.5, 56.0, 51.5, 42.7, 41.9, 40.4, 40.1, 35.8, 35.4, 35.0, 34.6, 32.2, 31.0, 30.8, 28.3, 28.2, 27.0, 26.6, 26.3, 24.2, 23.3, 20.8, 18.3, 12.0.

HRMS (ESI): m/z = [M+Na]$^+$: calculated for C$_{32}$H$_{53}$ NO$_6$Na$^+$ 570.3765, found: 570.3771.

6.6.12. 2-[(24-Methoxy-24-oxocholan-3-yl)oxy]-2-oxoethan-1-aminium

$C_{27}H_{45}NO_4$
Mwt= 447.66
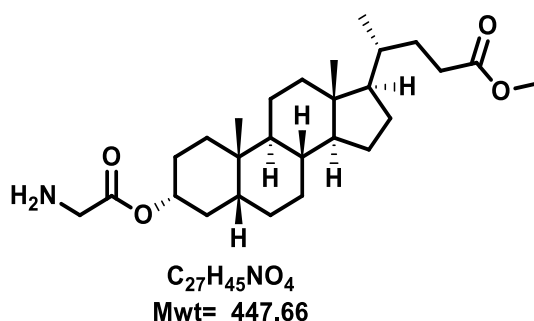
To remove the t-boc group, the previous compound (1.0 g, 1.83 mmol) was treated with a mixture of CH_2Cl_2/TFA (1/1, v/v). The reaction mixture was stirred at $0°C$ for 3 hours. The crude product was then precipitated with water (50 mL). The crude product was filtered off and evaporated to dryness without any further purification.

^{1}H NMR (400 MHz, CDCl$_3$) δ 4.89 – 4.75 (m, 1H), 3.78 (s, 2H), 3.68 (s, 3H), 3.39 (t, J = 10.1 Hz, 2H), 2.37 (ddd, J = 15.2, 10.1, 5.1 Hz, 1H), 2.29 – 2.18 (m, 1H), 2.03 – 1.00 (m, 26H), 0.95 (dd, J = 12.0, 6.5 Hz, 6H), 0.66 (s, 3H).

IR (FTIR) cm^{-1}: 1783 (C=O, ester), 1720 (C=O, ester), 1625 (C=O, amide), 3329 (NH$_2$), 2928-2863 (CH).

HRMS (ESI): m/z = [M+H]$^+$: calculated for $C_{27}H_{45}NO_4H^+$ 448.3421, found: 448.3428.

6.6.13 Methyl 3-{[N-(chloroacetyl)glycyl]oxy}cholan-24-oate

$C_{29}H_{46}ClNO_5$
Mwt= 524.14
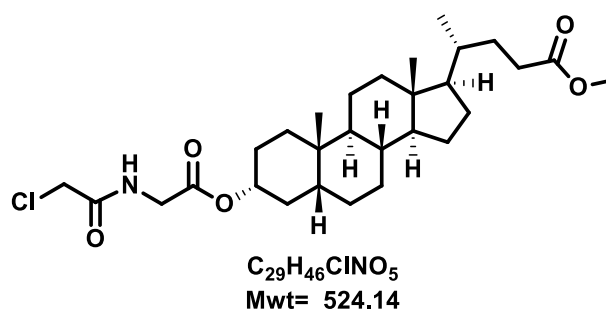
The crude product of the previous compound (1.0 g, 2.23 mmol, 1 eq.) was reacted with chloroacetyl chloride (0.28 g, 0.20 mL, 2.51 mmol, 1.1 eq.) in the presence of DMAP (0.07 g, 0.57 mmol, 0.25 eq.), anhydrous dichloromethane (50 mL) and an excess of triethylamine (0.33 g, 0.45 mL, 3.23 mmol); the basicity of the medium was checked using litmus paper. The reaction was run at 0 ºC, then left at room temperature for 18 hours. The resulting solid was treated with hydrochloric acid (1 N) until neutralisation, and then the crude product was extracted to the dichloromethane layer. The crude product was purified using column chromatography (SiO₂, 5% methanol in dichloromethane) to furnish the pure product as a white solid (0.60 g, 1.15 mmol, 51%).

¹H NMR (400 MHz, CDCl₃) δ 7.18 (t, *J* = 5.0 Hz, 1H), 4.81 – 4.69 (m, 1H), 4.10 – 4.03 (m, 2H), 4.00 (d, *J* = 5.3 Hz, 2H), 3.61 (s, 3H), 2.36 – 2.24 (m, 1H), 2.24 – 2.10 (m, 1H), 1.93 (d, *J* = 11.2 Hz, 1H), 1.88 – 0.93 (m, 26H), 0.92 – 0.83 (m, 6H), 0.60 (s, 3H).

¹³C NMR (101 MHz, CDCl₃) δ 174.7, 168.7, 166.2, 76.1, 56.4, 55.9, 51.4, 42.7, 42.4, 41.9, 41.7, 40.4, 40.1, 35.7, 35.3, 34.9, 34.5, 32.1, 31.0, 31.0, 28.1, 27.0, 26.5, 26.3, 24.1, 23.3, 20.8, 18.2, 12.0.

HRMS (ESI) : m/z = [M+Na]⁺: calculated for $C_{29}H_{46}ClNO_5Na^+$ 546.2957, found: 546.2968.

IR (FTIR) cm⁻¹: 1735 (C=O, ester), 1668 (C=O, amide), 2932-2861 (CH).

6.7 Long Ligand Synthesis

6.7.1 Octyl ({(E)-[1-(6-acetylpyridin-2-yl)ethylidene]amino}oxy)acetate
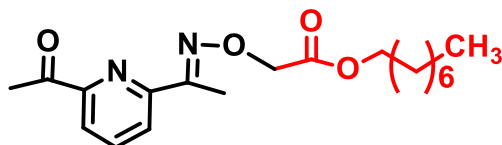
A round-bottomed flask was charged with potassium carbonate (1.5 g, 10.85 mmol) and placed in an ice bath was added a solution of ligand **1** (0.48 g, 2.69 mmol) in DMF (10 mL), and the mixture was stirred for an hour at room temperature before it was re-cooled. Another solution of octyl 2-chloroacetate (0.62 g, 3.0 mmol) in DMF:DCM (2:1) was added and the colour turned from yellow to colourless. The reaction mixture was stirred overnight at room temperature. The crude product was diluted with dichloromethane (50 mL) then washed with water (25 x 2 mL), brine (25 mL), and the compound was extracted to the organic layer. The compound was dried with $MgSO_4$, the solvent was evaporated and the crude product was purified by column chromatography (SiO_2, 3% methanol in dichloromethane) to afford a white solid (0.8 g, 2.30 mmol, 85%).

¹H NMR (400 MHz, $CDCl_3$) δ 8.07 (d, J = 7.9 Hz, 1H), 8.02 (d, J = 7.8 Hz, 1H), 7.79 (t, J = 7.8 Hz, 1H), 4.79 (s, 2H), 4.19 (t, J = 6.6 Hz, 2H), 2.75 (s, 3H), 2.47 (s, 3H), 1.70 – 1.59 (m, 2H), 1.38 – 1.16 (m, 10H), 0.86 (t, J = 6.8 Hz, 3H).

6.7.2 Decyl ({(E)-[1-(6-acetylpyridin-2-yl)ethylidene]amino}oxy)acetate
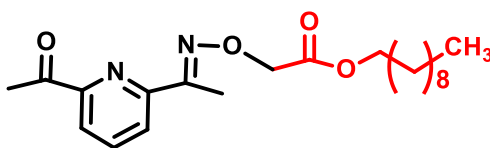
A round-bottomed flask was charged with potassium carbonate (1.5 g, 10.9 mmol) and put in an ice bath then a solution of ligand **1** (0.48 g, 2.69 mmol) in DMF (10 mL) was added and the mixture was stirred for an hour at room temperature before it was re-cooled. Another solution of decyl 2-chloroacetate (0.67 g, 2.85 mmol) in DMF:DCM (2:1) was added and the colour turned from yellow to colourless. The reaction mixture was stirred overnight at room temperature. The crude product was diluted with dichloromethane (50 mL), washed with water (25 x 2 mL) and then brine (25 mL). The crude compound was extracted to the organic layer, dried with MgSO$_4$ and the solvent was evaporated. The compound was purified by column chromatography (SiO$_2$, 3% methanol in dichloromethane) to afford a white solid (0.81 g, 2.15 mmol, 80%).

^{1}H NMR (400 MHz, CDCl$_3$) δ 8.08 (dd, J = 7.9, 0.9 Hz, 1H), 8.00 (dd, J = 7.7, 0.9 Hz, 1H), 7.79 (t, J = 7.8 Hz, 1H), 4.79 (s, 2H), 4.21 – 4.15 (m, 2H), 2.75 (s, 3H), 2.47 (s, 3H), 1.70 – 1.61 (m, 2H), 1.40 – 1.20 (m, 14H), 0.90 (t, J = 6.8 Hz 3H).

^{13}C NMR (101 MHz, CDCl$_3$) δ 200.1, 170.0, 157.1, 153.1, 152.5, 137.0, 124.1, 121.6, 71.2, 65.2, 31.9, 29.5, 29.3, 29.2, 28.6, 25.9, 25.7, 22.7, 14.1, 11.2.

HRMS (ESI) m/z: calculated for C$_{21}$H$_{32}$N$_2$O$_4$Na$^+$ [M+Na]$^+$ 399.2254, found: 399.2259 and calculated for C$_{21}$H$_{32}$ N$_2$O$_4$$^+$ [M+H]$^+$ 377.2435, found: 377.2437.

IR (FTIR) cm^{-1}: 3000-2852 (CH), 1741 (C=O), 1701 (C=O).

6.7.3 Octadecyl({(E)-[1-(6-acetylpyridin-2-yl)ethylidene]amino}oxy) acetate

A round-bottomed flask was charged with potassium carbonate (1.5 g, 10.85 mmol) and put in an ice bath then a solution of ligand **1** (0.48 g, 2.70 mmol) in DMF (10 mL) was added and the mixture was stirred for an hour at room temperature before it was re-cooled. Another solution of stearyl 2-chloroacetate (1.1 g, 3.17 mmol) in DMF:DCM (2:1) was added and the colour turned from yellow to colourless. The reaction mixture was stirred overnight at room temperature. The crude product was diluted with dichloromethane (50 mL) then washed with water (25 x 2 mL) and brine (25 mL). The organic layer was dried with $MgSO_4$ and the solvent was evaporated. The compound was purified by column chromatography (SiO_2, 3% methanol in dichloromethane) to afford a white solid (1.15 g, 2.35 mmol, 87%).

1H NMR (400 MHz, CDCl3) δ 8.07 (d, J = 8.0, 0.9 Hz, 1H), 7.98 (d, J = 7.7, 4.6, 1.1 Hz, 1H), 7.78 (t, J = 7.9 Hz, 1H), 4.18 (t, J = 6.7 Hz, 2H), 2.74 (s, 3H), 2.44 (s, 3H), 1.70 – 1.59 (m, 2H), 1.37 – 1.18 (m, 30H), 0.87 (t, J = 6.8 Hz, 3H).

6.7.4 (9Z)-Octadec-9-en-1-yl({(E)-[1-(6-acetylpyridin-2-yl)ethylidene] amino}oxy) acetate

$C_{29}H_{46}N_2O_4$
Exact Mass =486.35
Mwt =486.70

A round-bottomed flask was charged with potassium carbonate (1.5 g, 10.85 mmol) and put in an ice bath then a solution of ligand **1** (0.6 g, 3.37 mmol) in DMF (10 mL) was added and the mixture was stirred for an hour at room temperature before it was re-cooled. Another solution of (9Z)-octadec-9-en-1-yl chloroacetate (1.1 g, 3.19 mmol) in DMF:DCM (2:1) was added and the colour turned from yellow to colourless. The reaction mixture was stirred overnight at room temperature. The crude product was diluted with dichloromethane (50 mL) then washed with water (25 x 2 mL) and brine (25 mL). The organic layer was dried with MgSO₄ and the solvent was evaporated. The compound was purified by column chromatography (SiO₂, 3% methanol in dichloromethane) to afford a white solid (0.97 g, 1.99 mmol, 63%).

^{1}H NMR (400 MHz, CDCl₃) δ 8.10 (d, *J* = 7.7 Hz, 1H) 7.95 (d, *J* = 7.8 Hz, 1H), 7.82 (t, *J* = 8.0 Hz, 1H), 5.35 (td, *J* = 13.8, 9.9 Hz, 2H), 4.80 (s, 1H), 4.19 (t, *J* = 6.7 Hz, 2H), 4.07 (s, 2H), 2.76 (s, 3H), 2.46 (s, 3H), 2.00 (dd, *J* = 18.5, 6.1 Hz, 4H), 1.66 (dd, *J* = 12.8, 5.8 Hz, 2H), 1.29 (d, *J* = 13.7 Hz, 22H), 0.89 (t, *J* = 6.6 Hz, 3H).

6.7.5 Octyl{[(E)-(1-{6-[(1E)-N-hydroxyethanimidoyl]pyridin-2-yl} ethylidene)amino] oxy} acetate

$C_{19}H_{29}N_3O_4$

12 Mwt = 363.45

To a stirred solution of octyl ({(E)-[1-(6-acetylpyridin-2-yl)ethylidene]amino}oxy)acetate (0.7 g, 2.01 mmol) in 1:1 of chloroform/ethanol (20 mL), hydroxylamine hydrochloride (0.2 g, 2.88 mmol) and another solution of sodium acetate (0.045 g, 0.55 mmol) in water (1 mL) were added. The mixture was allowed to stir at room temperature for 18 hours and then was diluted with chloroform (50 mL). The organic layer was washed with brine (2 x 20 mL) then dried with anhydrous MgSO$_4$, the solvents were evaporated, and the crude product was purified by column chromatography on (SiO$_2$, 0-40% ethyl acetate in hexane) to yield a white solid (0.59 g, 1.62 mmol, 81%).

R$_f$. = 0.44 (20% ethyl acetate in hexane).

^{1}H NMR (400 MHz, CDCl$_3$) δ 9.13 (s, 1H), 7.87 (d, *J* = 7.8 Hz, 1H), 7.79 (d, *J* = 7.8 Hz, 1H), 7.64 (t, *J* = 7.8 Hz, 1H), 4.79 (s, 2H), 4.21 (t, *J* = 6.7 Hz, 2H), 2.45 (s, 3H), 2.40 (s, 3H), 1.71 – 1.61 (m, 2H), 1.40 – 1.19 (m, 10H), 0.88 (t, *J* = 6.9 Hz, 3H).

^{13}C NMR (101 MHz, CDCl$_3$) δ 170.3, 157.7, 157.1, 153.1, 152.8, 136.4, 120.6, 120.3, 71.1, 65.2, 31.8, 29.2, 28.6, 25.9, 22.6, 14.1, 11.3, 10.5.

HRMS (ESI) m/z: calculated for $C_{19}H_{29}$ $N_3O_4^+$ [M+H]$^+$ 364.2231, found: 364.2222.

6.7.6 Decyl{[(E)-(1-{6-[(1E)-N-hydroxyethanimidoyl]pyridin-2-yl} ethylidene) amino] oxy} acetate

C$_{21}$H$_{33}$N$_{3}$O$_{4}$
Mwt = 391.51

13

To a stirred solution of decyl ({(E)-[1-(6-acetylpyridin-2-yl)ethylidene]amino}oxy)acetate (0.70 g, 1.86 mmol) in 1:1 of chloroform:ethanol (20 mL) was added hydroxylamine hydrochloride (0.20 g, 2.88 mmol) and another solution of sodium acetate (0.045 g, 0.55 mmol) in water (1 mL). The mixture was allowed to stir at room temperature overnight, then was diluted with chloroform (50 mL) and the organic layer was washed with brine (2 x 20 mL). The organic layer was then dried with anhydrous MgSO$_4$ and the solvents were evaporated. The crude product was purified by column chromatography (SiO$_2$, 0-40% ethyl acetate in hexane) to yield a white solid (0.65 g, 1.66 mmol, 89%).

R$_f$. = 0.48 (20% ethyl acetate in hexane).

^{1}H NMR (400 MHz, CDCl$_3$) δ 9.09 (s, 1H), 7.87 (d, J = 7.8 Hz, 1H), 7.79 (d, J = 7.8 Hz, 1H), 7.64 (t, J = 7.8 Hz, 1H), 7.64 (t, J = 7.8 Hz, 1H), 4.80 (s, 2H), 4.21 (t, J = 6.7 Hz, 2H), 2.45 (s, 3H), 2.42 (s, 3H), 1.72 – 1.61 (m, 2H), 1.41 – 1.18 (m, 14H), 0.89 (t, J = 6.9 Hz, 3H).

^{13}C NMR (101 MHz, CDCl$_3$) δ 170.3, 157.7, 157.1, 153.1, 152.8, 136.4, 120.6, 120.3, 71.1, 65.2, 31.9, 29.5, 29.3, 29.2, 28.6, 25.9, 22.7, 14.1, 11.3, 10.5.

HRMS (ESI) m/z: calculated for C$_{21}$H$_{33}$N$_{3}$O$_{4}$$^+$ [M+H]$^+$ 392.2544, found: 392.2545.

IR (FTIR) cm^{-1}: 3261 (OH), 2959-2852 (CH), 1766 (C=O).

6.7.7 Octadecyl{[(E)-(1-{6-[(1E)-N-hydroxyethanimidoyl]pyridin-2-yl} ethylidene) amino] oxy} acetate

$C_{29}H_{49}N_3O_4$
Mwt= 503.72

14
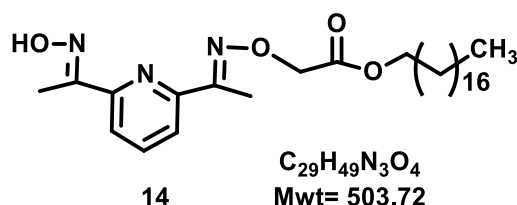
To a stirred solution of octadecyl ({(E)-[1-(6-acetylpyridin-2-yl) ethylidene] amino} oxy)acetate (1.0 g, 2.05 mmol) in 1:1 chloroform:ethanol (30 mL) was added hydroxylamine hydrochloride (0.3 g, 4.32 mmol) and another solution of sodium acetate (0.045 g, 0.55 mmol) in water (1 mL). The mixture was allowed to stir at room temperature for 18 hours, then diluted with chloroform (50 mL) and the organic layer was washed with brine (2 x 20 mL). The organic layer was then dried with anhydrous $MgSO_4$ and the solvents were evaporated. The crude product was purified by column chromatography (SiO_2, 0-40% ethyl acetate in hexane) to give 0.85 g of a white solid product. For the purification of the native compound; HPLC was used 70% THF in water for 10 min., 230 nm detection, compound retention time = 2.8 min. to yield a white solid (0.6 g, 1.19 mmol, 58%).
R_f. = 0.5 (20% ethyl acetate in hexane).

1H NMR (400 MHz, CDCl₃) δ 9.03(s, 1H), 7.88 (d, J = 7.7 Hz, 1H), 7.80 (d, J = 7.7 Hz, 1H), 7.66 (t, J = 7.8 Hz, 1H), 4.80 (s, 2H), 4.21 (t, J = 6.6 Hz, 2H), 2.44 (s, 6H), 1.71 – 1.61 (m, 2H), 1.27 (m, 30H), 0.90 (t, J = 6.5 Hz, 3H).

13C NMR (101 MHz, CDCl₃) δ 170.2, 157.7, 157.1, 153.1, 152.8, 136.4, 120.6, 120.4, 71.1, 65.2, 31.9, 29.7, 29.6, 29.5, 29.4, 29.2, 28.6, 25.9, 22.7, 14.1, 11.3, 10.5.

HRMS: calculated for $C_{29}H_{49}N_3O_4$ (M+H)⁺: 504.3796, found: 504.3797.

6.7.8 (9Z)-octadec-9-en-1-yl{[(E)-(1-{6-[(1E)-N-hydroxyethanimidoyl]pyridin-2-yl} ethylidene) amino]oxy}acetate

$C_{29}H_{47}N_3O_4$
Mwt= 501.36

15
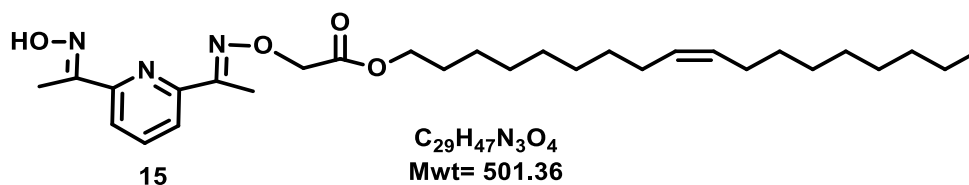
To a stirred solution of (9Z)-octadec-9-en-1-yl ({(E)-[1-(6-acetylpyridin-2-yl)ethylidene]amino}oxy)acetate (0.7 g, 1.44 mmol) in 1:1 of chloroform/ethanol (20 mL), hydroxylamine hydrochloride (0.11 g, 69.5 mmol) and another solution of sodium acetate (0.045 g, 0.55 mmol) in water (1 mL) were added. The mixture was allowed to stir at room temperature for 18 hours, and then diluted with chloroform (50 mL). The organic layer was washed with brine (2 x 20 mL) then was dried with anhydrous $MgSO_4$ and the solvents were evaporated. The crude product was purified by column chromatography (SiO_2, 0-40% ethyl acetate in hexane) to yield a white waxy product (0.65 g, 1.30 mmol, 90%).
R$_f$.= 0.5 (20% ethyl acetate in hexane).

^{1}H NMR (400 MHz, CDCl$_3$) δ 8.58 (s, 1H), 7.88 (dd, *J* = 7.8, 0.9 Hz, 1H), 7.81 (dd, *J* = 7.8, 0.9 Hz, 1H), 7.65 (t, *J* = 7.8 Hz, 1H), 5.42 – 5.32 (m, 2H), 4.80 (s, 2H), 4.21 (t, *J* = 6.7 Hz, 2H), 2.46 (s, 3H), 2.42 (s, 3H), 2.00 (ddd, *J* = 13.2, 6.5, 3.3 Hz, 4H), 1.66 (dd, *J* = 14.4, 6.9 Hz, 2H), 1.40 – 1.23 (m, 22H), 0.90 (t, *J* = 6.8 Hz, 3H).

^{13}C NMR (101 MHz, CDCl$_3$) δ 170.2, 157.7, 157.2, 153.1, 152.7, 136.4, 130.0, 129.8, 120.6, 120.3, 71.1, 65.1, 32.6, 31.9, 29.8, 29.7, 29.7, 29.5, 29.4, 29.3, 29.2, 28.60, 27.2, 27.2, 25.9, 22.7, 14.1, 11.3, 10.4.

HRMS: calculated for $C_{29}H_{47}N_3O_4$ (M+H)$^+$: 502.3639, found: 502.3646.

6.7.9 Cholest-5-en-3-yl({(E)-[1-(6-acetylpyridin-2-yl)ethylidene]amino} oxy) acetate

$C_{38}H_{56}N_2O_4$
Mwt = 604.88
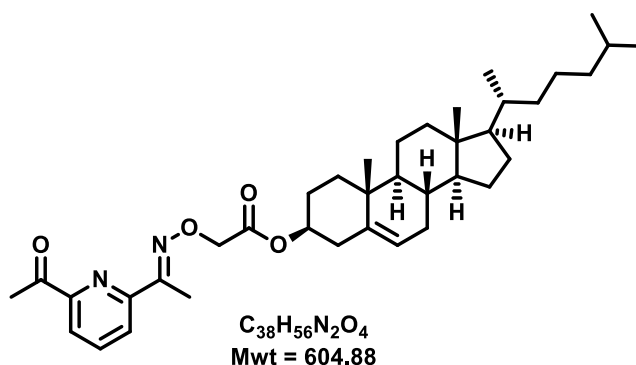
To a solution of compound **1** (0.38 g, 2.13 mmol, 1 eq.) in DMF (12 mL) at 0°C, potassium carbonate (1.95 g, 14.11 mmol, 6.5 eq.) was added after re-warming the solution to room temperature. The yellow mixture was stirred for 1 hour, before cooling to 0 °C, and adding a solution of cholesteryl 2-chloroacetate (1.0 g, 2.16 mmol, 1 eq.) in dichloromethane (5 mL) in which the solution went colourless. The reaction mixture was warmed to room temperature, and then allowed to stir for 16 hours, before diluting with dichloromethane (50 mL), and washed with brine (2 x 10 mL). The organic layer was dried with MgSO$_4$, filtered and the solvents were removed under high vacuum. The crude product was purified by column chromatography (SiO$_2$, 0-10% gradient of methanol in dichloromethane) to afford the product as a white solid (1.2 g, 1.98 mmol, 92%).

1H NMR (400 MHz, CDCl$_3$) δ 8.09 (d, J = 7.9 Hz, 1H), 8.01 (d, J = 7.7 Hz, 1H), 7.81 (t, J = 9.6 Hz, 1H), 5.39 (d, J = 5.0 Hz, 1H), 4.80 – 4.69 (m, 3H), 2.76 (s, 3H), 2.49 (s, 3H), 2.41 – 2.32 (m, 2H), 2.07 – 0.85 (m, 32H), 0.88 (d, J = 6.3 Hz, 6H), 0.69 (s, 3H).

13C NMR (101 MHz, CDCl$_3$) δ 200.1, 169.3, 157.1, 153.0, 152.5, 139.4, 136.9, 124.1, 122.9, 121.5, 74.8, 71.3, 56.7, 56.1, 5.0, 42.3, 39.7, 39.5, 38.1, 36.9, 36.6, 36.1, 35.8, 32.0, 31.8, 31.0, 28.2, 28.1, 27.8, 25.7, 24.3, 23.8, 22.9, 22.6 , 21.0, 19.3, 18.7, 11.9, 11.2.

HRMS (ES$^+$) m/z = 605.4 (M+H)$^+$: calculated for C$_{38}$H$_{56}$N$_2$O$_4$H$^+$ 605.4313, found: 605.4323.

6.7.10 Cholest-5-en-3-yl{[(E)-(1-{6-[(1E)-N-hydroxyethanimidoyl] pyridin-2-yl} ethylidene) amino] oxy}acetate

10

$C_{38}H_{57}N_3O_4$
Mwt = 619.89
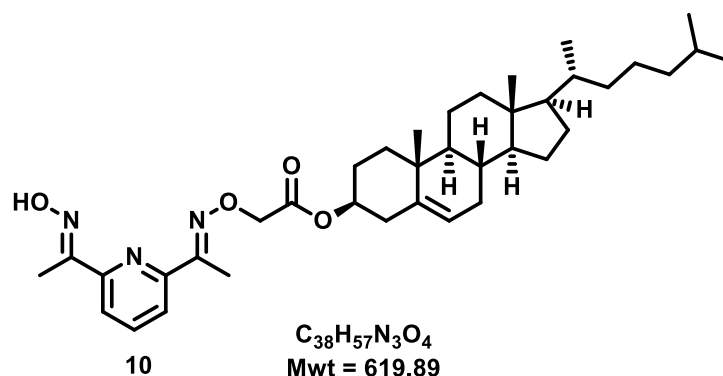
To a solution of previous compound (0.50 g, 0.83 mmol) in chloroform:ethanol (1:1, 10 mL), a solution of hydroxylamine hydrochloride (0.06 g, 0.86 mmol) in chloroform:ethanol (1:1, 2 mL) and a solution of sodium acetate (0.025 g, 0.31 mmol) in water (1 mL) were added. The mixture was heated to 60 °C for 16 hours before the solution was diluted with chloroform (50 mL) and washed with water (25 x 2 mL), then brine (25 mL). The organic layer was then dried with $MgSO_4$, and the solvents were evaporated. The compound was purified by column chromatography (SiO_2, 20% ethyl acetate in hexane) to afford a colourless compound (0.37 g, 0.60 mmol, 72%).

R_f. = 0.6 (20% ethyl acetate-hexane).

^{1}H NMR (400 MHz, CDCl$_3$) δ 9.10 (s, 1H), 7.87 (d, J = 7.8 Hz, 1H), 7.79 (d, J = 7.7 Hz, 1H), 7.64 (t, J = 7.8 Hz, 1H), 5.40 (s, 1H), 4.85 – 4.69 (m, 3H), 2.46 (s, 3H), 2.41 (d, J = 6.0 Hz, 3H), 2.08 – 0.91 (m, 34H), 0.88 (d, J = 6.3 Hz, 6H), 0.69 (s, 3H).

^{13}C NMR (101 MHz, CDCl$_3$) δ 169.6, 157.7, 157.0, 153.1, 152.8, 139.4, 136.4, 122.9, 120.6, 120.3, 74.8, 71.2, 56.7, 56.1, 5.0, 42.3, 39.7, 39.5, 38.1, 36.9, 36.6, 36.2, 35.8, 31.9, 31.8, 28.2, 28.0, 27.8, 24.3, 23.9, 22.8, 22.6, 21.0, 19.3, 18.7, 11.9, 11.5, 10.5.

HRMS (ES$^+$) m/z = 620.4 [M+H]$^+$: calculated for $C_{38}H_{57}N_3O_4H^+$ 620.4422, found: 620.4431., m/z = 642.4 [M+H]$^+$: calculated for $C_{38}H_{57}N_3O_4Na^+$ 642.4241, found: 642.4249.

HPLC: compound was found as one peak at 40.507 minutes, method run as 1% isopropyl alcohol in hexane over 60 minutes.

6.7.11.Methyl3-{[({(E)-[1-(6-acetylpyridin-2-yl)ethylidene]amino}oxy) acetyl]oxy} chol -5-en-24-oate

$C_{36}H_{52}N_2O_6$
Mwt = 608.82
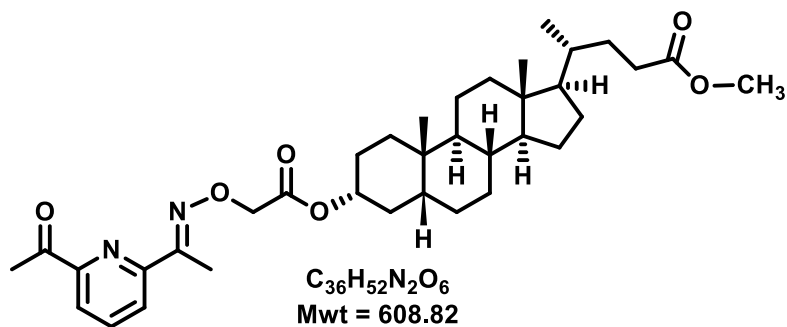
Potassium carbonate (0.34 g, 2.46 mmol) was added to a dry round-bottomed flask immersed in an ice bath and then a solution of compound **1** (0.40 g, 2.25 mmol) in DMF (5 mL) was added. The mixture was stirred for an hour at room temperature, then re-cooled to 0 °C and another solution of methyl 3α-chloroacetyloxy-5β-lithocholan-24-oate (1 g, 2.14 mmol) in dichloromethane (5 mL) was added. The final mixture was stirred at room temperature for 16 hours before diluted it with dichloromethane (50 mL) and filtered, then the organic layer was washed with water and brine (2 x 25 mL). The solvents were then evaporated under high vacuum. The crude product was purified using column chromatography (SiO₂, 0 – 30% ethyl acetate in hexane) to obtain a white solid (0.8 g, 1.31 mmol, 61%).
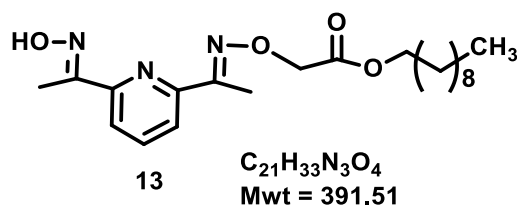
¹H NMR (400 MHz, CDCl₃) d 8.05 (d, *J* = 7.8 1H), 7.95 (d, *J* = 7.7 1H), 7.77 (t, *J* = 7.8 Hz, 1H), 4.88 – 4.76 (m, 1H), 4.73 (s, 2H), 3.64 (s, 3H), 2.71 (d, *J* = 6.2 Hz, 3H), 2.43 (d, *J* = 12.8 Hz, 3H), 2.38 – 2.09 (m, 2H), 1.98 – 0.76 (m, 26H),0.92 – 0.85 (m, 6H), 0.62 (s, 3H).

6.7.12. Methyl3-[({[(E)-(1-{6-[(1E)-N-hydroxyethanimidoyl]pyridin-2-yl} ethylidene) amino]oxy}acetyl)oxy]chol-5-en-24-oate

$C_{36}H_{53}N_3O_6$
Mwt = 623.84

11
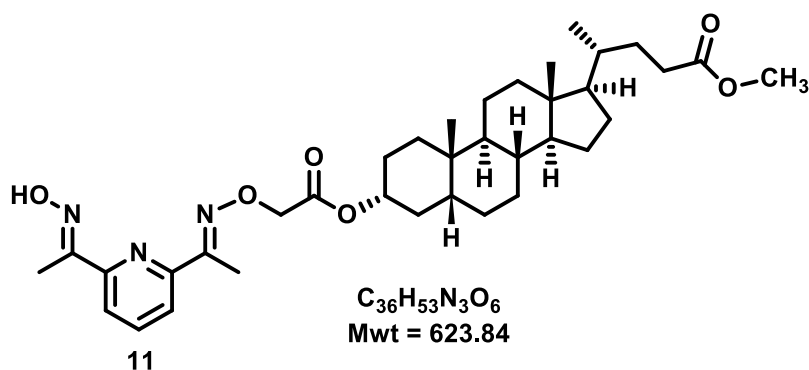
To a solution of methyl3-{[({(E)-[1-(6-acetylpyridin-2- yl)ethylidene] amino} oxy) acetyl]oxy}chol-5-en-24-oate (0.8 g, 1.31 mmol) in 30 mL 1:1 chloroform:ethanol), hydroxylamine hydrochloride (0.11 g, 1.58 mmol) and a solution of sodium acetate (0.5 g, 1.22 mmol) in water (2 mL) were added. The reaction mixture was allowed to stir at 60 °C for 16 hours. The solvents were evaporated under high vacuum and the compound was dissolved in dichloromethane (50 mL) and then filtered, washed with water, brine, and extracted to the organic layer. The crude product was purified using column chromatography (SiO_2, 20% ethyl acetate in hexane) to give a white solid (0.7 g, 1.12 mmol, 85%).
**R$_f$.** = 0.84 (1:1 ethyl acetate-hexane).

^{1}H NMR (400 MHz, CDCl$_3$) δ 8.66 (s, 1H), 7.88 (d, J = 7.8 Hz, 1H), 7.80 (d, J = 7.7 1H), 7.64 (t, J = 9.7 Hz, 1H), 4.91 – 4.80 (m, 1H), 4.76 (s, 2H), 3.69 (s, 3H), 2.46 (s, 3H), 2.42 (d, J = 4.4 Hz, 3H), 2.37 (dt, J = 7.3, 4.4 Hz, 1H), 2.24 (ddd, J = 15.7, 9.7, 6.4 Hz, 1H), 2.00 – 0.85 (m, 26H), 0.92 – 0.85 (m, 6H), 0.65 (d, J = 5.0 Hz, 3H).

^{13}C NMR (101 MHz, CDC$_{l3}$) δ 175.2, 169.7, 157.7, 157.0, 153.2, 152.7, 136.4, 120.5, 120.2, 75.3, 71.3, 56.5, 55.9, 51.6, 42.7, 41.8, 40.4, 40.1, 35.7, 35.4, 35.0, 34.5, 32.2, 31.0, 28.2, 27.0, 26.6, 26.3, 24.2, 23.3, 20.8, 18.2, 12.0, 11.3, 10.4.

HRMS (ESI) : m/z = [M+H]$^+$: calculated for C$_{36}$H$_{53}$ N$_3$O$_6$Na$^+$ 624.4007, found: 624.4014.

6.8 Azido Compounds

6.8.1 Ethyl azidoacetate

$C_4H_7N_3O_2$
Mwt = 129.12
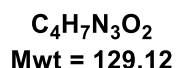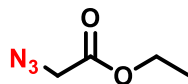
Sodium azide (5.0 g, 76.9 mmol) was added to a mixture of ethyl bromoacetate (6 mL, 9.06 g, 54.1 mmol) in water:acetone (4:12). The mixture was stirred for 40 minutes at room temperature then diluted with dichloromethane (100 mL). The organic layer was then washed with brine (2 x 25 mL), collected and was dried with MgSO$_4$. The solvent was removed to yield a colourless oil (5.50 g, 41.05 mmol, 76%) which was collected without further purification.

^{1}H NMR (400 MHz, CDCl$_3$) δ 4.23 (q, *J* = 7.1 Hz, 2H), 3.83 (s, 2H), 1.29 (t, *J* = 7.1 Hz, 3H).

^{13}C NMR (101 MHz, CDCl$_3$) δ 168.3 (C=O), 61.9 (CH$_2$), 50.4 (CH$_2$), 14.1 (CH$_3$).

IR(FTIR) cm $^{-1}$: 2985 (CH), 2105 (N=N=N), 1739 (C=O).

6.8.2 Octyl azidoacetate

$C_{10}H_{19}N_3O_2$
Mwt = 213.28
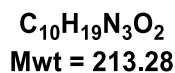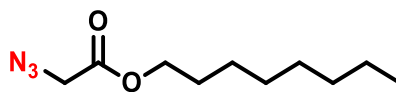
Sodium azide (0.33 g, 5.08 mmol) was added to a solution of octyl 2-chloroacetate (1.0 g, 4.84 mmol) in DMF (15 mL). The reaction mixture went from white to orange and was stirred at 70 °C overnight after which the solvent concentrated. The oil was dissolved in dichloromethane (50 mL) and the organic layer was washed with water (25 mL x 2), brine (25 x 2) and the solvents removed. The pure compound was obtained after purification using column chromatography (SiO$_2$, 3% methanol in dichloromethane) to afford a yellow oil (0.90 g, 4.22 mmol, 87%).

^{1}H NMR (400 MHz, CDCl$_3$) δ 4.25 – 4.18 (m, 2H), 3.88 (s, 2H), 1.74 – 1.62 (m, 2H), 1.44 – 1.22 (m, 10H), 0.90 (t, J = 6.9 Hz, 3H).

^{13}C NMR (101 MHz, CDCl$_3$) δ 168.4, 66.0, 50.4, 31.7, 29.7, 29.1, 28.5, 25.8, 22.6, 14.1.

IR (FTIR) cm^{-1}: 2926-2856 (CH), 2104 (-N=N=N), 1744 (C=O).

6.8.3 Decyl azidoacetate

$C_{14}H_{23}N_3O_2$
Mwt = 241.33
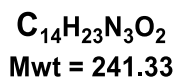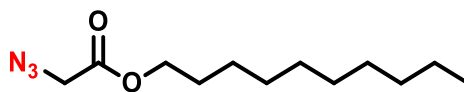
To a mixture of decyl 2-chloroacetate (1.0 g, 4.26 mmol) and sodium azide (0.33 g, 5.08 mmol), DMF (15 mL) was added. The reaction mixture went from white to orange, and it was stirred at 70 °C overnight after which the solvent concentrated. The oil was dissolved in dichloromethane (50 mL) and the organic layer was washed with water (25 mL x 2), brine (25 x 2) and the solvent was removed. The title compound was obtained after purification using column chromatography (SiO$_2$, 3% methanol in dichloromethane), yielding a yellow oil (0.85 g, 3.16 mmol, 74%).

^{1}H NMR (400 MHz, CDCl$_3$) δ 4.26 – 4.16 (m, 2H), 3.88 (s, 2H), 1.74 – 1.63 (m, 2H), 1.42 – 1.22 (m, 14H), 0.90 (t, J = 6.8 Hz, 3H).

^{13}C NMR (101 MHz, CDCl$_3$) δ 168.4, 66.1, 50.4, 31.9, 29.5, 29.5, 29.3, 29.2, 28.5, 25.8, 22.7, 14.1.

IR (FTIR) cm^{-1}: 2924-2854 (CH), 2106 (-N=N=N), 1744 (C=O).

6.8.4 Octadecyl azidoacetate

$C_{20}H_{39}N_3O_2$
Mwt= 353.54
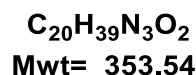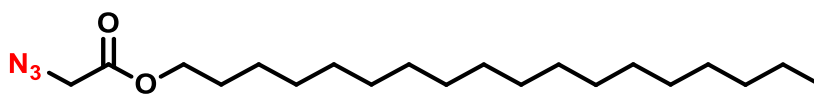
To octadecyl 2-chloroacetate (1.0 g, 2.88 mmol) in DMF (15 mL), sodium azide (0.33 g, 5.08 mmol) was added, and the reaction mixture went from white to orange. The solution stirred at 70 °C for 16 hours, then the solvent was concentrated. The resulting solid was dissolved in dichloromethane (50 mL) and was washed with water (25 mL x 2), brine (25 x 2). The crude compound was purified using column chromatography (SiO$_2$, 3% methanol in dichloromethane) to give a white solid (0.75 g, 2.12 mmol, 74%).

R$_f$. = 0.88 (25 % ethyl acetate in hexane).

^{1}H NMR (400 MHz, CDCl$_3$) δ 4.22 (t, J = 6.7 Hz, 2H), 3.89 (s, 2H), 1.74 – 1.63 (m, 2H), 1.40 – 1.26 (m, 30H), 0.90 (t, J = 6.8 Hz, 3H).

^{13}C NMR (101 MHz, CDCl$_3$) δ 168.4, 66.1, 50.4, 31.9, 29.7, 29.7, 29.6, 29.5, 29.4, 29.2, 28.5, 25.8, 22.7, 14.1.

IR (FTIR) cm^{-1}: 2923-2853 (CH), 2106 (-N=N=N), 1745 (C=O).

6.8.5 (9Z)-Octadec-9-en-1-yl azidoacetate

$C_{20}H_{37}N_3O_2$

Mwt= 351.53
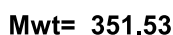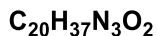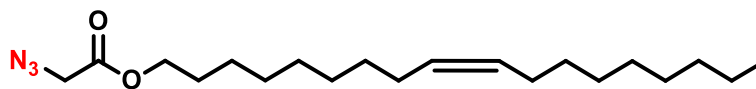
(9Z)-Octadec-9-en-1-yl chloroacetate (0.5 g, 1.45 mmol) in DMF (10 mL) was reacted with sodium azide (0.11 g, 1.7 mmol). The reaction mixture went from white to orange and stirred at 70 °C overnight before the solvent was concentrated. Then the crude product was dissolved in dichloromethane (30 mL) and was washed with water (25 mL x 2), brine (25 x 2) and extracted to the dichloromethane layer. The pure compound was obtained after purification using column chromatography (SiO$_2$, 3% methanol in dichloromethane) to give the product as a white solid (0.46 g, 1.31 mmol, 90%).

^{1}H NMR (400 MHz, CDCl$_3$) δ 5.44 – 5.29 (m, 2H), 4.22 (t, *J* = 6.7 Hz, 2H), 3.89 (s, 2H), 2.08 – 1.96 (m, 3H), 1.68 (dd, *J* = 14.1, 7.0 Hz, 2H), 1.44 – 1.24 (m, 22H), 0.90 (t, *J* = 6.8 Hz, 3H).

^{13}C NMR (101 MHz, CDCl$_3$) δ 168.4, 130.0, 129.8, 66.0, 50.4, 32.6, 31.9, 29.8, 29.7, 29.5, 29.4, 29.3, 29.2, 29.2, 28.5, 27.2, 3.2, 25.8, 22.7, 14.1.

IR (FTIR) cm^{-1}: 2923-2853 (CH), 2106 (-N=N=N), 1747 (C=O).

6.8.6 Methyl 3-[(azidoacetyl)oxy]chol-5-en-24-oate

$C_{29}H_{47}N_3O_2$
Mwt= 469.71
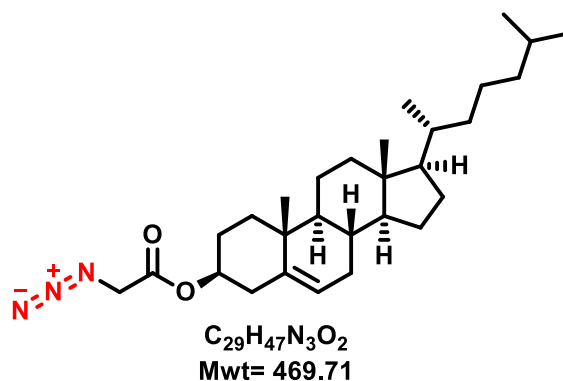
Cholesteryl 2-chloroacetate (0.5 g, 1.08 mmol) was treated with sodium azide (0.1 g, 1.5382 mmol) in DMF (20 mL) at 70 °C for 13 hours. The solvent was concentrated under high vacuum; solid was dissolved in dichloromethane (30 mL) and was washed with water, brine). Column chromatography was run to purify the crude product using SiO_2, 3% methanol in dichloromethane. The pure compound was isolated as a white solid (0.47 g, 0.992 mmol, 92%).

^{1}H NMR (400 MHz, CDCl$_3$) δ 5.40 (t, J = 7.4 Hz, 1H), 4.80 – 4.67 (m, 1H), 3.86 (s, 2H), 2.37 (t, J = 11.4 Hz, 2H), 2.10 – 0.90 (m, 32H), 0.89 (d, J = 6.6 Hz, 6H), 0.70 (s, 3H).

^{13}C NMR (101 MHz, CDCl$_3$) δ 167.7, 139.2, 123.2, 75.9, 56.7, 56.1, 50.5, 50.0, 42.3, 39.7, 39.5, 38.0, 36.9, 36.6, 36.2, 35.8, 31.9, 31.8, 28.2, 27.7, 27.6, 24.3, 23.9, 22.8, 22.5, 21.0, 19.3, 18.7, 11.9.

HRMS (ES+): m/z = [M+Na]$^+$: calculated for $C_{29}H_{47}N_3O_2Na^+$ 492.3566, found: 492.3555.

IR (FTIR) cm^{-1}: 2935-2867 (CH), 2107 (-N=N=N), 1748 (C=O).

6.8.7 Cholest-5-en-3-yl *N*-(azidoacetyl)glycinate

$C_{31}H_{50}N_4O_3$
Mwt= 526.77
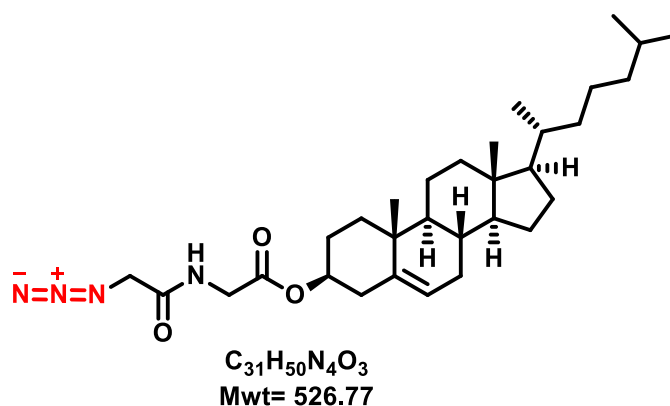
Cholest-5-en-3-yl N-(chloroacetyl)glycinate (0.13 g, 0.25 mmol) was treated with sodium azide (0.04 g, 0.62 mmol) in DMF (20 mL). The reaction mixture was stirred overnight at 70 °C, then the solvent was concentrated under high vacuum, and the crude product was dissolved in dichloromethane (50 mL), and then was washed with water (25 mL) and brine (3 x 25 mL). The crude product was extracted to the organic layer, and the solvent was removed by rotary evaporation. The crude product was then purified using column chromatography (SiO$_2$, 3% methanol in dichloromethane) to obtain a cream coloured solid (0.13 g, 0.25 mmol, 99%).

^{1}H NMR (400 MHz, CDCl$_3$) δ 6.84 (s, 1H), 5.40 (t, *J* = 7.4 Hz, 1H), 4.80 – 4.67 (m, 1H), 4.07 (d, *J* = 5.9 Hz, 4H), 2.36 (d, *J* = 7.8 Hz, 2H), 2.08 – 1.75 (m, 5H), 1.73 – 0.80 (m, 33H), 0.69 (s, 3H).

^{13}C NMR (101 MHz, CDCl$_3$) δ 168.8, 166.8, 139.2, 123.1, 75.7, 56.7, 56.1, 52.5, 50.0, 42.3, 41.4, 39.7, 39.5, 38.0, 36.9, 36.6, 36.2, 35.8, 31.9, 31.8, 28.2, 28.0, 27.7, 24.3, 23.8, 22.8, 22.6, 21.0, 19.3, 18.7, 11.9.

IR (FTIR) cm^{-1}: 1744 (C=O), 2112 (-N=N=N).

HRMS (TOF MS ES+): m/z = [M+Na]$^+$: calculated for C$_{31}$H$_{50}$N$_4$O$_3$Na$^+$ 549.3781, found: 549.3760.

6.8.8 Methyl 3-[(azidoacetyl)oxy]cholan-24-oate

C$_{27}$H$_{43}$N$_3$O$_4$
Mwt = 473.66
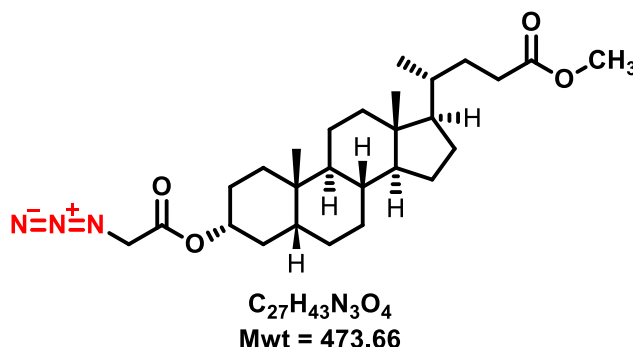
The procedure was modified from the literature procedure.[196]

Methyl 3α-(chloroacetoxy)-5β-cholan-24-oate (0.5 g, 1.07 mmol) was dissolved in DMF (15 mL) and then sodium azide (0.1 g, 1.54 mmol) was added. The mixture was stirred overnight at 60 °C, diluted with dichloromethane (50 mL) and washed with water (5 x 25 mL). The organic layer was then dried with MgSO$_4$ and the solvents evaporated. The obtained product was purified by column (SiO$_2$, dichloromethane:hexanes, 1:1) to give a white solid (0.4 g, 0.85 mmol, 79%). m.p. 106–109 °C.

1H NMR (400 MHz, CDCl$_3$) δ 4.94 – 4.73 (m, 1H, 3H), 3.84 (s, 2H, N$_3$CH$_2$CO), 3.66 (s, 3H, COOCH$_3$), 2.35 (dd, *J* = 10.2, 5.1 Hz, 1H), 2.27 – 2.13 (m, 1H), 2.01 – 0.96 (m, 26H), 0.96 – 0.85 (m, 6H), 0.64 (s, 3H).

13C NMR (101 MHz, CDCl$_3$) δ 174.7 (COOCH$_3$), 167.8 (COCH$_2$N$_3$), 76.4, 56.5, 56.0, 51.5, 50.6, 42.7, 41.9, 40.5, 40.1, 35.8, 35.4, 34.9, 34.6, 32.2, 31.1, 31.0, 28.2, 27.0, 26.6, 26.3, 24.2, 23.3, 20.8, 18.3, 12.0.

HRMS (ESI) : m/z = [M+Na]$^+$: calculated for C$_{27}$H$_{43}$N$_3$O$_4$Na$^+$ 496.3146, found: 496.3152.

IR (FTIR) cm^{-1}: 1753 (C=O), 1732 (C=O), 2105 (-N=N=N).

6.8.9 Methyl 3-{[N-(azidoacetyl)glycyl]oxy}cholan-24-oate

$C_{29}H_{46}N_4O_5$
Mwt = 530.70
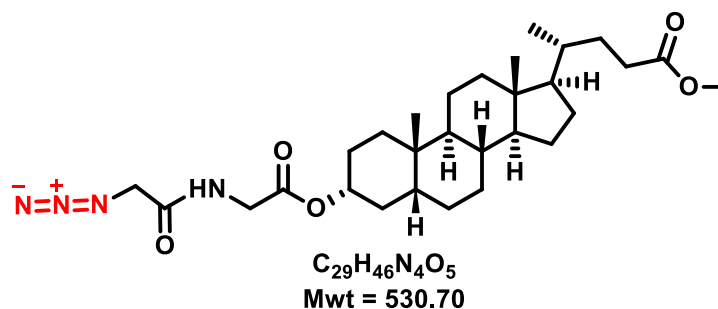
Methyl 3-{[N-(chloroacetyl)glycyl]oxy}cholan-24-oate (0.72 g, 1.37 mmol, 1 eq.) was reacted with sodium azide (0.18 g, 2.77 mmol, 2 eq.) in DMF (15 mL) at 70 °C for 16 hours. The mixture was diluted with dichloromethane (50 mL) and washed with water (5 x 25 mL) then brine (5 x 25 mL). The organic layer was dried with MgSO₄ and the solvents were evaporated. The obtained product was purified by column chromatography (SiO₂, 30% methanol in dichloromethane) to give a white solid, (0.65 g, 1.23 mmol, 89%).

¹H NMR (400 MHz, CDCl₃) δ 6.81 (s, 1H), 4.80 (s, 1H), 4.03 (t, J = 2.5 Hz, 4H), 3.65 (s, 3H), 2.32 (dd, J = 10.2, 5.1 Hz, 1H), 2.26 – 2.15 (m, 1H), 1.96 (d, J = 11.6 Hz, 1H), 1.90 – 0.96 (m, 26H), 0.96 – 0.85 (m, 6H), 0.63 (s, 3H).

¹³C NMR (101 MHz, CDCl₃) δ 174.8, 168.9, 166.8, 76.3, 56.4, 56.0, 52.5, 51.5, 42.7, 41.9, 41.4, 40.4, 40.1, 35.8, 35.5, 34.9, 34.6, 32.1, 31.1, 31.0, 28.2, 27.0, 26.6, 26.3, 24.2, 23.3, 20.84, 18.3, 12.1.

HRMS (ESI) : m/z = [M+Na]⁺: calculated for $C_{29}H_{46}N_4O_5Na^+$ 553.336, found: 553.3377.

IR (FTIR) cm⁻¹: 1666 (C=O, amide), 1731 (C=O, ester), 2101 (-N=N=N), 2931-2870 (CH).

6.9   Click Compounds

6.9.1   Octyl[4-({[(E)-(1-{6-[(1E)-N-hydroxyethanimidoyl]pyridin-2-yl} ethylidene) amino] oxy}methyl)-1H-1,2,3-triazol-1-yl]acetate

$C_{22}H_{32}N_6O_4$

MWt = 444.54

20
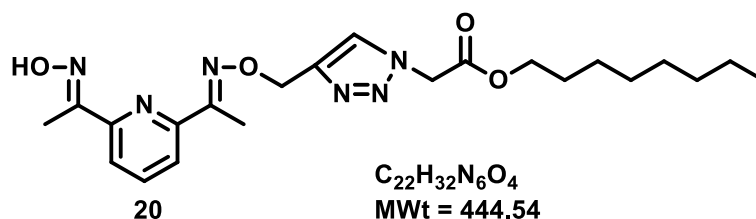
Compound **8** (0.33 g, 1.41 mmol) in anhydrous dichloromethane (16 mL) was reacted with octyl azidoacetate (0.30 g, 1.41 mmol) in the presence of CuI (0.54 g, 2.84 mmol) and DIPEA (4 mL). The reaction was running at room temperature for 15 hours, then the dark green-brown solution was treated with EDTA (20 mL, 0.1 M, pH = 8) to remove the copper (the aqueous layer turned to an azure colour). Then the solution diluted with dichloromethane (50 mL), and the product was extracted to the organic layer, dried with $MgSO_4$. The solvent was evaporated using a rotary evaporator, and the product was purified by column chromatography (SiO_2, 25-75% ethyl acetate: hexane) to furnish a white solid (0.55g, 1.24 mmol, 88%).

Rf. = 0.46 (1:1 ethyl acetate: hexane).

1H NMR (400 MHz, CDCl₃) δ 9.83 (s, 1H), 7.87 (d, J = 7.8 Hz, 1H), 7.80 (d, J = 7.2 Hz, 2H), 7.66 – 7.56 (m, 1H), 5.42 (s, 2H), 5.19 (s, 2H), 4.18 (t, J = 6.8 Hz, 2H), 2.40 (s, 3H), 2.36 (s, 3H), 1.68 – 1.54 (m, 2H), 1.35 – 1.19 (m, 10H), 0.87 (t, J = 6.9 Hz, 3H).

13C NMR (101 MHz, CDCl₃) δ 166.4, 156.8, 156.8, 153.3, 153.0, 145.2, 136.4, 124.6, 120.3, 120.2, 67.7, 66.6, 50.9, 31.7, 29.1, 28.3, 25.7, 22.6, 14.1, 11.2, 10.2.

HRMS (ES+) : m/z = [M+H]⁺: calculated for $C_{22}H_{32}N_6 O_4^+$ 445.2558, found: 445.2560.

IR (FTIR) cm⁻¹: 1744 (C=O), 3203 (OH).

6.9.2 Decyl{4-[({(E)-[1-(6-acetylpyridin-2-yl)ethylidene]amino}oxy) methyl]-1H-1,2,3-triazol-1-yl}acetate

$C_{24}H_{35}N_5O_4$
Mwt= 457.58
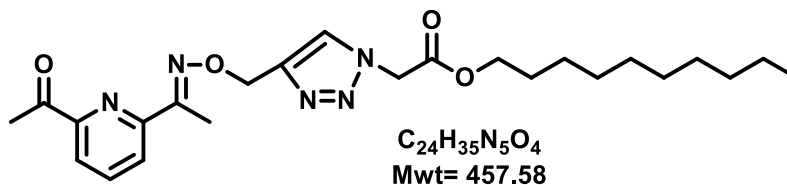
To a covered and evacuated round-bottomed flask containing a mixture of compound **7** (0.32 g, 1.48 mmol), decyl azidoacetate (0.33 g, 1.22 mmol), and CuI (0.5 g, 2.6 mmol) dry dichloromethane–DIPEA (as 8:2, 10 mL) was added. The resulting suspension was stirred at room temperature overnight, then the dark green-brown solution was treated with EDTA (20 mL, 0.1 M, pH = 8) to remove the copper (the aqueous layer turned to azure colour). The solution was diluted with dichloromethane (50 mL) and the product was extracted to the organic layer, dried with $MgSO_4$, the solvent was evaporated using a rotary evaporator, and the product was purified by column chromatography (SiO_2, ethyl acetate: hexane, 2:8) to furnish a white solid (0.53 g, 1.15 mmol, 94%).

¹H NMR (400 MHz, CDCl₃) δ 8.08 (d, *J* = 7.5 1H), 7.94 (d, *J* = 7.6 Hz, 1H), 7.78 – 7.73 (m, 2H), 5.39 (s, 2H), 5.15 (s, 2H), 4.16 (t, *J* = 6.7 Hz, 2H), 2.69 (s, 3H), 2.35 (s, 3H), 1.65 – 1.55 (m, 2H), 1.24 (m, 14H), 0.84 (t, *J* = 6.8 Hz, 3H).

¹³C NMR (101 MHz, CDCl₃) δ 200.1, 166.4, 156.2, 153.4, 152.6, 145.1, 137.0, 124.5, 124.0, 121.4, 68.0, 66.6, 50.9, 31.9, 29.5, 29.5, 29.3, 29.2, 28.4, 25.8, 25.7, 22.7, 14.2, 11.0.

IR (FTIR) cm⁻¹: 1741 (C=O), 2922 (CH).

HRMS calculated for $C_{24}H_{35}N_5O_4$ (M+H)⁺: 458.2762, found: 458.2749.

6.9.3 Decyl [4-({[(E)-(1-{6-[(1E)-N-hydroxyethanimidoyl]pyridin-2-yl} ethylidene) amino] oxy}methyl)-1H-1,2,3-triazol-1-yl]acetate

C$_{24}$H$_{36}$N$_6$O$_4$
Mwt= 472.59
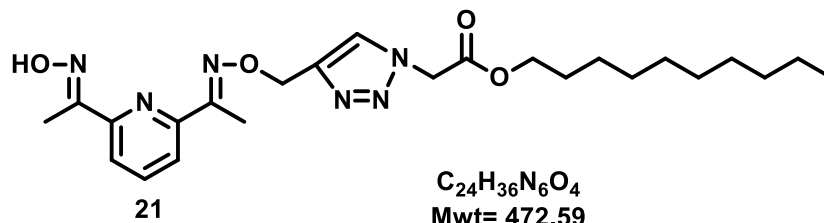
To a flask charged with the previous compound (0.50 g, 1.09 mmol), hydroxylamine hydrochloride (0.08 g, 1.2 mmol) and a mixture of chloroform:ethanol (1:1), and water (15:15:2 mL) was added and the mixture was stirred at 70 °C overnight. The solvents were removed under reduced pressure and the crude product (0.50 g) was purified using HPLC (55% THF in water, detection 240 nm, 20 min, compound's retention time = 10.73 min.) to yield a white solid (0.40 g, 0.87 mmol, 80%).

1H NMR (400 MHz, CDCl$_3$) δ 8.74 (s, 1H), 7.88 (d, *J* = 7.8 Hz, 1H), 7.79 (d, *J* = 7.8 Hz, 1H), 7.75 (s, 1H), 7.63 (t, *J* = 7.8 Hz, 1H), 5.41 (s, 2H), 5.17 (s, 2H), 4.18 (t, *J* = 6.8 Hz, 2H), 2.39 (s, 3H), 2.35 (s, 3H), 1.67 – 1.58 (m, 2H), 1.33 – 1.22 (m, 14H), 0.87 (t, *J* = 6.9 Hz, 3H).

13C NMR (101 MHz, CDCl$_3$) δ 166.5, 157.2, 156.9, 153.3, 153.2, 145.4, 136.5, 124.6, 120.5, 120.3, 67.9, 66.7, 51.0, 32.0, 29.6, 29.6, 29.4, 29.2, 28.5, 25.8, 22.8, 14.2, 11.3, 10.6.

IR (FTIR) cm^{-1}: 1742 (C=O), 2923 (CH), 3203 (OH).

HRMS (ES+): m/z = [M+H]$^+$: calculated for C$_{24}$H$_{36}$N$_6$ O$_4$$^+$ 473.2871, found: 473.2878.

6.9.4 Octadecyl[4-({[(E)-(1-{6-[(1E)-N-hydroxyethanimidoyl]pyridin-2-yl}ethylidene) amino] oxy}methyl)-1H-1,2,3-triazol-1-yl]acetate

C$_{32}$H$_{52}$N$_6$O$_4$
MWt = 584.41

To a covered and an evacuated round-bottomed flask containing a mixture of ligand **8** (0.2 g, 0.87 mmol) octadecyl azidoacetate (0.30 g, 0.85 mmol), and CuI (0.33 g, 1.73 mmol), dry dichloromethane–DIPEA (as 8:2, 20 mL) was added. The resulting suspension was stirred at room temperature for overnight. To remove the copper, the dark green-brown solution was treated with EDTA (50 mL, 0.1 M, pH = 8) and the aqueous layer turned azure in colour. The organic layer was diluted with dichloromethane (50 mL) and the product was extracted to the organic layer, dried with MgSO$_4$, the solvent was removed using a rotary evaporator. The product was purified by column chromatography (SiO$_2$ using a mixture of ethyl acetate: hexane (v/v = 2:8)) to yield a white solid (0.4 g, 0.68 mmol, 80%).
R$_f$. = 0.56 (1:1 ethyl acetate:hexane).

^{1}H NMR (400 MHz, CDCl$_3$) δ 8.31 (s, 1H), 7.91 (d, J = 7.8 Hz, 1H), 7.83 (d, J = 7.8 Hz, 1H), 7.77 (s, 1H), 7.66 (t, J = 7.8 Hz,1H), 5.44 (s, 2H), 5.19 (s, 2H), 4.21 (t, J = 6.8 Hz, 2H), 2.41 (s, 3H), 2.38 (s, 3H), 1.70 – 1.61 (m, 2H), 1.35 – 1.24 (m, 30H), 0.90 (t, J = 6.9 Hz, 3H).

^{13}C NMR (101 MHz, CDCl$_3$) δ 166.3, 157.1, 156.8, 153.2, 153.1, 145.3, 136.4, 124.4, 120.4, 120.2, 67.8, 66.6, 50.9, 31.9, 30.9, 29.7, 29.7, 29.6, 29.5, 29.4, 29.1, 28.4, 25.7, 22.7, 14.1, 11.2, 10.4.

HRMS (ES+): m/z = [M+H]$^+$: calculated for C$_{32}$H$_{52}$N$_6$ O$_4$$^+$ 585.4123, found: 585.4130.
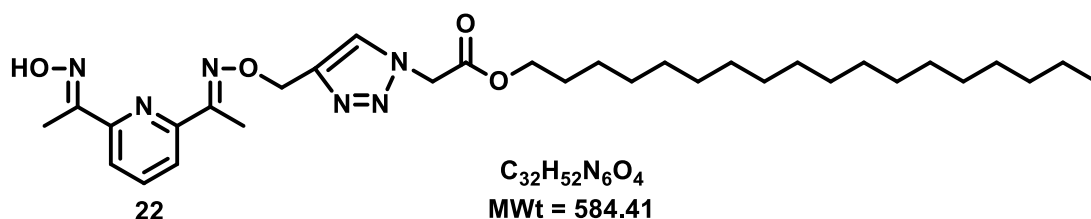
IR (FTIR) cm^{-1}: 1739 (C=O), 2916 (CH), 3261(OH).

6.9.5 (9Z)-octadec-9-en-1-yl[4-({[(E)-(1-{6-[(1E)-N-hydroxyethanimidoyl]pyridin-2-yl}ethylidene) amino]oxy}methyl)-1H-1,2,3-triazol-1-yl]acetate

$C_{32}H_{50}N_6O_4$
MWt = 582.39

23
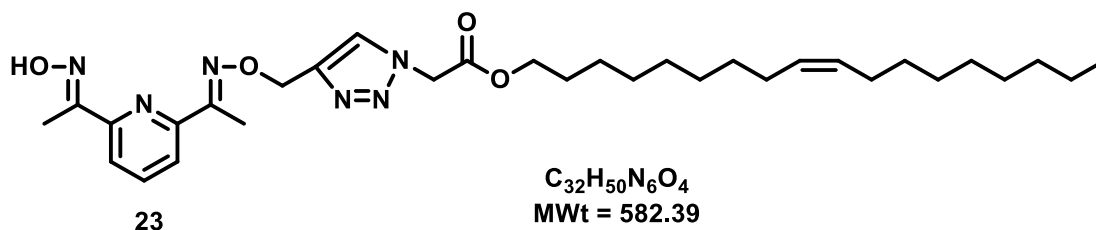
To a covered and evacuated round-bottomed flask containing a mixture of compound **8** (0.2 g, 0.87 mmol), (9Z)-octadec-9-en-1-yl azidoacetate (0.3 g, 0.85 mmol), and CuI (0.33 g, 1.73 mmol) a mixture of dry dichloromethane–DIPEA (as 8:2, 20 mL) was added. The resulting suspension was stirred at room temperature for overnight. To remove the copper, the dark green-brown solution was treated with EDTA (50 mL, 0.1 M, pH = 8) and the aqueous layer turned azure in colour. The organic layer was diluted with dichloromethane (50 mL) and the product was extracted to the organic layer, dried with $MgSO_4$, then the solvent was evaporated using a rotary evaporator. The product was purified by column chromatography (SiO_2, ethyl acetate: hexane, 2:8) to obtain a white solid (0.49 g, 0.84 mmol, 99%).

R$_f$. = 0.54 (1:1 ethyl acetate: hexane).

^{1}H NMR (400 MHz, CDCl$_3$) δ 8.56 (s, 1H), 7.91 (d, J = 7.8 Hz, 1H), 7.82 (d, J = 7.8 Hz, 1H), 7.77 (s, 1H), 7.66 (t, J = 7.8 Hz, 1H), 5.44 (s, 2H), 5.37 (td, J = 5.7, 3.4 Hz, 2H), 5.19 (s, 2H), 4.21 (t, J = 6.8 Hz, 2H), 2.42 (s, 3H), 2.38 (s, 3H), 2.02 (dt, J = 14.2, 6.9 Hz, 4H), 1.69 – 1.60 (m, 2H), 1.39 – 1.23 (m, 22H), 0.90 (t, J = 6.8 Hz, 3H).

^{13}C NMR (101 MHz, CDCl$_3$) δ 166.3, 157.2, 156.8, 153.2, 153.1, 145.3, 136.4, 130.0, 129.8, 124.4, 120.4, 120.2, 67.8, 66.6, 50.9, 32.6, 32.5, 31.9, 29.8, 29.7, 29.7, 29.6, 29.5, 29.4, 29.3, 29.2, 29.1, 28.4, 27.2, 27.2, 25.7, 22.7, 14.1, 11.2, 10.4.

HRMS (ES+): m/z = [M+H]$^+$: calculated for C$_{32}$H$_{50}$N$_6$ O$_4$$^+$: 583.3966, found: 583.3970.

IR (FTIR) cm^{-1}: 1746 (C=O), 2922 (CH), 3268 (OH).

6.9.6 Cholest-5-en-3-yl[4-({[(E)-(1-{6-[(1E)-N-hydroxyethanimidoyl]pyridin-2-yl}ethylidene)amino]oxy}methyl)-1H-1,2,3-triazol-1-yl]acetate

$C_{41}H_{60}N_6O_4$
Mwt = 700.79

Procedure modified from the literature [197]

To a covered and evacuated round-bottomed flask containing a mixture of alkyne ligand (0.08 g, 0.35 mmol, 1 eq.), methyl 3-[(azidoacetyl)oxy]chol-5-en-24-oate (0.20 g, 0.43 mmol, 1.2 eq), and CuI (0.13 g, 0.69 mmol, 2 eq.), a mixture of dry dichloromethane–DIPEA (as 8:2, 10 mL) was added. The mixture was stirred at room temperature overnight, the dark green-brown solution was treated with EDTA (20 mL, 0.1 M, pH = 8) to remove the copper (the aqueous layer turned azure). Then the solution diluted with dichloromethane (50 mL) and the product was extracted to the organic layer, dried with MgSO4, the solvent was removed using a rotary evaporator. The product was purified by column chromatography (SiO2, 0-50% ethyl acetate in hexane), to furnish a white solid, 0.24 g, 0.34 mmol, 99%).
Rf. = 0.7 (1:1 ethyl acetate:hexane).

1H NMR (400 MHz, CDCl3) δ 8.50 (s, 1H), 7.91 (d, J = 7.8 Hz, 1H), 7.82 (d, J = 7.8 Hz, 1H), 7.78 (s, 1H), 7.64 (t, J = 7.8 Hz, 1H), 5.44 (s, 2H), 5.37 (d, J = 3.9 Hz, 1H), 5.17 (s, 2H), 4.79 – 4.62 (m, 1H), 2.46 – 2.26 (m, 8H), 2.07– 0.81 (m, 39H), 0.69 (s, 3H).

13C NMR (101 MHz, CDCl3) δ 165.7, 157.1, 156.8, 153.2, 153.1, 145.3, 138.9, 136.4, 124.4, 123.3, 120.4, 120.2, 76.5, 67.8, 56.7, 56.1, 51.1, 49.9, 42.3, 39.7, 39.5, 37.9, 36.8, 36.5, 36.2, 35.8, 31.9, 31.8, 28.2, 28.0, 27.6, 24.3, 23.8, 22.8, 22.6, 21.0, 19.2, 18.7, 11.9, 11.1, 10.4.

HRMS (ES+): m/z = [M+H]+: calculated for $C_{41}H_{61}N_6O_4^+$ 701.5, found: 701.5.

6.9.7 Cholest-5-en-3-ylN-({4-[({(E)-[1-(6-acetylpyridin-2-yl)ethylidene] amino} oxy) methyl]-1H-1,2,3-triazol-1-yl}acetyl)glycinate

$C_{43}N_{62}N_6O_5$
Mwt = 743.01

To a covered and an evacuated round-bottomed flask containing a mixture of alkyne ligand **8** (0.056 g, 0.26 mmol) cholest-5-en-3-yl N-(azidoacetyl)glycinate (0.13 g, 0.25 mmol), and CuI (0.1 g, 0.53 mmol), a mixture of dry dichloromethane–DIPEA (as 8:2, 10 mL) was added. The resulting suspension was stirred at room temperature overnight, the dark green-brown solution was treated with EDTA (20 mL, 0.1 M, pH = 8) to remove the copper (the aqueous layer turned azure in colour). Then the solution was diluted with dichloromethane (50 mL), and the product was extracted to the organic layer, dried with MgSO$_4$, then the solvent was evaporated using a rotary evaporator. The product was purified by column chromatography (SiO$_2$, ethyl acetate: hexane, 2:8) to furnish a white solid (0.18 g, 0.24 mmol, 98%).

¹H NMR (400 MHz, CDCl₃) δ 8.11 (d, *J* = 7.9 Hz, 1H), 7.99 (d, *J* = 7.6 Hz, 1H), 7.88 (s, 1H), 7.80 (t, *J* = 7.8 Hz, 1H), 7.10 (t, *J* = 5.0 Hz, 1H), 5.39 (s, 2H), 5.35 (s, 1H), 5.18 (s, 2H), 4.61 (dd, *J* = 12.9, 7.9 Hz, 1H), 4.03 (d, *J* = 5.2 Hz, 2H), 2.74 (s, 3H), 2.47 – 2.22 (m, 5H), 2.05 – 1.73 (m, 5H), 1.65 – 0.77 (m, 35H), 0.67 (s, 3H).

¹³C NMR (101 MHz, CDCl₃) δ 200.2, 168.6, 165.4, 156.1, 153.3, 152.5, 145.2, 139.2, 137.0, 124.9, 124.0, 122.9, 121.5, 75.7, 67.6, 56.6, 56.1, 52.7, 49.9, 42.2, 41.7, 39.7, 39.5, 37.9, 36.8, 36.5, 36.2, 35.8, 32.0, 31.8, 29.7, 28.3, 28.0, 27.6, 25.7, 24.3, 23.9, 22.9, 22.6, 21.0, 19.3, 18.7, 11.8, 11.1.

6.9.8 Cholest-5-en-3-ylN-{[4-({[(E)-(1-{6-[(1E)-N-hydroxyethanimidoyl] pyridin-2-yl}ethylidene)amino]oxy}methyl)-1H-1,2,3-triazol-1-yl] acetyl}glycinate

$C_{43}N_{63}N_7O_5$
Mwt = 758.02

16

To a flask charged with the above mono oxime click compound (0.13 g, 0.18 mmol), hydroxyl amine hydrochloride (0.015 g, 0.22 mmol) and sodium acetate (0.045 g, 0.55 mmol) were added together with a mixture of 1:1 chloroform:ethanol (15 mL) and water (2 mL). The mixture was refluxed at 70 °C overnight, then the solvents were evaporated under high vacuum. The crude product was washed with water and brine (2 x 25 mL), then the product dried with $MgSO_4$ and purified using column chromatography (SiO_2, 20% ethyl acetate in hexane) to give a white solid (0.13 g, 0.17 mmol, 98%).

R$_f$. = 0.46 (4:6 dichloromethane/ ethyl acetate).

^{1}H NMR (400 MHz, CDCl$_3$) δ 8.70 (s, 1H), 7.87 (d, J = 7.8 Hz, 1H), 7.84 (s, 1H), 7.80 (d, J = 7.3 Hz, 1H), 7.63 (t, J = 7.8 Hz, 1H), 6.82 (t, J = 5.2 Hz, 1H), 5.47 – 5.31 (m, 3H), 5.15 (s, 2H), 4.72 – 4.56 (m, 1H), 4.01 (dd, J = 14.4, 6.2 Hz, 2H), 2.35 (dd, J = 27.4, 12.0 Hz, 8H), 2.09 – 1.74 (m, 6H), 1.67 – 0.81 (m, 32H), 0.69 (s, 3H).

^{13}C NMR (126 MHz, CDCl$_3$) δ 168.4, 165.3, 157.1, 156.8, 153.2, 153.0, 145.6, 139.2, 136.4, 124.6, 123.0, 120.4, 120.1, 108.0, 107.6, 106.8, 106.4, 75.8, 67.6, 56.7, 56.3, 52.8, 50.1, 42.4, 41.7, 39.8, 39.5, 38.0, 36.8, 36.6, 36.2, 35.7, 29.4, 29.1, 28.2, 27.8, 27.7, 24.2, 23.9, 22.7, 22.5, 21.0, 19.2, 18.7, 11.8, 11.1, 10.3.

HRMS: calculated for C$_{43}$H$_{63}$N$_7$ O$_5^+$ [M+H]$^+$ 758.4963, found: 758.4969.

6.9.9 Methyl3-({[4-({[(E)-(1-{6-[(1E)-N-hydroxyethanimidoyl]pyridin-2-yl}ethylidene)amino]oxy}methyl)-1H-1,2,3-triazol-1-yl]acetyl}oxy) cholan-24-oate

$C_{39}H_{56}N_6O_6$
Mwt = 704.91

To a covered and evacuated round-bottomed flask containing a mixture of alkyne ligand **8** (0.1 g, 0.43 mmol, 1 eq.), methyl 3-[(azidoacetyl)oxy] cholan-24-oate (0.21 g, 0.443 mmol, 1.03 eq.), and CuI (0.164 g, 0.861 mmol, 2 eq.), a mixture of dry dichloromethane–DIPEA (as 8:2, 10 mL) was added. The mixture was stirred at room temperature overnight, the dark green-brown solution was treated with EDTA (20 mL, 0.1 M, pH = 8) to remove the copper (the aqueous layer turned azure). Then the solution was diluted with dichloromethane (50 mL) and the product was extracted to the organic layer, dried with $MgSO_4$, then the solvent was evaporated using a rotary evaporator. The product was purified by column chromatography (SiO_2, 0-50% methanol in chloroform) to furnish a white solid (0.3 g). Further purification was done using HPLC (THF:water 40:60) to give the pure white solid product (0.25 g, 0.36 mmol, 82%).

Rf. = 0.7 (1:1 ethyl acetate: hexane)

¹H NMR (400 MHz, CDCl₃) δ 8.45 (s, 1H), 7.90 (d, *J* = 7.8 Hz, 1H), 7.83 (d, *J* = 7.8 Hz, 1H), 7.77 (s, 1H), 7.66 (t, *J* = 7.8 Hz, 1H), 5.44 (s, 2H), 5.16 (s, 2H), 4.89 – 4.78 (m, 1H), 3.69 (s, 3H), 2.41 (s, 3H), 2.37 (s, 3H), 2.24 (s, 1H), 2.02 – 0.97 (m, 29H), 0.93 (d, *J* = 6.9 Hz, 6H), 0.66 (s, 3H).

¹³C NMR (101 MHz, CDCl₃) δ 174.9, 165.8, 157.1, 156.6, 153.4, 153.0, 145.3, 136.4, 124.4, 120.4, 120.0, 77.1, 67.9, 56.4, 56.0, 51.5, 51.1, 42.7, 41.9, 40.4, 40.1, 35.8, 35.4, 34.9, 34.6, 32.1, 31.1, 30.9, 28.2, 27.0, 26.5, 26.3, 24.2, 23.3, 20.8, 18.3, 12.0, 11.2, 10.4.

HRMS (ESI): m/z = calculated for [M+H]⁺: $C_{39}H_{56}N_6O_6H^+$ 705.4348, found: 705.4334.

6.9.10. Methyl3-[(N-{[4-({[(E)-(1-{6-[(1E)-N-hydroxyethanimidoyl] pyridin-2-yl}ethylidene)amino]oxy}methyl)-1H-1,2,3-triazol-1-yl]acetyl} glycyl)oxy] cholan-24-oate

C$_{41}$H$_{59}$N$_7$O$_7$
Mwt = 761.97

18

To a covered and evacuated round-bottom flask containing a mixture of alkyne ligand **8** (0.1 g, 0.43 mmol, 1 eq.), methyl 3-{[N-(azidoacetyl)glycyl]oxy}cholan-24-oate (0.22 g, 0.42 mmol, 1.04 eq.), and CuI (0.17 g, 0.87 mmol, 2 eq.), a mixture of dry DCM–DIPEA (as 8:2, 10 mL) was added. The mixture was stirred at room temperature overnight, the dark green-brown solution was treated with EDTA (20 mL, 0.1 M, pH = 8) to remove the copper (the aqueous layer turned azure in colour). Then the solution diluted with dichloromethane (50 mL) and the product was extracted to the organic layer, dried with MgSO$_4$. The solvent was evaporated using a rotary evaporator, and the product was purified by column chromatography (SiO$_2$, 0-50% ethyl acetate in dichloromethane). The compound was obtained as a white solid (0.3 g, 0.40 mmol, 95%) with some residual DMF according to the slight excess in mass.

R$_f$. = 0.52 (6:4 ethyl acetate: dichloromethane).

^{1}H NMR (400 MHz, CDCl$_3$) δ 7.94 – 7.75 (m, 3H), 7.63 (t, J = 7.8 Hz, 1H), 6.85 (t, J = 5.0 Hz, 1H), 5.40 (s, 2H), 5.15 (s, 2H), 4.81 – 4.69 (m, 1H), 4.05 – 3.95 (m, 2H), 3.76 (d, J = 6.0 Hz, 1H), 3.68 (s, 3H), 2.40 (s, 3H), 2.35 (s, 3H), 2.25 (s, 1H), 2.28 – 0.96 (m, 27H), 0.92 (d, J = 8.0 Hz, 6H), 0.65 (s, 3H).

^{13}C NMR (101 MHz, CDCl$_3$) δ 174.89, 168.66, 165.41, 157.09, 156.91, 153.22, 152.99, 145.54, 136.43, 120.40, 120.21, 76.33, 67.65, 56.42, 55.96, 52.77, 51.53, 42.72, 41.88, 41.68, 40.42, 40.07, 35.76, 35.36, 34.91, 34.55, 32.09, 31.08, 31.00, 28.17, 26.97, 26.51, 26.27, 24.16, 23.96, 23.29, 20.83, 18.27, 12.04, 11.20, 10.45.

HRMS (ESI): m/z = [M+H]$^+$: calculated for C$_{41}$H$_{60}$N$_7$O$_7$$^+$ 762.4554, found: 762.4552.

6.10 Thiol Compounds Preparation:

Thiol compounds were prepared according to the following Scheme:
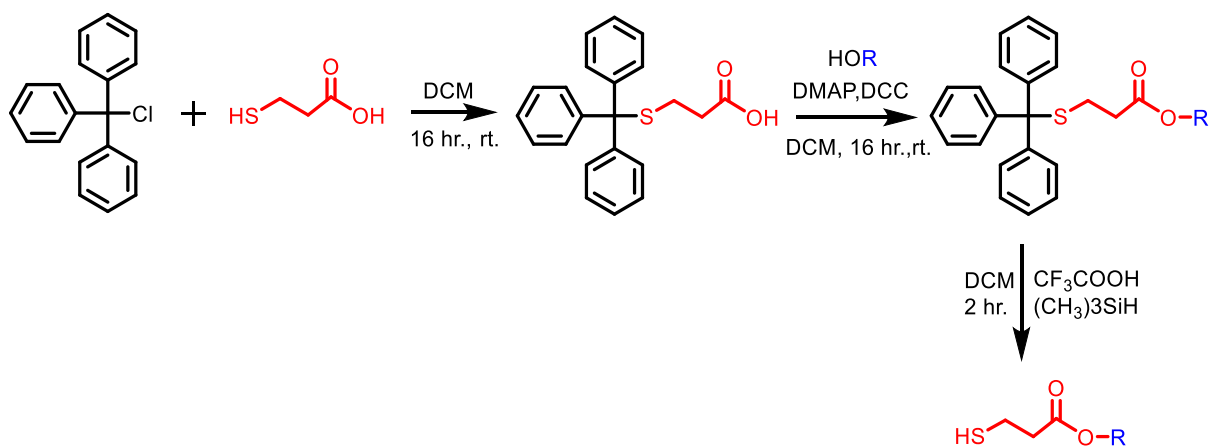
HOR = Cholesterol, lithocholic acid, protected Me-lithocholic acid, isopropyl alcohol

6.10.1 3-[(Triphenylmethyl)sulfanyl]propanoic acid
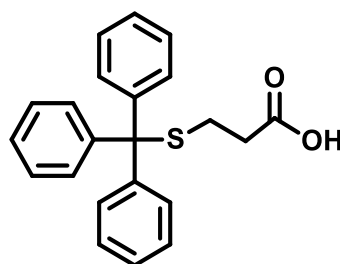
$C_{22}H_{20}O_2S$
Mwt = 348.46

The compound was prepared as described in literature.[198]

3-Mercaptopropanoic acid (3.05 g, 2.5 mL, 28.3 mmol) was dissolved in dichloromethane (30 mL). Triphenyl methyl chloride (7.0 g, 25.11 mmol) previously dissolved in dichloromethane (30 mL), was added dropwise, and the mixture was stirred for 16 hours at room temperature. The precipitate was filtered off and washed with diethyl ether. The pure product was isolated as a white powder (8.5 g, 24.4 mmol, 97%). m.p. 204–206 °C.

^{1}H NMR (400 MHz, DMSO–d_6) δ 12.23 (s, 1H, OH), 7.30-733 (m, 15H, phenyl), 2.29 (t, J = 7.1 Hz, 2H, CH$_2$COO), 2.17 (t, J = 7.0 Hz, 2H, CH$_2$S).

^{13}C NMR (101 MHz, DMSO–d_6) δ 173.2 (COOH), 144.8, 129.6 (phenyl), 128.5 (phenyl), 127.2 (phenyl), 66.6 (Ph$_3$CS), 33.4 (CH$_2$S), 27.2 (CH$_2$CO).

IR (FTIR) cm^{-1}: 3300-2400 (broad, OH), 1702 (C=O).

6.10.2 Propan-2-yl 3-[(triphenylmethyl)sulfanyl]propanoate
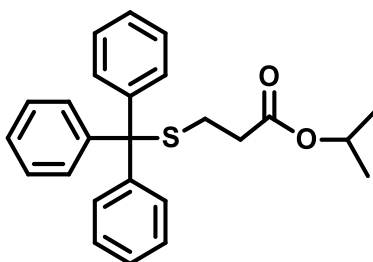
C$_{25}$H$_{26}$O$_2$S
Mwt = 390.54

3-[(Triphenylmethyl)sulfanyl]propanoic acid (1.0 g, 2.87 mmol), N,N-dimethylaminopyridine (0.35 g, 2.87 mmol) and dicyclohexylcarbodiimide (0.7 g, 3.39 mmol) were dissolved in dichloromethane (30 mL). Isopropyl alcohol (0.25 g, 0.32 mL, 4.16 mmol) was added to the mixture and the solution stirred at room temperature for 2 hours. The precipitate of dicyclohexylurea was removed by filtration. After concentration of the filtrate under reduced pressure, the crude product was purified by column chromatography (SiO$_2$, 20% ethyl acetate in hexane) to obtain the product as a white solid (0.9 g, 2.3 mmol, 80%).

^{1}H NMR (400 MHz, CDCl$_3$) δ 7.46 - 7.27 (m, 15H), 5.00 (sept, J = 12.5, 6.3 Hz, 1H), 2.47 (t, J = 7.4 Hz, 2H), 2.25 (t, J = 7.4 Hz, 2H), 1.23 (d, J = 6.3 Hz, 6H).

^{13}C NMR (101 MHz, CDCl$_3$) δ 171.4, 144.7, 129.6, 127.9, 126.7, 68.0, 33.9, 27.0, 21.8.

HRMS: calculated for C$_{25}$H$_{26}$OS (M+Na)$^+$: 413.1546, found: 413.1554.

6.10.3 Isopropyl 3-mercaptopropionate
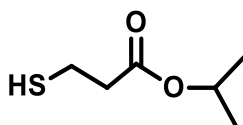
26

$C_6H_{12}O_2S$

Mwt = 148.22

Propan-2-yl 3-[(triphenylmethyl)sulfanyl]propanoate (0.7 g, 1.79 mmol) was treated with triethylsilane (288 μL, 0.21 g, 1.79 mmol) in the presence of trifluoroacetic acid (3 mL) in anhydrous dichloromethane (20 mL) at 0 °C. The mixture was stirred for 2 hours then the solvent was evaporated using a rotary evaporator, and the product was extracted to the ethyl acetate layer after neutralization with sodium bicarbonate (pH = 8). The pure compound was obtained after column chromatography (SiO₂ eluted with 20% diethyl ether in hexane) as a light-yellow oil (0.25 g, 1.69 mmol, 94%).

R$_f$. = 0.62 (2:8 diethyl ether in hexane).

¹H NMR (400 MHz, CDCl₃) δ 5.02 (sept, J = 6.3 Hz, 1H), 2.80 – 2.69 (m, 2H), 2.59 (t, J = 6.7 Hz, 2H), 1.61 (t, J = 8.4 Hz, 1H), 1.23 (d, J = 6.3 Hz, 6H).

¹³C NMR (101 MHz, CDCl₃) δ 171.1(C=O), 68.1 (C-O), 38.8 (CH₂), 21.9 (CH₃), 19.9 (CH₂).

IR (FTIR) cm⁻¹: 2981-2943 (CH), 1725 (C=O), 1372, 1105.

6.10.4 Cholest-5-en-3-yl 3-[(triphenylmethyl)sulfanyl]propanoate

$C_{49}H_{64}O_2S$
Mwt = 717.11
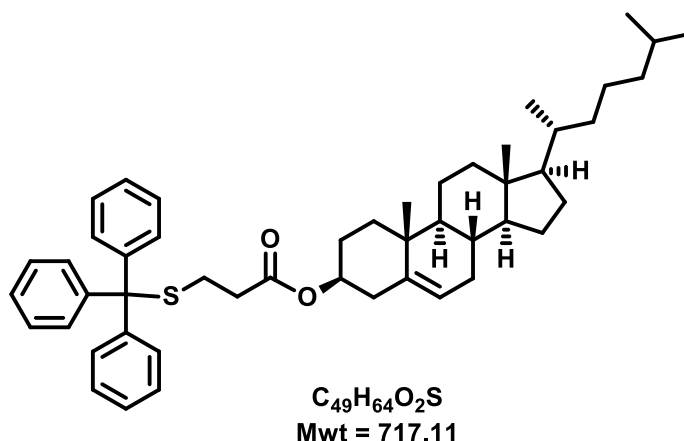
The compound was prepared by following the literature procedure.[198]

3-(Tritylmercapto) propanoic acid (1.0 g, 2.87 mmol), 4-dimethylaminopyridine (0.35 g, 2.87 mmol) and dicyclohexylcarbodiimide (0.7 g, 3.39 mmol) were dissolved in dichloromethane (40 mL). Cholesterol (1.2 g, 3.10 mmol) was added to the mixture and the solution was stirred at room temperature for 2 hours. The precipitate of dicyclohexylurea was removed by filtration. After concentration under reduced pressure, the crude product was purified by column chromatography (SiO$_2$, ethyl acetate: hexane, 2:8). The pure compound was obtained as a white powder (1.8 g, 2.65 mmol, 92%). m.p. 130–134 °C.

¹H NMR (400 MHz, CDCl$_3$) δ 7.50 – 7.19 (m, 15H, phenyl), 5.39 (d, J = 4.5 Hz, 1H, cholesterol), 4.67 – 4.52 (m, 1H, cholesterol), 2.45 (t, J = 7.3 Hz, 2H), 2.35 – 2.19 (m, 4H), 2.08 – 0.85 (m, 39H), 0.70 (s, 3H).

¹³C NMR (101 MHz, CDCl$_3$) δ 171.2 (CO ester), 144.7, 139.6, 129.6, 127.9, 126.7, 122.9, 74.3, 66.8, 56.7, 56.1, 50.0, 42.3, 39.7, 39.5, 38.1, 37.0, 36.6, 36.2, 35.8, 33.9, 31.9, 31.9, 31.0, 28.3, 28.0, 27.7, 27.0, 24.3, 23.9, 22.9, 22.6, 21.0, 19.3, 18.7, 11.9.

IR (FTIR) cm⁻¹: 3060-2870 (CH), 1729 (C=O).

HRMS: calculated for C$_{49}$H$_{64}$O$_2$SNa⁺ (M+Na)⁺ 739.4525; found: 739.4531.

6.10.5. Cholest-5-en-3-yl 3-sulfanylpropanoate

$C_{30}H_{50}O_2S$

Mwt = 474.79

24
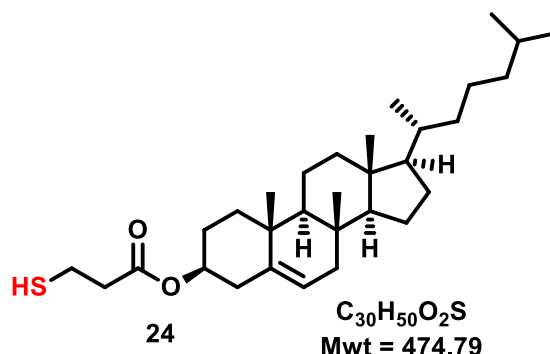
The compound was prepared as described in the literature.[198]

Cholesteryl 3-(tritylmercapto) propanoate (1.0 g, 1.39 mmol) and triethylsilane (223 µL, 0.16 g, 1.39 mmol) were dissolved in dichloromethane (20 mL) at 0 °C. Trifluoroacetic acid (3 mL) in dichloromethane (30 mL) was added dropwise to the cold mixture. After stirring for 1 hour, the mixture was concentrated under a vacuum. The crude product was dissolved in diethyl ether (50 mL) and washed with $NaHCO_3$ (to neutralise the solution). After drying, concentration under a vacuum, and column chromatography (SiO_2 eluted with 0-50% diethyl ether in hexane) the pure compound was obtained as a white solid (0.6 g, 1.264 mmol, 91%).

R$_f$. = 0.74 (2:8, ethyl acetate: hexane). m.p. 69–70 °C.

^{1}H NMR (400 MHz, CDCl$_3$) δ 5.38 (d, J = 4.2 Hz, 1H, cholesterol), 4.71 – 4.59 (m, 1H, cholesterol), 2.77 (dd, J = 15.0, 7.0 Hz, 2H), 2.62 (t, J = 6.7 Hz, 2H), 2.32 (d, J = 7.8 Hz, 2H), 2.00 (dt, J = 26.9, 10.4 Hz, 2H), 1.85 (t, J = 9.6 Hz, 2H), 1.67 – 0.84 (m, 34H), 1.54 (t, 1H, SH) 0.67 (s, 3H).

^{13}C NMR (101 MHz, CDCl$_3$) δ 171.0 (CO ester), 139.5, 129.5–126.4, 122.8, 74.4, 56.7, 56.1, 50.0, 42.3, 39.7, 39.5, 38.8, 38.1, 37.0, 36.6, 36.2, 35.8, 31.9, 31.9, 28.3, 28.0, 27.8, 24.3, 23.8, 22.9, 22.6, 21.0, 19.9, 19.3, 18.7, 11.9.

HRMS: calculated for $C_{30}H_{50}O_2SNa^+$ (M+Na)$^+$: 497.3424, found: 497.3428.

IR (FTIR) cm^{-1}: 2940-2851 (CH), 1729 (C=O).

6.10.6. Methyl3-({3-[(triphenylmethyl)sulfanyl]propanoyl}oxy)cholan-24-oate
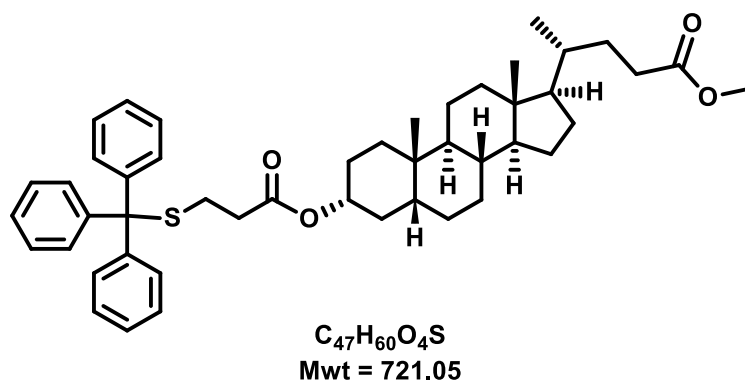
$C_{47}H_{60}O_4S$
Mwt = 721.05

3-(Tritylmercapto) propanoic acid (1.0 g, 2.87 mmol), N,N-dimethylaminopyridine (0.35 g, 2.87 mmol) and dicyclohexylcarbodiimide (0.70 g, 3.39 mmol) were dissolved in dichloromethane (40 mL). Methyl 3-hydroxycholan-24-oate (1.1g, 2.82 mmol) was added to the mixture and the solution was stirred at room temperature for 2 hours. The precipitate of dicyclohexylurea was removed by filtration. After concentration under reduced pressure, the crude product was purified by column chromatography (SiO$_2$, ethyl acetate:hexane, 2:8). The pure compound was obtained as a white powder (1.85 g, 2. 75 mmol, 91%).

^{1}H NMR (400 MHz, CDCl$_3$) δ 7.47 – 7.21 (m, 15H), 4.71 (s, 1H), 3.69 (s, 3H), 2.49 – 2.32 (m, 3H), 2.26 (dt, J = 7.5, 3.4 Hz, 3H), 2.03 – 0.97 (m, 26H), 0.94 (m, 6H), 0.67 (s, 3H).

^{13}C NMR (101 MHz, CDCl$_3$) δ 174.9, 171.4, 144.7, 129.6, 127.9, 126.7, 74.7, 66.8, 56.5, 56.0, 51.5, 42.8, 41.9, 40.4, 40.1, 35.7, 35.4, 35.0, 34.6, 33.9, 32.2, 31.1, 30.9, 28.2, 26.9, 26.6, 26.3, 24.2, 23.3, 22.7, 20.9, 18.3, 14.2, 12.1.

HRMS: calculated for $C_{47}H_{60}O_4SNa^+$ (M+Na)$^+$: 743.4105, found: 743.4112.

IR (FTIR) cm^{-1}: 2931-2868 (CH), 1732 (C=O).

6.10.7. Methyl 3-[(3-sulfanylpropanoyl)oxy]cholan-24-oate
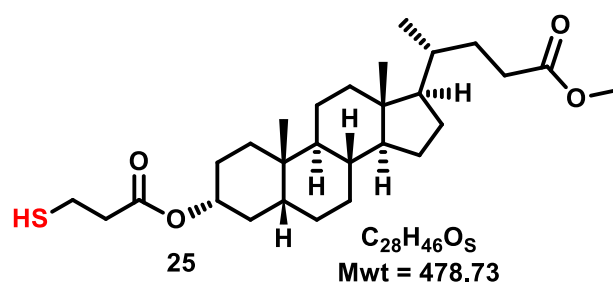
Methyl 3-({3-[(triphenylmethyl)sulfanyl]propanoyl}oxy)cholan-24-oate (1.0 g, 1.39 mmol) and triethylsilane (0.8 g, 6.98 mmol) were dissolved in dichloromethane (20 mL) at 0 °C. Trifluoroacetic acid (3 mL) dissolved in dichloromethane (30 mL) was added dropwise to the cold mixture. After stirring for 1 hour, the mixture was concentrated under a vacuum. The crude product was dissolved in diethyl ether and washed with a saturated solution of $NaHCO_3$. After drying and concentration under a vacuum, the crude product was purified using column chromatography (SiO_2, 0-50% diethyl ether in hexane). The pure compound was obtained as a white solid (0.55 g, 1.15 mmol., 83%).

R_f. = 0.43 (2:8, diethyl ether:hexane).

^{1}H NMR (400 MHz, $CDCl_3$) δ 4.83 – 4.73 (m, 1H), 3.68 (s, 3H), 2.83 – 2.74 (m, 2H), 2.62 (d, J = 7.4 Hz, 2H), 2.36 (td, J = 10.2, 5.0 Hz, 1H), 2.27 – 2.18 (m, 1H), 2.01 – 1.00 (m, 27H), 0.96 – 0.90 (m, 6H), 0.66 (s, 3H).

^{13}C NMR (101 MHz, $CDCl_3$) δ 174.8, 171.1, 74.8, 56.5, 56.0, 51.5, 42.7, 41.9, 40.4, 40.1, 38.9, 35.8, 35.4, 35.0, 34.8, 34.6, 32.3, 31.1, 31.0, 28.2, 27.0, 26.7, 26.3, 25.3, 24.2, 23.3, 22.7, 20.9, 19.9, 18.3, 14.1, 12.0.

HRMS: calculated for $C_{28}H_{46}O_4SNa^+$ $(M+Na)^+$: 501.3015, found : 501.3018.

IR (FTIR) cm^{-1}: 3328 (CH), 2931-2861(SH), 1732 (C=O).

6.11 Preparation of thiol compound with two polar head groups

The reaction scheme shows:

Starting material (cholic acid derivative with OH and carboxylic acid) reacts with:
- ^tBuOH
- trifluoroacetic anhydride
- THF, rt

to give the tert-butyl ester product:
$C_{28}H_{48}O_3$
Mwt = 432.69
Yield = 87%

+ (trityl protected thiol propanoic acid)

reacting with:
- DMAP, DCC
- dry DCM, 16 hrs.

to give:
$C_{50}H_{66}O_4S$
Mwt = 763.13
Yield = 85%

then via:
(i) dry DCM, TFA
(ii) dry DCM, TFA, $(C_2H_5)_3SiH$

to give final thiol product:
$C_{27}H_{44}O_4S$
Mwt = 464.71
Yield = 35%

6.11.1. Tert-butyl 3-hydroxycholan-24-oate

$C_{28}H_{48}O_3$
Mwt = 432.69

The product was prepared according to the published literature.[199] To a solution of lithocholic acid (1.0 g, 2.66 mmol, 1.0 eq.) in THF (24 mL) at 0 °C, trifluoracetic anhydride (3.0 mL, 21 mmol, 7.8 eq.) was added dropwise. After stirring for 1.5 hour at 0 °C, the mixture was treated with tert-butanol (7.0 mL, 73 mmol, 28 eq.) and left to stir at 0 °C for 12 hours. The reaction mixture was neutralised with saturated aq. NH_4OH (5 mL) and stirred at 23 °C for 5 hours. Then the mixture diluted with ether (20 mL) and washed with aq. NaOH (40 mL, 1 M), water (40 mL), and brine. The organic layer was dried with $MgSO_4$, filtered, and then was concentrated under reduced pressure. The product was recrystallised from acetonitrile to obtain a white precipitate, which was filtered and dried to yield a white solid (1.0 g, 2.31 mmol, 87%).

¹H NMR (400 MHz, CDCl₃) δ 3.69 – 3.58 (m, 1H), 2.32 – 2.22 (m, 1H), 2.19 – 2.08 (m, 1H), 1.96 (dt, J = 12.6, 3.0 Hz, 1H), 1.89 – 1.72 (m, 5H), 1.67 – 1.65 (m, 1H), 1.58 – 1.50 (m, 2H), 1.44 (s, 9H), 1.42 – 1.36 (m, 6H), 1.36 – 1.19 (m, 6H), 1.16 – 1.08 (m, 5H), 1.00 – 0.94 (m, 1H), 0.92 (s, 3H), 0.90 (d, J = 6.6 Hz, 3H), 0.66 (s, 3H).

¹³C NMR (101 MHz, CDCl₃) δ 173.8, 79.9, 71.9, 56.5, 56.0, 42.7, 42.1, 40.4, 40.2, 36.5, 35.9, 35.4, 35.3, 34.6, 32.6, 31.1, 30.6, 28.2, 28.1, 27.2, 26.4, 24.2, 23.4, 20.8, 18.3, 12.0.

6.11.2 Tert-butyl 3-({3-[(triphenylmethyl)sulfanyl]propanoyl}oxy)cholan-24-oate

$C_{50}H_{66}O_4S$
Mwt = 763.13
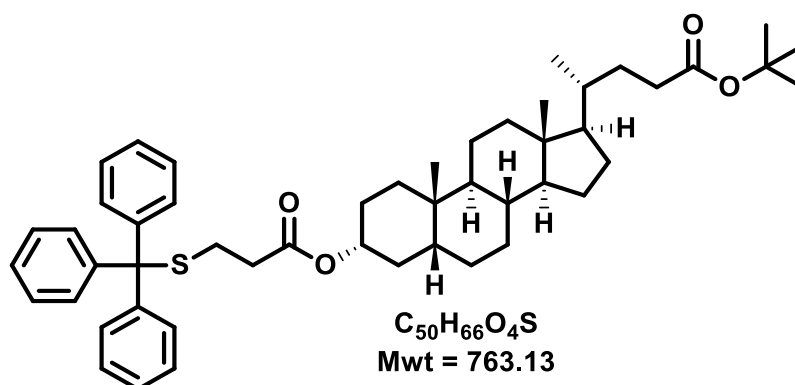
Tert-butyl 3-hydroxycholan-24-oate (0.60 g, 1.39 mmol, 1 eq.) was reacted with 3-[(triphenylmethyl)sulfanyl]propanoic acid (0.53 g, 1.52 mmol, 1.1 eq.) in the presence of DMAP (0.043 g, 0.35 mmol, 0.25 eq.) and DCC (0.32 g, 1.53 mmol, 1.1 eq.) in dry dichloromethane (40 mL). The reaction mixture was stirred for 16 hours, then the resulting cloudy solution was filtered to remove the DCU (dicyclohexylurea). The crude product was purified by flash column chromatography (SiO$_2$, ethyl acetate:hexane, 20:80) to afford white plate crystals (0.9 g, 1.18 mmol, 85%).

^{1}H NMR (400 MHz, CDCl$_3$) δ 7.48 – 7.21 (m, 15H), 4.78 – 4.66 (m, 1H), 2.46 (t, J = 7.3 Hz, 2H), 2.33 – 2.22 (m, 3H), 2.16 (ddd, J = 15.4, 8.1, 4.0 Hz, 1H), 2.08 – 1.49 (m, 10H), 1.48 (s, 10H), 1.45 – 0.99 (m, 16H), 0.94 (d, J = 4.9 Hz, 6H), 0.68 (s, 3H).

^{13}C NMR (101 MHz, CDCl$_3$) δ 173.7 (C=O), 171.3 (C=O), 144.7, 129.6 (phenyl), 127.9 (phenyl), 126.7 (phenyl), 79.9, 74.7, 66.8, 56.5, 56.1, 42.8, 41.9, 40.5, 40.2, 35.8, 35.3, 35.0, 34.6, 33.9, 32.6, 32.2, 31.1, 28.2, 28.2 (tert), 27.0, 26.6, 26.4, 24.2, 23.4, 20.9, 18.3, 12.1.

HRMS: calculated for $C_{50}H_{66}O_4SNa^+$ (M+Na)$^+$: 785.4580, found: 785.4555.

6.11.3. 3-[(3-Sulfanylpropanoyl)oxy]cholan-24-oic acid

27

$C_{27}H_{44}O_4S$
Mwt = 464.71
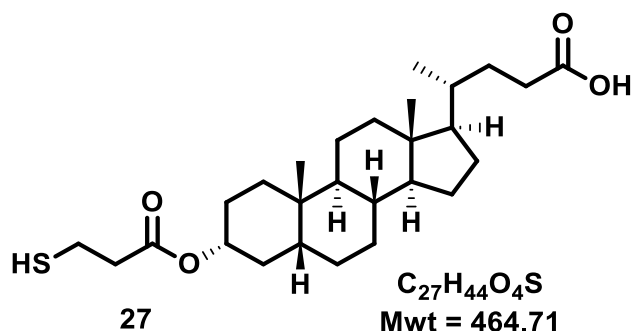
In an oven-dried round bottom flask, tert-butyl 3-({3-[(triphenylmethyl)sulfanyl]propanoyl}oxy)cholan-24-oate (0.28 g, 0.37 mmol.) was placed. The round bottom flask was covered and evacuated and anhydrous dichloromethane (10 mL) was added. While the round bottom flask was in an ice bath, TFA (0.2 mL) was added and the reaction mixture was stirred for 2 hours at 0 °C before triethylsilane (80 µL) was added. After 2 minutes, the reaction mixture colour turned from yellow to colourless. The reaction mixture was then stirred for 1.5 hours. The crude product was washed with water (25 mL x 2), brine (25 mL), then the organic layer was dried with MgSO4 and the solvent was evaporated. The title compound was obtained after column chromatography (SiO2, 0-50% ethyl acetate in hexane) as a white solid (0.06 g, 0.13 mmol. 35%).

1H NMR (400 MHz, CDCl3) δ 4.78 (dd, J = 10.4, 5.6 Hz, 1H), 2.79 (dd, J = 14.8, 7.1 Hz, 2H), 2.64 (t, J = 6.8 Hz, 2H), 2.39 (dd, J = 10.1, 4.9 Hz, 1H), 2.34 – 2.21 (m, 1H), 1.98 (d, J = 11.4 Hz, 1H), 1.93 – 1.68 (m, 6H), 1.63 (dd, J = 15.1, 6.7 Hz, 1H), 1.60 – 0.98 (m, 21H), 0.94 (d, J = 6.0 Hz, 6H), 0.66 (s, 3H).

13C NMR (101 MHz, CDCl3) δ 171.3, 75.0, 56.6, 56.1, 42.9, 42.0, 40.6, 40.3, 39.0, 35.9, 35.4, 35.1, 34.7, 32.4, 31.2, 30.9, 29.8, 28.3, 27.1, 26.8, 26.5, 24.3, 23.5, 21.0, 20.0, 18.4, 12.2.

HRMS: calculated for $C_{27}H_{44}O_4SNa^+$ (M+Na)$^+$: 487.2853, found: 487.2874.

IR (FTIR) cm^{-1}: 2925, 2868 (CH), 2569 (SH), 1700 (C=O).

Chapter 7 -   Appendix

7.1 Calibration Curve for *p*-Nitroaniline

To know the concentration of the *p*-nitroaniline that is released with time, a calibration curve was established.
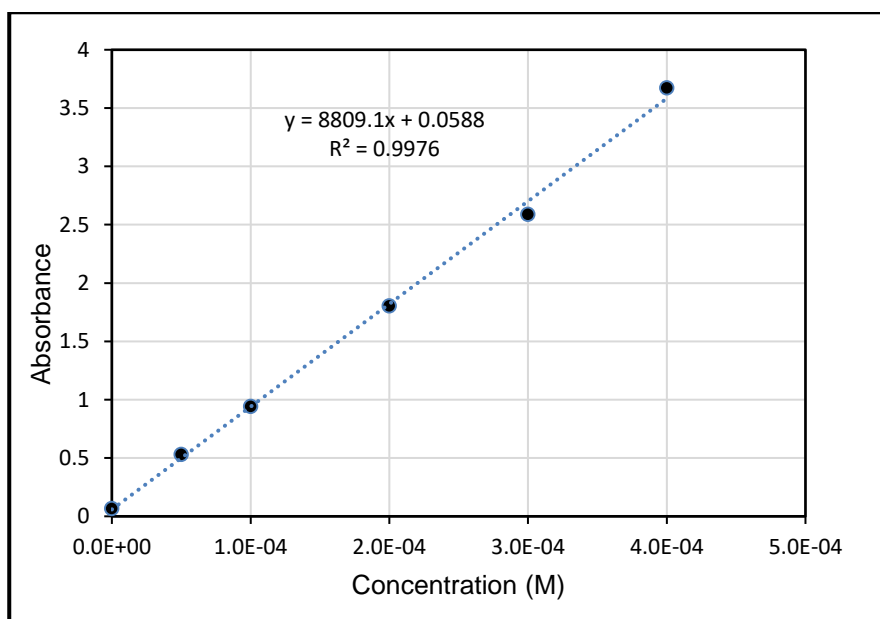
The absorbance at 410 nm versus different concentrations of *p*-nitroaniline in a buffer solution. The measurements were completed at 25 °C.

So the ε (efficient coefficient) to *p*-nitroaniline = 8809 L mol^{-1} cm^{-1}

Abs= $\varepsilon \times$ cell length $\times$ [product]

Abs/ (slope) = [product]

7.2 Calibration Curve for *p*-Nitrophenol:
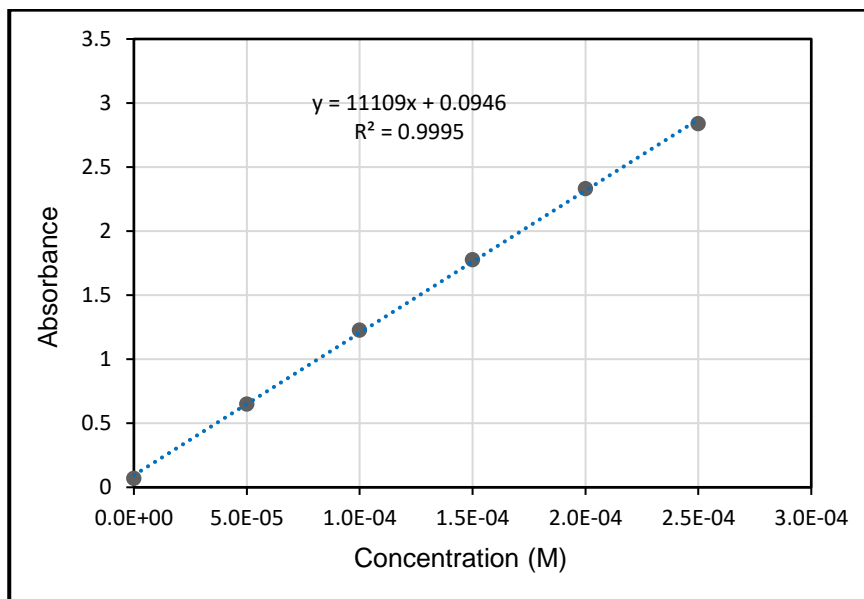
The absorbance at 400 nm versus different concentrations of *p*-nitrophenol in HEPES (100 mM, pH 7), the measurements were completed at 25 °C.

7.3 Calibration Curve for 8-Hydroxypyrene-1,3,6-trisulfonic acid trisodium salt:
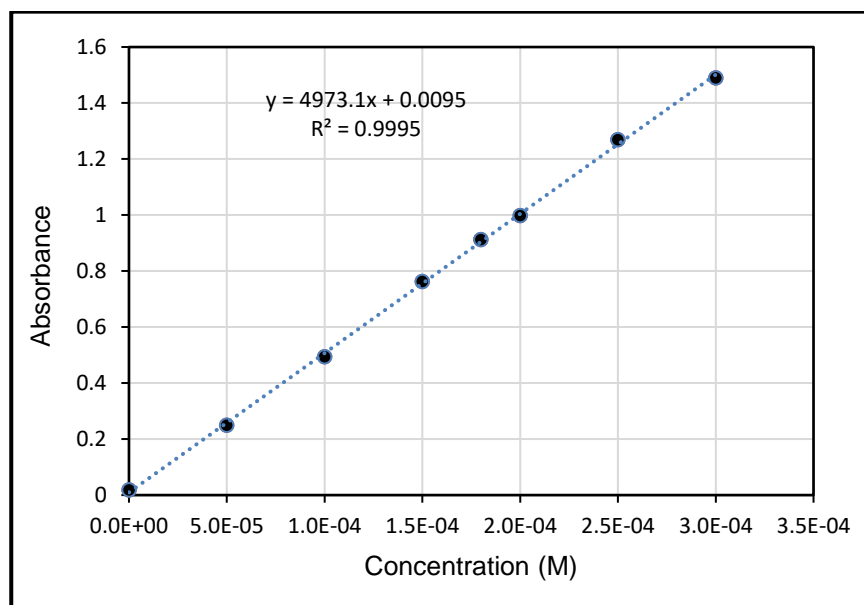
The absorbance at 450 nm versus different concentrations of 8-hydroxypyrene-1,3,6-trisulfonic acid trisodium salt in HEPES (100 mM, pH 7), the measurements were completed at 25 °C.

7.4 Equations to Fit the Data

The first-order equation was used to fit the data in Chapter 2: [200]

$$A = A_0 e^{-kt}$$

A is the absorbance after time, k is the observed rate constant, **A$_0$** is the absorbance and **t** is time

The equation was used to fit the data in Chapter 3: [200]

$$P = \frac{k_2 k_3 e_0 t}{k_2 + k_3} + \frac{k_2{}^2 e_0 \{1 - \exp[-(k_2 + k_3)\,t]\}}{(k_2 + k_3)^2}$$

k_2, k_3 the hydrolysis rate, **t** = time, **e$_0$** = initial catalyst concentration

Derivation of Equation 2-1

$$2ML \underset{\text{complex}}{\overset{K}{\rightleftharpoons}} (ML)_2 \quad \text{complex dimer} \qquad K = \text{equilibrium constant}$$

$$K = \frac{[(ML)_2]}{[ML]^2}$$

The total [ML] or $[ML]_T$ is the sum of all ML

$$[ML]_T = 2\,[(ML)]_2 + [ML]$$

Rearranging to give $[(ML)_2]$

$$[(ML)_2] = \frac{[ML]_T - [ML]}{2}$$

Substituting into above equation

$$K = \frac{[ML]_T - [ML]}{2\,[ML]^2}$$

Rearrangment this equation

$$2K\,[ML]^2 = [ML]_T - [ML]$$

$$2K\,[ML]^2 + [ML] - [ML]_T = 0$$

This is a quadratic and can be solved as

$$[ML] = \frac{-1 \pm \sqrt{1 + 8K[ML]_T}}{4K}$$

7.5   Some Selected DLS Reports

Brookhaven Instruments Corp.
ZetaPALS Particle Sizing Software Ver. 3.80

Date: Mar 2, 2019
Time: 16:27:18
Batch: 0

Sample ID   **vesicle of lipid only(mM) (Combined)**
Operator ID   **Layla**
Notes

Measurement Parameters:

Temperature	= 25.0 deg. C	Runs Completed	= 5
Liquid	= Water	Run Duration	= 00:02:00
Viscosity	= 0.890 cP	Total Elapsed Time	= 00:10:00
Ref.Index Fluid	= 1.330	Average Count Rate	= 1.8 Mcps
Angle	= 90.00	Ref.Index Real	= 1.590
Wavelength	= 660.0 nm	Ref.Index Imag	= 0.000
Baseline	= Auto (Slope Analysis)	Dust Filter	= Off

vesicle of lipid only(mM) (Combined)

Effective Diameter: 181.4 nm
Polydispersity: 0.223
Baseline Index: 9.7
Elapsed Time: 00:10:00
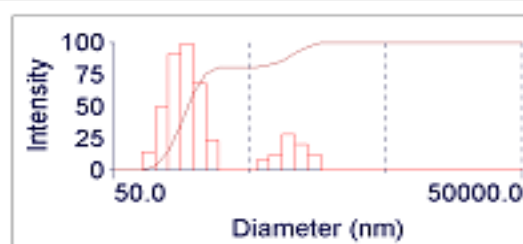
Multimodal Size Distribution

Run	Eff. Diam. (nm)	Half Width (nm)	Polydispersity	Baseline Index
1	179.6	81.0	0.203	9.5
2	175.4	83.0	0.224	9.5
3	180.5	83.9	0.216	8.9
4	185.7	90.0	0.235	8.9
5	184.3	86.5	0.220	9.4
Mean	181.1	84.9	0.220	9.2
Std. Error	1.8	1.6	0.005	0.1
Combined	181.4	85.6	0.223	9.7

The size distribution of a DOPC/DOPE pure vesicle sample (1. 6 mM) , data for Table 4-1.

217

Sample ID   **vesicle of lipid only(mM) (Combined)**
Operator ID   **Layla**
Notes

Elapsed Time	00:10:00
Mean Diam.	326.8 nm
Rel. Var.	1.188
Skew	1.893
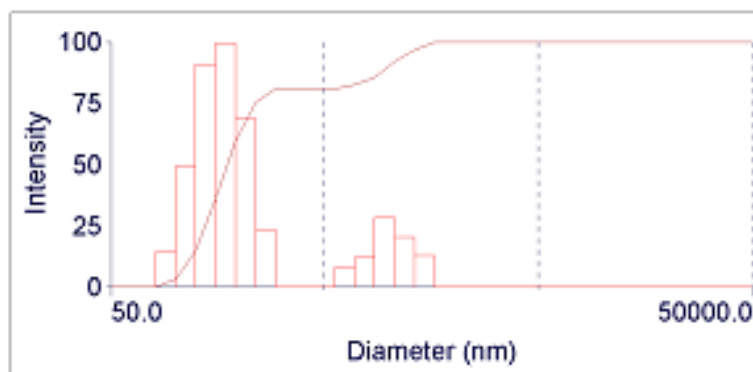
Multimodal Size Distribution

d(nm)	G(d)	C(d)	d(nm)	G(d)	C(d)	d(nm)	G(d)	C(d)
10.5	0	0	111.0	50	15	1172.7	20	97
13.0	0	0	137.5	91	36	1453.0	13	100
16.1	0	0	170.4	100	60	1800.3	0	100
20.0	0	0	211.1	69	76	2230.6	0	100
24.8	0	0	261.6	23	81	2763.8	0	100
30.7	0	0	324.1	0	81	3424.5	0	100
38.0	0	0	401.6	0	81	4243.0	0	100
47.1	0	0	497.6	0	81	5257.2	0	100
58.3	0	0	616.5	8	83	6513.8	0	100
72.3	0	0	763.9	12	86	8070.8	0	100
89.6	14	3	946.5	28	92	10000.0	0	100

The size distribution of a DOPC/DOPE pure vesicle sample (1. 6 mM), data for Table 4-1.

Brookhaven Instruments Corp.
ZetaPALS Particle Sizing Software Ver. 3.80

Date: Mar 2, 2019
Time: 16:27:18
Batch: 0

Sample ID   **vesicle of lipid only(mM) (Combined)**
Operator ID **Layla**
Notes

Elapsed Time	00:10:00
Eff. Diam.	181.4 nm
Mean Diam.	200.6 nm
Polydispersity	0.223
GSD	1.566

Lognormal Size Distribution
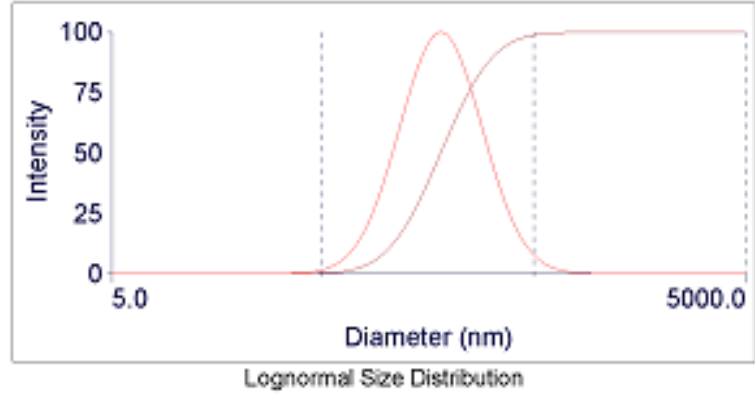
d(nm)	G(d)	C(d)	d(nm)	G(d)	C(d)	d(nm)	G(d)	C(d)
86.7	26	5	161.9	97	40	245.4	80	75
102.1	44	10	171.4	99	45	264.6	70	80
114.0	58	15	181.4	100	50	288.6	58	85
124.3	70	20	191.9	99	55	322.3	44	90
134.1	80	25	203.2	97	60	379.3	26	95
143.4	87	30	215.5	93	65			
152.6	93	35	229.4	87	70			

Brookhaven Instruments Corp.
ZetaPALS Particle Sizing Software Ver. 3.80

Date: Mar 2, 2019
Time: 16:27:18
Batch: 0

Sample ID   **vesicle of lipid only(mM) (Combined)**
Operator ID   **Layla**
Notes

Lognormal Distribution

Multimodal Size Distribution

Correlation Function

The size distribution of a DOPC/DOPE pure vesicle sample (1. 6 mM) , data for Table 4-1.

Date: Mar 2, 2019
Time: 18:09:59
Batch: 0

Sample ID   **2 mMvesicle +0.2 mM chol-SH ou (Combined)**
Operator ID   **Layla**
Notes

Measurement Parameters:

Temperature	= 25.0 deg. C	Runs Completed	= 5
Liquid	= Water	Run Duration	= 00:02:00
Viscosity	= 0.890 cP	Total Elapsed Time	= 00:10:00
Ref.Index Fluid	= 1.330	Average Count Rate	= 2.0 Mcps
Angle	= 90.00	Ref.Index Real	= 1.590
Wavelength	= 660.0 nm	Ref.Index Imag	= 0.000
Baseline	= Auto (Slope Analysis)	Dust Filter	= Off

2 mMvesicle +0.2 mM chol-SH ou (Combined)

Effective Diameter: **266.4 nm**
Polydispersity: **0.245**
Baseline Index: **9.8**
Elapsed Time: **00:10:00**

Multimodal Size Distribution

Run	Eff. Diam. (nm)	Half Width (nm)	Polydispersity	Baseline Index
1	236.8	115.0	0.236	9.8
2	253.3	126.3	0.249	8.3
3	255.4	138.8	0.295	8.7
4	303.0	149.8	0.245	9.5
5	281.4	148.3	0.278	8.2
Mean	266.0	135.6	0.260	8.9
Std. Error	11.7	6.6	0.011	0.3
Combined	266.4	131.7	0.245	9.8

Data for Table 4-1, for compound **24**, before the second purification for the vesicles using GPC column

Sample ID   **2 mMvesicle +0.2 mM chol-SH ou (Combined)**

Operator ID   **Layla**

Notes

Elapsed Time	00:10:00
Mean Diam.	517.1 nm
Rel. Var.	0.975
Skew	0.969

Multimodal Size Distribution
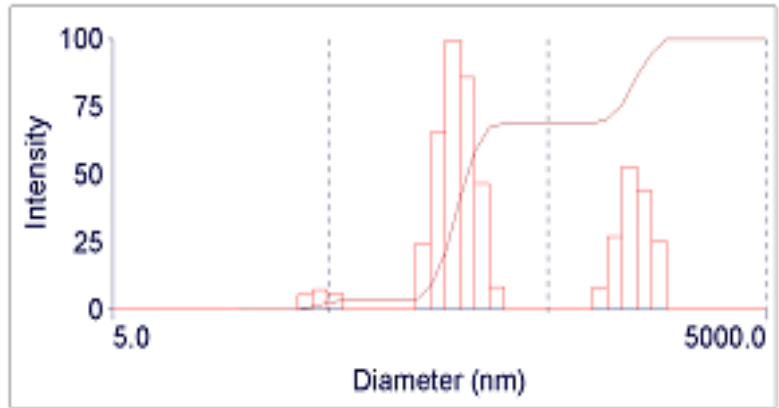
d(nm)	G(d)	C(d)	d(nm)	G(d)	C(d)	d(nm)	G(d)	C(d)
20.5	0	0	113.8	0	4	630.7	0	69
24.0	0	0	133.0	25	8	737.0	0	69
28.0	0	0	155.4	66	21	861.1	8	71
32.8	0	0	181.5	100	41	1006.2	27	76
38.3	5	1	212.1	86	58	1175.6	53	86
44.7	7	2	247.8	47	67	1373.7	44	95
52.2	6	4	289.6	8	69	1605.1	25	100
61.0	0	4	338.4	0	69	1875.5	0	100
71.3	0	4	395.4	0	69	2191.4	0	100
83.3	0	4	462.0	0	69	2560.5	0	100
97.4	0	4	539.8	0	69	2991.9	0	100

Brookhaven Instruments Corp.
ZetaPALS Particle Sizing Software Ver. 3.80

Date: Mar 2, 2019
Time: 18:09:59
Batch: 0

Sample ID   **2 mMvesicle +0.2 mM chol-SH ou (Combined)**
Operator ID   **Layla**
Notes

Elapsed Time	00:10:00
Eff. Diam.	266.4 nm
Mean Diam.	297.1 nm
Polydispersity	0.245
GSD	1.596

Lognormal Size Distribution
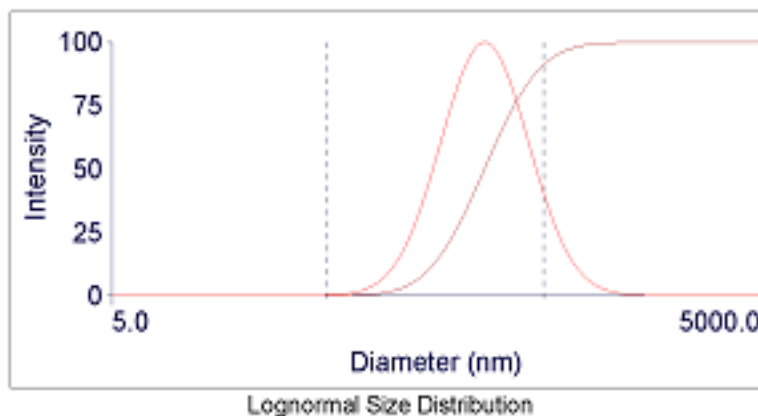
d(nm)	G(d)	C(d)	d(nm)	G(d)	C(d)	d(nm)	G(d)	C(d)
123.4	26	5	236.6	97	40	365.1	80	75
146.2	44	10	251.1	99	45	394.9	70	80
164.1	58	15	266.4	100	50	432.4	58	85
179.7	70	20	282.5	99	55	485.1	44	90
194.3	80	25	299.8	97	60	574.9	26	95
208.5	87	30	318.9	93	65			
222.5	93	35	340.3	87	70			

Data for Table 4-1, for compound **24**, before the second purification for the vesicles using GPC column.

Lognormal Distribution

Multimodal Size Distribution

Correlation Function

Data for Table 4-1, for vesicles incorporated with compound **24** before the second purification using GPC column

Brookhaven Instruments Corp.
ZetaPALS Particle Sizing Software Ver. 3.80

Date: Mar 2, 2019
Time: 19:03:20
Batch: 0

Sample ID **2 mMvesicle+ 0.2 mM Me-lithoSH (Combined)**
Operator ID **Layla**
Notes

Measurement Parameters:

Temperature	= 25.0 deg. C	Runs Completed	= 5
Liquid	= Water	Run Duration	= 00:02:00
Viscosity	= 0.890 cP	Total Elapsed Time	= 00:10:00
Ref.Index Fluid	= 1.330	Average Count Rate	= 1.6 Mcps
Angle	= 90.00	Ref.Index Real	= 1.590
Wavelength	= 660.0 nm	Ref.Index Imag	= 0.000
Baseline	= Auto (Slope Analysis)	Dust Filter	= Off

2 mMvesicle+ 0.2 mM Me-lithoSH (Combined)

Effective Diameter: 233.9 nm

Polydispersity: 0.271

Baseline Index: 9.3

Elapsed Time: 00:10:00
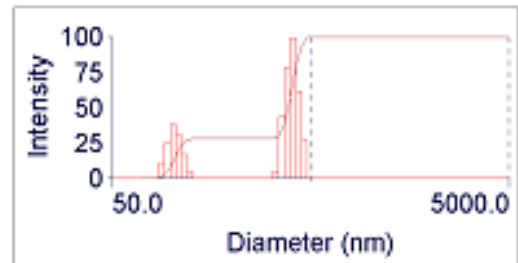
Multimodal Size Distribution

Run	Eff. Diam. (nm)	Half Width (nm)	Polydispersity	Baseline Index
1	235.0	121.7	0.268	8.1
2	231.3	122.6	0.281	10.0
3	234.7	120.7	0.264	8.8
4	231.3	116.9	0.255	8.4
5	238.2	127.3	0.286	8.1
Mean	234.1	121.8	0.271	8.7
Std. Error	1.3	1.7	0.006	0.3
Combined	233.9	121.8	0.271	9.3

225

Date: Mar 2, 2019
Time: 19:03:20
Batch: 0

Sample ID   **2 mMvesicle+ 0.2 mM Me-lithoSH (Combined)**
Operator ID   **Layla**
Notes

Elapsed Time   00:10:00
Mean Diam.   317.0 nm
Rel. Var.   0.189
Skew   -0.828
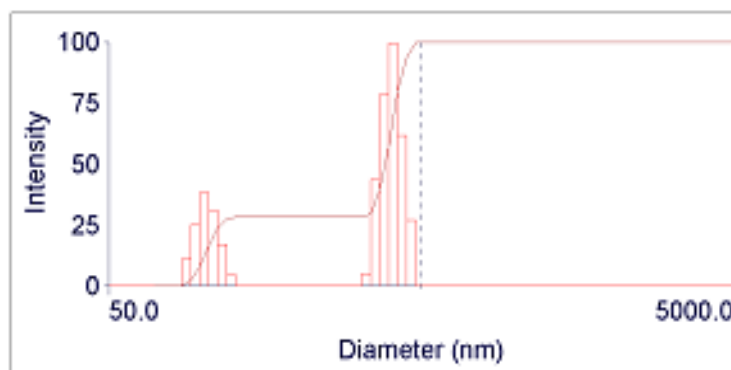
Multimodal Size Distribution

d(nm)	G(d)	C(d)	d(nm)	G(d)	C(d)	d(nm)	G(d)	C(d)
72.5	0	0	150.4	0	29	311.9	0	29
77.5	0	0	160.7	0	29	333.3	5	30
82.8	0	0	171.8	0	29	356.2	44	40
88.5	11	2	183.5	0	29	380.6	79	57
94.6	25	8	196.1	0	29	406.7	100	80
101.1	38	17	209.6	0	29	434.6	62	94
108.0	31	24	223.9	0	29	464.3	27	100
115.4	17	28	239.3	0	29	496.2	0	100
123.3	4	29	255.7	0	29	530.2	0	100
131.7	0	29	273.2	0	29	566.5	0	100
140.8	0	29	291.9	0	29	605.4	0	100

Data for Table 4-1, for vesicles incorporated with compound **25** before the second purification using GPC column

Sample ID   **2 mMvesicle+ 0.2 mM Me-lithoSH (Combined)**
Operator ID   **Layla**
Notes

Elapsed Time	00:10:00
Eff. Diam.	233.9 nm
Mean Diam.	263.7 nm
Polydispersity	0.271
GSD	1.632

Lognormal Size Distribution
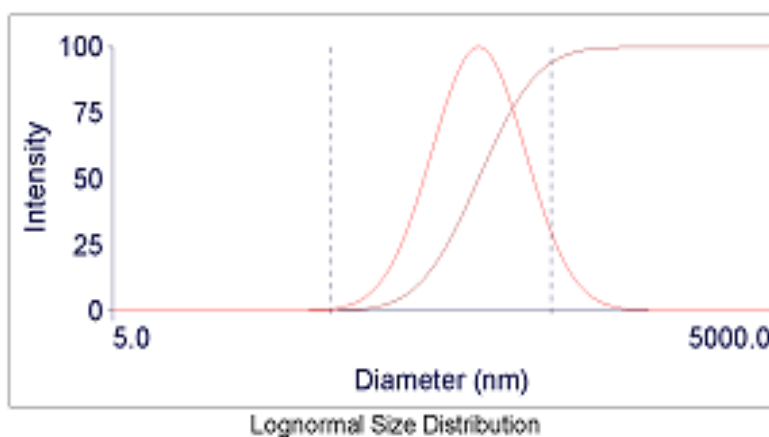
d(nm)	G(d)	C(d)	d(nm)	G(d)	C(d)	d(nm)	G(d)	C(d)
104.5	26	5	206.6	97	40	325.4	80	75
124.8	44	10	219.9	99	45	353.3	70	80
140.8	58	15	233.9	100	50	388.5	58	85
154.8	70	20	248.8	99	55	438.2	44	90
168.1	80	25	264.7	97	60	523.5	26	95
180.9	87	30	282.4	93	65			
193.7	93	35	302.3	87	70			

Data for Table 4-1, for vesicles incorporated with compound **25** before the second purification using GPC column

Lognormal Distribution

Multimodal Size Distribution

Correlation Function

Data for Table 4-1, for compound **25**, after purification the vesicles using GPC column.

Sample ID   **1.7mMvesiclesafter puri LithSH (Run 5)**
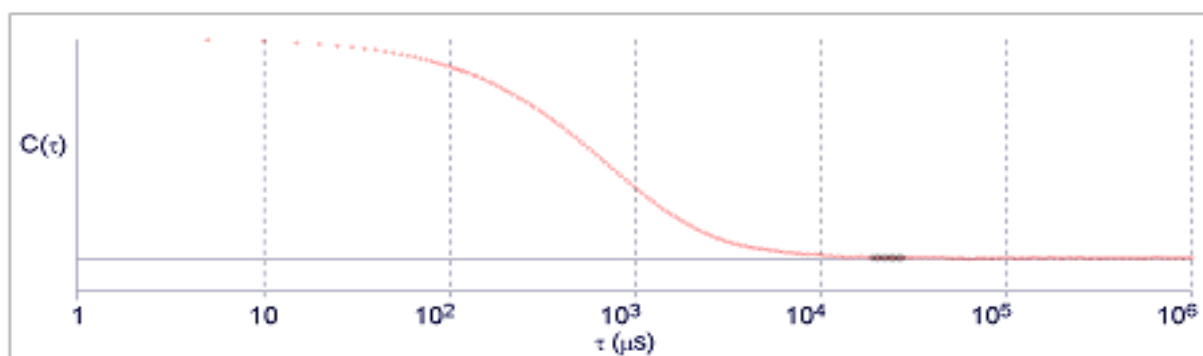Operator ID   Layla
Notes

Date: Mar 2, 2019
Time: 19:39:15
Batch: 0

Measurement Parameters:

Temperature	= 25.0 deg. C	Runs Completed	= 5
Liquid	= Water	Run Duration	= 00:02:00
Viscosity	= 0.890 cP	Total Elapsed Time	= 00:10:00
Ref.Index Fluid	= 1.330	Average Count Rate	= 2.0 Mcps
Angle	= 90.00	Ref.Index Real	= 1.590
Wavelength	= 660.0 nm	Ref.Index Imag	= 0.000
Baseline	= Auto (Slope Analysis)	Dust Filter	= Off

1.7mMvesiclesafter puri LithSH (Run 5)

Effective Diameter: 182.0 nm

Polydispersity: 0.297

Baseline Index: 7.2

Elapsed Time: 00:02:00

Multimodal Size Distribution

Run	Eff. Diam. (nm)	Half Width (nm)	Polydispersity	Baseline Index
1	199.6	92.8	0.216	9.8
2	200.5	95.4	0.226	8.9
3	212.3	103.5	0.238	8.3
4	189.4	99.5	0.276	8.5
5	182.0	99.2	0.297	7.2
Mean	196.8	98.1	0.251	8.5
Std. Error	5.2	1.8	0.015	0.4
Combined	197.6	98.1	0.246	9.4

Data for Table 4-1, for compound **25**, after purification the vesicles using GPC column

229

Brookhaven Instruments Corp.
ZetaPALS Particle Sizing Software Ver. 3.80

Date: Mar 2, 2019
Time: 19:39:15
Batch: 0

Sample ID   **1.7mMvesiclesafter puri LithSH (Run 5)**
Operator ID   **Layla**
Notes

Elapsed Time	00:02:00
Mean Diam.	199.2 nm
Rel. Var.	0.303
Skew	-0.555

Multimodal Size Distribution
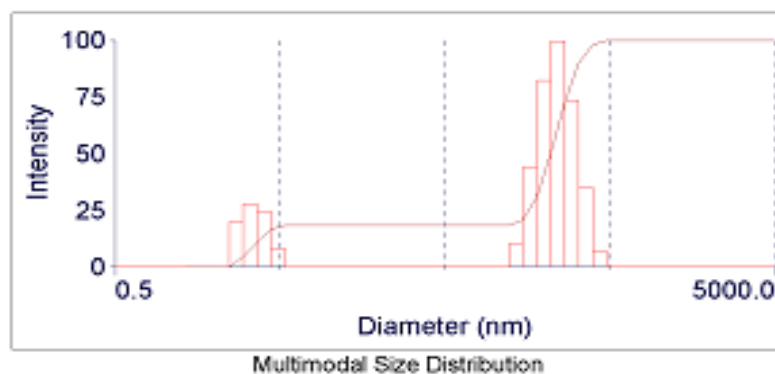
d(nm)	G(d)	C(d)	d(nm)	G(d)	C(d)	d(nm)	G(d)	C(d)
1.5	0	0	12.8	0	19	110.0	0	19
1.8	0	0	15.6	0	19	133.8	10	21
2.2	0	0	19.0	0	19	162.6	44	31
2.7	20	5	23.1	0	19	197.7	83	50
3.3	28	11	28.0	0	19	240.3	100	73
4.0	25	17	34.1	0	19	292.1	74	90
4.8	8	19	41.4	0	19	355.2	35	98
5.9	0	19	50.4	0	19	431.7	7	100
7.1	0	19	61.2	0	19	524.9	0	100
8.7	0	19	74.5	0	19	638.1	0	100
10.6	0	19	90.5	0	19	775.7	0	100

Data for Table 4-1. Vesicles incorporated with compound **25** after purification using GPC column.

Brookhaven Instruments Corp.
ZetaPALS Particle Sizing Software Ver. 3.80

Date: Mar 2, 2019
Time: 19:39:15
Batch: 0

Sample ID   **1.7mMvesiclesafter puri LithSH (Run 5)**
Operator ID   **Layla**
Notes

Elapsed Time	00:02:00
Eff. Diam.	182.0 nm
Mean Diam.	207.3 nm
Polydispersity	0.297
GSD	1.665

Intensity vs Diameter (nm) — Lognormal Size Distribution
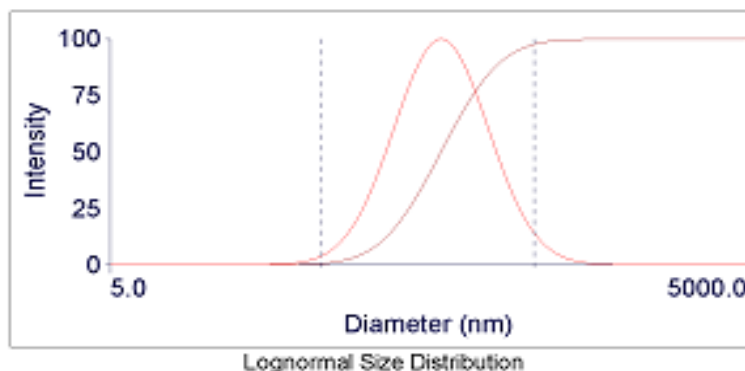
d(nm)	G(d)	C(d)	d(nm)	G(d)	C(d)	d(nm)	G(d)	C(d)
78.7	26	5	160.0	97	40	256.7	80	75
94.7	44	10	170.7	99	45	279.7	70	80
107.3	58	15	182.0	100	50	308.7	58	85
118.5	70	20	194.1	99	55	350.0	44	90
129.1	80	25	207.1	97	60	421.2	26	95
139.3	87	30	221.5	93	65			
149.6	93	35	237.8	87	70			

Data for Table 4-1. Vesicles incorporated with compound **25** after purification using GPC column.

Brookhaven Instruments Corp.
ZetaPALS Particle Sizing Software Ver. 3.80

Date: Mar 2, 2019
Time: 19:39:15
Batch: 0

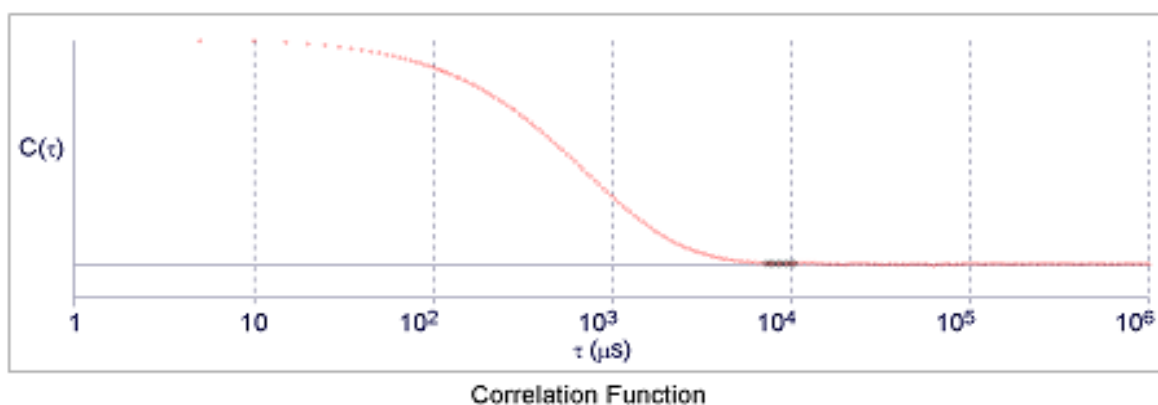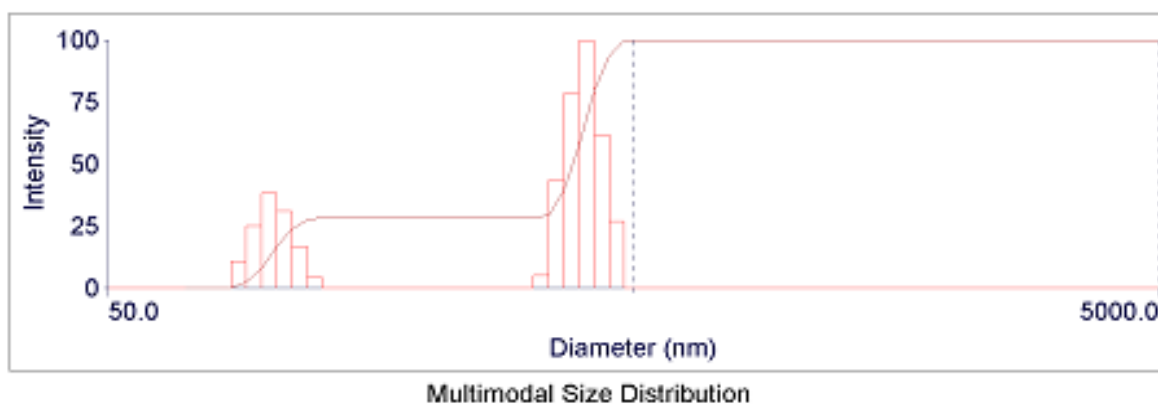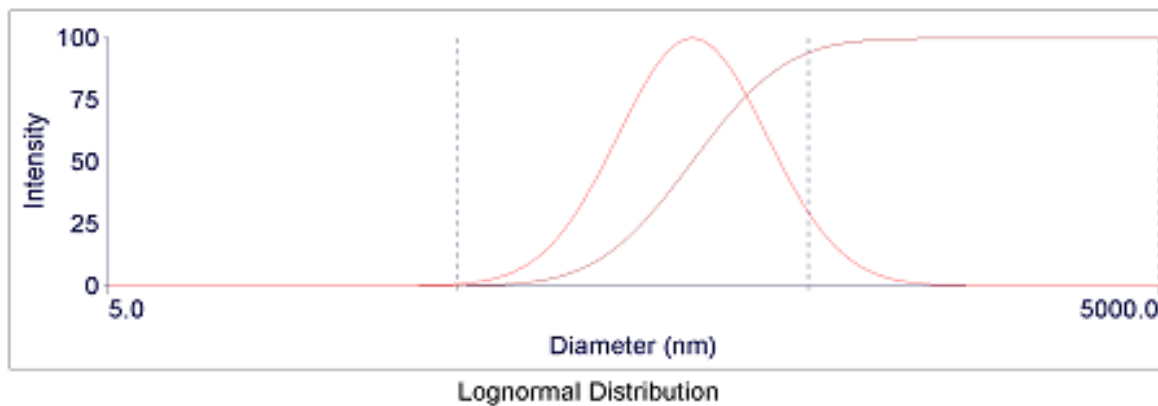Sample ID   **1.7mMvesiclesafter puri LithSH (Run 5)**
Operator ID   **Layla**
Notes
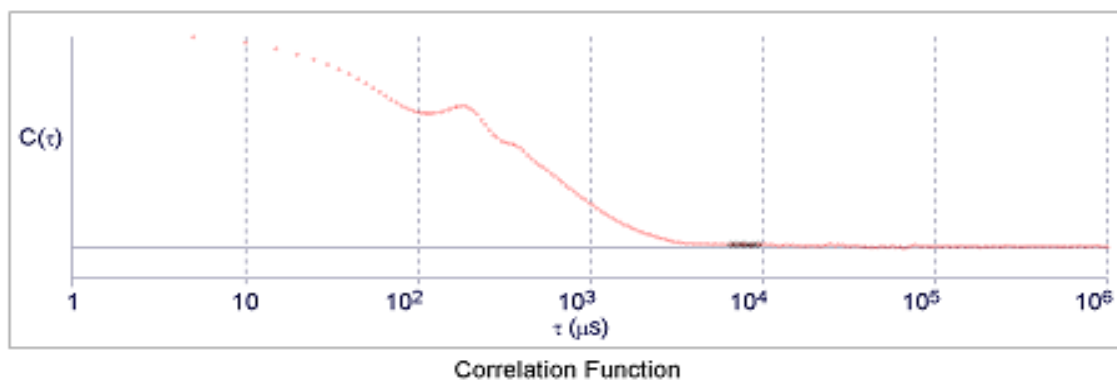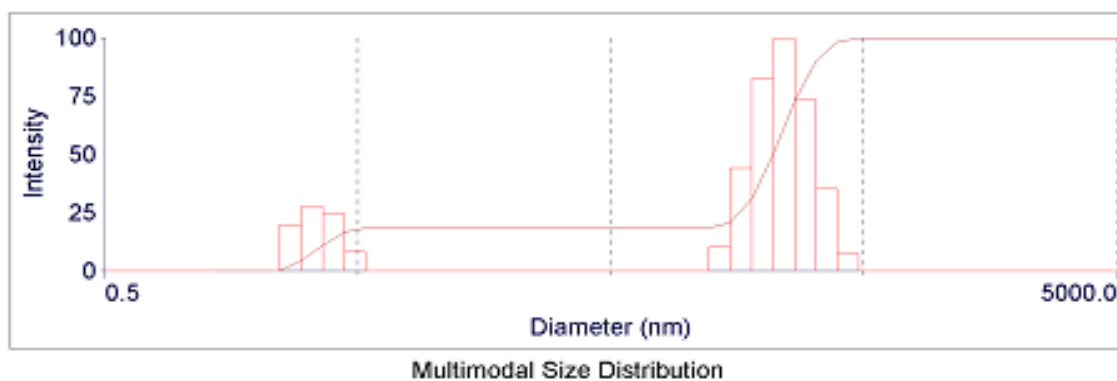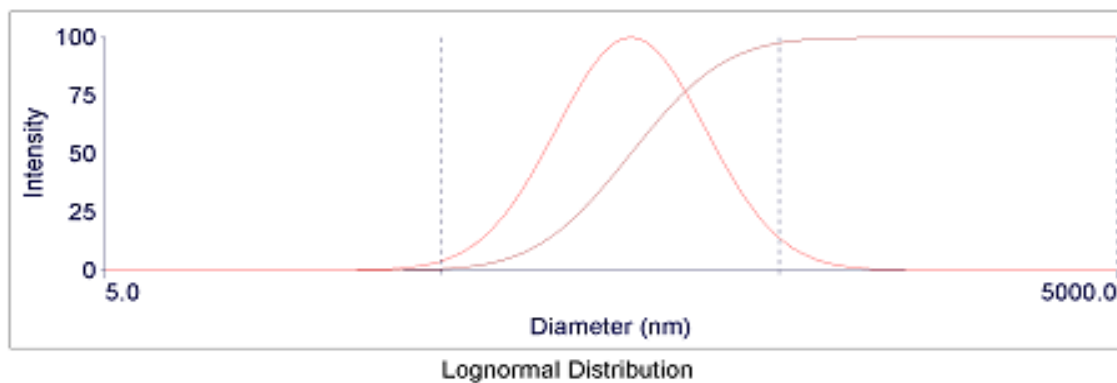
Data for Table 4-1. Vesicles incorporated with compound **25** after purification using GPC column

Sample ID **1.7mMvesiclesafter puri Cho-SH (Combined)**
Operator ID **Layla**
Notes

Elapsed Time	00:10:00
Mean Diam.	533.5 nm
Rel. Var.	1.194
Skew	1.323

Multimodal Size Distribution
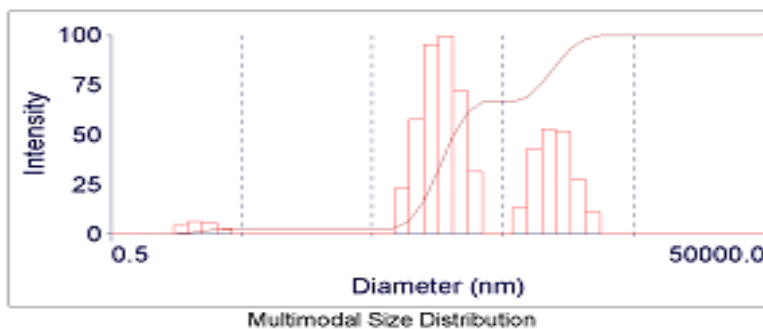
d(nm)	G(d)	C(d)	d(nm)	G(d)	C(d)	d(nm)	G(d)	C(d)
1.0	0	0	17.3	0	3	300.4	31	67
1.3	0	0	22.5	0	3	389.3	0	67
1.7	4	1	29.1	0	3	504.5	0	67
2.2	6	2	37.7	0	3	653.9	13	69
2.8	5	3	48.9	0	3	847.4	43	76
3.7	2	3	63.4	0	3	1098.3	53	85
4.7	0	3	82.1	23	7	1423.5	52	94
6.1	0	3	106.5	58	17	1844.9	27	98
8.0	0	3	138.0	96	33	2391.0	11	100
10.3	0	3	178.8	100	49	3098.9	0	100
13.4	0	3	231.7	72	61	4016.3	0	100

Data for Table 4-1. Vesicles incorporated with compound **24** after purification using GPC column.

Date: Mar 2, 2019
Time: 19:16:44
Batch: 0

Sample ID   **1.7mMvesiclesafter puri Cho-SH (Combined)**
Operator ID   **Layla**
Notes

Elapsed Time	00:10:00
Eff. Diam.	244.2 nm
Mean Diam.	273.9 nm
Polydispersity	0.257
GSD	1.614

Lognormal Size Distribution
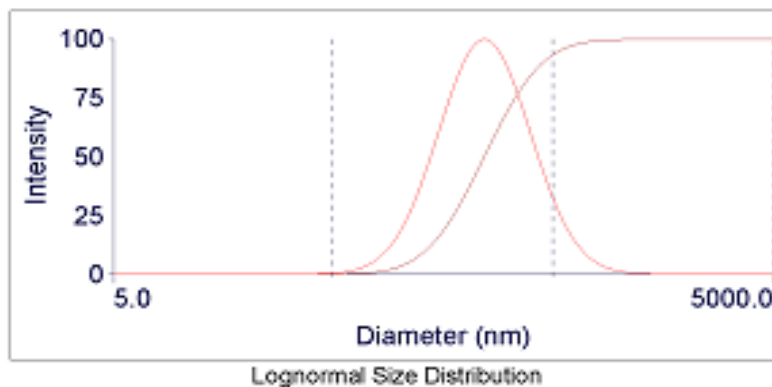
d(nm)	G(d)	C(d)	d(nm)	G(d)	C(d)	d(nm)	G(d)	C(d)
111.1	26	5	216.4	97	40	337.2	80	75
132.2	44	10	229.9	99	45	365.4	70	80
148.7	58	15	244.2	100	50	401.0	58	85
163.2	70	20	259.4	99	55	451.1	44	90
176.9	80	25	275.7	97	60	536.7	26	95
190.1	87	30	293.6	93	65			
203.1	93	35	313.8	87	70			

Data for Table 4-1. Vesicles incorporated with compound **24** after purification using GPC column.

Brookhaven Instruments Corp.
ZetaPALS Particle Sizing Software Ver. 3.80

Date: Mar 2, 2019
Time: 19:16:44
Batch: 0

Sample ID   **1.7mMvesiclesafter puri Cho-SH (Combined)**
Operator ID   **Layla**
Notes
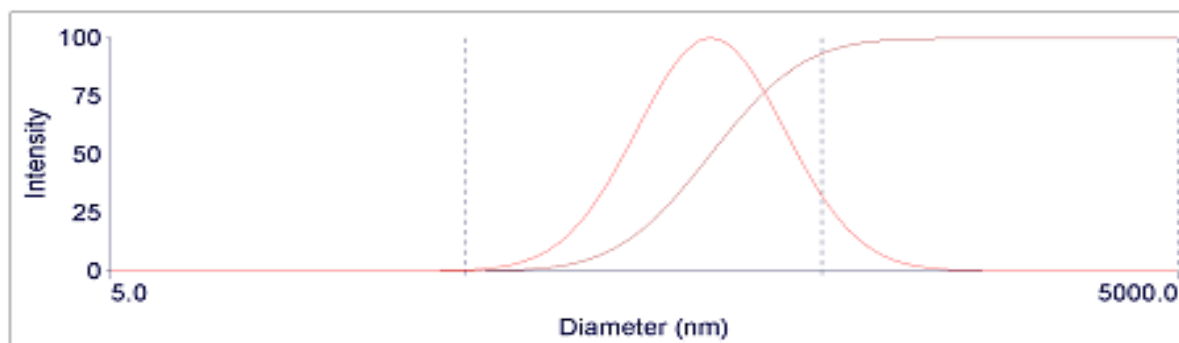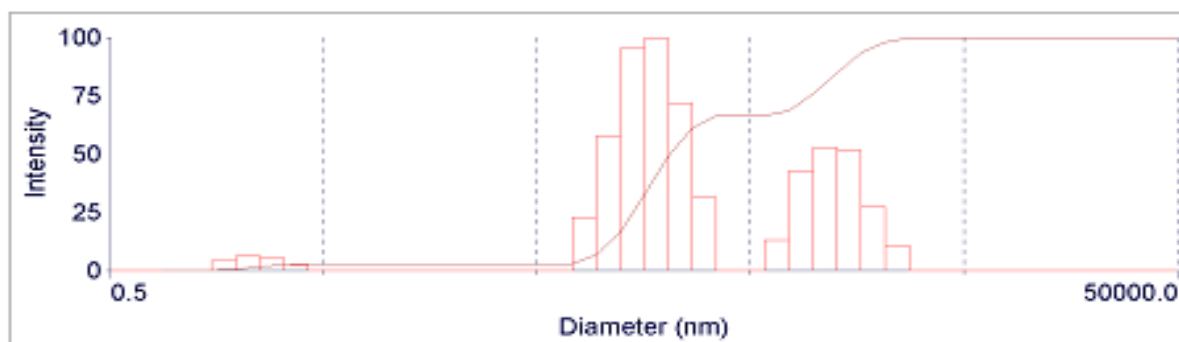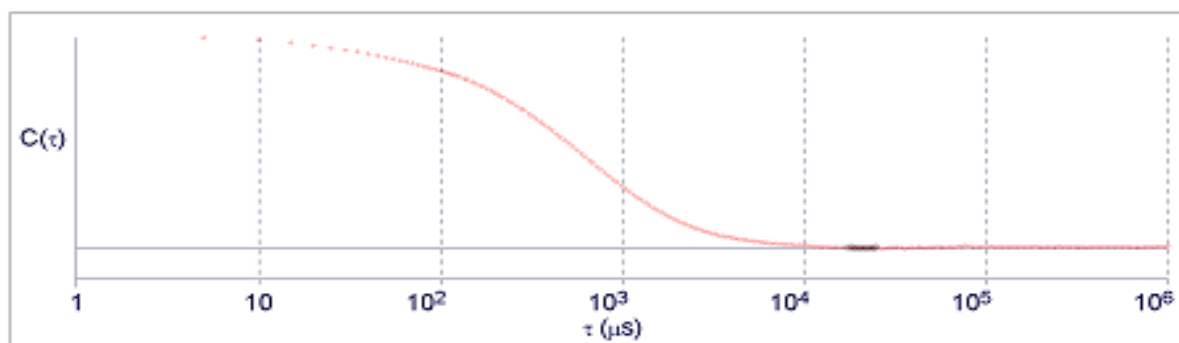
Data for Table 4-1. Vesicles incorporated with compound **24** after purification using GPC column.

7.6 NMR Spectra for the Final Compounds
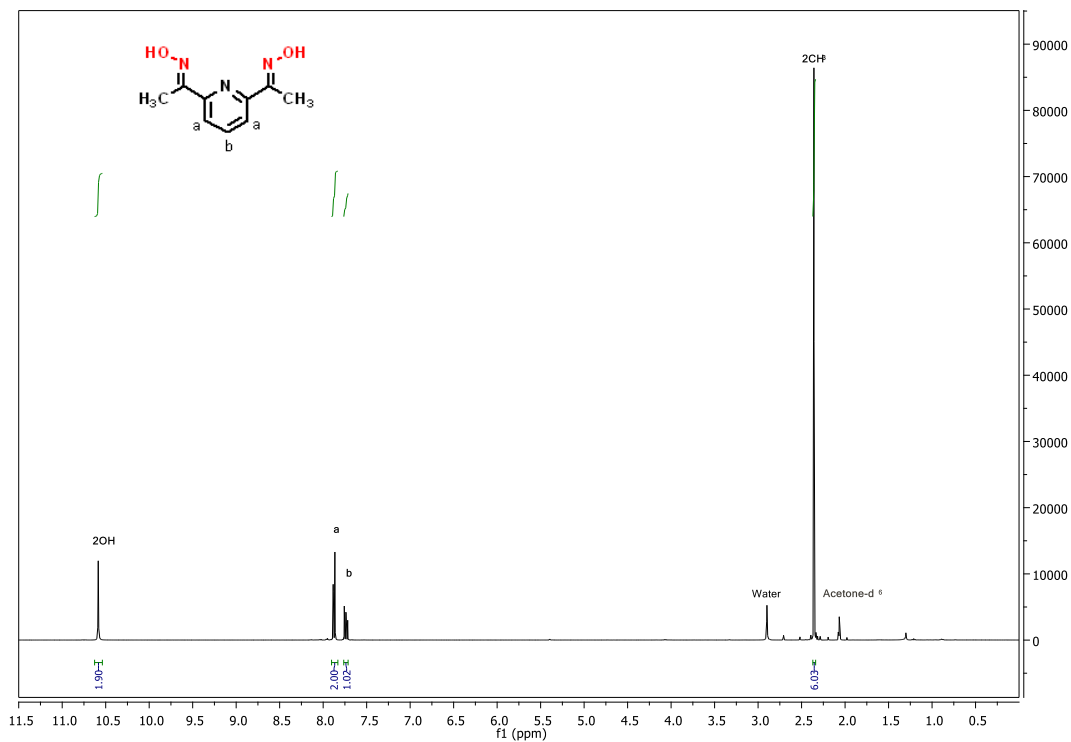
^{1}HNMR spectrum for compound **2**
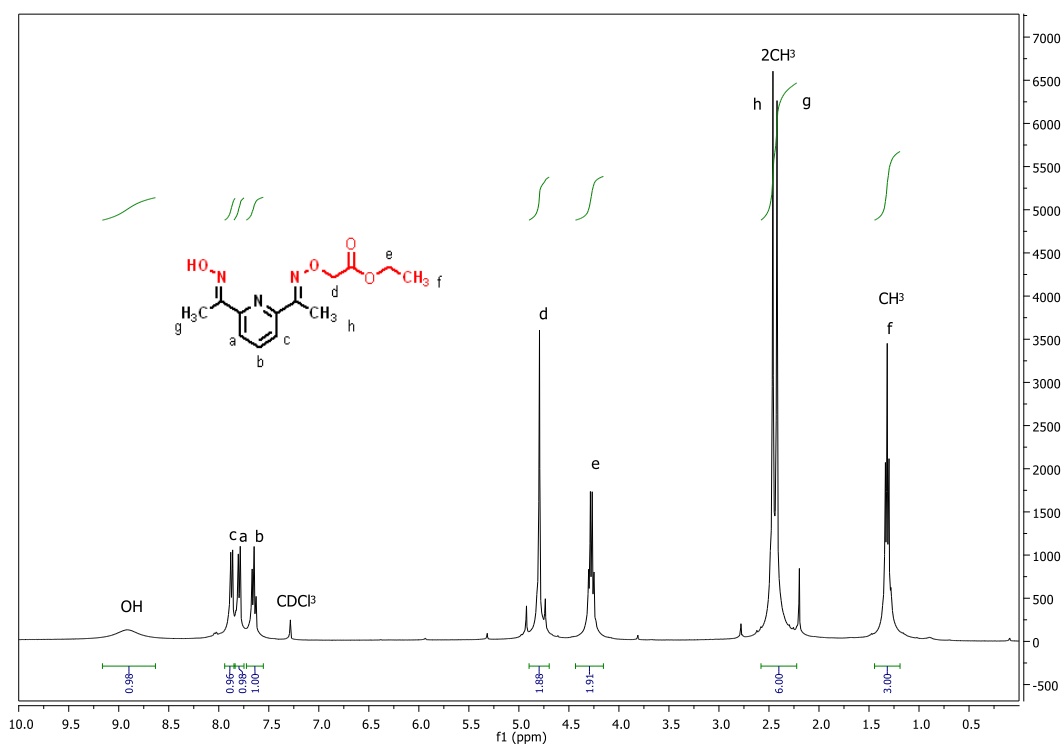
^{1}HNMR spectrum for compound **5**
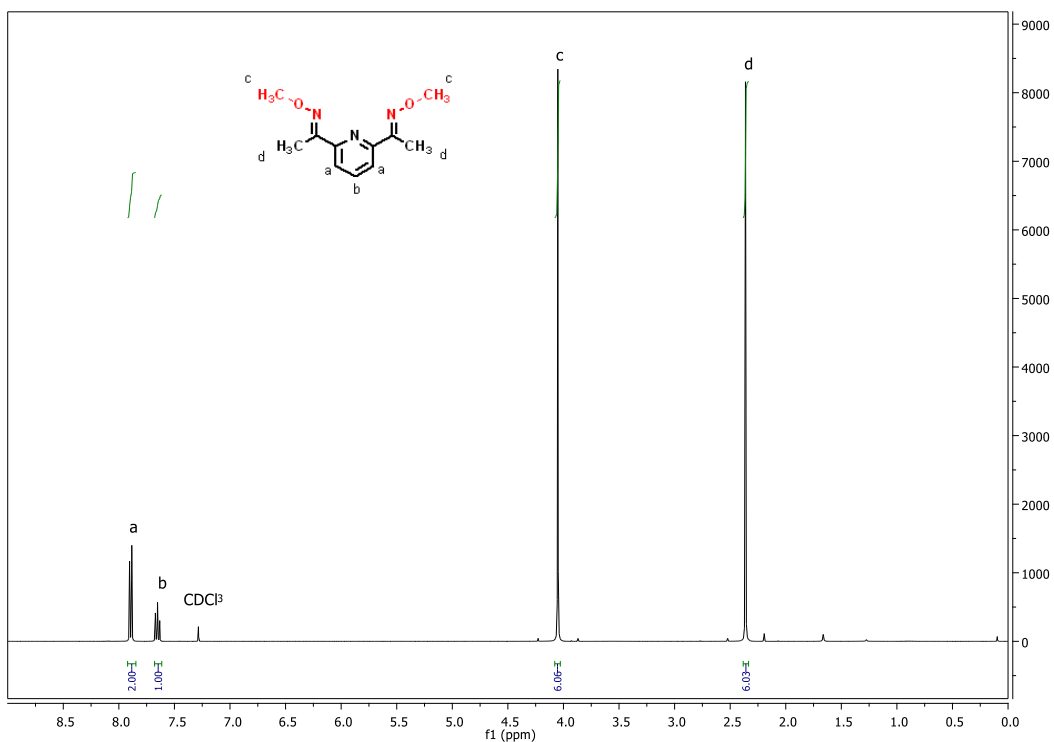
^{1}HNMR spectrum for compound **4**
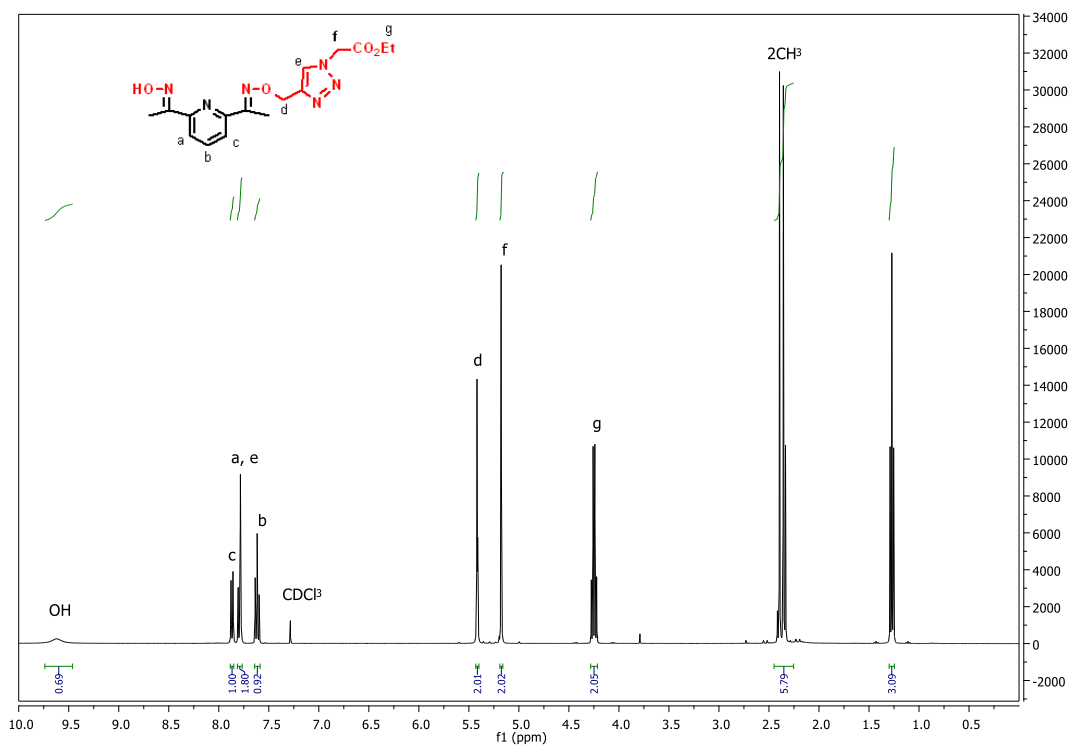
^{1}HNMR spectrum for compound **9**
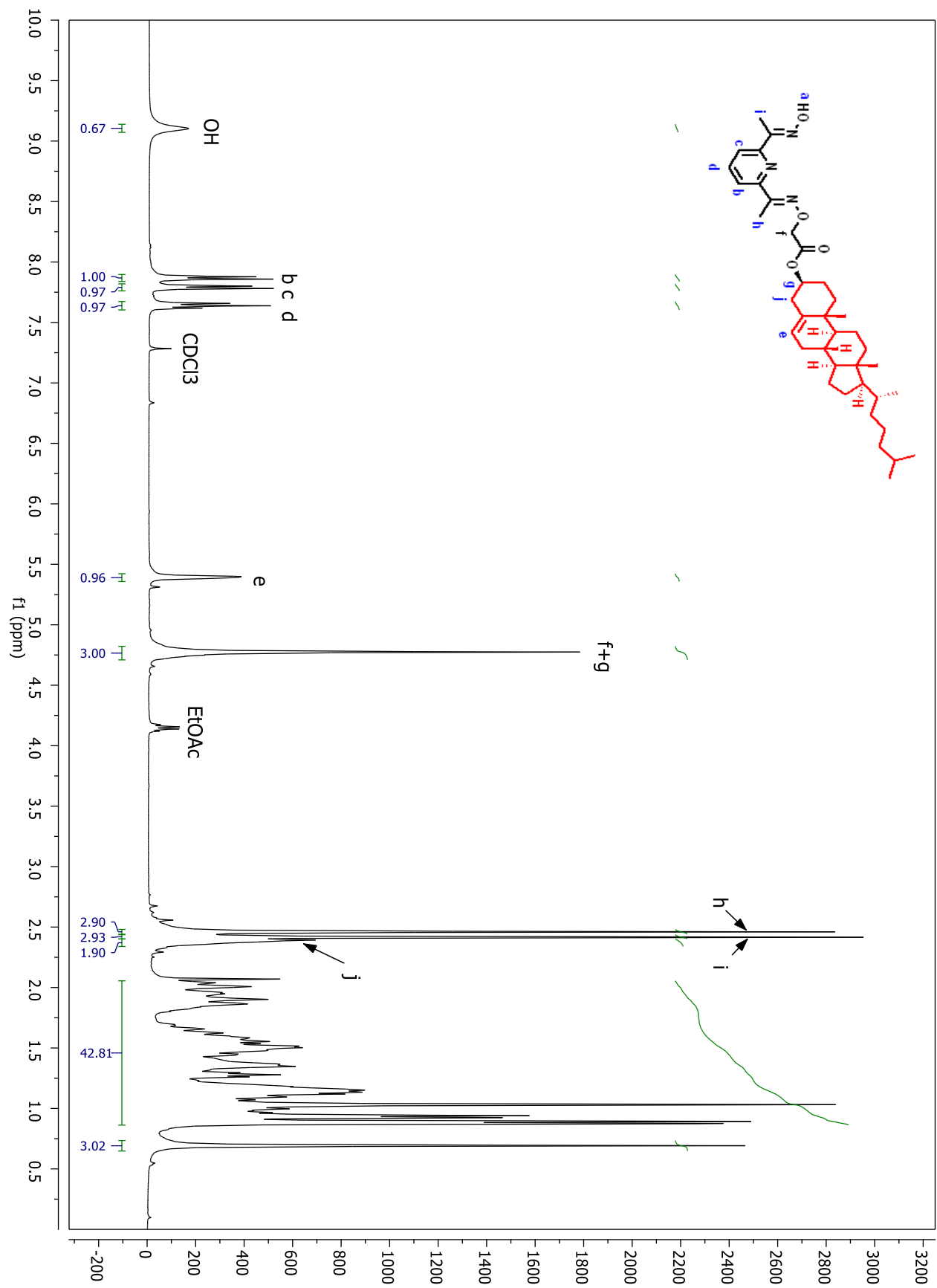
^{1}HNMR spectrum for compound **10**
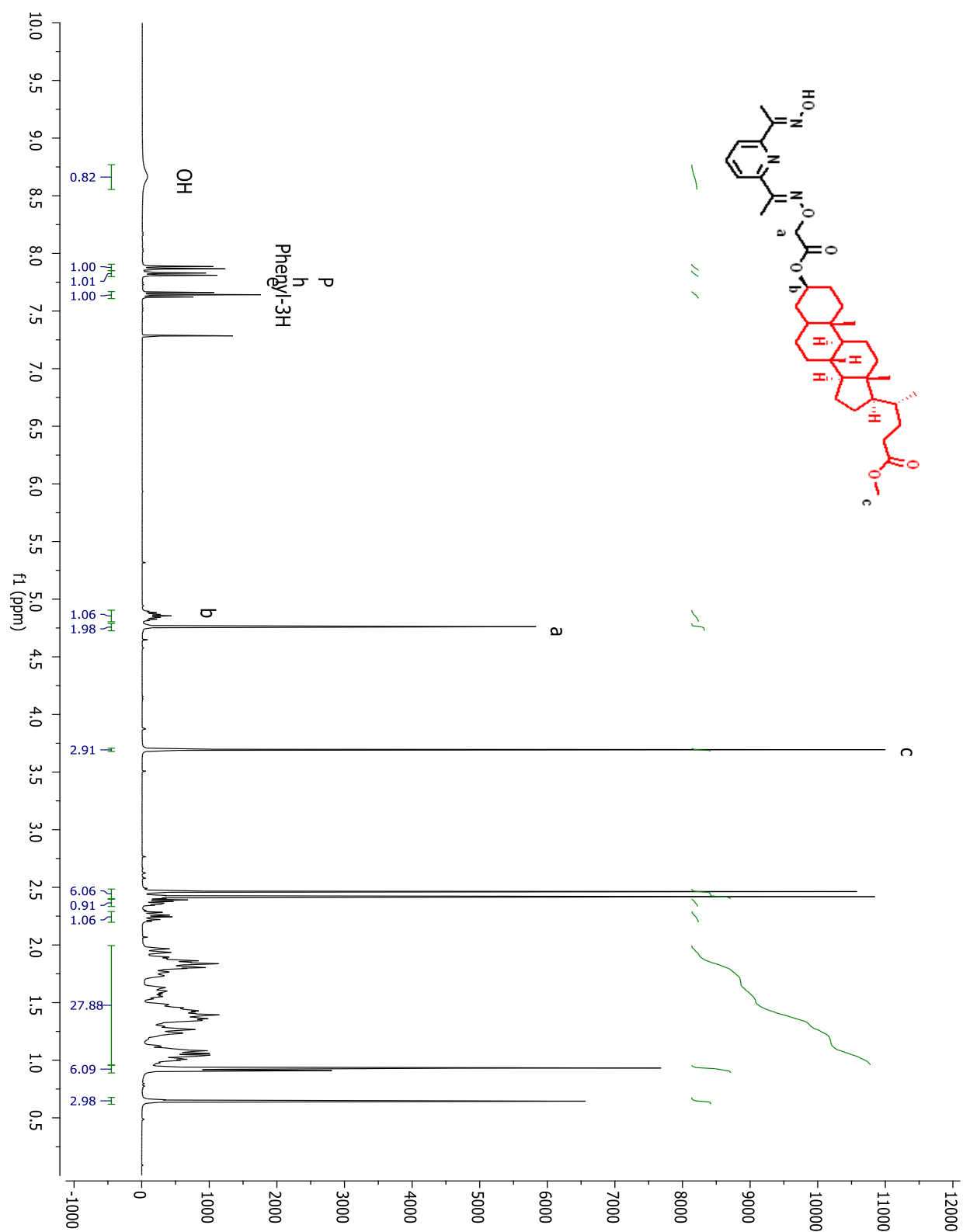
^{1}HNMR spectrum for compound **11**
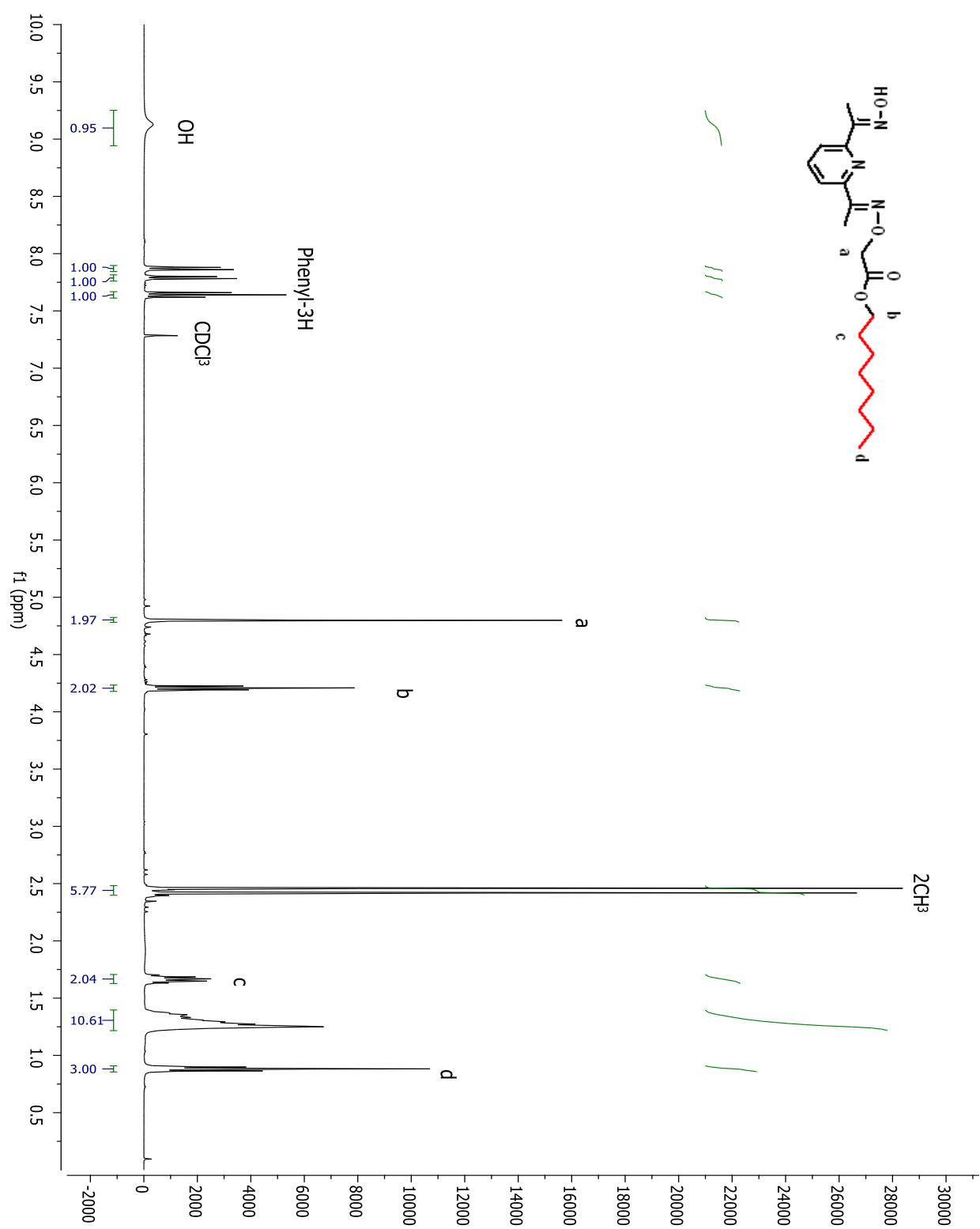
^{1}HNMR spectrum for compound 1**2**
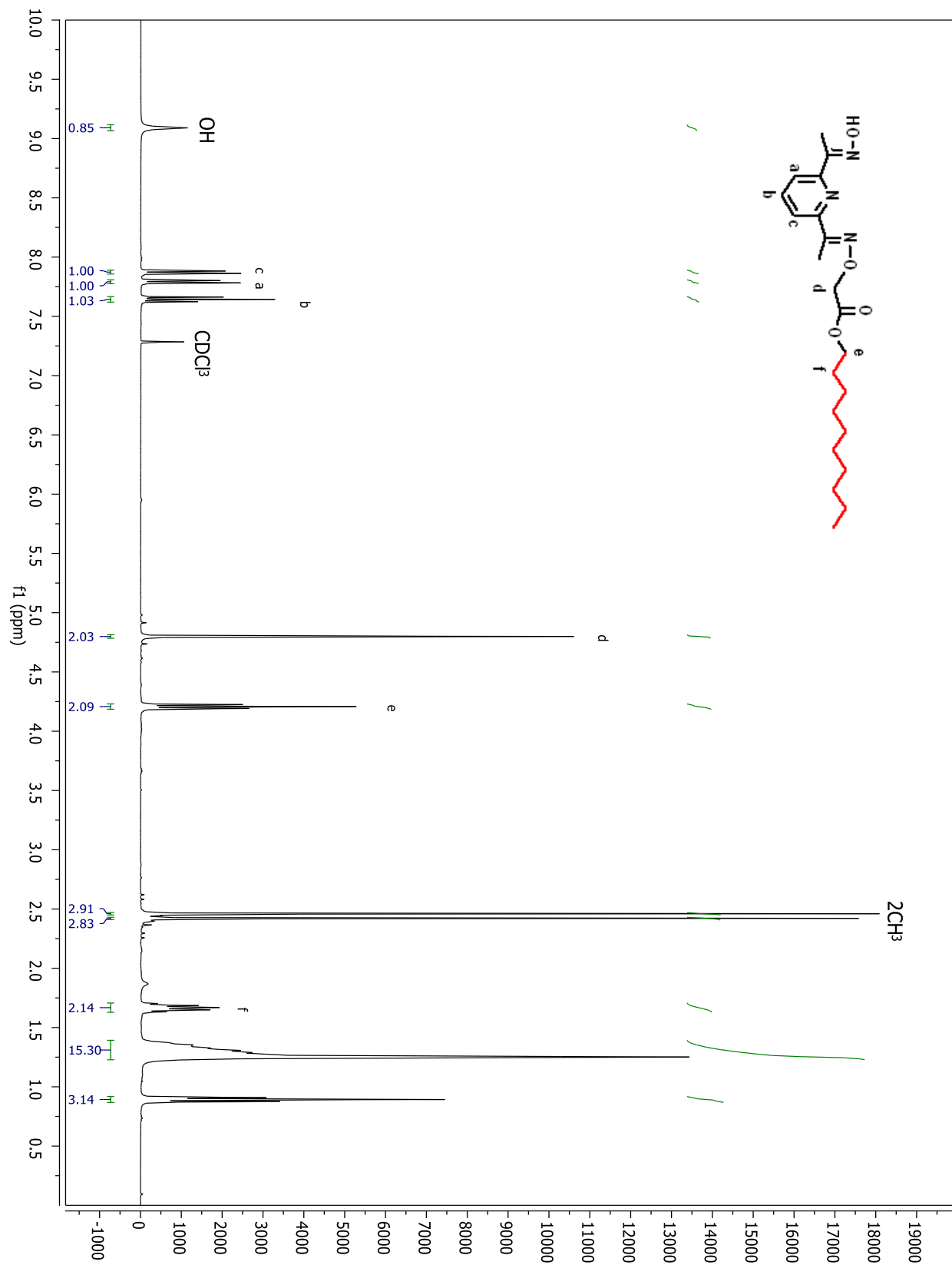
¹HNMR spectrum for compound **13**
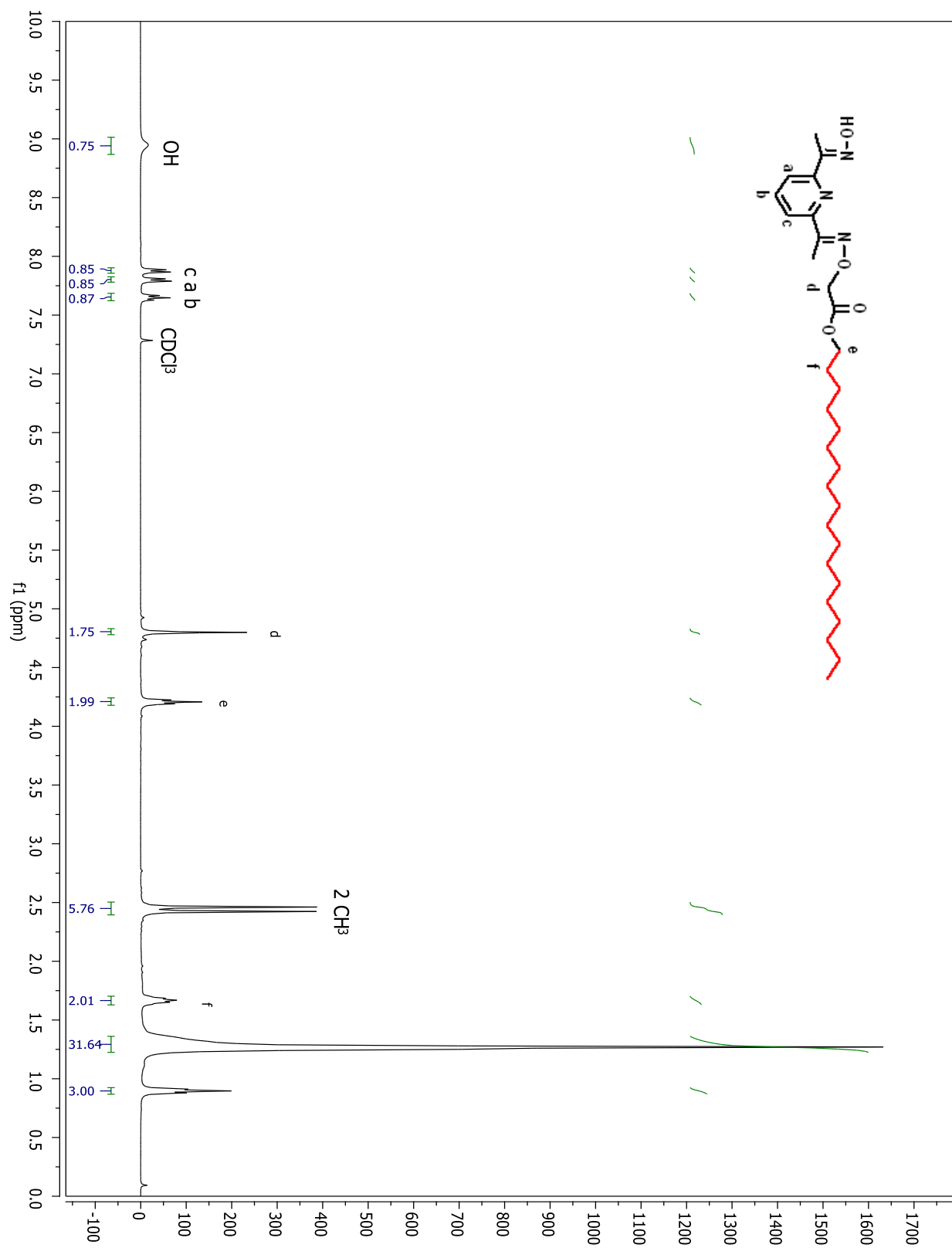
^{1}HNMR spectrum for compound **14**
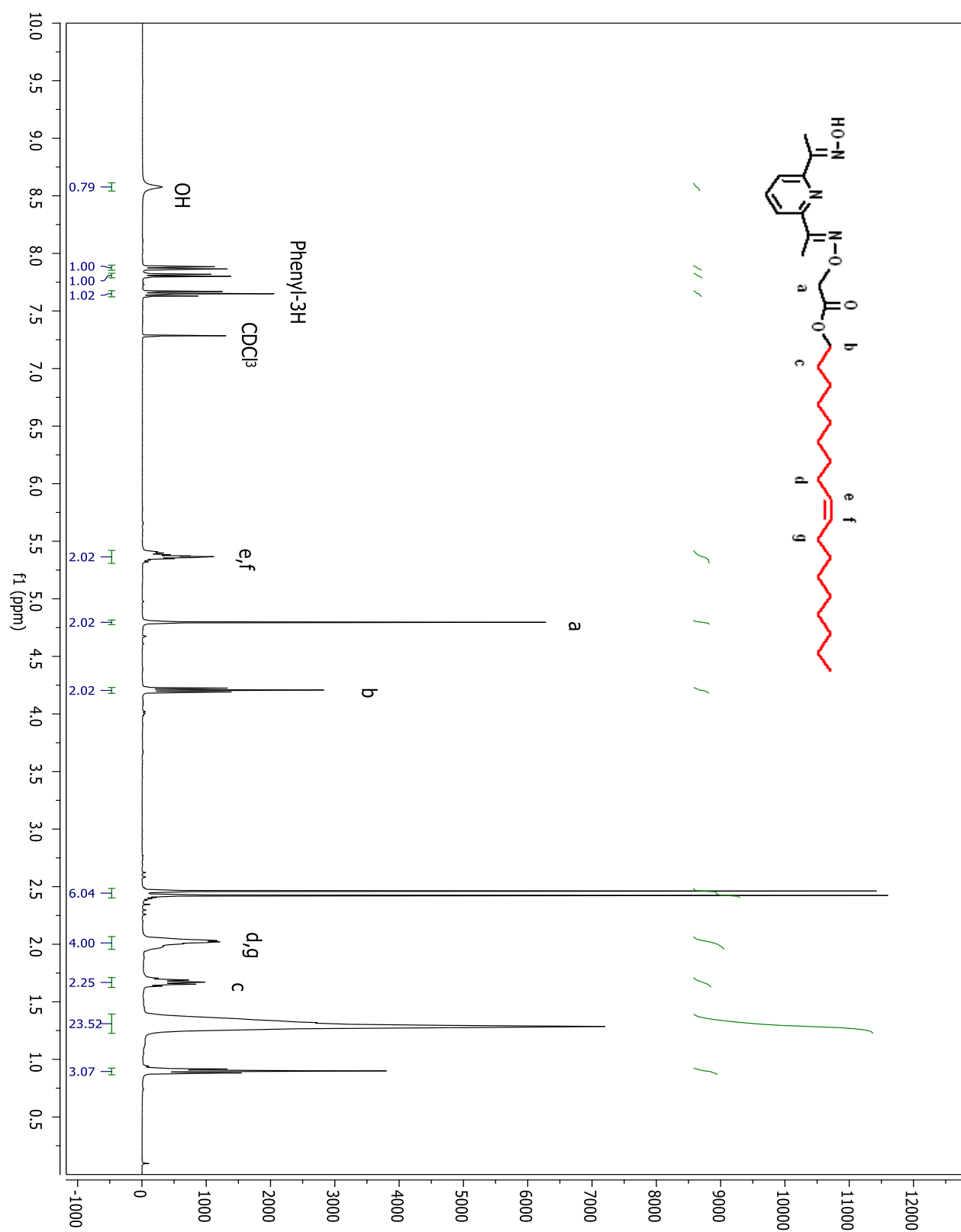
^{1}HNMR spectrum for compound **15**

243
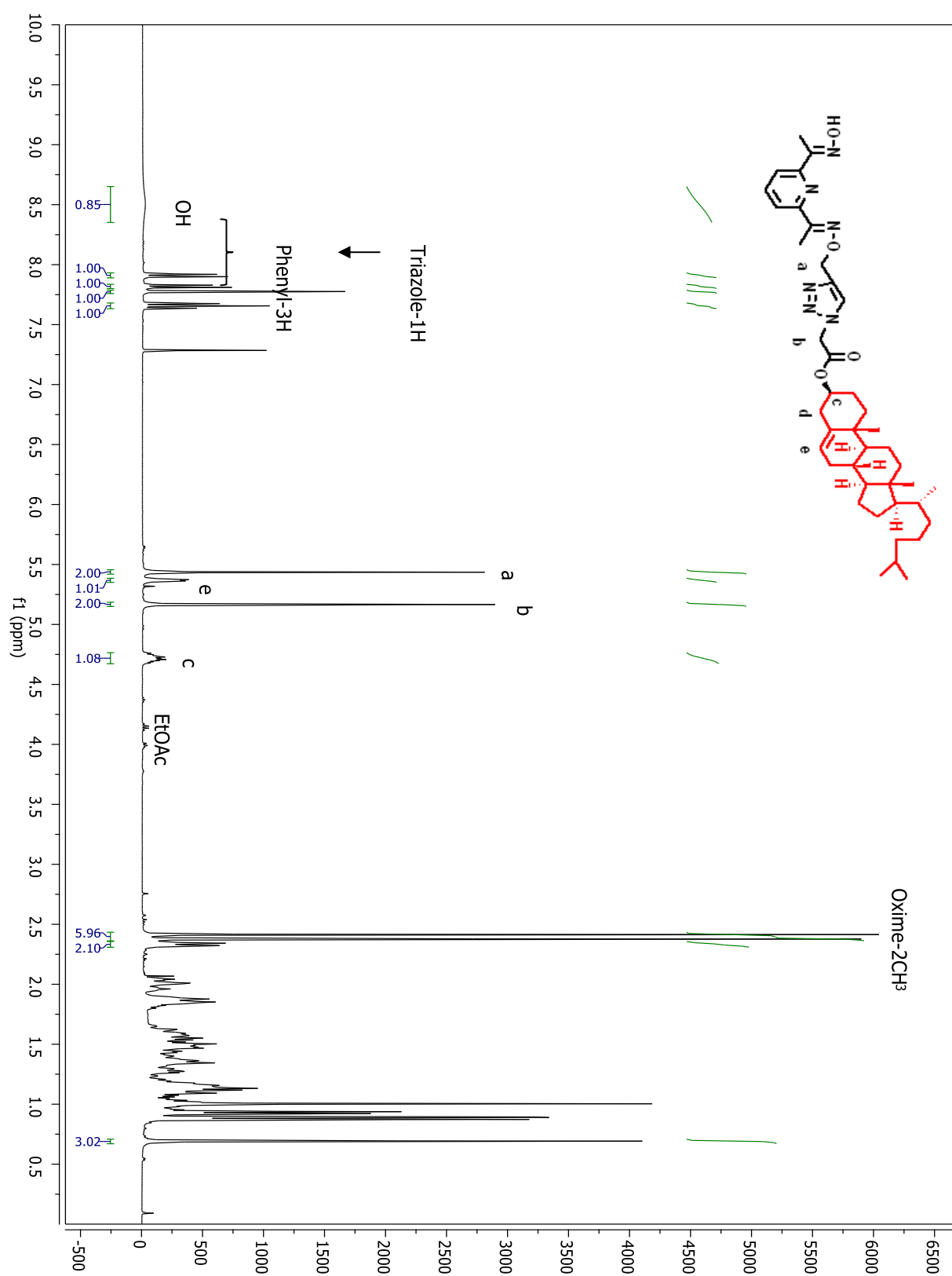
^{1}HNMR spectrum for compound **17**
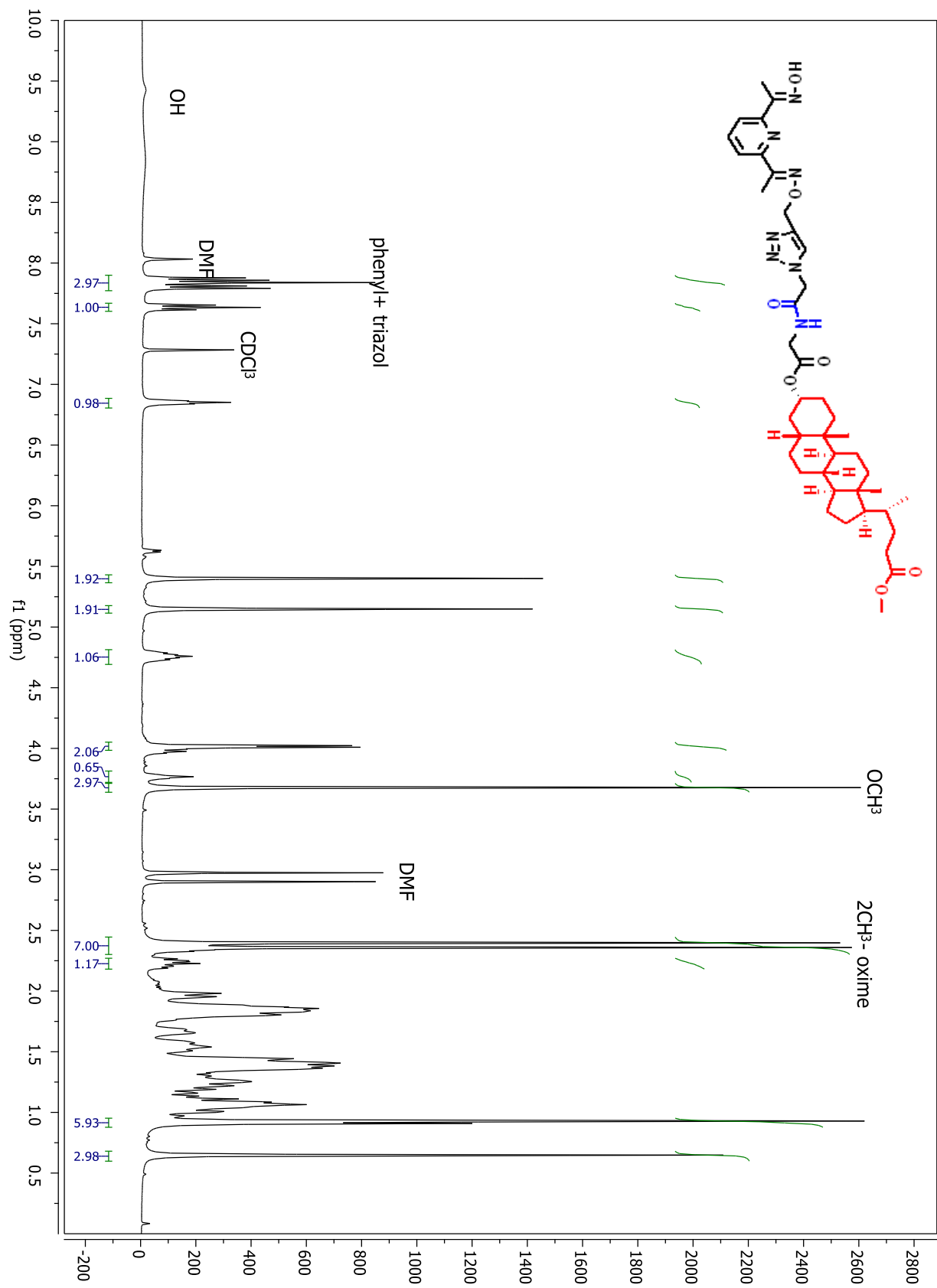
^{1}HNMR spectrum for compound **18**
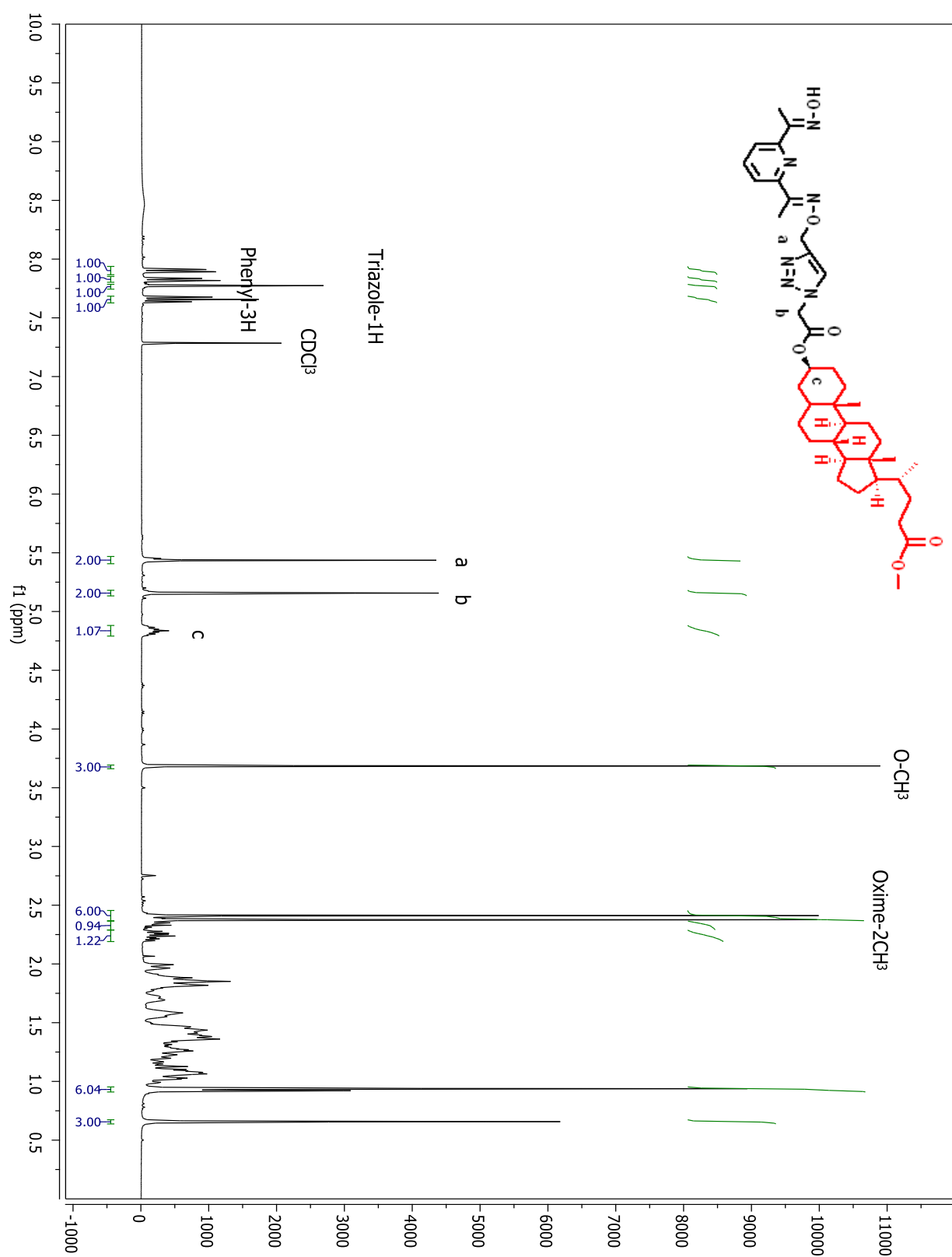
^{1}HNMR spectrum for compound **19**
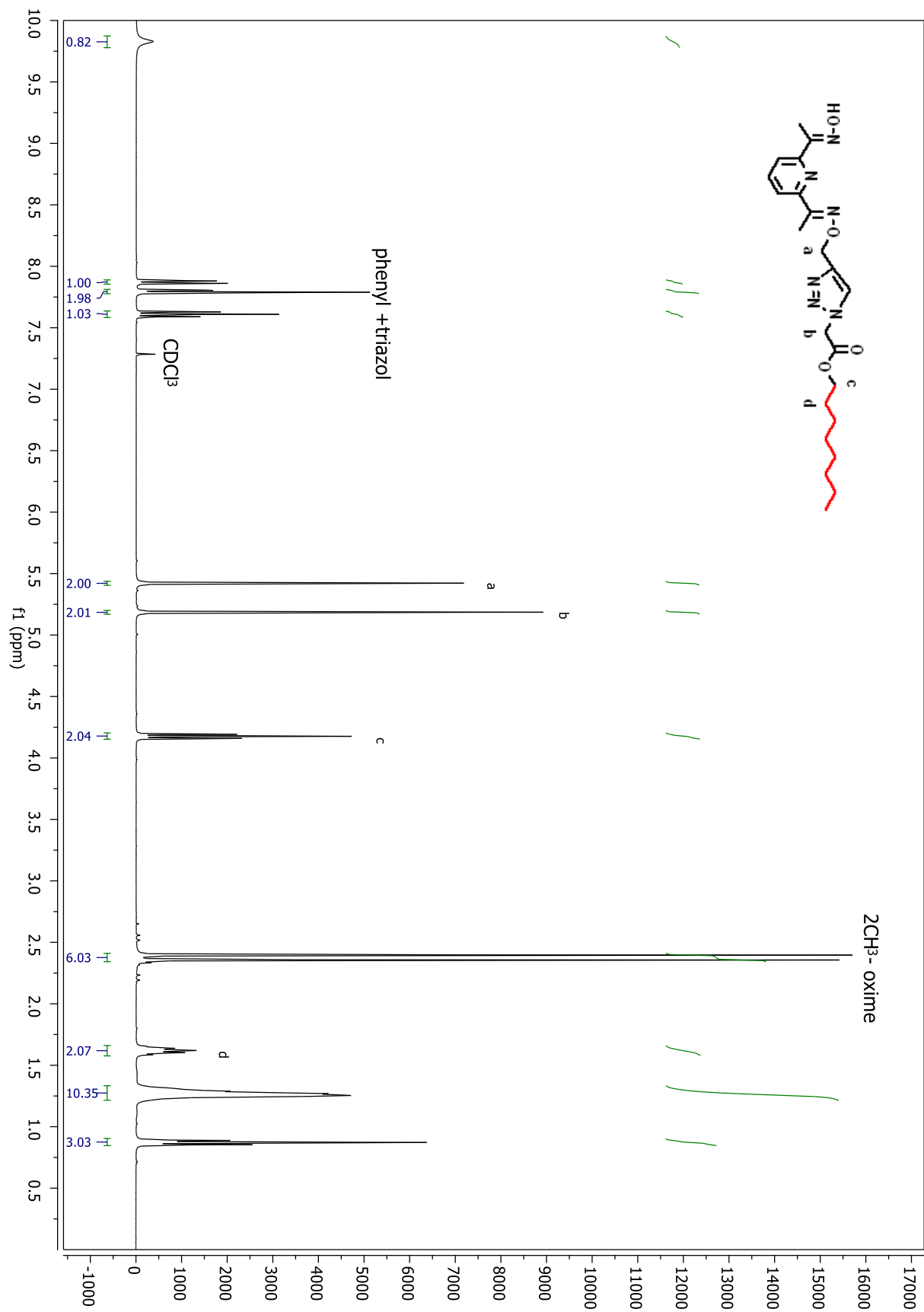
^{1}HNMR spectrum for compound **20**
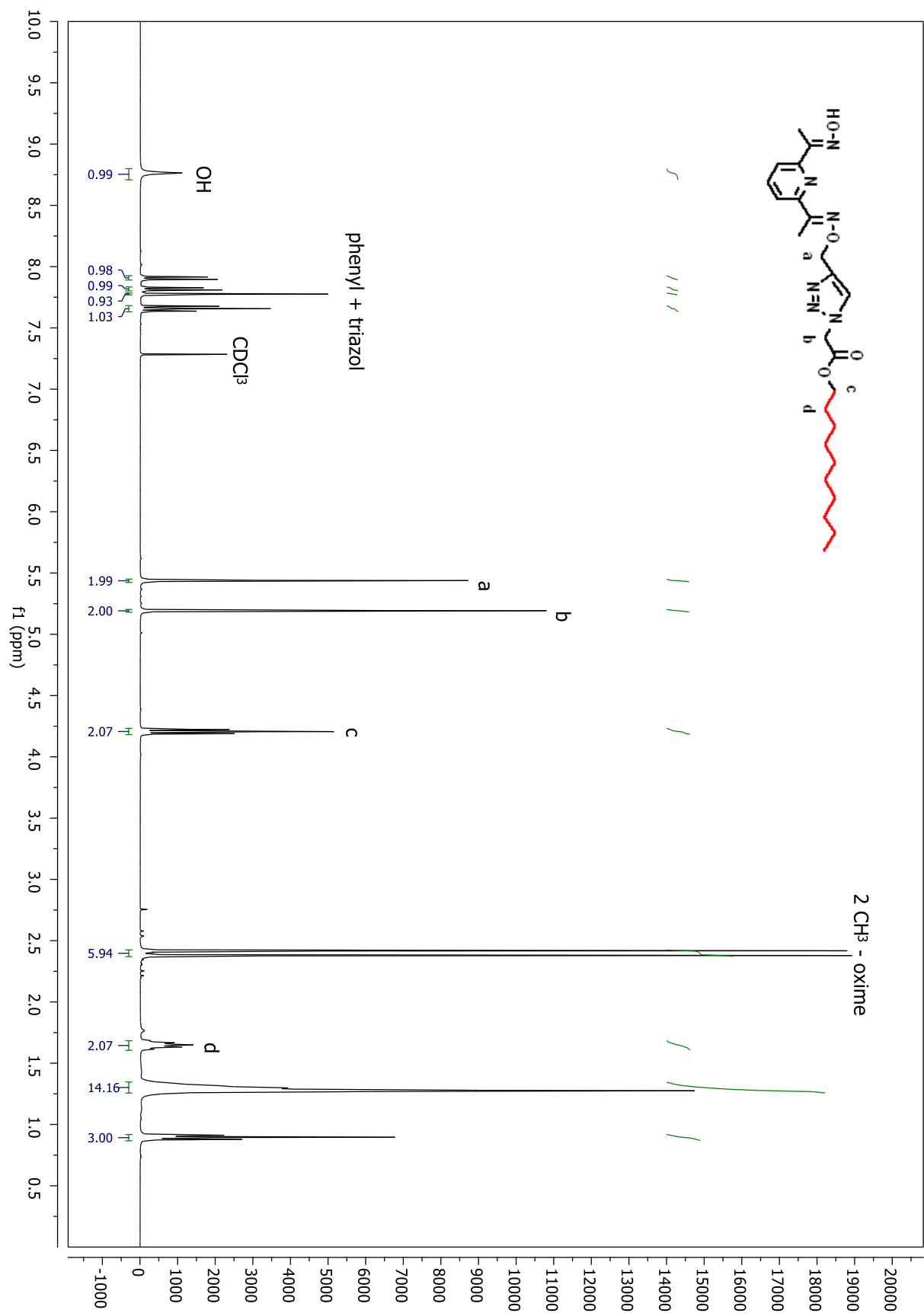
^{1}HNMR spectrum for compound **21**
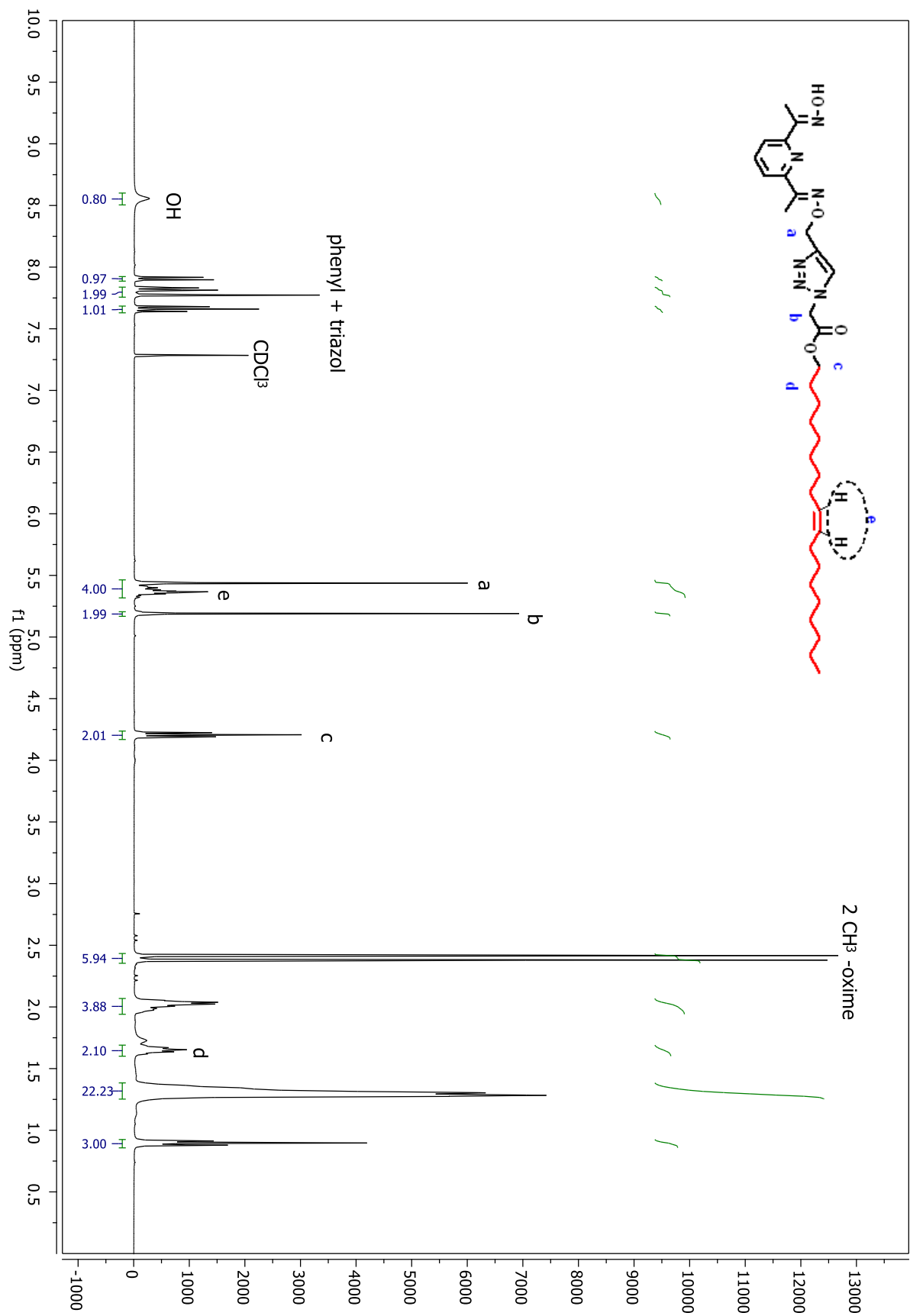
^{1}HNMR spectrum for compound **23**
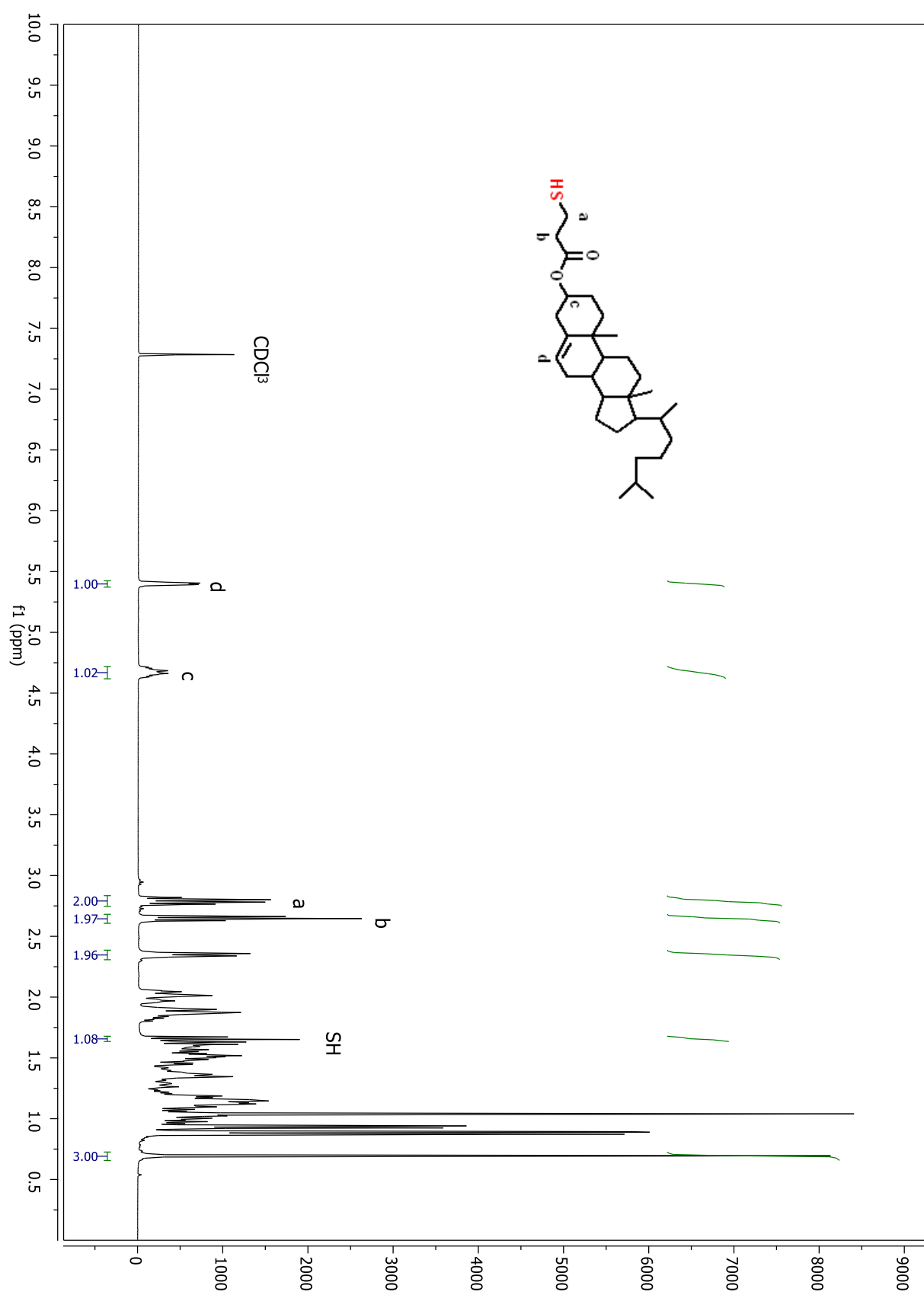
¹HNMR spectrum for compound **24**
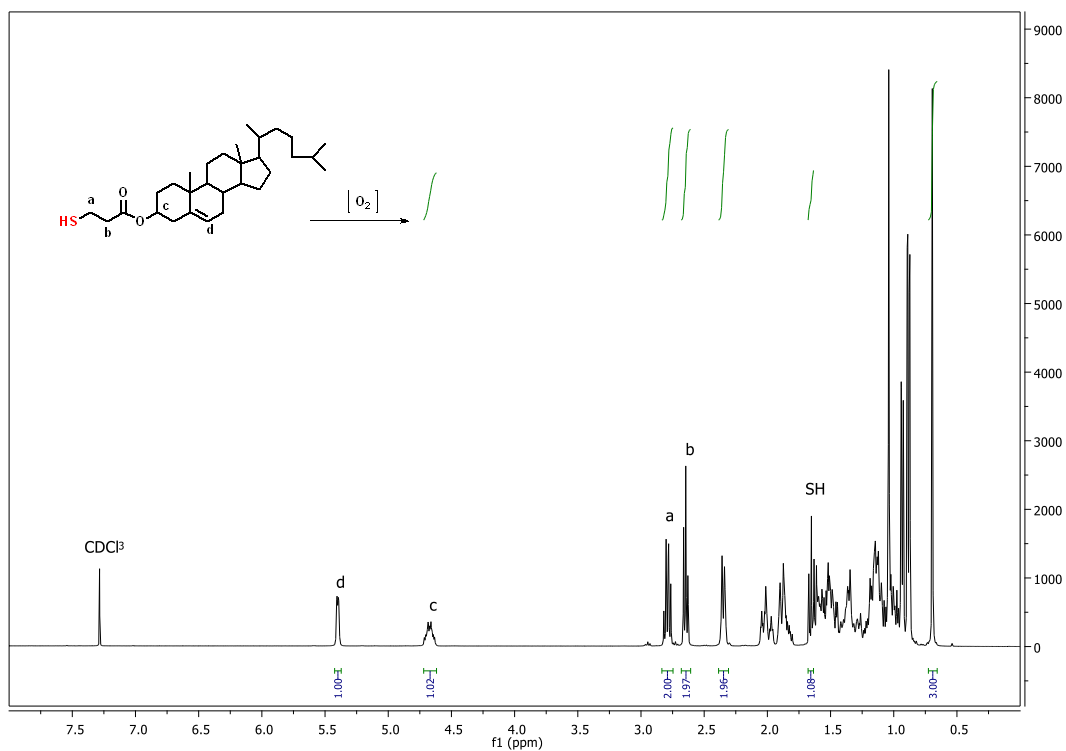
^{1}HNMR spectrum for compound **24** after exposing the sample 5 day to the air
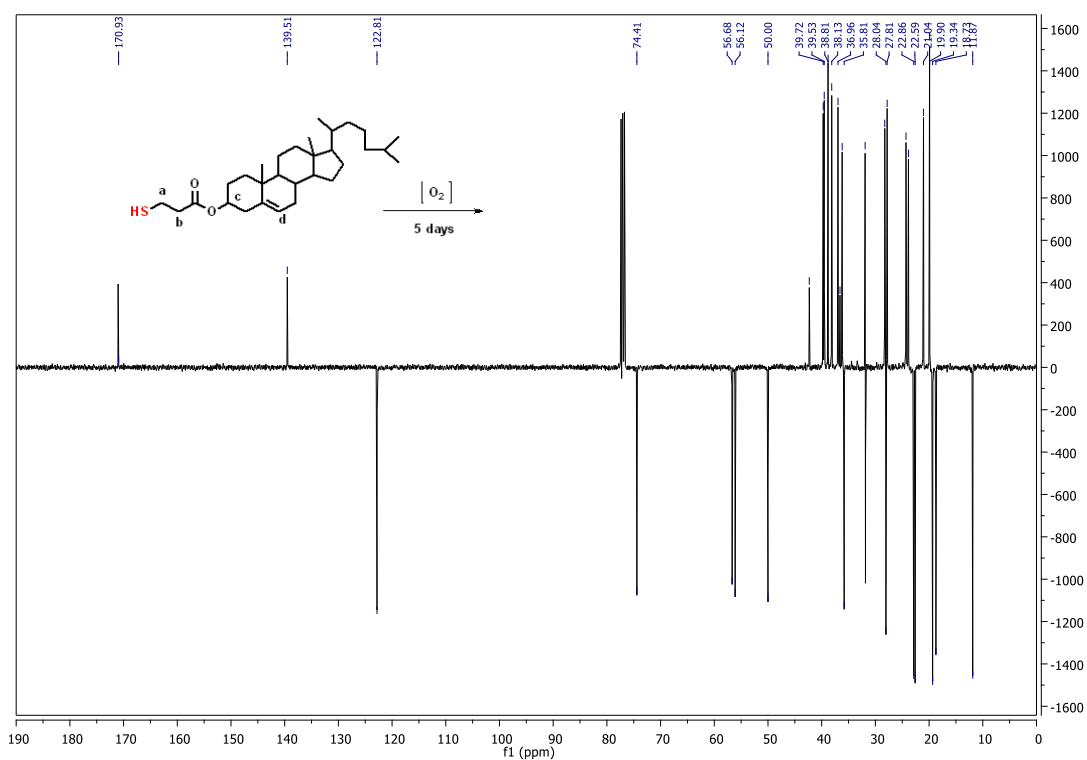
^{13}CNMR spectrum for compound **24** after exposing the sample 5 day to the air
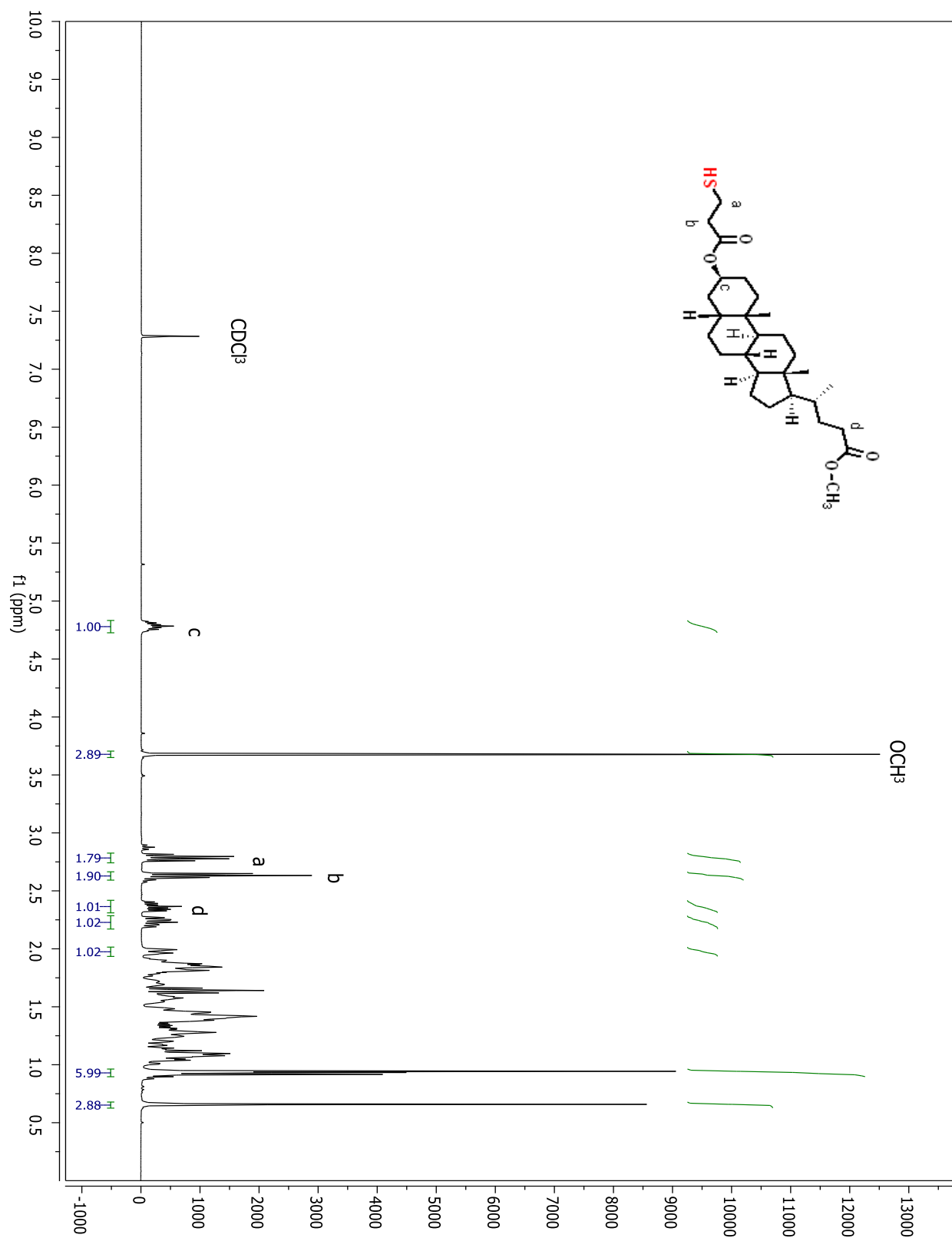
^{1}HNMR spectrum for compound **25**
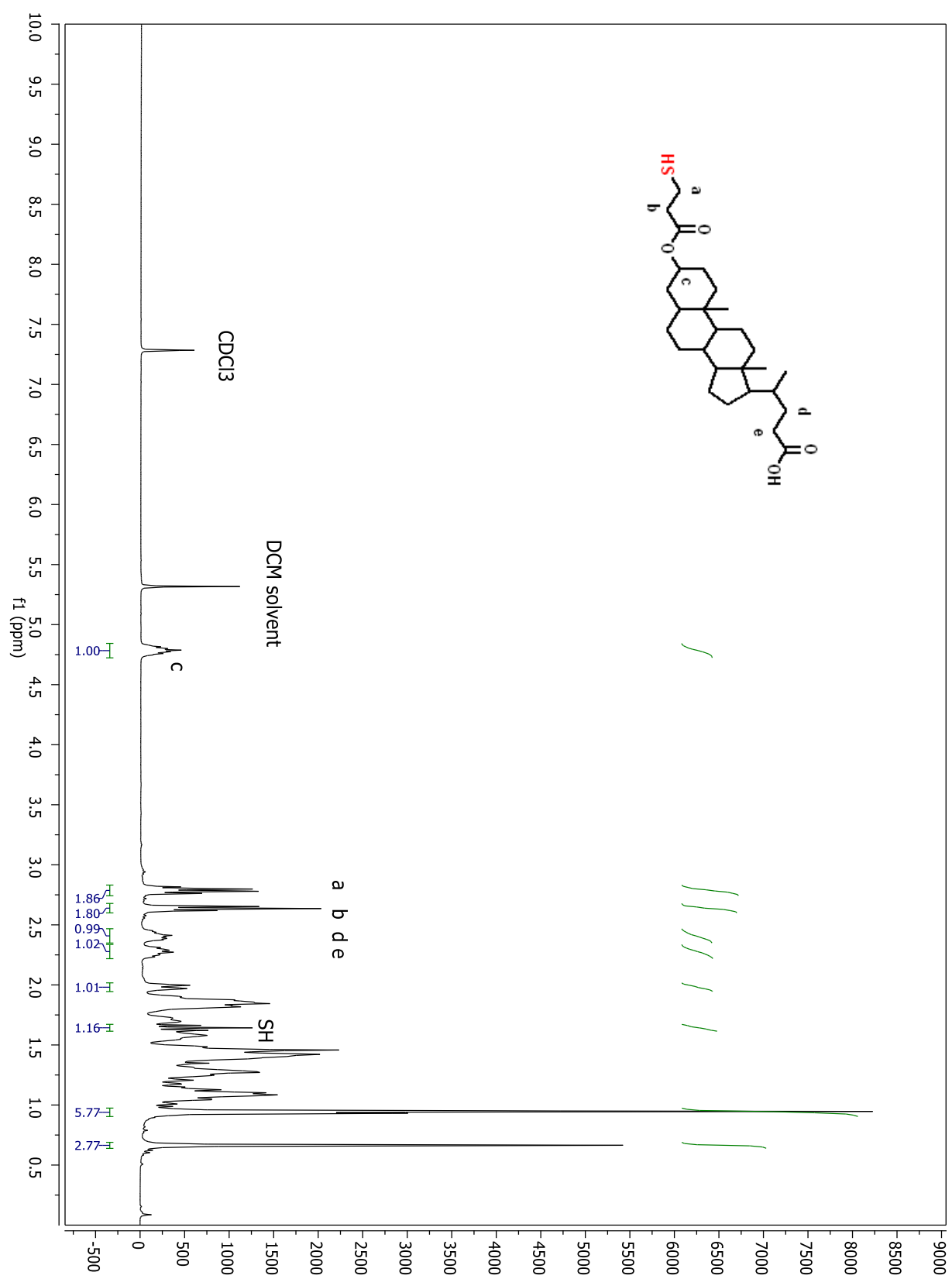
^{1}HNMR spectrum for compound **27**

7.7 HPLC Traces for the Final Compounds
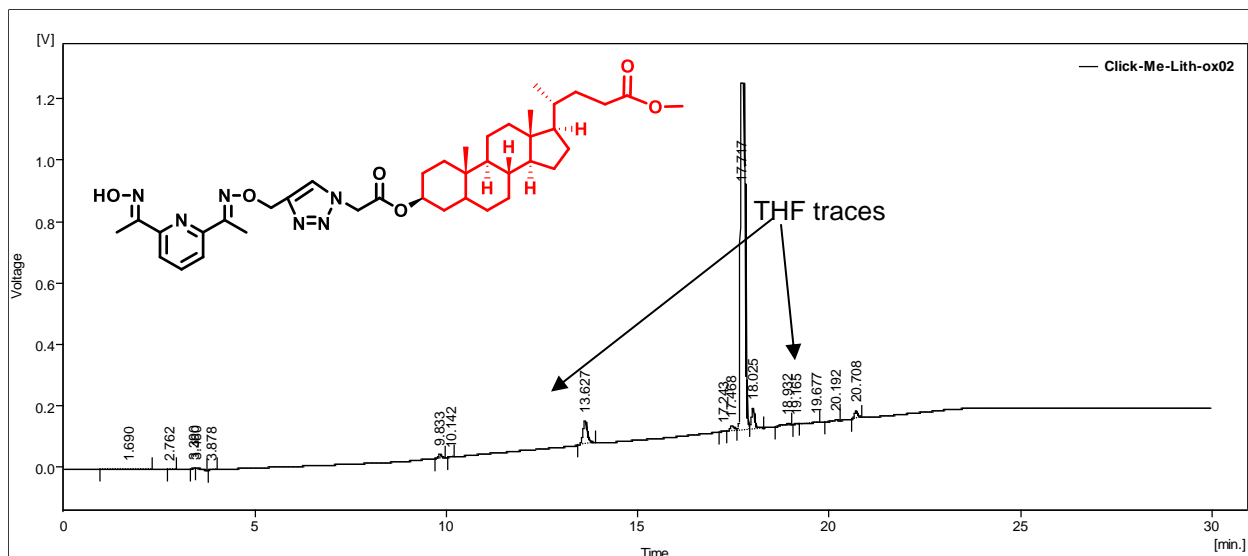
Compound (19) after purification using preparative HPLC, the compound was found as a major peak at 17.717 min., the method was run as 5-95% THF in water over 30 minutes followed by isocratic elution for a further 30 minutes. Data was recorded at 230 nm.
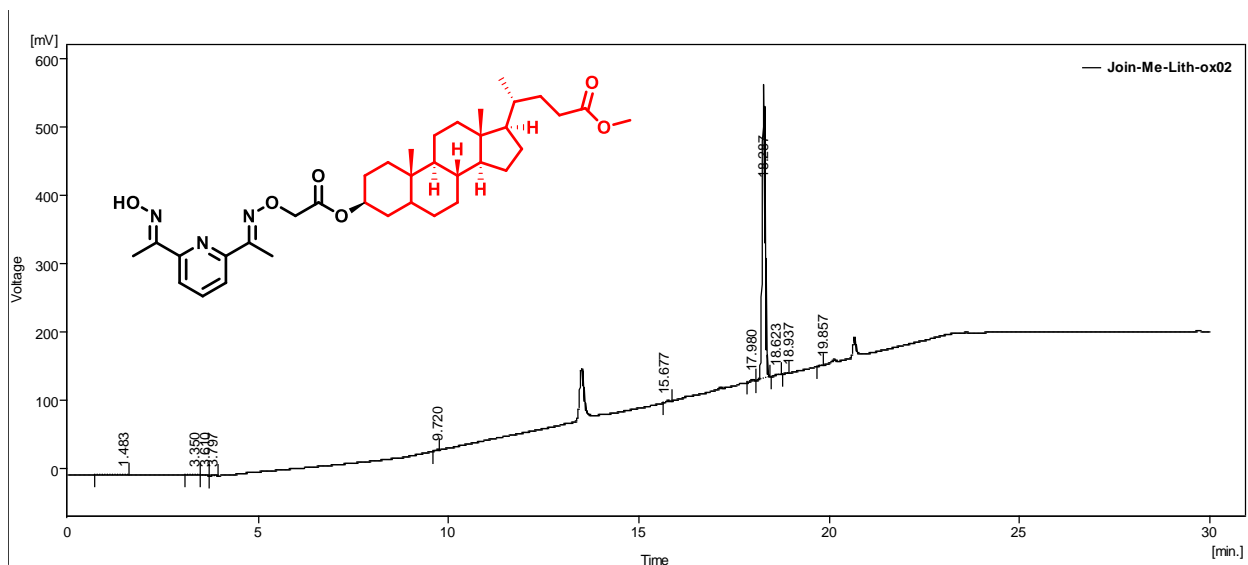
Compound (11) after purification using preparative HPLC, the compound was found as a major peak at 18.287 min., the method was run as 5-95% THF in water over 30 minutes followed by isocratic elution for a further 30 minutes. Data was recorded at 230 nm.
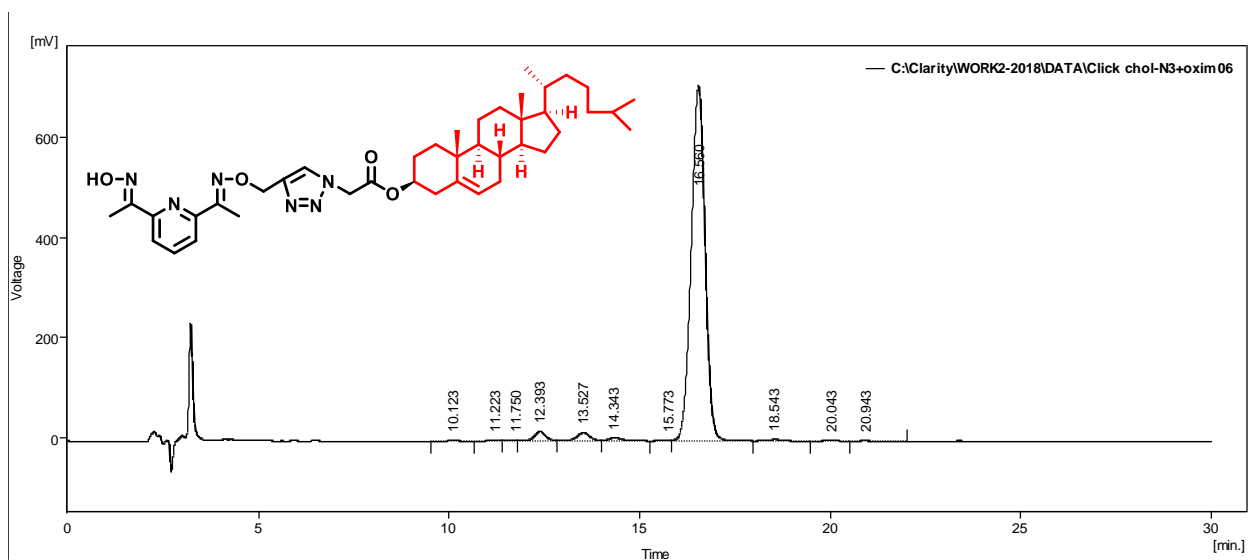
Compound (17) before purification using preparative HPLC, the compound was found as a major peak at 16.560 min., the method was run as 5-95% THF in water over 30 minutes followed by isocratic elution for a further 30 minutes. Data was recorded at 230 nm.
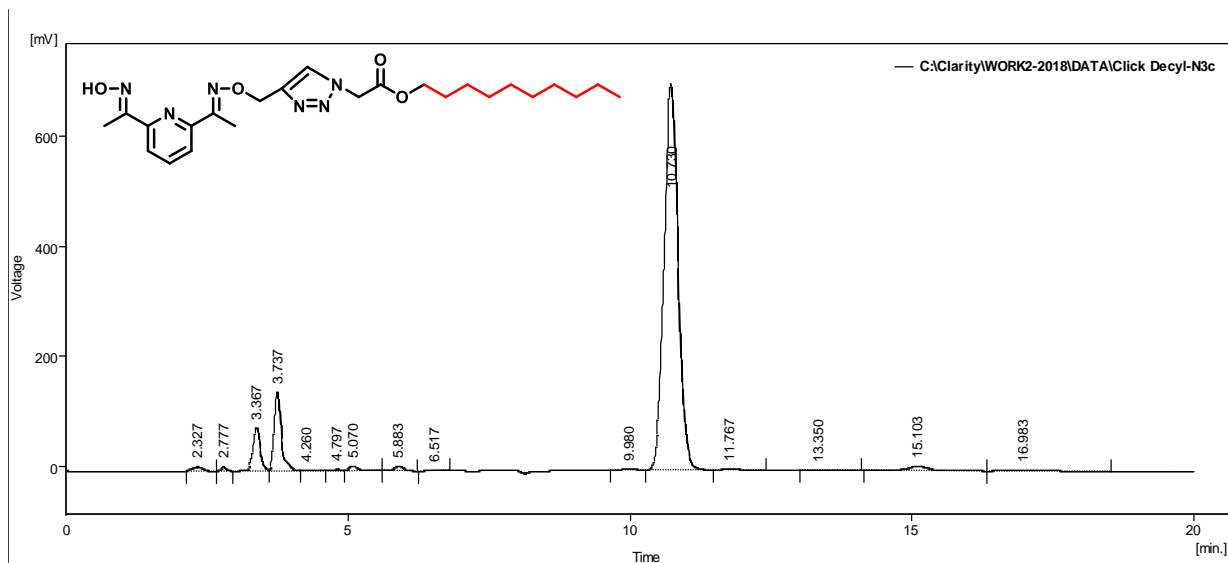
Compound (21) before purification using preparative HPLC, the compound was found as a major peak at 10. 730 min., the method was run as 5-95% THF in water over 30 minutes followed by isocratic elution for a further 30 minutes. Data was recorded at 230 nm.
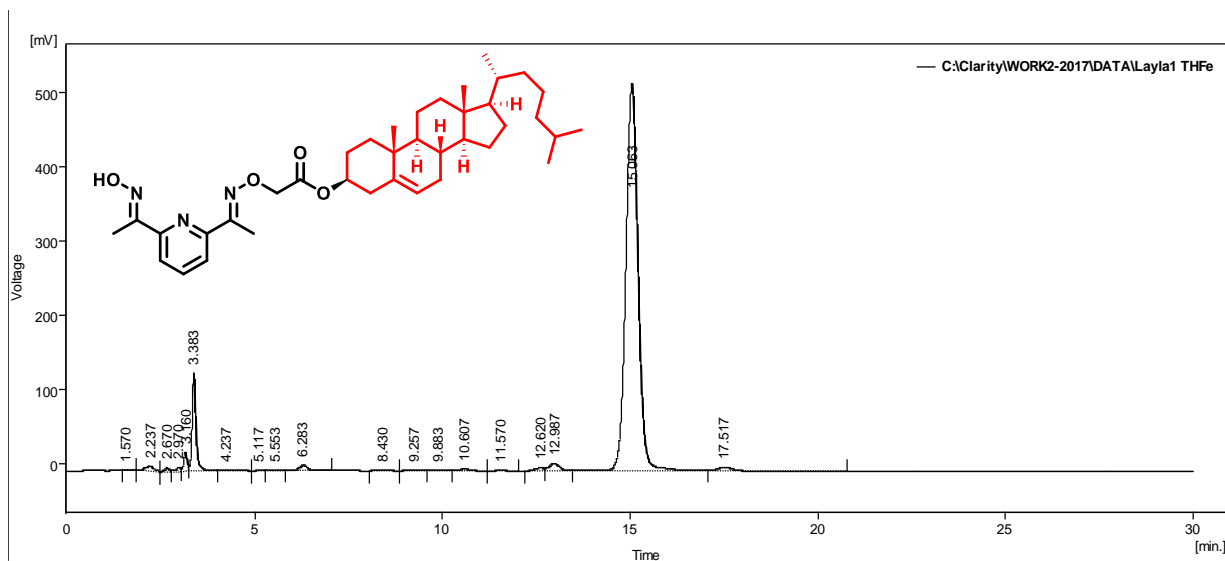
Compound (10) before purification using preparative HPLC, the compound was found as a major peak at 15.063 min., the method was run as 5-95% THF in water over 30 minutes followed by isocratic elution for a further 30 minutes. Data was recorded at 230 nm
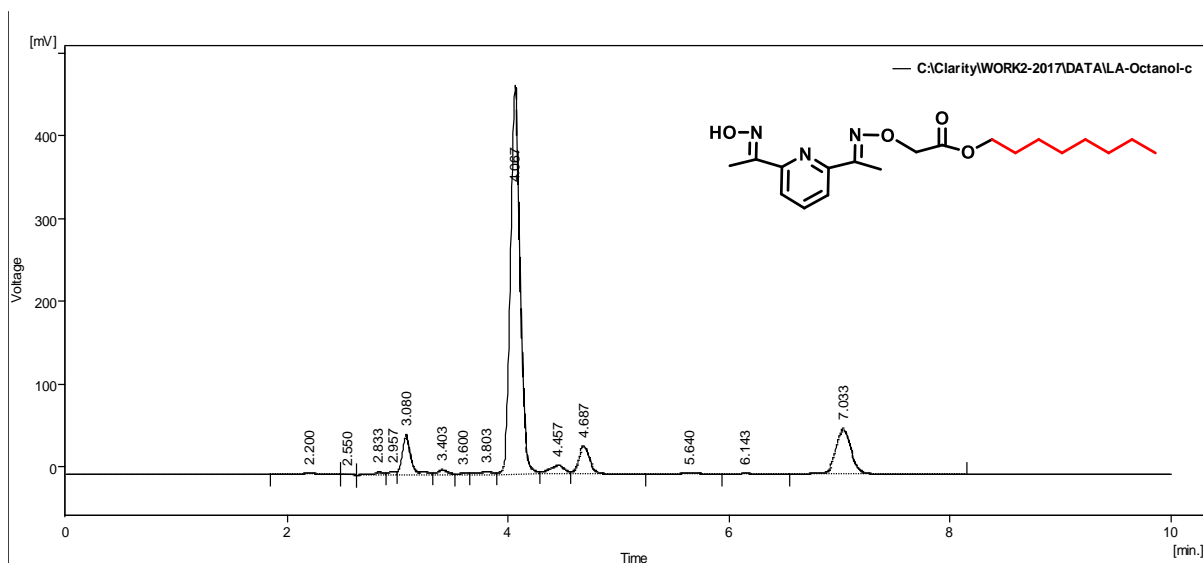
Compound (12) before purification using preparative HPLC, the compound was found as a major peak at 4.067 min., the method was run as 5-95% THF in water over 30 minutes followed by isocratic elution for a further 30 minutes. Data was recorded at 230 nm
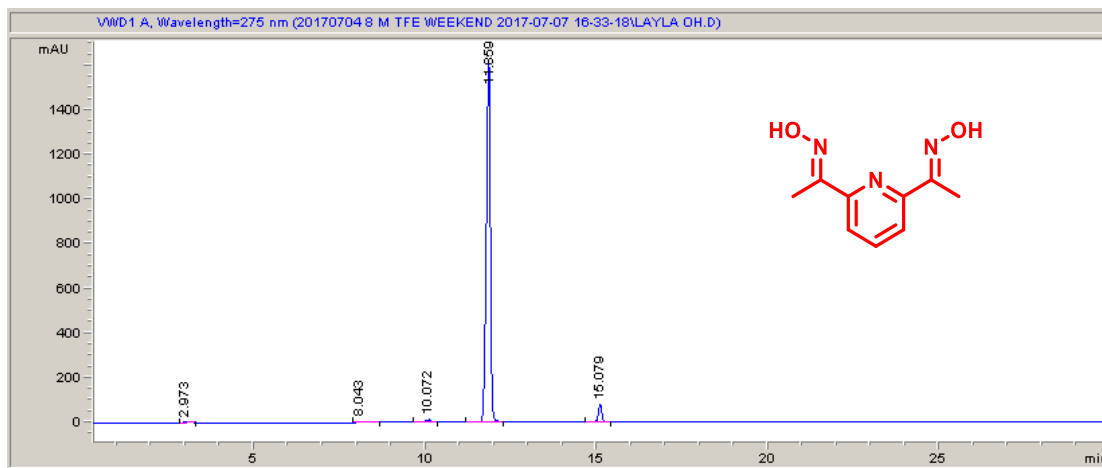
#	Time	Area	Height	Width	Area%	Symmetry
1	2.973	58	4.7	0.1814	0.408	0
2	8.043	86.4	6.7	0.1707	0.609	0.246
3	10.072	127.4	12.1	0.1414	0.897	2.426
4	11.859	13299.8	1629.9	0.1229	93.671	1.416
5	15.079	577.6	78.9	0.1131	4.068	1.045
6	74.21	49.1	2.1	0.3257	0.346	0.92

The compound was identified at 11.859 minutes as one single peak. The method was run as 5-95% ACN in water over 30 minutes followed by isocratic elution for a further 30 minutes. Data were recorded at 275 nm., 0.01 % v/v TFA was added to both mobile phase solvents.
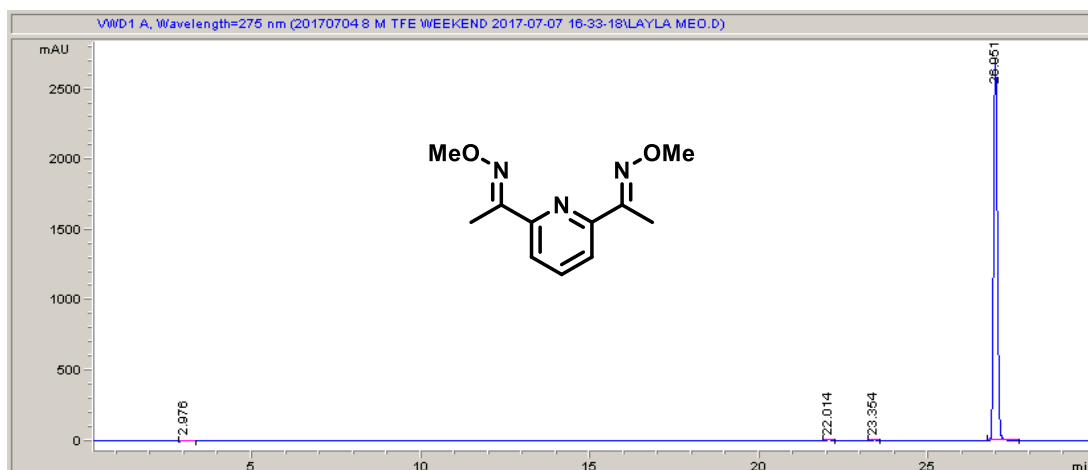
#	Time	Area	Height	Width	Area%	Symmetry
1	2.976	119.9	7.7	0.2151	0.571	0.349
2	22.014	43.4	6.2	0.1088	0.207	0.826
3	23.354	30.9	4.2	0.1144	0.147	0.816
4	26.951	20738.6	2704.4	0.1215	98.836	0.837
5	74.2	50.2	2.2	0.3215	0.239	0.903

The compound was identified at 26.951 minutes as one single peak. The method was run as 5-95% ACN in water over 30 minutes followed by isocratic elution for a further 30 minutes. Data were recorded at 275 nm., 0.01 % v/v TFA was added to both mobile phase solvents.

VWD1 A, Wavelength=275 nm (20170721 MATT AND LAYLA 2017-07-21 15-09-18\LAYLA ASYMMETRIC.D)
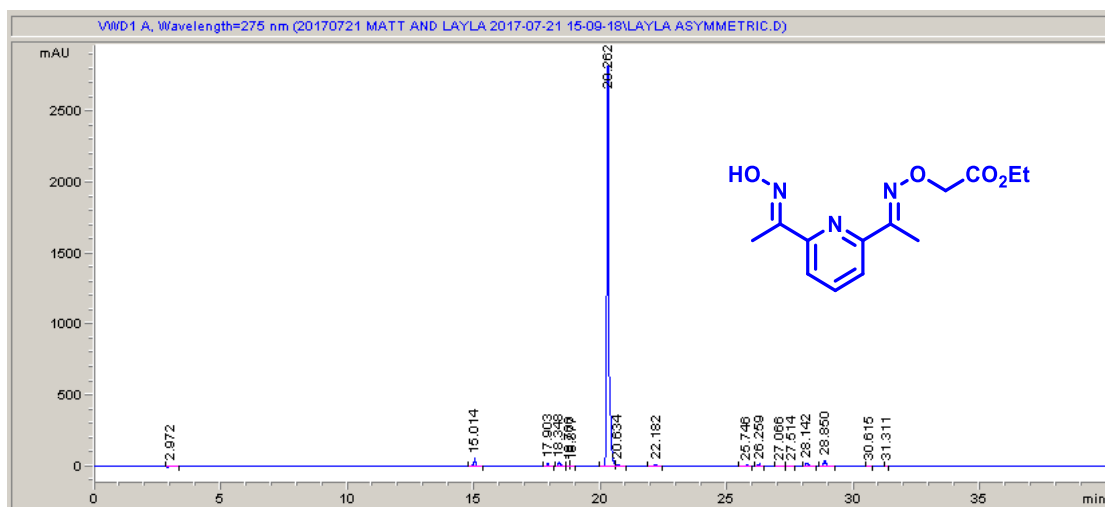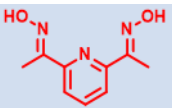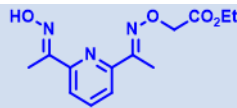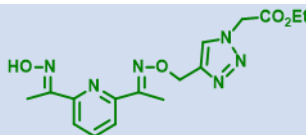
#	Time	Area	Height	Width	Area%	Symmetry
1	2.972	69.4	4.9	0.2013	0.313	0.259
2	15.014	414	58.6	0.1087	1.868	0.944
3	17.903	123.9	20.7	0.0932	0.559	0.836
4	18.348	162.8	26.8	0.0928	0.735	0.823
5	18.76	42.1	7.2	0.0889	0.190	0.98
6	18.877	33.3	5.8	0.0865	0.150	0.801
7	20.262	19951.2	2831.7	0.1055	90.040	0.653
8	20.634	104.7	11.8	0.1212	0.472	0.307
9	22.182	139.8	15.5	0.1284	0.631	1.368
10	25.746	79.1	8.6	0.1464	0.357	0.693
11	26.259	124.8	19.1	0.0995	0.563	0.802
12	27.066	20.3	2.4	0.1209	0.091	0.739
13	27.514	23.4	2	0.1553	0.106	0.706
14	28.142	147.5	21.3	0.1041	0.666	0.756
15	28.85	263	40.2	0.0983	1.187	0.794
16	30.615	11.2	1.8	0.0938	0.050	0.786
17	31.311	10.6	1.8	0.0892	0.048	0.877
18	42.393	390.3	4.4	1.0824	1.761	0.616
19	74.165	46.7	1.9	0.3456	0.211	0.925

The compound was observed at 20.262 min in good purity. No major impurities observed. The method was run as 5-95% ACN in water over 30 minutes followed by isocratic elution for a further 30 minutes. Data were recorded at 275 nm., 0.01 % v/v TFA was added to both mobile phase solvents.
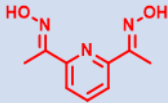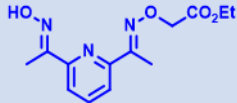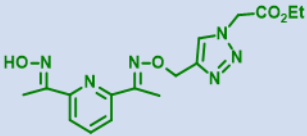
7.8   Rate Constants for Chapter Two

ZnCl$_2$ Concentration (mM)	k_{obs} (s^{-1})		
1.00	1.0×10^{-2}	1.6×10^{-3}	$1.4 \pm 0.4 \times 10^{-2}$
0.80	9.6×10^{-3}	1.7×10^{-3}	$1.1 \pm 0.03 \times 10^{-2}$
0.50	9.2×10^{-3}	1.3×10^{-3}	$8.3 \pm 0.1 \times 10^{-3}$
0.20	8.2×10^{-3}	7.0×10^{-4}	$4.8 \pm 0.4 \times 10^{-3}$
0.10	6.0×10^{-3}	4.2×10^{-4}	$2.8 \pm 0.2 \times 10^{-3}$
0.04	3.3×10^{-3}	2.1×10^{-4}	$1.3 \pm \times 10^{-3}$
0.00	2.4×10^{-5}	8.4×10^{-5}	3.4×10^{-6}

Data for Figure 2-12 (with sulfonate pyrine subs.), red data are average of two experiments

ZnCl$_2$ Concentration (mM)	k_{obs} (s^{-1})		
1.00	$7.4 \pm 0.4 \times 10^{-4}$	3.9×10^{-4}	1.9×10^{-3}
0.80	$7.8 \pm 0.6 \times 10^{-4}$	3.6×10^{-4}	1.8×10^{-3}
0.50	$8.6 \pm 0.5 \times 10^{-4}$	2.3×10^{-3}	1.4×10^{-3}
0.20	$9.3 \pm 0.4 \times 10^{-4}$	1.4×10^{-4}	7.2×10^{-4}
0.10	$8.2 \pm 0.6 \times 10^{-4}$	7.9×10^{-5}	4.2×10^{-4}
0.04	$4.8 \pm 0.2 \times 10^{-4}$	4.2×10^{-5}	2.1×10^{-4}
0.00	1.9×10^{-5}	7.8×10^{-6}	9.2×10^{-5}

Data for Figure 2-13 (with PNPA), red data are average of two experiments

Conc. of the Ligand (mM)	k_{obs} (s^{-1})		
0.20	7.43×10^{-4}	1.34×10^{-4}	1.04×10^{-3}
0.10	5.29×10^{-4}	5.34×10^{-5}	5.74×10^{-4}
0.07	4.20×10^{-4}	3.17×10^{-5}	3.25×10^{-4}
0.04	2.98×10^{-4}	1.65×10^{-5}	1.59×10^{-4}
0.02	2.49×10^{-4}	7.06×10^{-6}	4.84×10^{-4}

Data for Figure 2-18

pH	Conc. 0.2 mM		Conc. 0.02 mM	
	k_{obs} (s^{-1})	Log k_{obs}	k_{obs} (s^{-1})	Log k_{obs}
7.20	1.22×10^{-3}	-2.9132	9.0×10^{-5}	-4.0458
7.30	1.39×10^{-3}	-2.8562	1.00×10^{-4}	-4.0000
7.40	1.49×10^{-3}	-2.8283	1.20×10^{-4}	-3.9208
7.43	1.62×10^{-3}	-2.7913	1.51×10^{-4}	-3.8210
7.54	1.81×10^{-3}	-2.7419	1.89×10^{-4}	-3.7228
7.60	2.29×10^{-3}	-2.6411	3.36×10^{-4}	-3.4739
7.80	2.26×10^{-3}	-2.6469	3.29×10^{-4}	-3.4827
8.00	2.37×10^{-3}	-2.6257	3.44×10^{-4}	-3.4634

Data for Figure 2-19

Chapter 8 -   References

1.   Tian, W. J., Sasaki, Y., Fan, S. Di & Kikuchi, J. I. Switching of Enzymatic Activity through Functional Connection of Molecular Recognition on Lipid Bilayer Membranes. *Supramol. Chem.* **17**, 113–119 (2005).

2.   MacKinnon, R. Potassium Channels and the Atomic Basis of Selective Ion Conduction. *Angew. Chemie - Int. Ed.* **43**, 4265–4277 (2004).

3.   Barton, P., Hunter, C. A., Potter, T. J., Webb, S. J. & Williams, N. H. Transmembrane Signalling. **41**, 3878–3881 (2002).

4.   Davis, J. T., Okunola, O. & Quesada, R. Recent Advances in the Transmembrane Transport of Anions. *Chem. Soc. Rev.* **39**, 3843–3862 (2010).

5.   Pande, A. H., Qin, S. & Tatulian, S. A. Membrane Fluidity is a Key Modulator of Membrane Binding, Insertion, and Activity of 5-Lipoxygenase. *Biophys. J.* **88**, 4084–4094 (2005).

6.   Nomura, R., Inuo, C., Takahashi, Y., Asano, T. & Fujimoto, T. Two-Dimensional Distribution of G(i2α) in the Plasma Membrane: A Critical Evaluation by Immunocytochemistry. *FEBS Lett.* **415**, 139–144 (1997).

7.   Dacosta, C. J. B., Ogrel, A. A., McCardy, E. A., Blanton, M. P. & Baenziger, J. E. Lipid-Protein Interactions at the Nicotinic Acetylcholine Receptor. A Functional Coupling between Nicotinic Receptors and Phosphatidic Acid-Containing Lipid Bilayers. *J. Biol. Chem.* **277**, 201–208 (2002).

8.   Sharman, G. J. *et al.* The Roles of Dimerization and Membrane Anchoring in Activity of Glycopeptide Antibiotics Against Vancomycin-Resistant Bacteria. *J. Am. Chem. Soc.* **119**, 12041–12047 (1997).

9.   Pierce, K. L., Premont, R. T. & Lefkowitz, R. J. Signalling: Seven-Transmembrane Receptors. *Nat. Rev. Mol. Cell Biol.* **3**, 639–650 (2002).

10. Tamir, I. & Cambier, J. C. Antigen Receptor Signaling: Integration of Protein Tyrosine Kinase Functions. *Oncogene* **17**, 1353–64 (1998).

11. Levit, M. N., Liu, Y. & Stock, J. B. Stimulus Response Coupling in Bacterial Chemotaxis: Receptor Dimers in Signalling Arrays. *Mol. Microbiol.* **30**, 459–466 (1998).

12. Voskuhl, J. & Ravoo, B. J. Molecular Recognition of Bilayer Vesicles. *Chem. Soc. Rev.* **38**, 495–505 (2009).

13. Ichihashi, N. & Yomo, T. Positive Roles of Compartmentalization in Internal Reactions. *Curr. Opin. Plant Biol.* **22**, 93–100 (2014).

14. Bansho, Y. *et al.* Importance of Parasite RNA Species Repression for Prolonged Translation-Coupled RNA Self-Replication. *Chem. Biol.* **19**, 478–487 (2012).

15. Rasmussen, S., Chen, L., Nilsson, M. & Abe, S. Bridging Nonliving and Living Matter. *Artif. Life* **9**, 269–316 (2003).

16. Matsuura, T. *et al.* Effects of Compartment Size on the Kinetics of Intracompartmental Multimeric Protein Synthesis. *ACS Synth. Biol.* **1**, 431–437 (2012).

17. Grochmal, A., Prout, L., Makin-Taylor, R., Prohens, R. & Tomas, S. Modulation of Reactivity in the Cavity of Liposomes Promotes the Formation of Peptide Bonds. *J. Am. Chem. Soc.* **137**, 12269–12275 (2015).

18. Palivan, C. G., Fischer-Onaca, O., Delcea, M., Itel, F. & Meier, W. Protein–Polymer Nanoreactors for Medical Applications. *Chem. Soc. Rev.* **41**, 2800–2823 (2012).

19. Balaram, P. Synthesizing Life. *Curr. Sci.* **85**, 1509–1510 (2003).

20. Gruber, B. Functional Lipid Membranes : Bio-Inspired Nanomaterials for Sensing and Catalysis. *Dissertation* (Regensburg, 2012).

21. Song, Y., Han, X., Guo, X., Zeng, Q. & Jiang, F. Metallovesicular Catalytic Hydrolysis of *p*-Nitrophenyl Picolinate Catalyzed by Zinc(II) Complexes of Pyridyl Ligands in Vesicular Solution. *Colloids Surfaces, A Physicochem. Eng. Asp.* **392**, 110–115 (2011).

22. Pintre, I. C. & Webb, S. J. *Binding and Reactivity at Bilayer Membranes. Advances in Physical Organic Chemistry* vol. 47 (Elsevier Ltd., 2013).

23. Helmut Ringsdorf, Bernhard Schlarb, and J. V. Molecular Architecture and Function of Polymeric Oriented Systems: Models for the Study of Organization, Surface Recognition, and Dynamics of Biomembranes. *Angew. Chem.* **27**, 113–158 (1988).

24. Moss, A. Imidazole Mediated Acylation of Cholesterol in Functional Vesicles : A Simple Analogue of Lecithin:Cholesterol Acyltransferase. *Tetrahedron Lett.* **30**, No.37, 4905–4908 (1989).

25. Weijnen, J. G. J. & Engbersen, J. F. J. Hydrolysis of 4-Nitrophenyl Esters of Picolinic Acid and N-protected Amino Acids by Metalloenzyme Models in Vesicular Assemblies. *Recl. Trav. Chim. Pays-Bas* **112**, 525–530 (1993).

26. Gruber, B. & König, B. Self-Assembled Vesicles with Functionalized Membranes. *Chem. - A Eur. J.* **19**, 438–448 (2013).

27. Singer, S. J. & Nicolson, G. L. The Fluid Mosaic Model of the Structure of Cell Membranes. *Science (80-.).* **175**, 720–731 (1972).

28. Schneck, E., Sedlmeier, F. & Netz, R. R. Hydration Repulsion between Biomembranes Results from an Interplay of Dehydration and Depolarization. *Proc. Natl. Acad. Sci. U. S. A.* **109**, 14405–14409 (2012).

29. Finean, J. B. *Membranes and their Cellular Functions*. (Blackwell Scientific Publications, 1984).

30. Rawicz, W., Olbrich, K. C., Mcintosh, T., Needham, D. & Evans, E. Effect of Chain Length and Unsaturation on Elasticity of Lipid Bilayers. *Biophys. J.* **79**, 328–339 (2000).

31. Corvera, E., Mouritsen, O. G., Singer, M. A. & Zuckermann, M. J. The Permeability and the Effect of Acyl-Chain Length for Phospholipid Bilayers Containing Cholesterol: Theory and Experiment. *BBA - Biomembr.* **1107**, 261–270 (1992).

32. Needham, D. & Nunn, R. S. Elastic Deformation and Failure of Lipid Bilayer Membranes Containing Cholesterol. *Biophys. J.* **58**, 997–1009 (1990).

33. Bhattacharya, Santanu, S. H. Interactions between Cholesterol and Lipids in Bilayer Membranes. Role of Lipid Headgroup and Hydrocarbon Chain-Backbone Linkage. *Biochim. Biophys. Acta* **1467**, 39–53 (2000).

34. Boal, D. H. *Mechanics of the Cell*. (Cambridge University Press, 2012).

35. Rubenstein, J. hosphatidylcholines. L., Smith, B. A. & McConnell, H. M. Lateral Diffusion in Binary Mixtures of Cholesterol and Phosphatidylcholines. *Proc. Natl. Acad. Sci. U. S. A.* **76**, 15–18 (1979).

36. Homan, R. & Pownall, H. J. Transbilayer Diffusion of Phospholipids: Dependence on Headgroup Structure and Acyl Chain Length. *BBA - Biomembr.* **938**, 155–166 (1988).

37. Wimley, W. C. & Thompson, T. E. Transbilayer and Interbilayer Phospholipid Exchange in Dimyristoylphosphatidylcholine/Dimyristoylphosphatidylethanolamine Large Unilamellar Vesicles. *Biochemistry* **30**, 1702–1709 (1991).

38. Gurtovenko, A. A. & Vattulainen, I. Molecular Mechanism for Lipid Flip-Flops. *J. Phys. Chem. B* **111**, 13554–13559 (2007).

39. Dietrich, C., Volovyk, Z. N., Levi, M., Thompson, N. L. & Jacobson, K. Partitioning of Thy-1, GM1, and Cross-Linked Phospholipid Analogs into Lipid Rafts Reconstituted in Supported Model Membrane Monolayers. *Proc. Natl. Acad. Sci. U. S. A.* **98**, 10642–10647 (2001).

40. Janmey, P. A. & Kinnunen, P. K. J. Biophysical Properties of Lipids and Dynamic Membranes. *Trends Cell Biol.* **16**, 538–546 (2006).

41. Fahy, E., Cotter, D., Sud, M. & Subramaniam, S. Lipid Classification, Structures and Tools. *Biochim. Biophys. Acta - Mol. Cell Biol. Lipids* **1811**, 637–647 (2011).

42. Sud, M. *et al.* LMSD: LIPID MAPS Structure Database. *Nucleic Acids Res.* **35**, 527–532 (2007).

43. Sych, T., Mély, Y. & Römer, W. Lipid Self-Assembly and Lectin-Induced Reorganization of the Plasma Membrane. *Philos. Trans. R. Soc. B Biol. Sci.* **373**, (2018).

44. Fong, W. K. *et al.* Understanding the Photothermal Heating Effect in Non-Lamellar Liquid Crystalline Systems, and the Design of New Mixed Lipid Systems for Photothermal On-Demand Drug Delivery. *Phys. Chem. Chem. Phys.* **16**, 24936–24953 (2014).

45. Kugimiya, S., Lazrak, T., Blanchard-Desce, M. & Lehn, J.-M. Electron Conduction Across Vesicular Bilayer Membranes Induced by a Caroviologen Molecular Wire. *J. Chem. Soc. Chem. Commun.* 1179–1182 (1991).

46. Dijkstra, H. P. *et al.* Transmission of Binding Information Across Lipid Bilayers. *Chem. Eur. J.* **13**, 7215–7222 (2007).

47. Heldin, C. & Ericsson, J. RIPping Tyrosine Kinase Receptors Apart. *Science (80).* **294**, 2111–2113 (2001).

48. Sasaki, D. Y. Control of Membrane Structure and Organization through Chemical Recognition. *Cell Biochem. Biophys.* **39**, 145–161 (2003).

49. Marchi-Artzner, V., Brienne, M. J., Gulik-Krzywicki, T., Dedieu, J. C. & Lehn, J. M. Selective Complexation and Transport of Europium Ions at the Interface of Vesicles. *Chem. - A Eur. J.* **10**, 2342–2350 (2004).

50. Jose, D. A., Ghosh, A. & Schiller, *A. Supramolecular Receptors for the Recognition of Bioanalytes. Discovering the Future of Molecular Sciences* (editor Pignataro, B.) 1–30 (Wiley-VCH Verlag GmbH & Co. KGaA, 2014).

51. Ariga, K., Nakanishi, T. & Michinobu, T. Immobilization of Biomaterials to Nano-assembled Films (Self-assembled Monolayers, Langmuir-Blodgett Films, and Layer-by-Layer Assemblies) and Their Related Functions. *J. Nanosci. Nanotechnol.* **6**, 2278–2301 (2006).

52. Lehn, J.-M. *Supramolecular Chemistry and Concepts and Perspectives. Proceedings of the National Academy of Sciences of the United States of America* (Wiley-VCH Verlag GmbH, Weinheim, Cambridge, 1995).

53. Mathews C. K, and Holde. K. E. V. *Biochemistry*, second edition (1996).

54. Müller-Dethlefs, K. & Hobza, P. Noncovalent Interactions: A Challenge for Experiment and Theory. *Chem. Rev.* **100**, 143–168 (2000).

55. Bianchi, A., Bowman-James, K., and Garcia-Espana, E. *Supermolecular Chemistry of Anions*. (Wiley-VCH Verlag GmbH, 1997).

56. Banerjee, S., Bhuyan, M. & König, B. Tb(III) Functionalized Vesicles for Phosphate Sensing: Membrane Fluidity Controls the Sensitivity. *Chem. Commun.* **49**, 5681 (2013).

57.   Ambrosi, G. *et al.* A Macrocyclic Ligand as Receptor and Zn(II)-Complex Receptor for Anions in Water: Binding Properties and Crystal Structures. *Chem. Eur. J.* **17**, 1670–82 (2011).

58.   Das, P., Bhattacharya, S., Mishra, S. & Das, A. Zn(II) and Cd(II)-based Complexes for Probing the Enzymatic Hydrolysis of $Na_4P_2O_7$ by Alkaline Phosphatase in Physiological Conditions. *Chem. Commun.* **47**, 8118–8120 (2011).

59.   Hargrove, A. E., Nieto, S., Zhang, T., Sessler, J. L. & Anslyn, E. V. Artificial Receptors for the Recognition of Phosphorylated Molecules. *Chem. Rev.* **111**, 6603–6782 (2011).

60.   Singer, J. Intercellular Communication and Cell-cell Adhesion. *Science (80).* **255**, 1671–1677 (1992).

61.   Tolar, P., Hanna, J., Krueger, P. D. & Pierce, S. K. The Constant Region of the Membrane Immunoglobulin Mediates B Cell-Receptor Clustering and Signaling in Response to Membrane Antigens. *Immunity* **30**, 44–55 (2009).

62.   Wang, X., Mart, R. J. & Webb, S. J. Vesicle Aggregation by Multivalent Ligands: Relating Crosslinking Ability to Surface Affinity. *Org. Biomol. Chem.* **5**, 2498–2505 (2007).

63.   Gruber, B., Kataev, E., Aschenbrenner, J., Stadlbauer, S. & König, B. Vesicles and Micelles from Amphiphilic Zinc(II)-cyclen Complexes as Highly Potent Promoters of Hydrolytic DNA Cleavage. *J. Am. Chem. Soc.* **133**, 20704–20707 (2011).

64.   Gruber, B., Balk, S., Stadlbauer, S. & König, B. Dynamic Interface Imprinting: High-Affinity Peptide Binding Sites Assembled by Analyte-induced Recruiting of Membrane Receptors. *Angew. Chemie - Int. Ed.* **51**, 10060–10063 (2012).

65.   Kyung, K. I. M. S., Dong Hoon, L. E. E., Hong, J. I. N. & Yoon, J. Chemosensors for Pyrophosphate. *Acc. Chem. Res.* **42**, 23–31 (2009).

66. Nguyen, B. T. & Anslyn, E. V. Indicator-Displacement Assays. *Coord. Chem. Rev.* **250**, 3118–3127 (2006).

67. Gruber, B., Stadlbauer, S., Woinaroschy, K. & König, B. Luminescent Vesicular Receptors for the Recognition of Biologically Important Phosphate Species. *Org. Biomol. Chem.* **8**, 3704–3714 (2010).

68. Gruber, B. *et al.* Modular Chemosensors from Self-Assembled Vesicle Membranes with Amphiphilic Binding Sites and Reporter Dyes. *Angew. Chemie Int. Ed.* **49**, 7125–7128 (2010).

69. Garavito, R. M. & Ferguson-Miller, S. Detergents as Tools in Membrane Biochemistry. *J. Biol. Chem.* **276**, 32403–32406 (2001).

70. Akbarzadeh, A., Rezaei-sadabady, R., Davaran, S., Joo, S. W. & Zarghami, N. Liposome : Classification, Preparation, and Applications. *Nanoscale Res. Lett.* **8(1)**, 1–9 (2013).

71. Stevenson, S. A. & Blanchard, G. J. Investigating Internal Structural Differences between Micelles and Unilamellar Vesicles of Decanoic Acid/Sodium Decanoate. *J. Phys. Chem. B* **110**, 13005–13010 (2006).

72. Schröter, J. A. *et al.* Monolayer Properties of a New Family of Amphiphiles with an Unusual Head-Group Topology. *Langmuir* **13**, 796–800 (1997).

73. Griffiths, P. C., Fallis, I. A., Tatchell, T., Bushby, L. & Beeby, A. Aqueous Solutions of Transition Metal Containing Micelles. *Adv. Colloid Interface Sci.* **144**, 13–23 (2008).

74. Zhang, J., Meng, X.-G., Zeng, X.-C. & Yu, X.-Q. Metallomicellar Supramolecular Systems and Their Applications in Catalytic Reactions. *Coord. Chem. Rev.* **253**, 2166–2177 (2009).

75. Chin, J. Developing Artificial Hydrolytic Metalloenzymes by a Unified Mechanistic Approach. *Acc. Chem. Res.* **24**, 145–152 (1991).

76. Hermann Dugas and Christopher Penney. *Bioorganic Chemistry A Chemical Approach to Enzyme Action.* (Springer-Varlay, 1981).

77. Chin, J. Developing Artificial Hydrolytic Metalloenzymes by a Unified Mechanistic Approach. *Acc. Chem. Res.* **24**, 145 (1991).

78. Koike, T. & Kimura, E. Roles of Zinc(II) ion in Phosphatases. A Model Study with Zinc(II)-macrocyclic Polyamine Complexes. *J. Am. Chem. Soc.* **113**, 8935–8941 (1991).

79. Mancin, F., Tecilla, P. & Tonellato, U. Metallomicelles Made of Ni (II) and Zn (II) Complexes of 2-Pyridinealdoxime-Based Ligands as Catalyst of the Cleavage of Carboxylic Acid Esters. *Langmuir* **16**, 227–233 (2000).

80. Polyzos, A., Hughes, A. B. & Christie, J. R. Catalysis of Aryl Ester Hydrolysis in the Presence of Metallomicelles Containing a Copper(II) Diethylenetriamine Derivative. *Langmuir* **23**, 1872–1879 (2007).

81. Bhattacharya, S. & Kumari, N. Metallomicelles as Potent Catalysts for the Ester Hydrolysis Reactions in Water. *Coord. Chem. Rev.* **253**, 2133–2149 (2009).

82. Melhado, L. L. & Gutsche, C. D. Association Phenomena. 2. Catalysis of the Decomposition of Acetyl Phosphate by Chelate Micelles and by Amine-Ammonium Micelles. *J. Am. Chem. Soc.* **100**, 1850–1856 (1978).

83. Vizitiu, D., Kriste, A. G., Stewart Campbell, A. & Thatcher, G. R. J. Inhibition of Phosphatidylinositol-Specific Phospholipase C: Studies on Synthetic Substrates, Inhibitors and a Synthetic Enzyme. *J. Mol. Recognit.* **9**, 197–209 (1996).

84. Fallis, A., *Gemini Surfactant Synthesis, Interfacial and Solution-Phase Behavior, and Applications*. (MARCEL DEKKER, INC, NewYork 2013).

85. Qiu, L. G., Xie, A. J. & Shen, Y. H. Metallomicellar Catalysis: Hydrolysis of *p*-Nitrophenyl Picolinate Catalyzed by Cu(II) Complexes of Triazole-based Ligands in Cationic Gemini Surfactant Micelles. *J. Mol. Catal. A Chem.* **244**, 58–63 (2006).

86. Fendle, J. H. and W. L. H. Reactivity Control in Micelles and Surfactant Vesicles. Kinetics and Mechanism of Base-Catalyzed Hydrolysis of 5,5'-Dithiobis(2-nitrobenzoic acid) in Water, Hexadecyltrimethylammonium Bromide Micelles, and Dioctadecyldimethylammonium Chloride Surfactant. *J.Am.Chem.Soc* **103**, 5439–5447 (1981).

87. Fornasier, R., Milani, D., Scrimin, P. & Tonellato, U. Functional Micellar Catalysis. Part 8. Catalysis of the Hydrolysis of *p*-Nitrophenyl Picolinate by Metal-Chelating Micelles Containing Copper(II) or Zinc(II). *J. Chem. Soc. Perkin Trans. II,* 233 (1986).

88. Fuhrhop, J.-H. & Mathieu, J. Routes to Functional Vesicle Membranes without Proteins. *Angew. Chemie Int. Ed. English* **23**, 100–113 (1984).

89. Waichiro Tagaki, Kenji Ogino, Osamu Tanaka, Koji Machiya, Nobuyuki Kashihara, T. Y. Hydrolytic Metalloenzyme Models.Micellar Effect on the Activation of the Hydroxyl Groups of N-Alkyl-2-(hydroxymethyl)-Imidazole Ligands by Cu in the Transacylation of *p*-Nitrophenyl Picolinate. *Bull.Chem.Soc.Jpn.,* **64**, 74–80 (1991).

90. Sharma, R. *et al.* Degradation of Organophosphate Pesticides Using Pyridinium Based Functional Surfactants. *ACS Sustain. Chem. Eng.* **4**, 6962–6973 (2016).

91. Liu, Y., Meng, X. G., Li, J. M. & Li, X. H. Hydrolysis of Phosphodiester Catalyzed by Metallomicelles with Histidine Residue: Kinetics and Mechanism. *Colloids Surfaces A Physicochem. Eng. Asp.* **436**, 839–845 (2013).

92. Fornasier, R., Scrimin, P., Tecilla, P. & Tonellato, U. Bolaform and Classical Cationic Metallomicelles as Catalysts of the Cleavage of p-Nitrophenyl Picolinate. *J. Am. Chem. Soc.* **111**, 224–229 (1989).

93. Scrimin, P., Tecilla, P. & Tonellato, U. Metallomicelles as Catalysts of the Hydrolysis of Carboxylic and Phosphoric Acid Esters. *J.Org.Chem.* **56**, 161–166 (1991).

94. Fubin, J., Bingying, J., Yong, C., Xiaoqi, Y. & Xiancheng, Z. Metallomicellar Catalysis: Effects of Bridge-Connecting Ligands on the Hydrolysis of PNPP Catalyzed by Cu(II) Complexes of Ethoxyl-Diamine Ligands in Micellar Solution. *J. Mol. Catal. A Chem.* **210**, 9–16 (2004).

95. Gunnlaugsson, T., O'Brien, J. E. & Mulready, S. Glycine-alanine Conjugated Macrocyclic Lanthanide ion Complexes as Artificial Ribonucleases. *Tetrahedron Lett.* **43**, 8493–8497 (2002).

96. Li, F., Feng, F., Yu, L. & Xie, J. The Metallomicelle of Lanthanide Metal (Ce, La) Aza-Macrocyclic Complexes with a Carboxyl Branch: The Catalytic Activity and Mechanism in the Hydrolysis of a Phosphate Diester. *J. Solution Chem.* **43**, 1331–1343 (2014).

97. Shang, H., Yu, L., Li, S. & Xie, J. Activity of a New Metallomicelle Catalytic System on the Hydrolysis of Bis (4-nitrophenyl) Phosphate Ester. *J. Dispers. Sci. Technol.* **2691**, 411–417 (2014).

98. Cai, S. *et al.* Hydrolysis of BNPP Catalyzed by Metallomicelles Made of Pr(III) Complexes. *J. Dispers. Sci. Technol.* **35**, 93–97 (2014).

99. Fendler, J.H. *Membrane Memetic Chemistry*. (Wiley, NewYork, 1982).

100. Sissi, C. *et al.* Dinuclear Zn^{2+} Complexes of Synthetic Heptapeptides as Artificial Nucleases. *J. Am. Chem. Soc.* **123**, 3169–3170 (2001).

101. Yan, J. & Breslow, R. An Enzyme Mimic that Hydrolyzes an Unactivated Ester with Catalytic Turnover. *Tetrahedron Lett.* **41**, 2059–2062 (2000).

102. Kirby, A. J. Enzyme Mimics. *Angew Chem. Int. Ed. Engl.* **33**, 551–553 (1994).

103. Williams, N. H., Takasaki, B., Wall, M. & Chin, J. Structure and Nuclease Activity of Simple Dinuclear Metal Complexes: Quantitative Dissection of the Role of Metal Ions. *Acc. Chem. Res.* **32**, 485–493 (1999).

104. Liang, X., Campopiano, D. J. & Sadler, P. J. Metals in Membranes. *Chem. Soc. Rev.* **36**, 968–992 (2007).

105. Jiang, W. *et al.* Cleavage of Phosphate Diesters Mediated by Zn(II) Complex in Gemini Surfactant Micelles. *J. Colloid Interface Sci.* **311**, 530–536 (2007).

106. Mikkola, S. *et al.* The Mechanism of the Metal Ion Promoted Cleavage of RNA Phosphodiester Bonds Involves a General Acid Catalysis by the Metal Aquo Ion on the Departure of the Leaving Group. *J. Chem. Soc. Perkin Trans. 2* 1619–1626 (1999).

107. Molenveld, P., Engbersen, J. F. J. & Reinhoudt, D. N. Dinuclear Metallo-Phosphodiesterase Models: Application of Calix[4]arenes as Molecular Scaffolds. *Chem. Soc. Rev.* **29**, 75–86 (2000).

108. Moss, R. A. & Jiang, W. Lanthanide-Mediated Cleavages of Micellar Phosphodiesters. *Langmuir* **16**, 49–51 (2000).

109. Jiang, F. *et al.* Metallomicellar Catalysis: Hydrolysis of Phosphate Monoester and Phosphodiester by Cu(II), Zn(II) Complexes of Pyridyl Ligands in CTAB Micellar Solution. *J. Colloid Interface Sci.* **303**, 236–242 (2006).

110. Menger, F. M., Gan, L. H., Johnson, E. & Durst, D. H. Phosphate Ester Hydrolysis Catalyzed by Metallomicelles. *J. Am. Chem. Soc.* **109**, 2800 (1987).

111. Mancin, F., Scrimin, P. & Tecilla, P. Progress in Artificial Metallonucleases. *Chem. Commun.* **48**, 5545–5559 (2012).

112. Schroeder, G. K., Lad, C., Wyman, P., Williams, N. H. & Wolfenden, R. The Time Required for Water Attack at the Phosphorus Atom of Simple Phosphodiesters and of DNA. *Proc. Natl. Acad. Sci. U. S. A.* **103**, 4052–4055 (2006).

113. Korhonen, H., Mikkola, S. & Williams, N. H. The Mechanism of Cleavage and Isomerisation of RNA Promoted by an Efficient Dinuclear Zn [2+] Complex. *Chem. A Eur. J.* **18**, 659–670 (2012).

114. Brown, R. S. *et al.* Dinuclear Zn(II) Catalysts as Biomimics of RNA and DNA Phosphoryl Transfer Enzymes: Changing the Medium from Water to Alcohol Provides Enzyme-Like Rate Enhancements. *J. Phys. Org. Chem.* **23**, 1–15 (2010).

115. Manea, F., Houillon, F. B., Pasquato, L. & Scrimin, P. Nanozymes: Gold-Nanoparticle-Based Transphosphorylation Catalysts. *Angew. Chemie - Int. Ed.* **43**, 6165–6169 (2004).

116. Diez-Castellnou, M., Mancin, F. & Scrimin, P. Efficient Phosphodiester Cleaving Nanozymes Resulting from Multivalency and Local Medium Polarity Control. *J. Am. Chem. Soc.* **136**, 1158–1161 (2014).

117. Hay, R. W., Govan, N. & Parchment, K. E. A Metallomicelle Catalysed Hydrolysis of a Phosphate Triester, a Phosphonate Diester and O-Isopropyl Methylfluorophosphonate (Sarin). *Inorg. Chem. Commun.* **1**, 228–231 (1998).

118. Jiang, B. *et al.* Hydrolysis of *p*-Nitrophenyl Picolinate Catalyzed by Divalent Metal Ion Complexes Containing Imidazole Groups in Micellar Solution. *Colloids Surfaces A Physicochem. Eng. Asp.* **235**, 145–151 (2004).

119. Poznik, M. & König, B. Cooperative Hydrolysis of Aryl Esters on Functionalized Membrane Surfaces and in Micellar Solutions. *Org. Biomol. Chem.* **12**, 3175–3180 (2014).

120. Bunton, A., Fendler, E. J., Sepulveda, L. & Yang, K. Micellar-Catalyzed Hydrolysis of Nitrophenyl Phosphates. *J. Am. Chem. Soc.* **2806**, 5512–5518 (1968).

121. Grochmal, A., Ferrero, E., Milanesi, L. & Tomas, S. Modulation of In-Membrane Receptor Clustering upon Binding of Multivalent Ligands. *J. Am. Chem. Soc.* **135**, 10172–10177 (2013).

122. Melvin I. Simon, Strathmann, M. P. & Gautam, N. Diversity of G Proteins in Signal Transduction. *Science (80).* **252**, 802–808 (1991).

123. Schlessinger, J. Cell Signaling by Receptor Tyrosine Kinases. *Cell* **103**, 211–225 (2000).

124. Langton, M. J., Keymeulen, F., Ciaccia, M., Williams, N. H. & Hunter, C. A. Controlled Membrane Translocation Provides a Mechanism for Signal Transduction and Amplification. *Nat. Chem.* **9**, 426–430 (2017).

125. Langton, M. J., Williams, N. H. & Hunter, C. A. Recognition-Controlled Membrane Translocation for Signal Transduction Across Lipid Bilayers. *J. Am. Chem. Soc.* **139**, 6461–6466 (2017).

126. Langton, M. J., Scriven, L. M., Williams, N. H. & Hunter, C. A. Triggered Release from Lipid Bilayer Vesicles by an Artificial Transmembrane Signal Transduction System. *J. Am. Chem. Soc.* **139**, 15768–15773 (2017).

127. Xiancheng, Z., Yuanqin, Z., Xiaoqi, Y. & Anmin, T. Metallomicellar Catalysis. Cleavage of *p*-Nitrophenyl Picolinate in Copper(II) Coordinating N-Myristol-N-(B-hydroxyethyl)ethylenediamine in CTAB micelles. *Langmuir* **15**, 1621–1624 (1999).

128. Menger, F. M. & Portnoy, C. E. On the Chemistry of Reactions Proceeding inside Molecular Aggregates. *J. Am. Chem. Soc.* **89**, 4698–4703 (1967).

129. Moroi, Y. Distribution of Solubilizates among Micelles and Kinetics of Micelle-Catalyzed Reactions. *J. Phys. Chem* **84**, 2186–2190 (1980).

130. Lugo-González, J. C., Gómez-Tagle, P., Huang, X., M. Del Campo, J. & Yatsimirsky, A. K. Substrate Specificity and Leaving Group Effect in Ester Cleavage by Metal Complexes of an Oximate Nucleophile. *Inorg. Chem.* **56**, 2060–2069 (2017).

131. Mancin, F., Tecilla, P. & Tonellato, U. Activation of Oximic Nucleophiles by Coordination of Transition Metal Ions. *European J. Org. Chem.* **2000,** 1045–1050 (2000)

132. Singh, N., Karpichev, Y., Tiwari, A. K., Kuca, K. & Ghosh, K. K. Oxime Functionality in Surfactant Self-Assembly: An Overview on Combating Toxicity of Organophosphates. *J. Mol. Liq.* **208**, 237–252 (2015).

133. Morales-Rojas, H. & Moss, R. A. Phosphorolytic Reactivity of O-Iodosylcarboxylates and Related Nucleophiles. *Chem. Rev.* **102**, 2497–2521 (2002).

134. Soukup, O. *et al.* The Interaction of Standard Oxime Reactivators with Hemicholinium-3 Sensitive Choline Carriers. *Toxicol. Lett.* **212**, 315–319 (2012).

135. Davey, S. Analysing the α-Effect. *Nat. Chem.* **3**, 753–753 (2011).

136. Yatsimirsky, A. K., Gmez-Tagle, P., Escalante-Tovar, S. & Ruiz-Ramfrez, L. Kinetics and Mechanism of Ester Hydrolysis by Metal Complexes of 2,6-Diacetylpyridine Dioxime. *Inorganica Chim. Acta* **273**, 167–174 (1998).

137. Gómez-Tagle, P., Lugo-González, J. C. & Yatsimirsky, A. K. Oximate Metal Complexes Breaking the Limiting Esterolytic Reactivity of Oximate Anions. *Chem. Commun.* **49**, 7717–7719 (2013).

138. Buncel, E., Cannes, C., Chatrousse, A. P. & Terrier, F. Reactions of Oximate α-Nucleophiles with Esters: Evidence from Solvation Effects for Substantial Decoupling of Desolvation and Bond Formation. *J. Am. Chem. Soc.* **124**, 8766–8767 (2002).

139. Suh, J., Han, O. & Chang, B. Catalysis by Binuclear Zinc Ions in Ester Hydrolysis. *J. Am. Chem. Soc.* **108**, 1839–1842 (1986).

140. Satchell, D. P. & Satchell, R. S. Kinetic Studies of Metal Ion Catalysis of Heterolytic Reactions. *Annu. Reports Prog. Chem. Sect. A Phys. Inorg. Chem.* **75**, 25–48 (1978).

141. Nanjappan, P. & Czarnik, A. W. Metal Ion Catalyzed Reactions of Acrylonitrile, Acrylamide, and Ethyl Acrylate by way of Their Diels—Alder Cycloadducts. *J. Am. Chem. Soc.* **109**, 1826–1833 (1987).

142. Suh, J., Cheong, M., and Han, H. Multifunctional Catalysis by Metal Complexes. *Bioorg. Chem.* **12**, 188–196 (1984).

143. Suh, J. & Han, H. Zinc Ion-catalyzed Ester Hydrolysis of O-acetyl-2-acetylpyridineketoxime: Bimolecular Participation of Hydroxozinc(II) Ion. *Bioorg. Chem.* **12**, 177–187 (1984).

144. Suh, J., Cho, W. & Chung, S. Carboxypeptidase A-Catalyzed Hydrolysis of a-(Acylamino)cinnamoyl Derivatives of L-β-Phenyllactate and L-Phenylalaninate: Evidence for Acyl-Enzyme Intermediates. *J. Am. Chem. Soc.* **107**, 4530–4535 (1985).

145. Cappuccio, F. E., Suri, J. T., Cordes, D. B., Wessling, R. A. & Singaram, B. Evaluation of Pyranine Derivatives in Boronic Acid Based Saccharide Sensing: Significance of Charge Interaction Between Dye and Quencher in Solution and Hydrogel. *J. Fluoresc.* **14**, 521–533 (2004).

146. Wang, P. S. P., Nguyen, J. B. & Schepartz, A. Design and High-Resolution Structure of a β3-Peptide Bundle Catalyst. *J. Am. Chem. Soc.* **136**, 6810–6813 (2014).

147. M. Orama, H. Saarinen, J. K. Formation, Redox Structural Properties of Nickel. *Acta Chem. Scand.* **43**, 407–412 (1989).

148. Saarinen, H. & Orama, M. Equilibrium and Structural Studies on Metal Complexes of Oxime Ligands. Formation of Nickel(II) Complexes of Two Methyl-Substituted Pyridine Oxime Ligands in Aqueous Solution. *Acta Chemica Scandinavica* vol. 52 1209–1213 (1998).

149. Schäfer, B., Orbán, E., Kele, Z. & Tömböly, C. Tritium Labelling of a Cholesterol Amphiphile Designed for Cell Membrane Anchoring of Proteins. *J. Label. Compd. Radiopharm.* **58**, 7–13 (2015).

150. Doyle, E. L., Hunter, C. a, Phillips, H. C., Webb, S. J. & Williams, N. H. Cooperative Binding at Lipid Bilayer Membrane Surfaces. *J. Am.Chem.Soc.,* **125**, 4593–4599 (2003).

151. K.E. Suckling, H.A.F. Blair, G. S. B. I. F. C. and B. R. M. The Importance of The Phospholipid Bilayer and The Length of The Cholesterol Molecule in Membrane Structure. *Biochim. Biophys. Acta,* **551**, 10–21 (1979).

152. Mukai, M., Krause, M. R. & Regen, S. L. Peptide Recognition of Cholesterol in Fluid Phospholipid Bilayers. *J. Am. Chem. Soc.* **137**, 12518–12520 (2015).

153. Kikuchi, J. I., Ariga, K. & Ikeda, K. Signal Transduction Mediated by Artificial Cell-Surface Receptors: Activation of Lactate Dehydrogenase Triggered by Molecular Recognition and Phase Reorganization of Bile Acid Derivatives Embedded in a Synthetic Bilayer Membrane. *Chem. Commun.* 547–548 (1999)

154. Smondyrev, A. M. & Berkowitz, M. L. Structure of Dipalmitoylphosphatidylcholine/Cholesterol Bilayer at Low and High Cholesterol Concentrations: Molecular Dynamics Simulation. *Biophys. J.* **77**, 2075–2089 (1999).

155. Fuhrhop, J.-H. and Koning, J. Membrane and Molecular Assemblies: the Synkinetic Approach. (Royal Society of Chemistry, 1994).

156. Potter, T. J. Transmembrane Signalling. PhD thesis, (2002).

157. Findlay, H. E., Rutherford, N. G., Henderson, P. J. F. & Booth, P. J. Unfolding Free Energy of a Two-Domain Transmembrane Sugar Transport Protein. *Proc. Natl. Acad. Sci.* **107**, 18451–18456 (2010).

158. Charalambous, K., Miller, D., Curnow, P. & Booth, P. J. Lipid Bilayer Composition Influences Small Multidrug Transporters. *BMC Biochem.* **9**, 1–12 (2008).

159. Jose, D. A. & König, B. Polydiacetylene Vesicles Functionalized with N-Heterocyclic Ligands for Metal Cation Binding. *Org. Biomol. Chem.* **8**, 655–662 (2010).

160. Menger, F. M. & Azov, V. A. Cytomimetic Modeling in Which One Phospholipid Liposome Chemically Attacks Another. *J. Am. Chem. Soc.* **122**, 6492–6493 (2000).

161. Menger, F. M., Caran, K. L. & Seredyuk, V. A. Chemical Reaction between Colliding Vesicles. *Angew. Chemie - Int. Ed.* **40**, 3905–3907 (2001).

162. Hansen, M., Li, F., Sun, L. & König, B. Photocatalytic Water Oxidation at Soft Interfaces. *Chem. Sci.* **5**, 2683–2687 (2014).

163. Bizzigotti, G. O. Thiol-Disulfide Interchange Reaction between Ellman's Reagent (5,5′-Dithiobis(2-nitrobenzoic acid)) and Functionalized Thiol Vesicles. *J. Org. Chem.* **48**, 2598–2600 (1983).

164. Balk, S., Maitra, U. & König, B. Terbium(III)-Cholate Functionalized Vesicles as Luminescent Indicators for the Enzymatic Conversion of Dihydroxynaphthalene Diesters. *Chem. Commun.* **50**, 7852–7854 (2014).

165. Svobodová, H., Noponen, V., Kolehmainen, E. & Sievänen, E. Recent Advances in Steroidal Supramolecular Gels. *RSC Adv.* **2**, 4985–5007 (2012).

166. Chakrabarty, A., Maitra, U. & Das, A. D. Metal Cholate Hydrogels: Versatile Supramolecular Systems for Nanoparticle Embedded Soft Hybrid Materials. *J. Mater. Chem.* **22**, 18268–18274 (2012).

167. Nagy, P. Kinetics and Mechanisms of Thiol–Disulfide Exchange Covering Direct Substitution and Thiol Oxidation-Mediated Pathways. *Antioxid. Redox Signal.* **18**, 1623–1641 (2012).

168. Ohvo-Rekilä, H., Ramstedt, B., Leppimäki, P. & Peter Slotte, J. Cholesterol Interactions with Phospholipids in Membranes. *Prog. Lipid Res.* **41**, 66–97 (2002).

169. Homaei, A. A., Sajedi, R. H., Sariri, R., Seyfzadeh, S. & Stevanato, R. Cysteine Enhances Activity and Stability of Immobilized Papain. *Amino Acids* **38**, 937–942 (2010).

170. Sanner, T. and Pihl, A. Studies on the Active -SH Group of Papain and on the Mechanism of Papain Activation by Thiols. *J. Biol. Chem.* **238**, 165–171 (1963).

171. Smith, E. L. Active Site of Papain and Covalent High-Energy Bonds of Proteins. *J. Biol. Chem.* **233**, 1392–1397 (1958).

172. Smith, L. & Finkle, J. Crystalline Papain : Number and Reactivity of Thiol Group; Chromatographic Behavior. *J. Biol. Chem.,* **230**, 669–690 (1958).

173. Mole, J. E. & Horton, H. R. Kinetics of Papain-Catalyzed Hydrolysis of α-N-Benzoyl-L-arginine-P-nitroanilide. *Biochemistry* vol. 12 816–822 (1973).

174. Whitaker, J. R. & Bender, M. L. Kinetics of Papain-Catalyzed Hydrolysis of α-N-Benzoyl-L-arginine Ethyl Ester and α-N-Benzoyl-L-argininamide. *Journal of the American Chemical Society* vol. 87 2728–2737 (1965).

175. E. L. Smith, V. J. Chavere, P. M. J. Kinetics of Papain Action. I. Hydrolysis of Benzoyl-L-argininamide. *J. Biol. Chem.* **230** (1), 283–293 (1958).

176. Smith, Emil L., A. S. Kinetics of Papain Action I. Hydrolysis of Benzoyl-L-argininamide. **227(1)**, 1–26 (1957).

177. Lowe, G. & Yuthavong, Y. pH-Dependence and Structure-Activity Relationships in The Papain-Catalysed Hydrolysis of Anilides. *Biochem. J.* **124**, 117–22 (1971).

178. Sluyterman, L. A. Æ. The Activation Reaction of Papain. *Biochim. Biophys. Acta* **139**, 430–438 (1967).

179. Klein, I. B. & Kirsch, J. F. The Mechanism of the Activation of Papain. *Biochem. Biophys. Res. Commun.* **34**, 575–581 (1969).

180. Kanazawa, H., Fujimoto, S., Ohara, A. On the Mechanism of Inactivation of Active Papain by Ascorbic Acid in the Presence of Cupric Ions. *Biol. Pharm. Bull.* **17**, 789–793 (1994).

181. Schrader, T., Maue, M. & Ellermann, M. Entirely Artificial Signal Transduction with Adrenaline. *J. Recept. Signal Transduct.* **26**, 473–485 (2006).

182. Langton, M. J., Williams, N. H. & Hunter, C. A. Recognition-Controlled Membrane Translocation for Signal Transduction across Lipid Bilayers. *J. Am. Chem. Soc.* **139**, 6461–6466 (2017).

183. Bernitzki, K., Maue, M. & Schrader, T. Artificial Signal Transduction with Primary and Secondary Messengers. *Chem. - A Eur. J.* **18**, 13412–13417 (2012).

184. Lister, F. G. A., Le Bailly, B. A. F., Webb, S. J. & Clayden, J. Ligand-Modulated Conformational Switching in a Fully Synthetic Membrane-Bound Receptor. *Nat. Chem.* **9**, 420–425 (2017).

185. Thiol and Sulfide Quantitation Kit (T-6060) Information Product. 1–5 (2001).

186. Singh, R., Blättler, W. A. & Collinson, A. R. Assay for Thiols Based on Reactivation of Papain. *Analytical Biochemistry* vol. 213 49–56 (1993).

187. Falvey, P. *et al.* Bilayer Vesicles of Amphiphilic Cyclodextrins: Host Membranes That Recognize Guest Molecules. *Chem. - A Eur. J.* **11**, 1171–1180 (2005).

188. Glynn, C. W. & Turnbull, M. M. Complexes of 2,6-Diacetylpyridine Dioxime (dapdoH2). Crystal Structures of [M(dapdoH$_2$)$_2$](ClO$_4$)$_2$(M = Cu and Mn). *Transit. Met. Chem.* **27**, 822–831 (2002).

189. Obłak, E., Piecuch, A., Krasowska, A. & Łuczyński, J. Antifungal Activity of Gemini Quaternary Ammonium Salts. *Microbiol. Res.* **168**, 630–638 (2013).

190. Dega-szafran, Z., Dulewicz, E. & Brycki, B. Synthesis and Characterization of 1-Carbalkoxymethyl-4-hydroxy-1-methylpiperidinium Chlorides. *ARKIVOC* **vi**, 90–102 (2007).

191. Deck, L. M., Baca, M. L., Salas, S. L., Hunsaker, L. A. & Jagt, D. L. Vander. 3-Alkyl-6-Chloro-2-pyrones : Selective Inhibitors of Pancreatic Cholesterol Esterase. **42**, 4250–4256 (1999).

192. Zhang, X., Guo, H., Yang, F. & Yuan, J. Ion Complexation-Controlled Columnar Mesophase of Calix [4] arene – Cholesterol Derivatives with Schiff-Base Bridges. *Tetrahedron Lett.* **57**, 905–909 (2016).

193. Sreekanth, V. *et al.* Design, Synthesis, and Mechanistic Investigations of Bile Acid-Tamoxifen Conjugates for Breast Cancer Therapy. *Bioconjug. Chem.* **24**, 1468–1484 (2013).

194. Singh, M., Singh, A., Kundu, S., Bansal, S. & Bajaj, A. Deciphering the Role of Charge, Hydration, and Hydrophobicity for Cytotoxic Activities and Membrane Interactions of Bile Acid Based Facial Amphiphiles. *Biochim. Biophys. Acta - Biomembr.* **1828**, 1926–1937 (2013).

195. Ha, W. *et al.* Self-Aggregates of Cholesterol-Modified Carboxymethyl Konjac Glucomannan Conjugate: Preparation, Characterization, and Preliminary Assessment as a Carrier of Etoposide. *Carbohydr. Polym.* **86**, 513–519 (2011).

196. Erzunov, D. A., Latyshev, G. V., Averin, A. D., Beletskaya, I. P. & Lukashev, N. V. CuAAC Synthesis and Anion Binding Properties of Bile Acid Derived Tripodal Ligands. *European J. Org. Chem.* **2015**, 6289–6297 (2015).

197. Stuhr-Hansen, N. *et al.* Synthesis of Cholesterol-Substituted Glycopeptides for Tailor-Made Glycocalyxification of Artificial Membrane Systems. *ChemBioChem,* **17***,* 1403–1406 (2016).

198. Wathier, M., Polidori, A., Ruiz, K., Fabiano, A. S. & Pucci, B. Stabilization of Polymerized Vesicular Systems: An Application of the Dynamic Molecular Shape Concept. *Chem. Phys. Lipids* **115**, 17–37 (2002).

199. Szewczyk, S. M., Zhao, Y., Sakai, H. A., Dube, P. & Newhouse, T. R. α, β-Dehydrogenation of Esters with Free O-H and N-H Functionalities via Allyl-Palladium Catalysis. *Tetrahedron* **74**, 3293–3300 (2018).

200. Cornish-Bowden, A. *Fundamentals of Enzyme Kinetics*. (Weinheim : Wiley-Blackwell, 2012).